MAGNETOTELLURIC INVESTIGATION OF THE APPALACHIANS , NEWFOUNDLAND, CANADA

GARY WAYNE McNEICE

INFORMATION TO USERS

This manuscript has been reproduced from the microfilm master. UMI films the text directly from the original or copy submitted. Thus, some thesis and dissertation copies are in typewriter face, while others may be from any type of computer printer.

The quality of this reproduction is dependent upon the quality of the copy submitted. Broken or indistinct print, colored or poor quality illustrations and photographs, print bleedthrough, substandard margins, and improper alignment can adversely affect reproduction.

In the unlikely event that the author did not send UMI a complete manuscript and there are missing pages, these will be noted. Also, if unauthorized copyright material had to be removed, a note will indicate the deletion.

Oversize materials (e.g., maps, drawings, charts) are reproduced by sectioning the original, beginning at the upper left-hand corner and continuing from left to right in equal sections with small overlaps. Each original is also photographed in one exposure and is included in reduced form at the back of the book.

Photographs included in the original manuscript have been reproduced xerographically in this copy. Higher quality 6" x 9" black and white photographic prints are available for any photographs or illustrations appearing in this copy for an additional charge. Contact UMI directly to order.

UMI

A Bell & Howell Information Company
300 North Zeeb Road, Ann Arbor MI 48106-1346 USA
313/761-4700 800/521-0600

MAGNETOTELLURIC INVESTIGATION OF THE APPALACHIANS, NEWFOUNDLAND, CANADA

by

Gary Wayne McNeice

A thesis submitted to the
School of Graduate Studies
in partial fulfilment of the
requirements for the degree of
Master of Science

Department of Earth Sciences
Memorial University of Newfoundland

January 1998

St.John's Newfoundland

ABSTRACT

Data from 77 magnetotelluric (MT) soundings across the Appalachian orogen in Newfoundland, Canada, are analysed to determine the conductivity structure of major tectonic boundaries of the orogen and the regional conductivity structure. An extended Groom-Bailey tensor decomposition analysis is developed and employed to remove galvanic distortion effects produced by the complex near surface geology of Newfoundland. In the proposed decomposition analysis a global minimum is sought to determine the most appropriate strike direction and telluric distortion parameters for a range of frequencies and a set of sites. The recovered 2D responses are representative of regional-scale structures and 2D inversion algorithms can be employed to recover the regional conductivity structure.

The regional conductivity structure of the orogen suggests that the Baie Verte Line, Red Indian Line and Dover fault - Hermitage flexure represent significant crustal tectonic boundaries. The conductivity structure changes both across and along strike in Newfoundland. The magnetotelluric data do not support a near two-dimensional model of three lower crustal blocks but indicate a more complex three-dimensional geometry in southern Newfoundland.

The Baie Verte Line is imaged as an upper-middle crustal boundary separating the deformed and duplicated passive margin of Laurentia (Humber zone) and resistive arc terrain of the Notre Dame subzone. The Red Indian Line marks the boundary between the Notre Dame and Exploits subzones of the Dunnage zone and is roughly coincident with a change in lower crustal conductivity. The Dover fault is imaged as a near vertical boundary between upper-middle crusts of contrasting electrical properties, extending to a depth of at least 20 km.

The sharp change in upper-middle crustal conductivity observed in the magnetotelluric data suggest that orogen parallel motions were important in the development of many of the major boundaries of the orogen. The data support a three part division of the lower crust.

TABLE OF CONTENTS

LIST OF TABLES

LIST OF FIGURES

ACKNOWLEDGEMENTS

I am grateful to Dr. James A. Wright and Dr. Alan G. Jones for their support, supervision and patience throughout this long project. As well, I thank Dr. David E. Boerner, Dr. Ronald D. Kurtz and Dr. Ross W. Groom who provided advice on various aspects of this thesis, the Geological Survey of Canada for the use of research facilities and Memorial University of Newfoundland for financial support through a graduate student fellowship. This research was additionally supported through a Lithoprobe grant to Dr. James A. Wright. Finally, I am grateful to Kelly, my wife, for her initial encouragement and continued understanding support.

CHAPTER 1

Introduction

The Appalachians of Newfoundland record a Wilson-cycle (Wilson, 1966) of ocean creation and destruction. The Iapetus Ocean opened in the Late Precambrian between the Laurentian plate of North American affinity in the west and the Gondwanan plate of African affinity in the east. Closing during the Ordovician - Silurian resulted in the collision of the Laurentian and Gondwanan plates squeezing between them the arc-derived rocks of the Iapetus Ocean.

The interpretations of the marine deep seismic reflection data north of Newfoundland (Keen et al., 1986) and in the Gulf of St. Lawrence (Marillier et al., 1989) inferred a division of the lower crust of Newfoundland into three blocks: the western Grenville, the Central and the eastern Avalon. The upper crust of the orogen is subdivided into four main tectono-stratigraphic zones, the Humber, Dunnage, Gander, and Avalon from west to east, respectively (Williams, 1979) (Fig. 1.1). The Laurentian plate is represented by the continental rocks of the Humber zone and by the Grenville lower crustal block whereas the Gondwanan plate is represented by the continental rocks of the Avalon zone and by the Avalon lower crustal block. The Dunnage and Gander zone rocks, lying between the two plates, represent island-arc and back-arc basin rocks of the destroyed ocean and the eastern passive margin of the Iapetus Ocean. The Central lower crustal block is of unknown affinity between the Grenville and Avalon blocks (Fig. 1.1).

The early interpretation in terms of three lower crustal blocks was based entirely on reflection seismic data offshore (Keen et al., 1986; Marillier et al., 1989) and surface

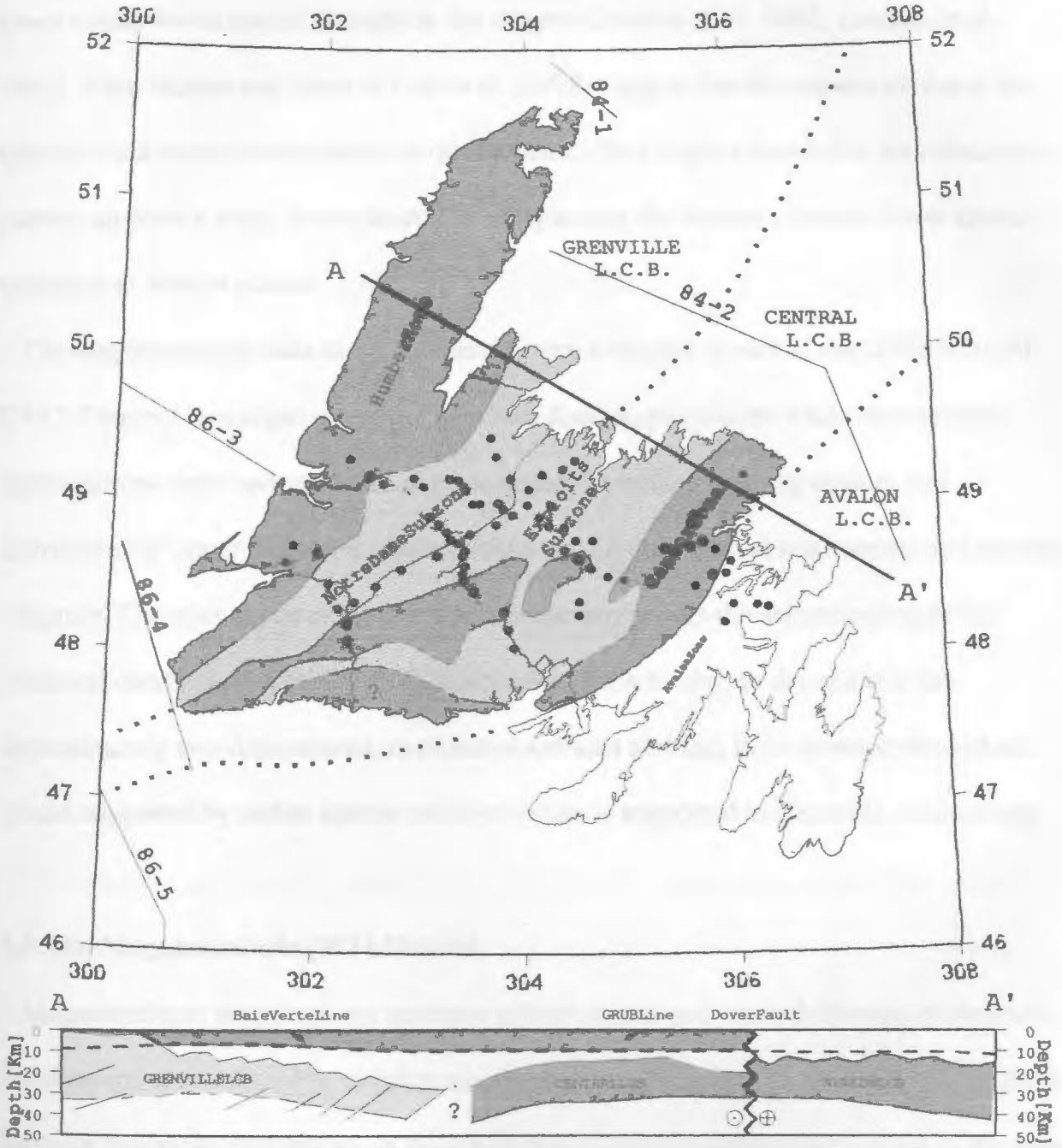

Figure 1.1 Map of the Newfoundland showing the four tectono-stratigraphic zones of the orogen and boundaries of the three lower crustal blocks inferred on the basis of marine seismic investigations (after Marillier et al., 1989; cross section AA' is based on Keen et al .(1986) interpretation of seismic lines 84-1,2) .

geological mapping on the island of Newfoundland (Williams, 1979). More recent interpretations of the seismic data onshore have called into question the applicability of the

lower crustal block model throughout the orogen (Quinlan et al., 1992; Quinlan et al., 1993). Their studies and those of Hall et al. (1998) suggest that the seismic evidence for three distinct lower crustal blocks is questionable. They argue instead that the reflectivity pattern supports a single lower crustal block spanning the Avalon / Gander lower crustal boundary at least in places.

The magnetotelluric data discussed herein were collected as part of the LITHOPROBE EAST Transect investigations of the Newfoundland Appalachians. Multi-disciplinary investigations were undertaken to provide better constraints on the geometry and distribution of upper and lower crustal blocks and on their mutual relationship and internal structure. The main focus of the electromagnetic survey was the determination of the electrical conductivity of the middle-lower crust, in particular, to determine if the approximately two-dimensional, northeast-southwest striking, three-lower-crustal-block model suggested by earlier marine seismic studies is supported in electrical conductivity.

1.1 The Magnetotelluric (MT) Method

Magnetotelluric soundings are sensitive to both lateral and vertical changes in electrical conductivity. The method is an integrating technique and as such is sensitive to changes in the bulk electrical conductivity of the subsurface. Electrical conductivity is one of the most variable properties of rocks and minerals (Haak and Hutton, 1986), providing the method with resolution not attained by other integrating techniques (gravity and surface wave studies). The method is complementary to seismic reflection investigations as it is sensitive

to different physical properties and is capable of resolving the distribution of electrical conductivity of the subsurface, as opposed to faults, lithological boundaries and intrusions resolved in normal incident reflection surveys (Jones, 1987).

In the MT method, time-varying electric and magnetic fields, observed at the subsurface of the Earth, are recorded as a function of frequency. These fields are the sum of a naturally occurring external magnetic field, the magnetotelluric source, and electric and secondary magnetic fields induced by the interaction of the external magnetic field with the conductivity structure of the Earth. The depth of source interaction is frequency dependent, governed by a skin depth relationship. This depth dependence enables one to image the conductivity structure of the Earth by examining relationships between the observed fields as a function of frequency (pseudo depth).

1.2 The LITHOPROBE EAST Magnetotelluric Experiment

The electromagnetic data of the LITHOPROBE EAST Transect investigations consist of 77 magnetotelluric soundings recorded in 1989 and 1991. The magnetotelluric sites were located to provide reasonable areal coverage of the island and to complement seismic refraction (Hall et al., 1991) and reflection (Quinlan et al., 1992) investigations. During the field campaigns care was taken to place sites distant from known near surface conductive structures that can produce severe telluric distortion and reduce the effective depth of investigation. The location of the 77 magnetotelluric sites is shown in Fig. 1.1.

The magnetotelluric data were collected by Phoenix Geophysics Ltd. using a five

component (*Ex, Ey, Hx, Hy, Hz*) MAGNETOTELLURIC-system with 2-component (*RHx, RHy*) hard-wired remote magnetic reference. Natural time-varying electromagnetic signals were filtered and collected into three frequency bands: 10,000 - 72 Hz, 384 - 9 Hz, and 0.1 - 2000 s. Recording times were approximately 1 x 4 hours, 1 x 4 hours, and 2 x 20 hours respectively. The lowest frequency band was processed using a robust variant of Wight and Bostick's (1980) cascade decimation scheme. A comparison of the Phoenix robust processing with more rigorous M-regression robust estimation demonstrated that both yield estimates of the mean values that lie within error tolerances (Chave and Jones 1997). However, the parametric error estimates from the Phoenix processing were shown to be too small for a large number of degrees of freedom, and too large for a small number of degrees of freedom, compared to nonparametric jackknife estimates. This means that the errors in the frequency range 12 - 0.5 Hz are probably too small. Consequently, the poor misfit of either a distortion model and/or a conductivity model in this range should not be taken necessarily as an indicator of an inadequate model, manifesting either three-dimensional effects or insufficient structure.

The data quality was, overall, excellent. However, because of the problems in the calibration of the very high frequency induction coils, the data from the first decade (10,000 - 1,000 Hz) could not be used. Also, given that the objective of this study is the large-scale structure of the Newfoundland Appalachians, and that the site separation was more than 5 km, data from the first half of the second decade (1,000 - 384 Hz) were also not used further.

Although, care was taken during the field campaign to avoid near surface conductive features, the magnetotelluric data collected in Newfoundland proved to be one of the most complex data sets ever collected as part of LITHOPROPE electromagnetic investigations. Outcropping graphitic units distorted the natural electromagnetic fields, particularly the electric fields, yielding responses that are very sensitive to analysis procedures. Thus extreme care had to be taken when analysing, modelling and inverting the data to models of the conductivity structure.

1.3 Thesis Outline

This thesis is organized into seven chapters and one appendix. In chapter two the regional geology and crustal tectonics of the Newfoundland Appalachians are reviewed. As well, the results of crustal geophysical investigations are summarized to present a picture of our current understanding of the middle and lower crust of the orogen.

Chapter three begins with a mathematical derivation of the magnetotelluric impedance tensor. Methods of interpretation of the impedance tensor through the traditional assumptions of one and two dimensional earth conductivity models are discussed, along with the extension of these models through mathematical and physical decompositions.

In chapter four an extension of Groom-Bailey decomposition is developed. The extended decomposition analysis is applied to a number of synthetic data sets to demonstrate the method's recovery of regional impedances in the presence of experimental noise. The advantages and superiority of distortion analysis over simple data rotation are outlined.

The regional conductivity structure of Newfoundland is discussed in chapter five. An estimate of the coast effect in Newfoundland is found through three-dimensional modelling of the Newfoundland coast and surrounding bathymetry. Regional strike, induction vectors and determinant phases are examined to delineate important changes in conductivity structure of the orogen.

In chapter six the conductivity structure of the Humber-Dunnage zone, Notre Dame - Exploits subzone and Gander-Avalon zone boundaries is examined through two-dimensional inversion. The tectonic significance of the structure observed at these boundaries is discussed. Conclusions, along with recommendations for future work are discussed in chapter seven.

CHAPTER 2

Regional Setting and Tectonics

2.1 Introduction

The island of Newfoundland records a late Precambrian to mid-Paleozoic cycle of ocean creation and destruction. This cycle was first proposed by Wilson (1966) on the basis of contrasting early Paleozoic faunal realms. The Appalachian-Caledonian orogen extending from Scandinavia in the north to the United States in the south contains the remnants of this pre-Atlantic ocean, termed Iapetus by Harland and Gayer (1972) (Fig. 2.1). Since the initial proposal of the Iapetus ocean, the orogen has been the focus of a large number of geological and geophysical studies. Newfoundland provides the most complete and best exposed cross-section through the orogen.

Late Precambrian rifting of the North American craton led to the development of the early Paleozoic Iapetus ocean (see review by Williams, 1979). By the late Ordovician, destructive processes operating within Iapetus led to closure of the ocean and subsequent Silurian continent-continent collision. Williams (1978, 1979) divided the Appalachian orogen into five tectono-stratigraphic zones based on stratigraphic and structural contrasts inherited during the development and destruction of Iapetus (Fig. 2.2). The zones are from west to east, the Humber, Dunnage, Gander, Avalon and Meguma zones. Zones east of the North American craton (Humber zone) are viewed as suspect terranes, accreted to North America during the destruction of Iapetus (Williams and Hatcher, 1982, 1983). This subdivision of the Appalachian Orogen and evolutionary concept has provided a

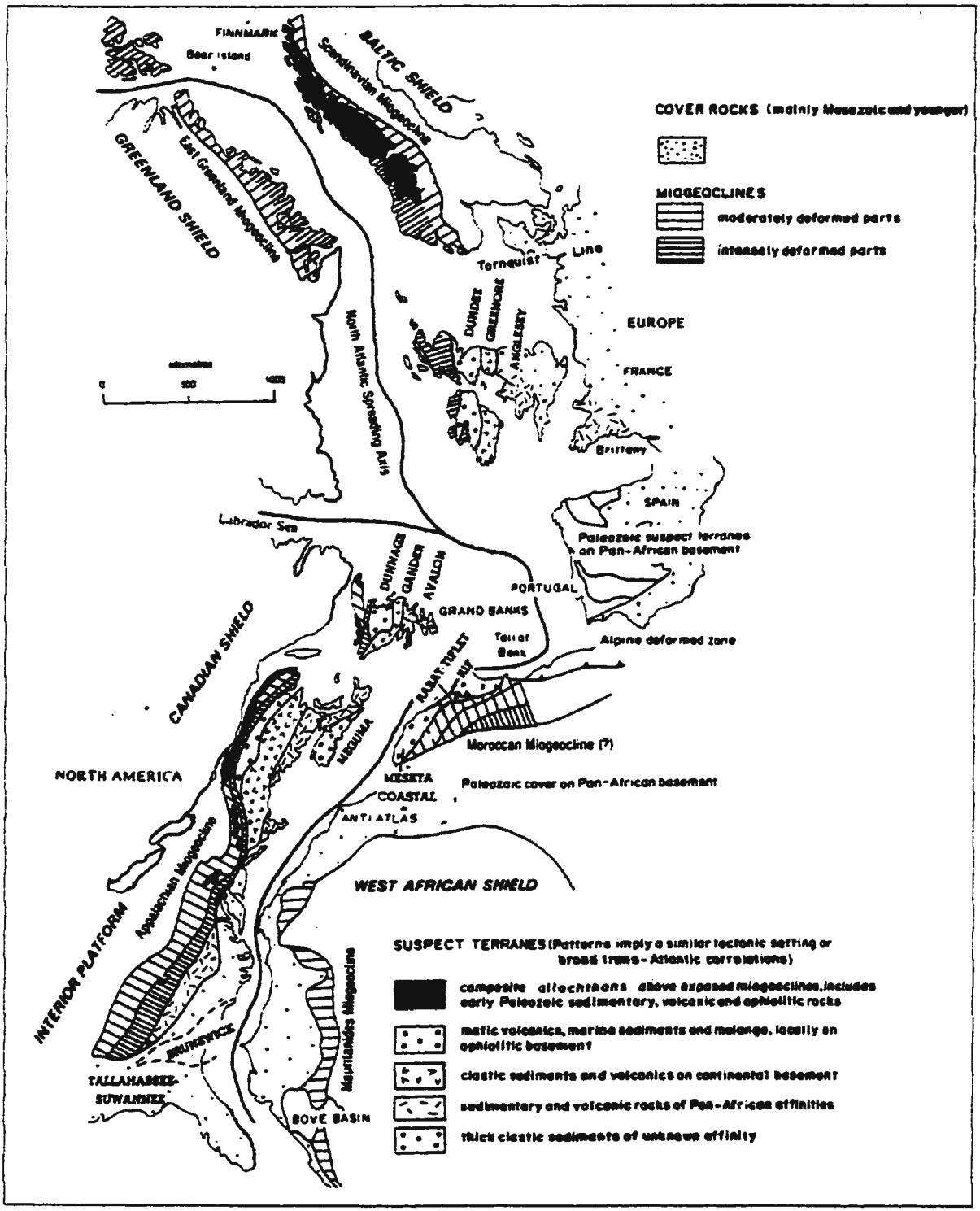

Figure 2.1 Reconstruction of the North Atlantic (Williams, 1979).

framework for tectonic models of the Orogen and constraints on the tectonic development of the Orogen.

While the surface geology of Newfoundland can be divided into zones of contrasting stratigraphic and structural histories, the relationship of these surface zones to boundaries in the mid-lower crust of the Orogen are poorly resolved. Lithoprobe geophysical and supporting geoscience investigations were designed primarily to resolve the relationship between the observed surface geology and the geology of the mid-lower crust. An understanding of how structures observed at surface relate to those of the mid-lower crust is essential to fully understand the tectonic processes involved in the destruction of Iapetus.

Early Lithoprobe marine deep seismic reflection profiles across the Appalachians in waters north and south of the island of Newfoundland (Fig. 2.3) divided the lower crust of the Orogen into three lower crustal blocks (LCB) (Keen et al., 1986; Marillier et al., 1989). This division of the lower crust is based primarily on contrasts in reflectivity character within the lower crust and in particular at or near the reflection Moho. The western LCB is interpreted as the North American craton (Laurentia) and the two eastern LCBs represent parts of Gondwanda accreted during the development of the orogen. The division of the lower crust into three LCBs implies both allochthonous and autochthonous settings for the five tectono-stratigraphic zones recognized at the surface. The zones are interpreted to have been carried and deformed above the three LCBs, which remained as essentially rigid plates throughout the development of the orogen (Stockmal et al., 1987, 1990). An allochthonous setting for one of the zones (Dunnage) is supported by earlier gravity

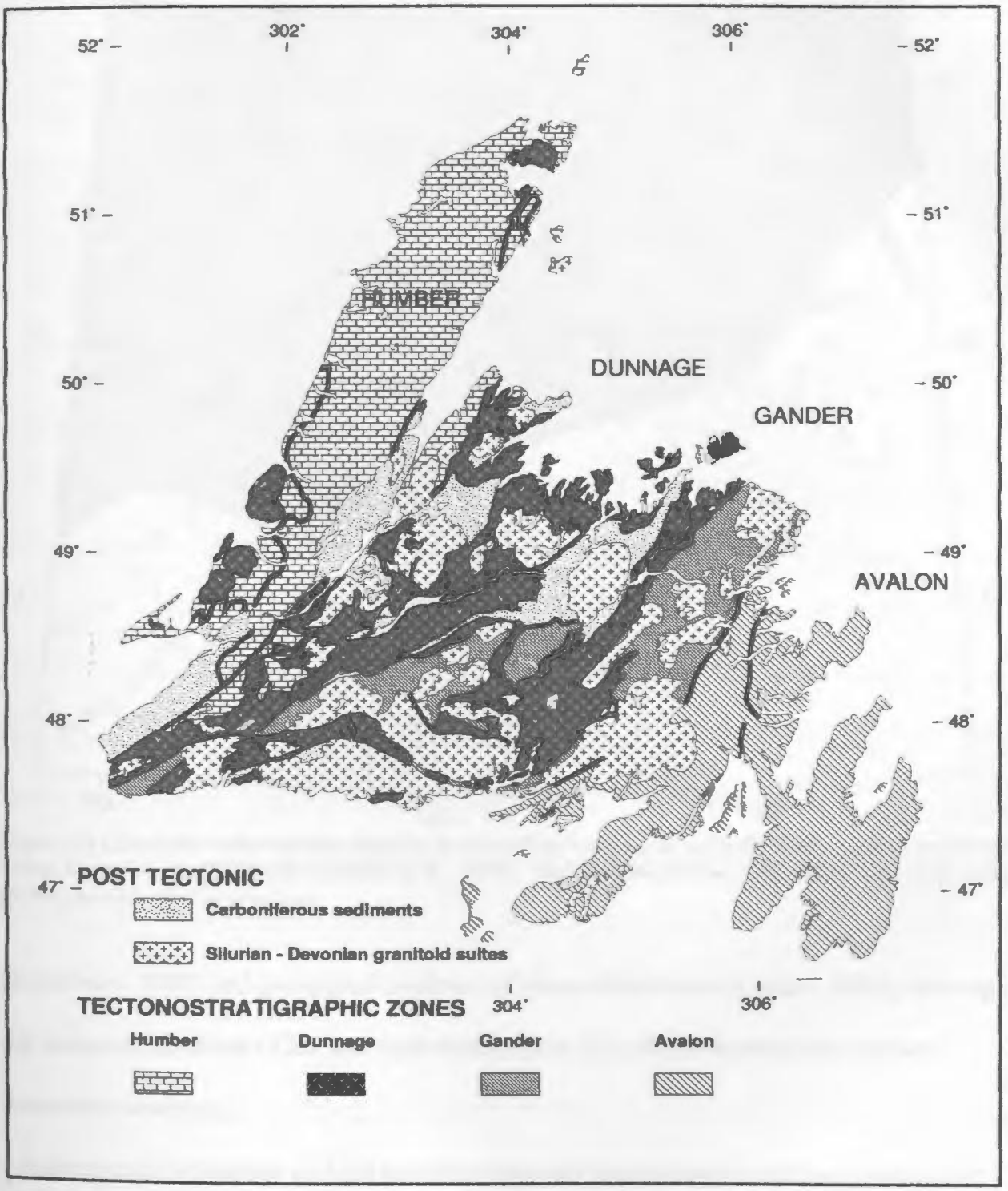

Figure 2.2 Tectono-stratigraphic zones of Newfoundland (after Colman-Sadd et al., 1990).

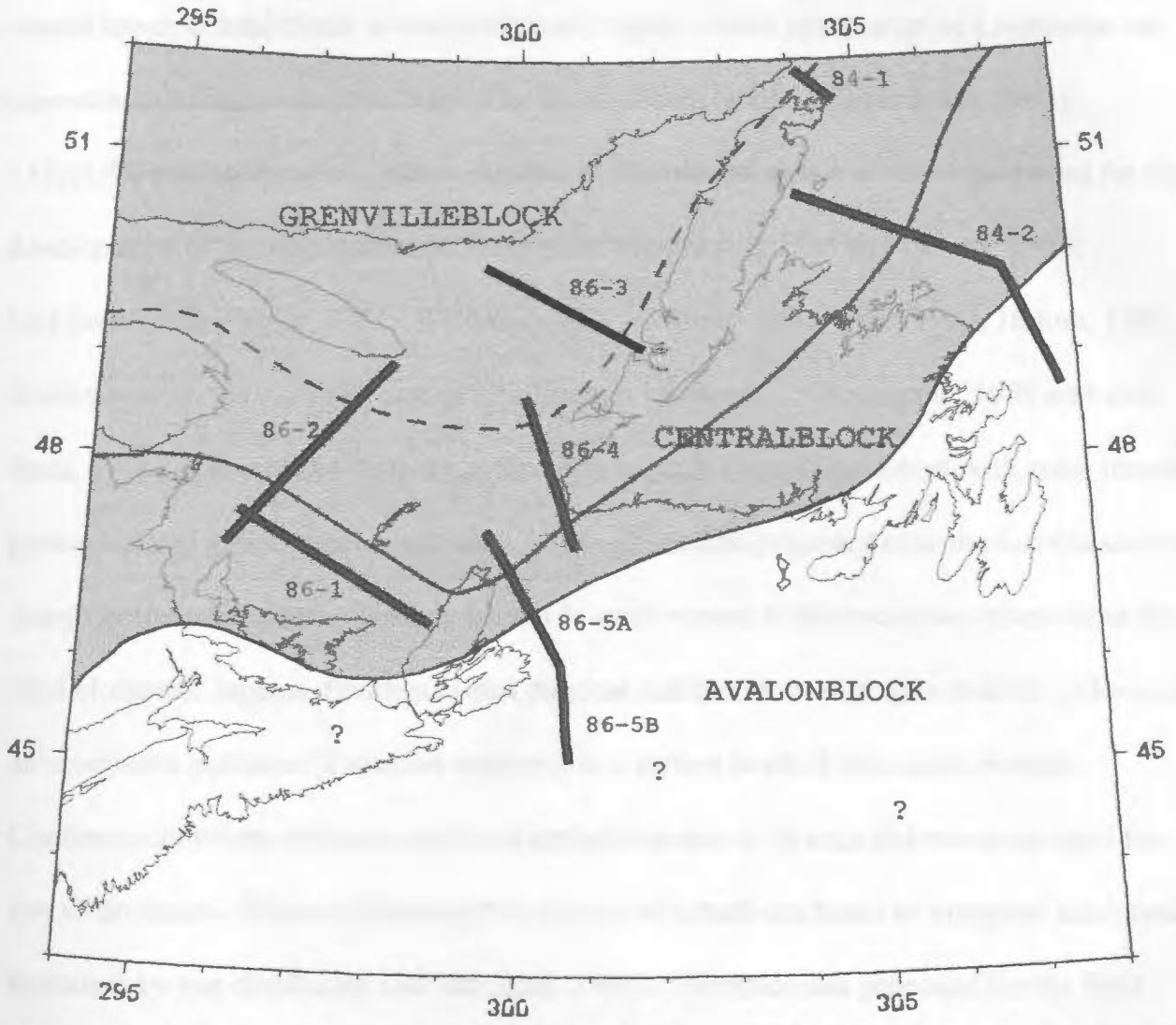

Figure 2.3 Lithoprobe marine seismic reflection division of the lower crust into a Grenville, Central and Avalon Lower Crustal Blocks (LCB) (after Marillier et al., 1989). The location of Lithoprobe marine seismic reflection profiles are indicated by grey lines.

(Karlstrom, 1983) and geological evidence (Colman-Sadd and Swinden, 1984), although the nature of the three LCBs and their relationship to surface observations remains somewhat uncertain.

Subsequent Lithoprobe on land seismic reflection investigations contrast with earlier seismic investigations suggesting a two part division of the lower crust. In this model the

central lower crustal block is interpreted as a region where lower crust of Laurentian and Gonwandan affinities are interleaved by tectonic processes (Quinlan et al., 1992).

Over the past twenty-five years a number of tectonic models have been proposed for the development of the Appalachian-Caledonides orogen (e.g. Bird and Dewey, 1970; McKerrow and Ziegler, 1971; Williams, 1979; Colman-Sadd, 1980, 1982; Hutton, 1987; Stockmal et al., 1987, 1990; van der Pluijm and van Staal, 1988; Keppie, 1989 and van Staal, 1994). Many of the features in the early models are not consistent with more recent geological and geophysical constraints, although models proposed over the last decade have many common elements, differing primarily with respect to the processes involved in the final closure of Iapetus. Southeastward directed subduction resulting in middle Ordovician arc-continent collision (Taconian orogeny) is common to all of the recent models. Continent-continent collision and the complete closure of Iapetus did not occur until the late Ordovician - Silurian following the closure of a back-arc basin or marginal sea (termed Iapetus II by van der Pluijm and van Staal, 1988). The processes proposed for the final closure of Iapetus include: lithospheric delamination allowing for "blind subduction" to continue after the Taconian collision of North America with an island arc and closure of the back-arc basin as a result of crustal shortening (Colman-Sadd, 1980, 1982 and Stockmal et al., 1987, 1990), and abandonment of southeast directed subduction after continent-arc collision and the development of north westward subduction in the back-arc basin (van der Pluijm and van Stall, 1988; Keppie, 1989 and van Staal, 1994). Uncertainties about the processes involved in the final closure of Iapetus stem partially

from the lack of lower crustal information and the fact that surface observations are possibly obscured by orogen parallel transcurrent motions (e.g. Currie and Piasecki, 1989). Relationships along strike within the Orogen may also be complicated by offsets (Promontories) in the original rifted margins of Iapetus (Thomas, 1977; Stockmal et al., 1987, 1990 and Currie and Piasecki, 1989).

2.2 Tectono-stratigraphic zones and Boundaries

Much of our present understanding of the tectonics of the Appalachian orogen in Newfoundland is derived from the recognition of surface zones of contrasting geological properties and the relationships between these zones. An understanding of the relationships between the remnants of the Iapetus ocean contained within the Dunnage zone and the margins of Iapetus contained in the Humber and Gander zones is essential to an understanding of the tectonics of the orogen. The following description of the tectono-stratigraphic zones and their inter-relationships is based mainly on the works of Williams et al. (1988, 1989), Cawood et al. (1988), Piasecki et al. (1990), Colman-Sadd et al. (1992) and Piasecki (1995).

The Humber zone extends from the western limit of Appalachian deformation eastward to the Baie Verte-Brompton line and Long Range Fault (Fig. 2.4). The zone records the development and destruction of the Cambrian-Ordovician western passive margin of Iapetus. Development of the margin was initiated by Late Precambrian rifting and was followed by the deposition of clastic sediments and a shallow-marine carbonate sequence. Sedimentation on the passive margin ceased in the early to middle Ordovician with the

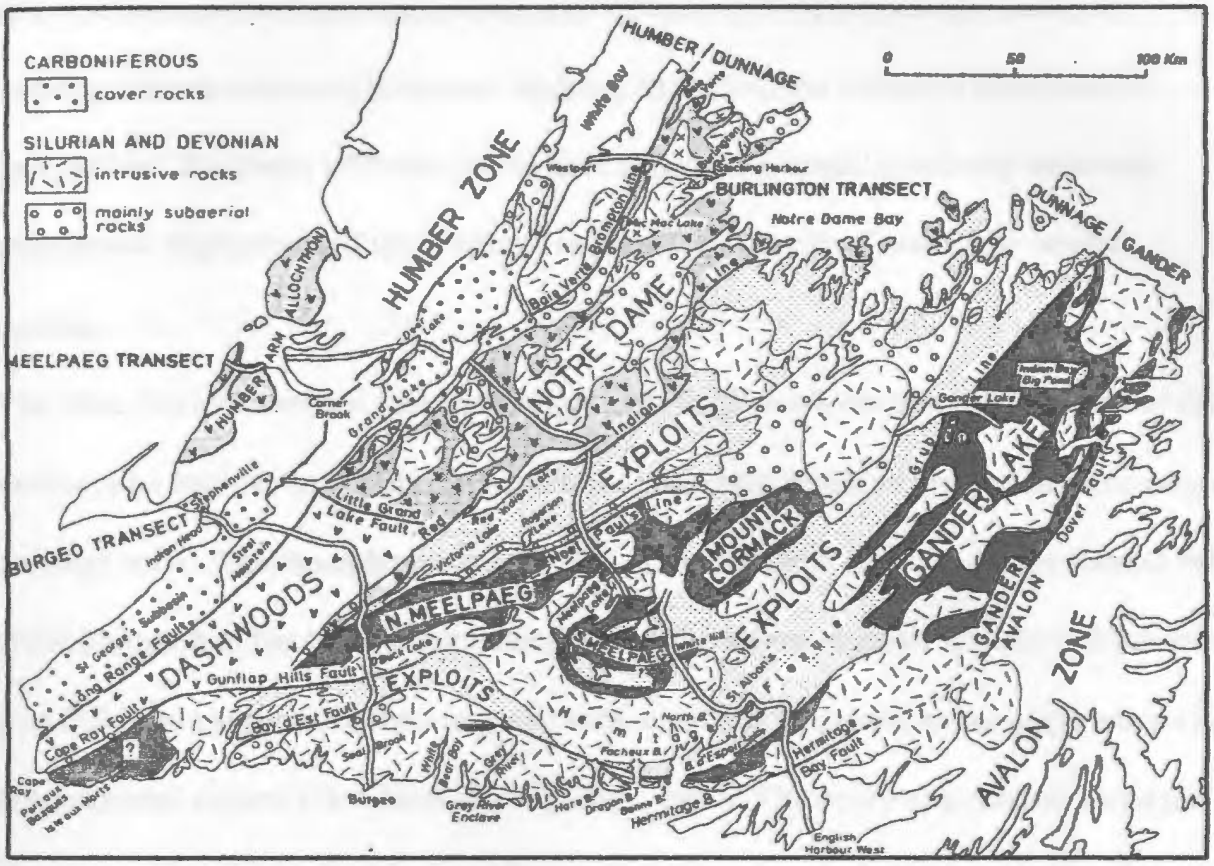

Figure 2.4 Tectono-stratigraphic zone and subzone boundaries of Newfoundland (Piasecki et al., 1990).

structural emplacement of Taconian allochthons over the shelf (Cawood et al., 1995) and the development of a middle Ordovician foredeep (Quinn, 1995). The Taconian allochthons are thrust stacks consisting of basal slices of nearby continental margin rocks and higher slices of ophiolite suites. The ophiolitic suites represent oceanic crust and mantle thrust onto the margin during continent-arc collision and attempted subduction of the passive margin (Cawood and Suhr, 1992; Cawood et al., 1995).

Deformation of the western passive margin of Iapetus did not cease with the mid-Ordovician continent-arc collision. Rocks of the Humber Zone were subsequently deformed in the Late Ordovician-Devonian development of the Orogen, resulting in

northwest transport and uplift. Cawood and Williams (1988) proposed a model of involving delamination and basement wedging to explain the observed deformation. Stockmal and Waldron (1990 and 1993) have proposed a model involving westward transport and duplication of the platform sequence as a result of northwest vergent thrusting.

The Baie Verte-Brompton line and Long Range Fault mark the eastern boundary of the Humber zone and the transition from crust of continental origin to crust of oceanic origin (Dunnage zone). This boundary was the locus of deformation from the Ordovician to the Carboniferous, and has had a complicated history of deformation with westward thrusting being followed by eastward thrusting and both sinistral and dextral strike-slip motions in a transpressional regime (Goodwin and Williams, 1990). The strike-slip motion along the boundary separating the Humber and Dunnage zones suggests that the pre-strike-slip histories of the two tectono-stratigraphic zones are unlikely to be similar, with contrasts across the boundary possibly dependent on strike-slip motion rather than older tectonic events (Taconian thrusting and destruction of the western passive margin of Iapetus) (Goodwin and Williams, 1990; Currie and Piasecki, 1989).

The Dunnage zone contains vestiges of arc, arc-related and back-arc rocks of an oceanic domain, deformed during the closure of the Iapetus ocean. The Dunnage zone in Newfoundland extends from the North American migeocline (Humber zone) eastward to the Gander River Ultrabasic Belt (GRUB line), southeast to the Day Cove thrust and south to the Bay d'Est fault (Hermitage Flexure) (Fig. 2.4).

Dating of ophiolite sequences in the Dunnage zone and within the Taconian allochthons of the Humber zone indicates that the majority of ophiolites formed in a relatively narrow time range between 495 and 478 Ma (Early Ordovician) (Dunning and Krogh, 1985). Arc volcanics located primarily in the central Dunnage zone have a greater spread in ages, ranging from 513 Ma (Late Cambrian) to 462 Ma (Middle Ordovician) (Dunning et al., 1991). Evidence of arc volcanism predating ophiolite formation within the Orogen implies that the ophiolites of the Dunnage zone do not represent vestiges of the main ocean basin (Jenner et al., 1991; Dunning et al., 1991). This conclusion is further supported by island-arc geochemical signatures of the Dunnage ophiolites (Jenner et al. 1991 and references therein). The ophiolite sequences preserved within the Dunnage zone therefore represent fragments of oceanic crust formed in a supra-subduction zone environment and record some or all stages of arc evolution.

Although, the ophiolites of the Dunnage zone formed in a similar supra-subduction zone setting over a short time period the zone is internally divisible on the bases of contrasting stratigraphy, faunas, structure, metamorphism and plutonism (Williams et al., 1988; Currie and Piasecki, 1989; Colman-Sadd et al., 1992; Williams et al., 1995). The Dunnage zone is commonly divided into the Dashwood, Notre Dame and Exploits subzones, each of which developed independently until at least the Late Ordovician (Many authors consider the Dashwood subzone to be part of the Notre Dame subzone).

The Dashwood and Notre Dame Subzones abut the Humber zone forming the western side of the Dunnage Zone (Fig. 2.4). These two subzones are interpreted as parts of an arc

terrane accreted to North America during the Taconian orogeny (Cawood et al., 1995: Dec et al., 1997). Contrasting lithologies, metamorphic grade and plutonism indicate that the two subzones developed at different structural levels (Currie and Piasecki, 1989; Piasecki, 1995). The deeper crustal rocks of the Dashwoods subzone have been juxtaposed against the swallower crustal Notre Dame subzone (Piasecki, 1995).

A high angle fracture termed the Red Indian Line separates the Dashwoods and Notre Dame subzones from the Exploits subzone (Fig. 2.4) (Williams et al., 1988). In the southwest this boundary is marked by the Cape Ray fault which separates rocks of the Dashwoods subzone from those of the Gander zone (Dubé et al., 1996). Similarities between the ophiolites of the Notre Dame and Exploits subzones are the principal reason for grouping them together in the Dunnage zone, although these similarities are misleading since stratigraphic, structural and faunal information suggests that the two subzones were not linked until the Late Ordovician to Early Silurian. A sediment provenance and U/Pb age study (Colman-Sadd et al., 1992) indicates that the oceanic rocks of the Exploits subzone were emplaced onto the eastern margin of Iapetus during the late Arenig (Early Ordovician). This event correlates with the Penobscot Orogeny of Maine and was approximately synchronous with the Taconian Orogeny, in which ophiolites of the Notre Dame subzone where emplaced westward onto the North American margin (Humber zone). The direction of transport within the two subzones was therefore in opposite directions and onto opposite margins.

Contrasting Early to Middle Ordovician faunas (Celtic versus North American) of the

Notre Dame and Exploits subzone indicate that the deformation that occurred at both margins of Iapetus did not result in the complete closure of the Iapetus ocean (Neuman and Max, 1989; Williams et al., 1995). Stratigraphy of the subzones imply a Late Ordovician to Early Silurian linkage for the Exploits and Notre Dame subzones (Williams et al., 1988). The relative movements of the Notre Dame and Exploits subzone and the processes responsible for their linkage remain unresolved. The importance of Silurian orogen parallel sinistral movements within the Orogen and arc volcanism post dating the Taconian and Penobscot Orogenies (462 Ma) suggest that the linkage of the Exploits and Notre Dame subzones was accompanied by sinistral transcurrent movements and or subduction (Keppie, 1989; Currie and Piasecki, 1989; Piasecki, 1995).

The GRUB (Gander river ultrabasic belt) line , Day Cove Thrust and Bay d'Est Fault (Hermitage Flexure) mark the boundary between the Exploits subzone and the eastern margin of Iapetus represented in Newfoundland by the Gander zone. Rocks of the Gander zone consist of pre-Middle Ordovician clastic sediments of predominantly continental origin. Their sedimentary provenance suggest a continental or continental-margin environment that did not experience volcanism (Williams et al., 1988). The rocks of the Gander zone therefore are interpreted as remnants of an eastern passive margin of Iapetus.

The Gander zone is divided into three subzones: the Meelpaeg, Mt. Cormack and Gander Lake subzones (Fig. 2.4). The Mt. Cormack and Meelpaeg subzones are surrounded by Dunnage zone rocks and are interpreted as structural windows of Gander zone rocks exposed through the structural cover of the Dunnage zone (Colman-Sadd and

Swinden, 1984; Colman-Sadd et al., 1992). Structural relationships at the boundaries of these subzones and observations of an ophiolite substrate to Dunnage zone rocks at observed contacts between the Dunnage and Gander zones indicates that the Exploits subzone (Dunnage zone) is allochthonous and transported over Gander zone rocks. Xenoliths and zircons contained within intrusive and volcanic rocks of the Dunnage zone (Exploits subzone) indicate that a continental substrate may extend as far west as the Red Indian line (Dunning at al., 1987 and Greenough et al. 1990). The Exploits subzone and Gander zone therefore probably form a composite crust in the eastern Dunnage zone and have developed as such since the Early Ordovician emplacement of Exploit subzone rocks onto the eastern margin of Iapetus (Penobscot Orogeny) (Colman-Sadd et al., 1992; Piasecki, 1995).

The final closure of Iapetus in Newfoundland is therefore marked by the amalgamation of the Exploits and Notre Dame subzones in the Late Ordovician to Early Silurian. This amalgamation signifies the collision of the previously deformed eastern and western margins of Iapetus (continent-continent collision).

The closure of Iapetus was followed by continued deformation throughout the Silurian and Devonian and is recorded as telescoping of the orogen and the development of successor basins over the destroyed margins of Iapetus. Devonian deformation is termed the Acadian Orogeny by some authors, but the importance of Silurian events suggest that deformation may be the result of two distinct events (Dunning et al., 1990). The emplacement of batholiths, regional metamorphism and subaerial volcanicity in the Silurian

indicate a distinct orogenic peak in Newfoundland, similar to the Scandian or Salinic Orogeny observed elsewhere in the Appalachian-Caledonian Orogen (Dunning et al., 1991). The Silurian orogenic event was followed by the intrusion of granite and the brittle reactivation of earlier structures in the Devonian Acadian Orogeny.

The orogen parallel movements observed on northeast trending faults of the orogen and north over south thrusts are related to the Silurian orogenic event. These movements were accompanied by plutonism and were more intense in the easterly zones of the Orogen. Thrusting of the Notre Dame subzone over the Dashwood subzone and sinistral movements along the Baie Verte - Brompton line noted earlier are probably related to this orogenic event (Cawood et al., 1994 and Currie and Piasecki, 1989). Deformation also occurred along the eastern side of the Dunnage zone, with sinistral strike-slip motions on the GRUB line and thrusting along the Hermitage Flexure indicting that the rocks of the Exploits subzone were transported to the southwest (Orogen parallel) over the Gander zone rocks (see Hanmer, 1981; Piasecki, 1988 and Currie and Piasecki, 1989). The Silurian event may be related to continued oblique convergence after the closure of Iapetus and possibly to the accretion of the Avalon zone.

The Dover Fault and its southern extension, the Hermitage Bay Fault, form the eastern boundary of continental passive margin rocks (Gander zone) (Cawood et al., 1988). To the east of this high-angle fault system lies the Avalon zone consisting of Precambrian igneous and sedimentary rocks overlain by Paleozoic shallow marine and terrestrial sedimentary rocks and minor volcanics. The Gander/Avalon boundary is marked by a sharp contrast in

deformation intensity, intensely deformed Gander zone rocks are juxtaposed against the mildly deformed rocks of the Avalon zone. This contrast in deformation intensity and the lack of overthrust allochthons at the boundary of the zones suggests that the Avalon zone was accreted late in the development of the Orogen and that accretion was accomplished primarily by strike-slip motion. The complete lack of correlatable features across the boundary implies that lateral displacement was significant (Holdsworth, 1991).

Kinematic indicators observed along the Gander-Avalon boundary preserve a three phase history for the boundary comprising: early ductile sinistral transpression, later ductile dextral transpression, and brittle dextral faulting (Holdsworth, 1991). The early sinistral motions on the boundary are associated with plutonism and appear to be analogous to deformation along the Hermitage Flexure. The later dextral motions along the Dover - Hermitage Bay Faults indicate a reversal of motion and may mark the onset of the Acadian Orogeny. Motions on both the Hermitage Flexure and Dover - Hermitage Bay Faults are locked by Devonian granites, which provide an upper age limit to motions on the faults and suggest a near synchronous end to faulting (Dunning and O'Brien, 1989).

Tectonostratigraphic zone boundaries along the south coast of Newfoundland are obscured by deformation and plutonism associated with the Hermitage Flexure. The swing in structural trends in this region suggest a departure from the near two dimensional zone geometry observed in northern Newfoundland. Rocks south of the Hermitage Flexure in central Newfoundland (shown as part of Gander zone in Fig. 2.4) have Precambrian to earliest Palaeozoic U/Pb ages and form a unique zone intermediate between the lower

Palaeozoic Dunnage zone and Precambrian Avalon zone (Dunning and O'Brien, 1989). O'Brien et al. (1991a) have interpreted this region to be of Avalonian affinity and possibly representing surface exposures of the basement on which the Gander Zone was deposited. The Hermitage Bay Fault therefore, may not represent the Gander - Avalon boundary in southern Newfoundland, but a boundary within a larger composite Avalon Zone.

Currie and Piasecki (1989) have suggested a kinematic model for southwestern Newfoundland in which the sinistral strike-slip movements and north over south thrusts of the Orogen are related to Silurian orogen parallel movements around an Avalonian promontory in south - central Newfoundland (Fig. 2.5). If this model is substantiated it may be able to explain the swing in structural trends observed in Newfoundland and the presence of rocks of Avalonian affinity in southern Newfoundland. This model may also explain the outcrop pattern of the Orogen and apparent relationship of thrusting and strike-slip motion within the Orogen.

Despite uncertainties about the processes operating during the development of the Appalachian Orogen, it appears certain that orogen parallel motions are important in the post continent-continent collision history of the Orogen in Newfoundland. The importance of strike-slip motions has been recognized in other parts of the Appalachian-Caledonides (Hutton, 1987, 1989 and Soper et al., 1992). Strike-slip motions similar to those observed in Newfoundland are interpreted to be important in the evolution of the British and Irish Caledonides (Hutton, 1987; Soper et al., 1992).

The recognition of contrasting surface tectono-stratigraphic zones in the Appalachians of

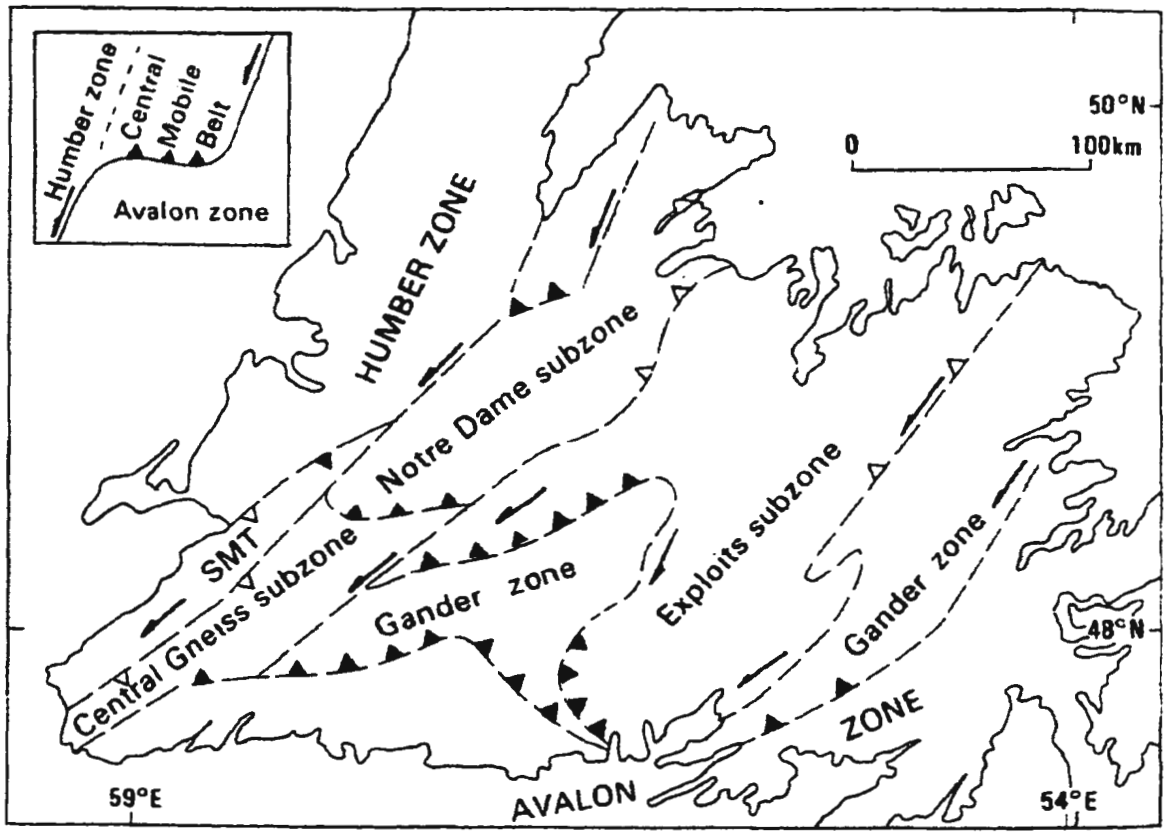

Figure 2.5 Silurian kinematic model for Newfoundland (Currie and Piasecki, 1989).

Newfoundland provides insight into the tectonic development of the Appalachian Orogen and provides constraints on the tectonic processes operating during the evolution of the Orogen. The tectonic constraints provided by surface observations can be summarized, as follows:

- Orogenic events in the Early Ordovician resulted in the destruction of both the eastern and western passive margins of Iapetus. Destruction of the western margin of Iapetus occurred during the Taconian Orogeny as a result of continent - arc collision (Humber zone - Notre Dame subzone collision). The destruction of the

eastern margin (Exploits subzone - Gander zone collision) correlates with the Penobscot Orogeny of Maine, although the processes involved in this orogenic event remain unresolved.

- The destruction of the margins of Iapetus did not result in complete closure of the ocean. Complete closure of Iapetus occurred in the Late Ordovician to Early Silurian and is marked by the linkage of the Notre Dame and Exploits subzones.
- Ophiolites obducted onto the two margins of Iapetus formed in a supra-subduction zone setting and do not represent fragments of the main Iapetus ocean. This implies that both the Taconian and Penobscot Orogenies involved subduction processes.
- Continued deformation in the Silurian, following the closure of Iapetus, involved significant sinistral orogen parallel movements, volcanism and plutonism. This deformation may be related to the Salinic Orogeny observed elsewhere in the Orogen.
- Accretion of the Avalon zone occurred primarily as a result of strike-slip motion. Similarities in the deformation along the Gander/Avalon boundary with that along other boundaries of the Orogen suggest that accretion of the Avalon zone may be linked to Silurian deformation of the Orogen.
- A reversal in strike-slip motion occurred late in the development of the Orogen. Dextral strike-slip motions and the intrusion of Late Silurian - Devonian plutons may be the result of the Acadian Orogeny.

Although, the surface geology provides many constraints on the tectonics of the Appalachian Orogen a full understanding of the development of the Orogen requires information on the relationship of surface features to the properties of the deeper crust.

2.3 Crustal Structure

Much of our present understanding of the deep crustal structure of the Canadian Appalachians has been provided by seismic and supporting geoscience investigations carried out as part of the Canadian Lithoprobe East transect. Information on the crustal structure of the Appalachians in Canada prior to the onset of Lithoprobe investigations was primarily provided by seismic refraction, regional electromagnetic and potential field investigations. These early investigations determined the gross structure of the Orogen and delineated some anomalous aspects of the deep crust. The results of Lithoprobe East investigations have advanced our understanding of the crust of the Orogen and it is clear that changes in crustal structure and geophysical properties can be roughly related to major changes in the surface geology. Although advances have been made, it remains unclear what the changes in crustal structure signify with respect to collisional tectonics of the Orogen.

The early seismic refraction investigations of the Appalachian Orogen in Canada are summarized by Dainty et al. (1966) and Keen et al.(1989). These early investigations primarily provided estimates of crustal thickness and regional velocity structure of the Orogen. The crust below the Dunnage and Gander Zones was found to be 45 km in

thickness. In contrast the crust of the Avalon Zone and Grenville crust (Humber Zone and westward) were found to be thinner having crustal thicknesses of 35 km and 30-40 km respectively. These investigations indicated that crustal velocities of the Orogen are typical of normal continental crust with velocities ranging from 6.1 to 6.3 km/s with the exception of a basal high velocity layer (7.3 km/s) coincident with a zone of increased crustal thickness below the Dunnage and Gander Zones. High velocities were also observed within the upper crust of the Dunnage Zone at depths less than 10 km. This upper crustal high velocity zone was attributed to vestiges of oceanic crust observed at the surface, implying a shallow root for the oceanic remnants of the Dunnage Zone.

Potential field investigations of the Orogen have been reviewed by Miller (1990). Examination of Bouguer anomalies of the Island of Newfoundland indicates the edge of the Palaeozoic continental margin (Humber Zone) is marked by a major eastward increase in Bouguer anomalies (Fig. 2.6). This transition from negative to positive anomalies can be traced throughout most of the Canadian Appalachians and the 400 km offset observed in this trend between Newfoundland and Quebec has been interpreted by Thomas (1977) to represent an offset in the rifted western margin of Iapetus. Whether this regional variation in Bouguer gravity anomalies is related to changes in crustal thickness and/or composition of the lower crust has yet to be demonstrated. Wiseman and Miller (1994) suggest that gravity anomalies observed in southwestern Newfoundland can be explained by upper crustal structures.

In central Newfoundland the Dunnage Zone is characterized by positive anomalies (Fig.

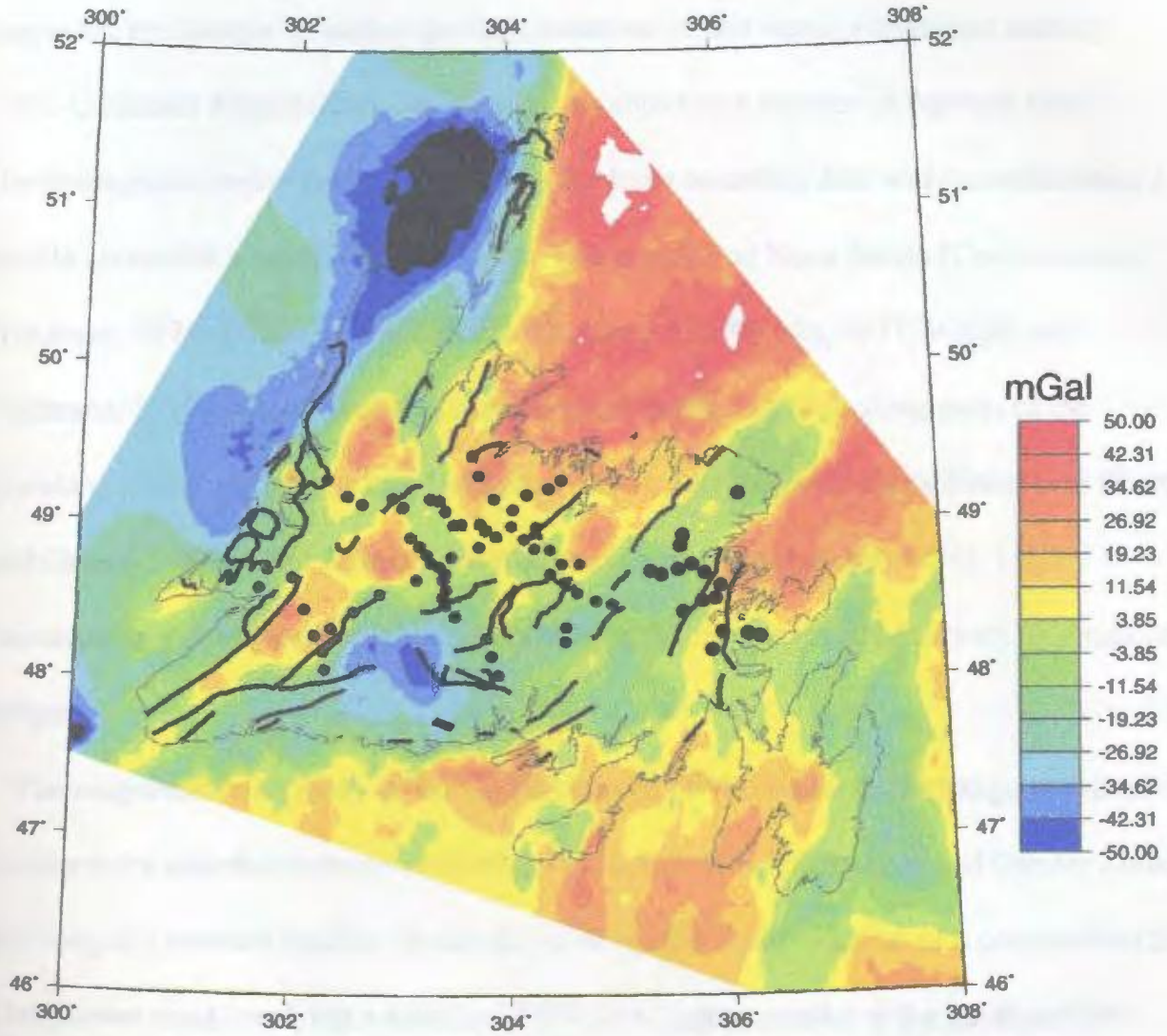

Figure 2.6 Bouguer anomaly map of Newfoundland and surrounding waters. The location of Lithoprobe East magnetotelluric soundings are indicated by black dots.

2.6). Gravity models proposed for the Dunnage Zone suggest that the dense oceanic rocks observed at the surface are responsible for the observed positive anomalies, implying that the Dunnage Zone is allochthonous over crust of continental origin (Karlstrom, 1983).

To the east, the Gander Zone is marked by negative Bouguer anomalies (Fig. 2.6). The offset observed in these Bouguer anomalies in central Newfoundland, suggests that the

structure of the Orogen changes significantly along strike. This change in structure is supported by changes in surface geology observed in this region (discussed earlier).

The Canadian Appalachians have been the subject of a number of regional scale electromagnetic investigations. Geomagnetic depth sounding data was recorded along a profile across the orogen in Quebec, New Brunswick and Nova Soctia (Cochrane and Hyndman, 1974) and in Newfoundland (Cochrane and Wright, 1977; Wright and Cochrane, 1980). Magnetotelluric measurements were recorded along parts of the mainland profile (Cochrane and Hyndman, 1974), and profiles in New Brunswick (Kurtz and Garland, 1976), and Prince Edward Island (Jones and Garland, 1986). These investigations delineated a number of important features of the conductivity structure of the orogen.

The magnetotelluric study of Kurtz and Garland (1976) indicated a change in crustal conductivity structure occurs within the central mobile belt (Dunnage and Gander Zone) of the orogen. Grenville crust to the northeast of this boundary consists of a conductive (200 Ω·m) lower crust overlying a resistive (5000 Ω·m) upper mantle: to the southeast the situation is reversed with a resistive (1000 Ω·m) crust overlying a conductive (100 Ω·m) upper mantle. Geomagnetic depth sounding in Newfoundland indicated the presence of a conductive lower crust and/or mantle associated with the Gander Zone (Wright and Cochrane, 1980). The structural position of these lower crustal/ upper mantle transitions within the orogen suggests that they may mark the closure of the Iapetus ocean (Kurtz and Garland, 1976; Wright and Cochrane, 1980). The conductivity anomalies observed in

Canada may be extensions or equivalents of the low resistivity layer observed in the lower crust and upper mantle of the Caledonian orogeny of Scotland (Jones and Hutton, 1977, 1979a, 1979b; Hutton and Jones, 1980; Sule and Hutton, 1986) and Ireland (Whelan et al., 1990). The conductive zone in Scotland is interpreted as being related to ancient subduction associated with the closure of Iapetus.

Seismic reflection investigations carried out as part of the Lithoprobe East transect in the waters north and south of the island of Newfoundland have provided constraints on the deep structure of the Appalachian orogen. Results from these marine reflection profiles (Fig. 2.3) have divided the lower crust of the orogen into three "lower crustal blocks" (LCBs) characterized by diagnostic reflection signatures.

The first seismic reflection results were provided by marine reflection profiles collected north of Newfoundland (Fig. 2.7) (Lines 84-1 and 84-2 in Fig. 2-8). Interpretation of these data (Keen et al., 1986) indicated that the Baie Verte and GRUB line, marking the western and eastern boundaries of the Dunnage Zone, do not extend into the deep crust and are therefore only upper crustal boundaries. The lower crust beneath the Humber and western Dunnage Zones displays a reflective character distinct from that below the eastern Dunnage and Gander Zones. The lower crust beneath the Humber Zone has been termed the Grenville LCB and is interpreted as representing the North American craton (Laurentia). The lower crust to the east, below the Gander Zone, has been termed the Central LCB and represents crust of the eastern margin of Iapetus (Gondwanda). The

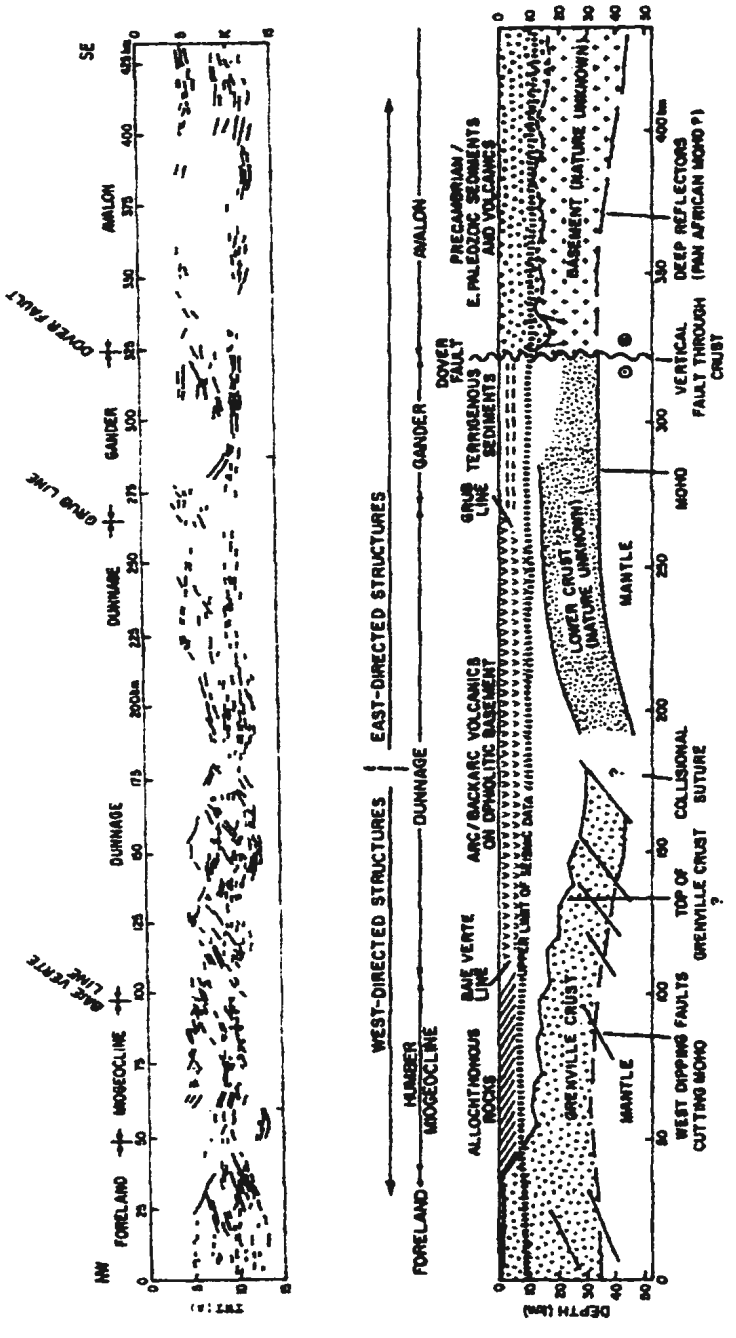

Figure 2.7 Interpretation of Lithoprobe marine seismic reflection profiles 84-1 and 84-2 (Kean et al., 1986). The location of these profiles is shown in figure 2.8A.

reflective character at the boundary between the Grenville and Central LCBs indicates that

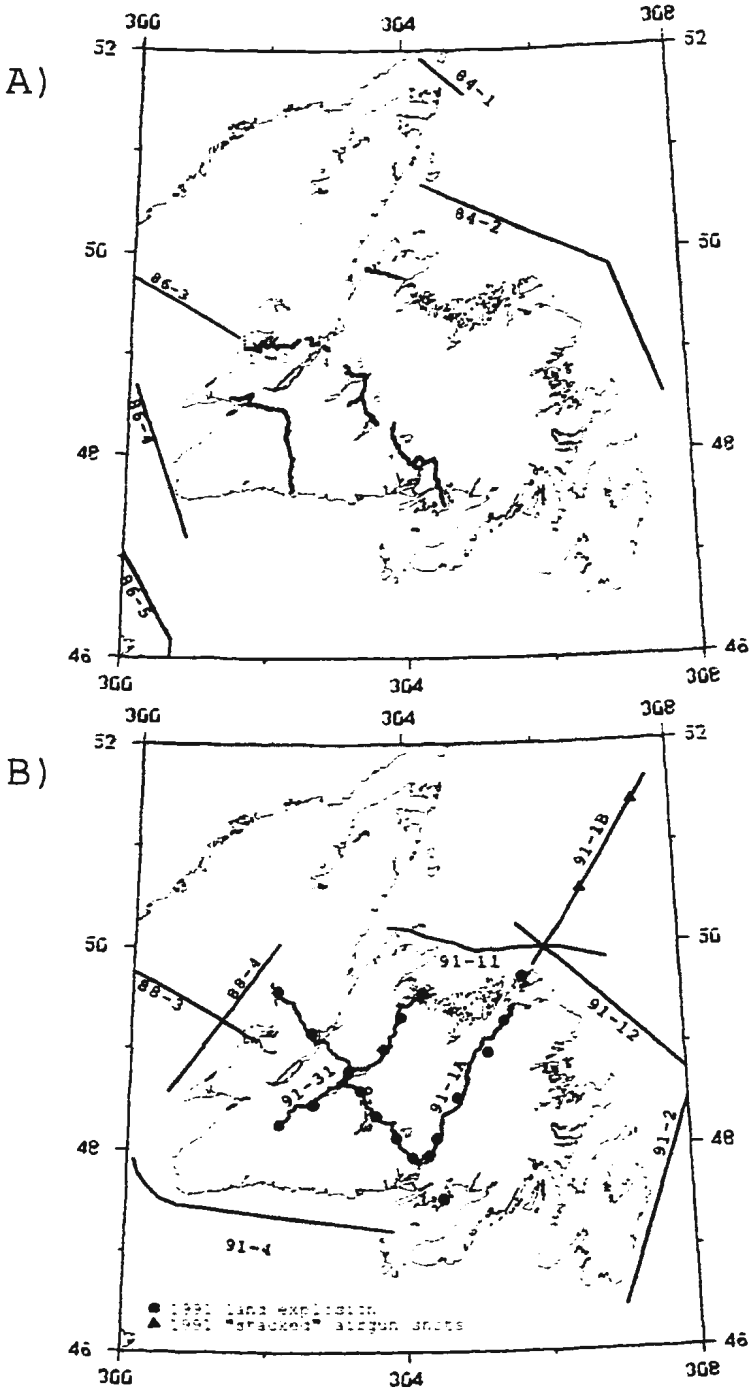

Figure 2.8 Location map showing the position of Lithoprobe seismic investigations, seismic reflection experiments are shown in A, seismic refraction in B.

they have a collisional relationship below the Dunnage Zone, which is allochthonous above

the two LCBs. This collisional zone is marked by northwest dipping shear zones, related to the closure of the Iapetus ocean (Hall et al., 1990). This collisional zone represents the Iapetus suture.

The deep seismic structure of the Avalon Zone appears to be unrelated to Appalachian tectonics and is distinct from that of the of the Central LCB. The Dover fault marks the boundary between the Central and Avalon LCBs as well as the surface boundary between the Gander and Avalon Zones. This boundary is also marked by an offset in the reflection Moho.

The results of marine reflection profiles collected in 1986 in the Gulf of St. Lawrence and south of Newfoundland (Marillier et al., 1989) (Lines 86-3, 86-4 and 86-5 in Fig. 2.8) support the conclusions of the earlier marine reflection profiles and distinguishes the three LCBs south of Newfoundland (Fig. 2.3). Taken together, the marine profiles map the three-dimensional geometry of the orogen. The relationships between the three LCBs south of Newfoundland are similar to those north of the island, implying that similar tectonics along the strike of the orogen. Hovever, the boundary between the Central and Avalon LCBs is not marked by an offset in the Moho south of Newfoundland.

The marine profiles were successful in mapping the lower crustal reflective character of the Orogen, although few reflectors could be correlated with tectonic boundaries observed at the surface. This lack of surface correlation is in part due to water-bottom multiples which mask upper crustal reflectors in the marine data. Vibroseis seismic reflection data were collected along three transects across the island of Newfoundland in 1989 (Hall et al.,

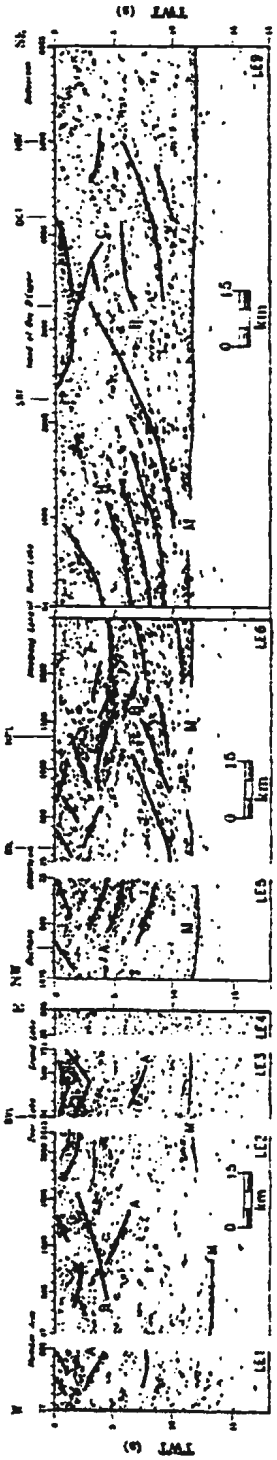

Figure 2.9 Lithoprobe on land seismic reflection profiles 1, 2, 3, 4, 5, 6 and 9 (Quinlan et el., 1992). The location of these profiles is shown in figure 2.8A.

1990; Quinlan et al., 1991; Quinlan et al., 1992) (Fig. 2.8). These data were intended to improve surface correlations with the deep seismic structure of the orogen and test the conclusions drawn from the offshore data.

The onshore seismic reflection data record many of the reflector patterns observed in the marine data. Although not all of the reflectors observed can be traced to the surface, some of the reflectors can be correlated with dated surface faults, allowing for the determination of age relationships between the observed reflectors (Quinlan et al., 1992).

Three reflector packages are recognized in the onshore data (A, B and C reflectors Fig. 2.9). Southeast dipping reflectors (A reflectors) are common at the northwest ends of the three transects (Fig. 2.8). These reflectors are related to northwest vergent thrusts associated with the Taconian to Acadian deformation of the western margin of Iapetus (Quinlan et al., 1992). The southeast dipping reflectors are truncated by northwest dipping reflectors (B reflectors) below the Dunnage Zone. Surface correlations and reflector relationships imply that these reflectors are related to the Middle-Ordovician to Middle-Silurian development of the Orogen and closure the Iapetus ocean. The northwest dipping reflectors define a collisional zone between Laurentia (Grenville LCB) and Gondwana (Central LCB), and are observed on all of the offshore and onshore profiles across the orogen (Hall et al., 1990). The northwest dipping reflectors may be truncated by younger southeast dipping reflectors (C reflector) in southeastern Newfoundland.

The onshore data's greater upper crustal resolution, enables an alternative interpretation of the lower crustal reflectivity of the Orogen. The temporal relationships and spatial extent

of the reflectors observed in the onshore seismic reflection data suggests that these reflection patterns are produced or reactivated by Appalachian tectonics data (Quinlan et al., 1992), rather than being inherent to pre-existing crustal blocks as suggested by the marine reflection data. In addition, the lower crustal reflective character of the Avalon Zone is not distinguishable from that of central Newfoundland as indicated on the marine profiles, suggesting that the division of the lower crust at the Gander-Avalon zone boundary may be unnecessary at least in Southern Newfoundland. Additional constraints on the composition of the lower crust are required to resolve the origin of the observed lower crustal reflectivity.

In 1991 offshore-onshore seismic refraction/wide-angle reflection data was collected by Lithoprobe along profiles both across and along strike of the Orogen (Fig. 2.8). The intent of this experiment was to determine the velocity structure of the crust and in particular velocities of the lower crust. Results of this experiment indicate that the crust of the orogen thins from 44 km west of Newfoundland and 40 km east of Newfoundland to 35 km under the central part of the Orogen (Dunnage Zone) (Marillier et al., 1994). These crustal thicknesses conflict with earlier refraction results which indicated a thick crust below the central part of the Appalachian Orogen, thinning to the east and west (See above).

Velocity models of the Lithoprobe refraction data indicate that lower crustal velocities of the Orogen are typical of continental crust (6.7-6.8 km/s) (Fig. 2.10), in agreement with the earlier results (Marillier et al., 1994; Hughes et al., 1994). The observed lower crustal velocities, bulk crustal Poison's ratio of 0.23 to 0.24 along with the extraction of large

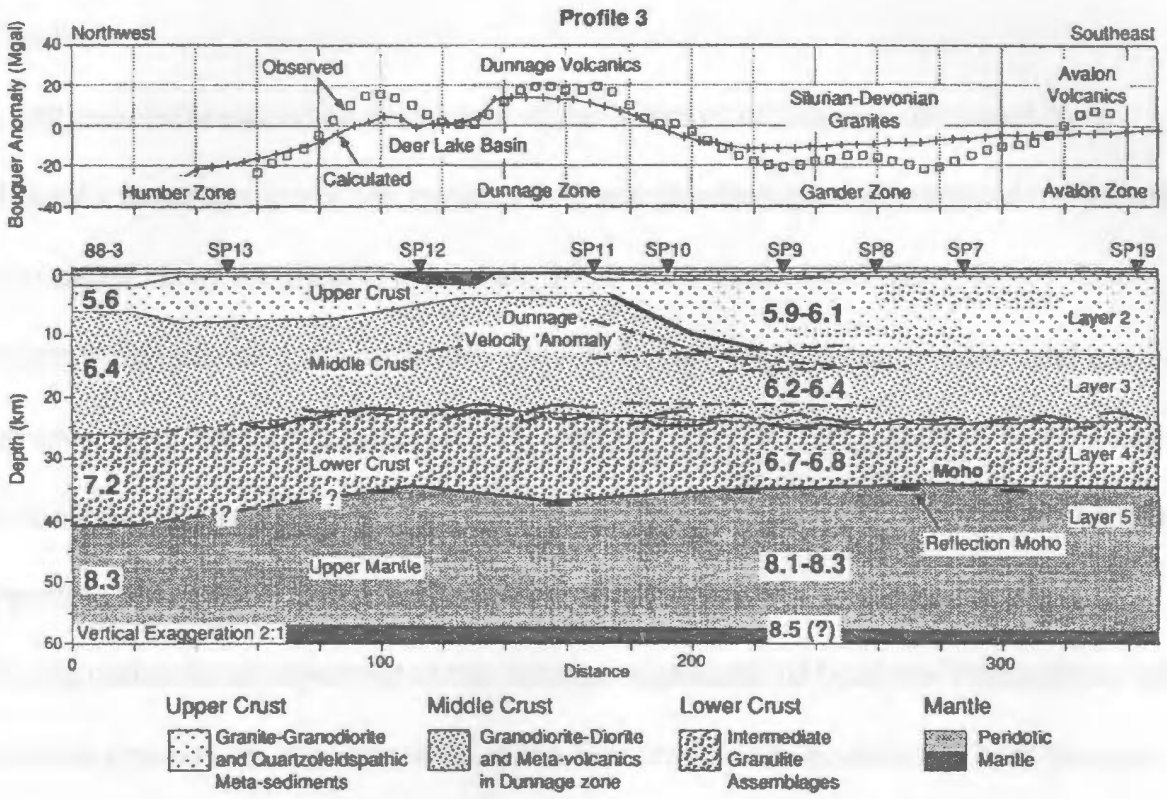

Figure 2.10 Interpretation of seismic refraction Profile 91-3(Hughes et al, 1994). The location of this profile is shown in figure 2.8B.

volumes of granitic melt required to produce the granites observed at surface suggest an intermediate granulite assemblage for the composition of the lower crust (Hughes et al., 1994).

The lower crustal blocks defined on the basis of vertical incidence reflection character do not show significant variations in velocity (Marillier et al., 1994). West of Newfoundland a high velocity (approximately 7.2 km/s) lower crustal layer was observed on refraction line 88-4 (Fig. 2.8) (Marillier et al., 1994). The on land refraction data, however suggests that this high velocity layer does not extend east of the Baie Verte Line (Hughes et al., 1994),

although, the exact position and nature of the high velocity layer's southeastern limit is unresolved.

Additional information on the nature of the lower crust has been provided by a Lithoprobe investigation of the regional isotopic geochemistry of granitoid intrusions across the island of Newfoundland (Fryer et al., 1992; Kerr et al., 1995; Kerr, 1996). The isotopic signatures of these intrusions provide insight into the composition and age of the deep crust from which the intrusions are partially derived. The results of these studies provide a number of constraints on the deep crustal structure of the orogen and are largely supportive of the three LCB division of the lower crust.

Strong contrasts are observed in the isotopic signatures of both late Precambrian and Devonian granites on opposite sides of the Gander-Avalon boundary. These isotopic contrasts indicate that the Dover-Hermitage Bay fault is a major isotopic break in Newfoundland, supporting the lower crustal division proposed on the basis of marine seismic reflection data (Fryer et al., 1992; Kerr et al., 1995). The lower crust of the Avalon zone is interpreted as late Precambrian in age with "Juvenile" affinities. To the northwest of the Dover-Hermitage Bay fault, the lower crust of the Exploits subzone and Gander zone appears to be late Precambrian in age including older components. Contrasts in the Precambrian basements of the Gander and Avalon zones suggests that the Dover-Hermitage Bay fault may be approximately coincident with an older (Precambrian) structure or that the two zones were spatially separated during their development.

Another isotopic break is observed at the approximate position of the of the Red Indian

line (central Dunnage zone) (Fig. 2.4). Intrusions to the northwest of the Red Indian line have relatively juvenile isotopic signatures in comparison to those to the southeast. This boundary is supportive of the lower crustal collisional zone observed on all of the reflection profiles, although the juvenile signatures west of this boundary do not support the presence of Grenvillian (Laurentian) basement rocks beneath the northwest Dunnage zone. The juvenile signatures are perhaps signatures of an arc-system accreted to North America (Laurentia) prior to collision with Gondwana (Fryer et al., 1992).

Taken together, investigations of the deep crust to date indicate at least two important changes in crustal structure occur across the strike of the orogen. The most important of these crustal structure changes occurs in the vicinity of the Red Indian line. The second crustal boundary occurs at the Gander-Avalon boundary (Dover-Hermitage Bay fault).

Below the Dunnage Zone, in the vicinity of the Red Indian line, a major transition in the lower crust is marked by:

- A change in reflective character and northwest dipping shear zones, which can be traced along the strike of the orogen. These shear zones are dated as Mid-Ordovician to Mid-Silurian in age (Quinlan et al., 1992).
- Early electromagnetic investigations indicate that a change in lower crustal and upper mantle conductivity is roughly coincident with this boundary (Kurtz and Garland, 1976; Wright and Cochrane, 1980).
- The results of seismic refraction investigations of the orogen, indicate that the crust in the vicinity of this boundary is thinner than the crust of bordering regions.

Additionally, this boundary marks a significant change in upper-middle crustal velocity structure (Marillier et al., 1994; Hughes et al., 1994).

- Isotopic investigations suggest this boundary marks a break in isotopic signatures (Fryer et al., 1992).

In addition to being a major lower crustal transition this boundary is recognized at the surface as a boundary between contrasting structures, stratigraphy and fauna (discussed above). The boundary probably marks the Iapetus suture, the site of continent-continent or arc-continent collision.

The second lower crustal boundary occurs at the Dover-Hermitage Bay fault (Gander-Avalon boundary). This boundary is indicated by a change in reflective character observed on the marine reflection profiles across the Orogen. This fault offsets the reflection Moho north of Newfoundland and is recognized as an isotopic break along its length in Newfoundland. Surface relationships and the lack of correlatable features across the fault indicate that the boundary is a crustal scale strike-slip fault.

2.4 Summary

Four tectono-stratigraphic zones are recognized in the Newfoundland Appalachians. These are from west to east the Humber zone, interpreted as the ancient margin of Laurentia, the Dunnage zone, consisting of vestiges of the Iapetus ocean (island arc and back arc basin rocks), the Gander zone possibly representing the opposing margin of Iapetus, and the Avalon zone, a late Proterozoic province of Gondwana. The Dunnage zone is divided into the Notre Dame and Exploits subzones, based on stratigraphic, faunal

and structural differences. Destructive processes operating in Iapetus resulted in the destruction of both continental margins prior to late Ordovician - Silurian continent-continent collision. The Notre Dame subzone, an arc terrain, was accreted to Laurentia during the Taconian orogeny (arc - continent collision) and the Exploits subzone was thrust over the Gander zone during the Penobscot Orogeny. Closure of Iapetus was marked by the linkage of the Notre Dame and Exploits subzones in the late Ordovician - early Silurian. Subsequent continent-continent collision resulted in Silurian volcanism, plutonism and orogen parallel movements. In the late Silurian - early Devonian the Avalon zone was accreted possibly as a result of orogen parallel motions.

Reflection seismic and isotopic investigations suggest that two boundaries observed at the surface appear to have expressions in the lower crust, the Notre Dame - Exploits subzone boundary (Red Indian Line) and the Dover-Hermitage Bay fault. Isotopic evidence suggests that the lower crust of the Exploits and Gander zone which lies between these boundaries is distinct from that of the Avalon and possibly the Notre Dame subzone. The Red Indian line may roughly mark the boundary between lower crust of Gondwana and Laurentian affinities and the Dover-Hermitage Bay fault may mark a boundary between two Gondwandan terrains.

CHAPTER 3

The Magnetotelluric Tensor: Distortion and Interpretation

3.1 Introduction

In the magnetotelluric (MT) method time-varying electric and magnetic fields observed at the surface of the Earth are measured in order to determine information on the conductivity structure of the Earth. The fields measured are the sum of the naturally occurring magnetic field external to the Earth (source) and electric and secondary magnetic field induced by the interaction of the external magnetic field with the conductivity structure of the Earth. The naturally occurring magnetic field, the source in the MT method, results primarily as a result of interactions of ejected solar plasma with the Earth's magnetosphere for periods greater than 1 s and as the result of lightning storms for shorter periods. Implicit to the MT method is the assumption that the measured electric and magnetic fields have the same linear dependence on the external magnetic field (source) and therefore the relationship between the measured electric and magnetic fields is independent of the source. Although, there is no complete proof that this assumption holds for all conductivity structures the assumption is a reasonable approximation in most instances (Madden and Nelson, 1964). Under the above assumption the linear transfer function relating the observed fields, the impedance tensor, is a function solely of the Earth's conductivity structure, the period of observation and the observer's position with respect to the conductivity structure.

The impedance tensor and magnetic transfer functions calculated from relationships

between the electric and magnetic fields measured in the magnetotelluric method can be regarded as the input response function of the conductivity structure of the Earth. By studying the input response function's dependence on period and position one can determine the Earth's conductivity structure. Unfortunately, for arbitrary Earth structures there is no obvious means of deriving a set of parameters describing the conductivity structure of the Earth.

Traditionally, interpretation of the impedance tensor has been approached by assuming that the conductivity of the Earth is a function of one or two dimensions. Under either of these assumptions the impedance tensor assumes a simplified form which is readily interpreted with the use of one or two dimensional forward and inverse algorithms.

The plane wave source field and potential depth of investigation of the MT method makes the technique most useful in the study of large scale features of the conductivity structure of the Earth. As surveys are often designed with this goal in mind, the recognition of regionally significant information becomes an integral part of interpretation. Regional scale sampling of the conductivity structure often results in a situation where smaller scale local structure effectively becomes noise, distorting the response of the larger scale regional structure. This distortion of the regional response is particularly important in crystalline regions with complex surface geology.

Over the past twenty years a number of parameterizations of the impedance tensor have been proposed to attempt to separate regional and local information. These parameterizations can be divided into two groups, mathematical and physical

decompositions of the impedance tensor. The mathematical decompositions are based solely on mathematical properties of the impedance tensor, while the physical decompositions attempt to fit the impedance tensor to a physical model of the conductivity structure. To date the physical decompositions have been the most successful as the parameters derived are readily interpretable.

3.2 Impedance Tensor

All electromagnetic phenomena are governed by Maxwell's equations, the fundamental equations of electromagnetism. These equations describe the propagation and attenuation of electromagnetic waves which occur in the Earth as the result of naturally occurring time-varying electromagnetic fields external to the Earth. By making several assumptions about the properties of the Earth and the electromagnetic source field Maxwell's equations can be used to derive a linear transfer function relating the horizontal electric and magnetic fields measured in the magnetotelluric method to the conductivity structure of the Earth (Madden and Nelson, 1964). This linear transfer function is termed the "impedance tensor" and under the assumptions implicit to the MT method is independent of the source field and dependent solely on the conductivity structure of the Earth as a function of position and period of observation.

In a source free medium, such as the Earth, Maxwell's equations are:

$$\nabla \times \vec{H} = \frac{\partial \vec{D}}{\partial t} + \vec{J}, \qquad (3.1)$$

$$\nabla \times \vec{E} = -\frac{\partial \vec{B}}{\partial t}, \tag{3.2}$$

$$\nabla \cdot \vec{D} = \rho_f, \tag{3.3}$$

$$\nabla \cdot \vec{B} = 0. \tag{3.4}$$

H is the magnetic field, B is the magnetic induction field, E is the electric field, D is the electric displacement, J is the current density and ρ_f is the free charge density. Maxwell's equations are not all independent of one another. Using the vector identity $\nabla \cdot \nabla \times = 0$ equation 3.1 becomes

$$\nabla \cdot \nabla \times \vec{H} = \nabla \cdot \vec{J} + \nabla \cdot \frac{\partial \vec{D}}{\partial t} = 0, \tag{3.5}$$

or, inverting the order of operations,

$$-\frac{\partial}{\partial t}(\nabla \cdot \vec{D}) = \nabla \cdot \vec{J}. \tag{3.6}$$

Since charge is conserved

$$\nabla \cdot \vec{J} = -\frac{\partial \rho_f}{\partial t}. \tag{3.7}$$

Using the law of conservation of free charge equation (3.7) we can rewrite equation (3.6)

as

$$\nabla \cdot \vec{D} = \rho_f + C \,, \tag{3.8}$$

where C is some quantity independent of time. If we assume that at sometime either in the past or future both $\nabla \cdot D$ and ρ_f are simultaneously equal to zero, then the constant of integration must equal zero and equation (3.8) equals equation (3.3). Equation (3.1) is not independent of equation (3.3). Similarly, taking the divergence of equation (3.2),

$$\nabla \cdot \nabla \times \vec{E} = -\nabla \cdot \frac{\partial \vec{B}}{\partial t} = 0 \,, \tag{3.9}$$

inverting the order of operation,

$$-\frac{\partial}{\partial t}(\nabla \cdot \vec{B}) = 0 \,. \tag{3.10}$$

Assuming that the divergence of B is equal to 0 at some time in the past or future, then the divergence of B is equal to zero as given by equation (3.4). Under this assumption equations (3.2) and (3.4) are not independent. The propagation of the magnetotelluric waves in a source free medium can therefore be fully described by equations (3.1) and (3.2).

Equation (3.1) is a form of Ampere's law, which states that a magnetic field is generated in space by current flow and that the field is proportional to the total current (conduction

plus displacement) and displacement. Equation (3.2) is a form of Faraday's law which states that an electric field exists in the a region of a time varying magnetic field and that the electromotive force (emf) induced is proportional to the negative rate of change of the magnetic flux.

In addition to Maxwell's equations there are three relationships which describe characteristics of the medium (Earth materials). If we assume that earth materials are linear and isotropic,

$$\vec{B} = \mu\vec{H}, \tag{3.11}$$

$$\vec{D} = \epsilon\vec{E}, \tag{3.12}$$

$$\vec{J} = \sigma\vec{E}, \tag{3.13}$$

where μ, ϵ, and σ are respectively the permeability, permittivity, and conductivity of the medium. Earth materials are also assumed to be homogeneous. Under these assumptions permittivity, permeability and conductivity are constants independent of E and B, and independent of direction and position.

The magnetotelluric source has a statistical nature and is contaminated by noise. It is therefore desirable to utilize the frequency domain so that parameters derived can be stacked to reduce the signal to noise ratio. Decomposing the fields into their frequency domain components also allows us to take advantage of the frequency dependence of

attenuation (see below). Assuming all fields have a $e^{i\omega t}$ time dependence, Maxwell's equations (3.1) and (3.2) can be rewritten as (using equations (3.11), (3.12) and (3.13)) as:

$$\nabla\times\vec{H} = \sigma\vec{E} - i\omega\epsilon\vec{E}\,, \tag{3.14}$$

and

$$\nabla\times\vec{E} = i\omega\mu\vec{H}\,. \tag{3.15}$$

Using the law of conservation of free charge (equation 3.7) and Ohm's law (equation 3.13) we can show that charge density ρ_f given by equation (3.3) is zero for earth materials,

$$\nabla\cdot\vec{J} = -\frac{\partial\rho_f}{\partial t} = \sigma\nabla\cdot\vec{E} = \sigma\frac{\rho_f}{\epsilon}\,, \tag{3.16}$$

and

$$\rho_f = \rho_{f_0} e^{-(\sigma/\epsilon)t}\,. \tag{3.17}$$

The free charge given by equation (3.17) can only decrease with time, reaching an equilibrium value in a very short time ($t = \epsilon/\sigma$). Thus,

$$\nabla\cdot\vec{J} = 0\,, \tag{3.18}$$

and using equations (3.12) and (3.13),

$$\nabla\cdot\vec{D} = \nabla\cdot\vec{E} = 0\ . \qquad (3.19)$$

Taking the curl of equation (3.14) and (3.15) and using the vector identity $\nabla\times(\nabla\times A) = \nabla(\nabla\cdot A) - \nabla^2 A$ we get finally (noting that $\nabla\cdot H = \nabla\cdot E = 0$ from equations (3.4) and (3.19)) that,

$$\nabla^2\vec{E} = i\omega\mu\sigma\vec{E} + \omega^2\mu\epsilon\vec{E} \qquad (3.20)$$

$$\nabla^2\vec{H} = i\omega\mu\sigma\vec{H} - \omega^2\mu\epsilon\vec{H}\ . \qquad (3.21)$$

These are the electromagnetic wave equations for the propagation of electric and magnetic field vectors in the Earth. The first term on the right hand side of equations (3.20) and (3.21) is related to conduction currents and the second-term to displacement currents. For the frequencies recorded in the MT method and typical Earth characteristics the fields propagating in the Earth decay to negligible amplitudes within a fraction of a wavelength. Mathematically this can be stated as

$$|\mu\omega^2\epsilon| \ll |i\sigma\mu\omega|\ . \qquad (3.22)$$

Equations (3.20) and (3.21) therefore reduce to diffusion equations in the MT method,

$$\nabla^2\vec{E} = i\omega\mu\sigma\vec{E}\ , \qquad (3.23)$$

and

$$\nabla^2 \vec{H} = i\omega\mu\sigma\vec{H} . \qquad (3.24)$$

In general the diffusion equations (3.23) and (3.24) are difficult to solve, with solutions being dependent on the properties of the medium and electromagnetic source exciting the medium. The solution's spatial dependence on the source is removed by assuming that the MT source field is a plane wave normally incident on a flat Earth. The source field under these assumptions is uniform over any plane parallel to the Earth's surface, removing the diffusion spatial equation's dependence on the source, and making use of the MT method feasible. Wait (1962) has shown that the flat Earth assumption has negligible effects as long as the depth being probed is a small fraction of the radius of the Earth. The plane wave assumption can not be rigorously proven, although Madden and Nelson (1964) have shown that it is a reasonable assumption for typical Earth conductivity structures.

For the simplest case, when the Earth is considered to be a halfspace of constant conductivity σ_0. The diffusion equation equations have solutions of the form

$$A(\omega)e^{-\gamma z + i\omega t} + B(\omega)e^{\gamma z + i\omega t}, \qquad (3.25)$$

where

$$\gamma = \sqrt{i\mu\omega\sigma_0} = (1+i)\sqrt{\frac{\mu\omega\sigma_0}{2}} = (1+i)k ,$$

and

$$k = \sqrt{\frac{\mu\omega\sigma_0}{2}}.$$

The solution is a linear combination of two decaying waves, one travelling down and the other travelling up. In a halfspace there are no sources or boundaries to reflect the down going wave and as a result $B(\omega) = 0$. The solution in a halfspace therefore has a form

$$A(\omega)e^{-\gamma z + i\omega t} = A(\omega)e^{-kz}e^{-ikz}e^{i\omega t}. \qquad (3.26)$$

Examination of equation (3.26) indicates that the electromagnetic wave varies sinusoidally with t and z, and attenuates as z increases. The electromagnetic wave reduces in amplitude by a factor $1/e$ in a distance δ (skin depth), given by

$$\delta = \sqrt{\frac{2}{\omega\mu\sigma_0}}. \qquad (3.27)$$

The solution (3.26) to the diffusion equations has an amplitude $A(\omega)$ which has a dependency on the amplitude of the source. We are therefore unable to derive any information about the conductivity (σ) of the medium from a single field measurement, without knowing the source amplitude. This dependence on source amplitude can be removed by taking the ratio of perpendicular components of the electric and magnetic field, which are linearly related through Maxwell's equations (3.14) and (3.15). For example, we have from equation (3.14) (neglecting displacement currents) that

$$\nabla \times \vec{E} = -i\mu\omega\vec{H}, \tag{3.28}$$

which reduces to

$$H_y = -\frac{1}{i\mu\omega}\frac{\partial E_x}{\partial z}, \tag{3.29}$$

for the perpendicular components E_x and H_y in a halfspace.

Taking

$$E_x(z,\omega) = A(\omega)e^{-\gamma z + i\omega t}, \tag{3.30}$$

equation (3.29) gives

$$H_y = \frac{\gamma}{i\mu\omega}A(\omega)e^{-\gamma z + i\omega t}. \tag{3.31}$$

The ratio of the two fields, is given by

$$Z(\omega) = \frac{E_x}{H_y} = \sqrt{\frac{\mu\omega}{2\sigma_0}} + i\sqrt{\frac{\mu\omega}{2\sigma_0}} = -\frac{E_y}{H_x}, \tag{3.32}$$

a complex scalar depending solely on the conductivity of the medium and the period of the electromagnetic wave. This ratio is termed the electromagnetic impedance.

The scalar impedance relation derived for the halfspace is valid for a 1-D earth, where conductivity is a function of depth only. For more complex 2-D and 3-D conductivity

structures this simple scalar relationship breaks down. The impedance, defined by the ratio of perpendicular components, becomes dependent on the coordinate orientation. In addition, the electric field measured in an arbitrary direction may depend on magnetic variations both perpendicular and parallel to its direction and the vertical magnetic field is non-zero. The relationship between the field components is given by a set of linear equations:

$$E_x = Z_{xx}H_x + Z_{xy}H_y, \tag{3.33}$$

$$E_y = Z_{yx}H_x + Z_{yy}H_y, \tag{3.34}$$

and

$$H_z = T_{zx}H_x + T_{zy}H_y. \tag{3.35}$$

In matrix notation the horizontal fields are described by

$$\vec{E} = Z\vec{H}, \tag{3.36}$$

where

$$Z = \begin{bmatrix} Z_{xx} & Z_{xy} \\ Z_{yx} & Z_{yy} \end{bmatrix}. \tag{3.37}$$

Z is termed the impedance tensor and relates the horizontal electric and magnetic fields as a

function of the conductivity structure, coordinate orientation and period of the electromagnetic wave. The impedance tensor is independent of the source amplitude and polarization.

The complex vector $T = (T_{zx}, T_{zy})$ relates the horizontal and vertical magnetic fields. T is called the tipper as it "tips" the horizontal magnetic field into the vertical magnetic field (also known as transfer functions).

3.3 Conventional Interpretation of the Impedance Tensor

The MT impedance tensor maps the subsurface conductivity structure of the Earth as a function of period and measurement position. In interpreting MT impedance data, one attempts to derive parameters from the impedance tensor's dependence on position and period which are interpretable in terms of the conductivity structure of the Earth. In practice this is a difficult task, since for arbitrary Earth structures there is no obvious means of deriving the desired parameters.

Traditionally interpretation of the impedance tensor has been approached by assuming that the Earth's conductivity structure is either one (1-D) or two dimensional (2-D). Under either of these assumptions the impedance tensor assumes a simplified form, which is readily interpreted with available forward modelling and inversion codes.

The simplest model of the earth is a 1-D or layered model where the impedance tensor is given by the expression:

$$Z_{1D}(\omega) = \begin{bmatrix} 0 & Z(\omega) \\ -Z(\omega) & 0 \end{bmatrix}. \qquad (3.38)$$

The conductivity structure of the earth is described by two model parameter per frequency, the magnitude and complex phase of the scalar impedance Z_{1D} (Cagniard, 1953). If known precisely at all periods, $Z(\omega)$ completely determines the subsurface conductivity (Bailey, 1970).

As a next order of complexity, the conductivity structure can be assumed to be 2-D (uniform along one horizontal axis). In a 2-D earth there exists two special field polarizations for which Maxwell's equations (3.14) and (3.15) decouple. A primary field in either of these polarizations will induce a secondary field in that same polarization. One of these polarizations is termed the E-polarization or transverse electric (TE) mode, corresponding to an electromagnetic wave whose electric field is parallel to the strike axis of the structure. The other polarization is that of an electromagnetic wave whose magnetic field is parallel to strike, termed the H-polarization or transverse magnetic (TM) mode. When the measurement axis corresponds to principal axes (coordinate axes of the 2-D structure), the impedance tensor has the form

$$Z_{2D}(\omega) = \begin{bmatrix} 0 & Z_{TE}(\omega) \\ -Z_{TM}(\omega) & 0 \end{bmatrix}. \qquad (3.39)$$

where Z_{TE} is the impedance associated with the transverse electric mode and Z_{TM} is the

impedance of the transverse magnetic mode. When the measurement axis are not aligned with the principal axis of the structure, the measured impedance tensor Z_m is given by

$$Z_m = R(\theta) Z_{2D} R^t(\theta) , \qquad (3.40)$$

where R is a rotation operator,

$$R = \begin{pmatrix} \cos\theta & \sin\theta \\ -\sin\theta & \cos\theta \end{pmatrix} ,$$

and θ is the angle between the measurement frame and the principal frame. A 2-D conductivity structure is therefore described by five parameters per frequency, the two complex impedances Z_{TE} and Z_{TM} and the strike angle θ.

For a true 2-D conductivity structure θ is given by

$$\theta = \frac{1}{2}\tan^{-1}\left(\frac{Z_{yy}-Z_{xx}}{Z_{xy}-Z_{yx}} \right) \pm \frac{\pi}{2} \qquad (3.41)$$

where Z_{xx}, Z_{yy}, Z_{xy} and Z_{yx} are elements of the measured impedance tensor. In the presence of noise equation (3.40) is not a stable method of determining the 2-D strike angle. In practice the strike angle is determined by minimizing the functional

$$|Z_{xx}|^2 + |Z_{yy}|^2 \qquad (3.42)$$

as a function of rotation angle (Swift, 1967). This method provides a strike angle θ for

which the measured tensor is as close as possible to an ideal 2-D tensor, in a least squares sense. Swift (1967) defined a rotationally invariant measure of two-dimensionality (skew), which attempts to quantify the departure of the impedance tensor from an ideal 2-D form

$$skew = \frac{Z_{xx}+Z_{yy}}{Z_{xy}-Z_{yx}} . \qquad (3.43)$$

For a true 2-D conductivity structure the skew is 0, although in the presence of galvanic distortion the skew can be non-zero for 2-D conductivity structures (see below).

3.4 Impedance tensor Decomposition

In the interpretation of experimental data, it is often found that there is no coordinate axis system in which the diagonal elements of the impedance tensor disappear. In this situation 1-D and 2-D conductivity models are unable to explain the impedance tensor and a three-dimensional (3-D) conductivity distribution must be invoked. The "three-dimensionality" of the impedance tensor often becomes a significant problem in the interpretation MT data and the interpretive errors introduced by using 1-D and 2-D conductivity models are difficult to quantify. 3-D forward modelling programs are available, although they are slow and require considerable computer resources to handle complex conductivity structures.

The dimensionality of the conductivity structure of the Earth is often a function of scale. When examined at a small scale most Earth structures exhibit significant three-dimensionality, although when examined at increasingly larger scales the assumptions of

one or two dimensionality often become reasonable. The plane wave source field of the MT method makes the method most useful in the study of the large scale properties of the Earth. As a result, MT surveys are usually designed with the resolution of large scale features in mind. This further complicates the interpretation of the impedance tensor, since sampling of the earth conductivity structure is often insufficient to resolve complicated small scale 3-D conductivity structures. The goal in interpreting the MT impedance tensors is therefore usually to resolve the large scale features of the conductivity structure, treating the smaller scale 3-D features as geological noise. Of course in some situations the Earth will be three dimensional at all scales of investigation and therefore a method of determining dimensionality is essential in any interpretation scheme.

The "three-dimensionality" of the impedance tensor has led to the development of a number of paramaterization schemes which attempt to decompose the impedance tensor into a minimum number of parameters characteristic of the conductivity structure. These methods can be divided into two groups: mathematical treatments of the impedance tensor in which no assumptions are made about the physical model (Berdichevsky and Dmitriev, 1976; Eggers, 1982; Spitz, 1985; LaTorraca et al., 1986; Yee and Paulson, 1987); and methods which assume a 1-D or 2-D conductivity structure and extract parameters of the assumed model from the elements of the impedance tensor (Larsen, 1977; Zhang et al., 1987; Bahr, 1988; Groom and Bailey, 1989, 1991; Chakridi et al., 1992; Chave and Smith, 1994; Smith, 1995).

3.4.1 Mathematical Decompositions

The "effective impedances" proposed by Berdichevsky and Dmitriev (1976) are the simplest in the class of mathematical treatments of the impedance tensor. They are rotationally invariant averages of the impedance tensor, defined in terms of the elements of the impedance tensor by

$$Z_{ave} = \frac{1}{2}(Z_{xy} - Z_{yx}), \qquad Z_{det} = \sqrt{Z_{xx}Z_{yy} - Z_{xy}Z_{yx}}. \tag{3.44}$$

The effective impedances reduce the impedance tensor to two parameters per period and are thought to minimize multi-dimensional effects. The use of effective impedances for multi-dimensional structures has been studied by a number of authors (Ranganayaki, 1984; Ingham, 1988; Park and Livelybrooks, 1989; Agarwal et al., 1993). These authors have shown that the success of models derived from the inversion of the effective impedances is structure dependent. The models are unsuccessful at imaging structure beneath a finite conductor and deep structure in the vicinity of a finite resistor. As a result, the models derived from the interpretation of the effective impedances must always be verified with multi-dimensional programs.

A number of parameterizations have been proposed based on mathematical treatments of the impedance tensor as a complex rank 2 tensor (Eggers, 1982; Spitz, 1985; LaTorraca et al., 1986; Yee and Paulson, 1987). These methods represent the impedance tensor with eight parameters, retaining all the information contained in the tensor. Since no assumptions are made about the conductivity structure of the Earth in these

parameterizations, the physical significance of the extracted parameters is difficult to determine. Groom and Bailey (1991) reviewed these parameterizations and show that only Spitz's (1985) second parameterization and Yee and Paulson (1987) parameterization offer a significant improvement over Swift's (1967) conventional 2-D parameterization in recovering information about the regional conductivity structure. These methods however have not yet been developed to enable their utilization in normal processing circumstances.

3.4.2 Physical Decompositions

The second class of parameterization methods is based on the assumption that the impedance tensor is the result of the superposition of large scale (regional) and small scale (local inhomogeneity) conductivity anomalies. The regional conductivity structure is assumed to be one or two dimensional and distorted by local two or three dimensional conductivity anomalies.

If the local inhomogeneity is small compared to the skin depth and wavelength of the electromagnetic wave in the regional structure, a condition which is reasonable at long periods if there is sufficient scale difference between the local and regional anomalies, the spatial gradients of the regional field are small over the inhomogeneity. Under the above condition it can be assumed that the inhomogeneity is excited by a uniform electric field. The small size of the inhomogeneity allows us to assume in addition, that the inhomogeneity is inductively small and as such induced secondary electric fields can be neglected. Under these assumptions the local inhomogeneity results in an electrostatic

(Galvanic) distortion of the regional electric field and an anomalous magnetic field produced as a result of the anomalous electric field.

The validity of the galvanic distortion model can only be judged by the success or failure of the model to explain observed data, since the observer has no information about the scale of the local inhomogeneity and possibly little information about the regional geoelectrical structure. The validity of the model is both dependent on the period of observation and location, with the assumptions generally holding at long periods and in locations removed from sharp boundaries in the regional structure where the regional field gradients are small. Numerous authors have discussed the conditions of validity of galvanic distortion (Berdichevsky and Dmitriev, 1976; Larsen, 1977; Jones, 1983; Park, 1985; West and Edwards, 1985; Bahr, 1988; Groom and Bailey, 1991; Groom and Bahr, 1992; Chave and Smith, 1994), to which the reader is referred for further details.

The electric field measured in the presence of a distorter is related to the regional electrical field through a 3x3 electric distortion matrix C_3 (Chave and Smith, 1994). The elements of this distortion matrix will be real if the distorting inhomogeneity is inductively small. Under the assumptions usually made in the magnetotelluric method (observer at surface flat Earth), normal electric currents vanish at the surface of the Earth and the distortion matrix reduces to a 2x2 distortion tensor $\boldsymbol{C}$. The electric field measured at the surface of the Earth is therefore given by,

$$\vec{E}_{meas} = C\,\vec{E}_{regional}$$
$$= \begin{bmatrix} C_1 & C_2 \\ C_3 & C_4 \end{bmatrix} \vec{E}_{regional} . \qquad (3.45)$$

The anomalous magnetic field produced as a result of a galvanic distortion is related to the regional electric field through a 3x3 magnetic distortion matrix D_3 (Chave and Smith, 1994). At the surface of the Earth this distortion matrix reduces to a 2x2 tensor D which describes the distortion of the horizontal magnetic field and a 2-element row vector Q which describes distortion of the vertical magnetic field (Chave and Smith, 1994). The elements of D and Q will be real under the same conditions as the electric distortion tensor. The anomalous horizontal magnetic field produced by the distorter is given by

$$\vec{H}_{h\ anomalous} = D\,\vec{E}_{regional}$$
$$= \begin{bmatrix} -\gamma & \alpha \\ -\beta & \varepsilon \end{bmatrix} \vec{E}_{regional} , \qquad (3.46)$$

and the anomalous vertical magnetic field by

$$\vec{H}_{z\ anomalous} = Q\,\vec{E}_{regional}$$
$$= \left[Q_{zx}, Q_{zy}\right] \vec{E}_{regional} . \qquad (3.47)$$

The horizontal and vertical magnetic fields measured in the presence of a galvanic distortion therefore become the sum of the regional and anomalous magnetic fields,

$$\vec{H}_{h\,meas} = \vec{H}_{h\,regional} + D\vec{E}_{regional} \tag{3.48}$$

and

$$H_{z\,meas} = H_{z\,regional} + Q\vec{E}_{regional}\,. \tag{3.49}$$

The impedance tensor measured in the regional coordinate system is given by

$$\begin{aligned} Z_{meas} &= \frac{\vec{E}_{meas}}{\vec{H}_{h\,meas}} \\ &= \frac{C\,\vec{E}_{regional}}{\vec{H}_{h\,regional} + D\,\vec{E}_{regional}} \\ &= \frac{C\,Z_{regional}}{I + D\,Z_{regional}}\,, \end{aligned} \tag{3.50}$$

where $Z_{regional}$ is the response of the regional one or two dimensional conductivity structure. The magnetic transfer functions $T\,(T_{zx}, T_{zy})$ relating the observed vertical and horizontal magnetic fields are given by

$$\vec{T}_{meas} = \frac{H_{z\,meas}}{\vec{H}_{h\,meas}}$$

$$= \frac{H_{z\,regional} + Q\vec{E}_{regional}}{\vec{H}_{h\,regional} + D\vec{E}_{regional}} \qquad \textbf{(3.51)}$$

$$= \frac{\vec{T}_{regional}}{\left(I + DZ_{regional}\right)} + \frac{QZ_{regional}}{\left(I + DZ_{regional}\right)}.$$

Using equation 3.50 the measured transfer function can be expressed as

$$\vec{T}_{meas} = \frac{\vec{T}_{regional}}{(1 + DZ_{regional})} + \frac{QZ_{meas}}{C}. \qquad \textbf{(3.52)}$$

Examination of the equation for the distorted impedance tensor (3.50) indicates that although the distortion matrices C and D are both constants for any given distorter, only the electric field distortion matrix C will have a frequency independent effect on the measured impedances. The distortion of the electric field (C) results in measured impedances which are distortion dependent combinations of the regional impedances, while the magnetic distortion matrix D results in impedances which are frequency and distortion dependent mixtures of the regional impedances. The frequency dependence of magnetic distortion stems from the magnitude of the regional impedance tensor's ($|Z_{regional}|$) dependence on frequency. Figure 3.1 shows the effect of magnetic distortion (D of 0.08) on the magnitude of the scalar impedance calculated for a 5000 Ω·m halfspace. The

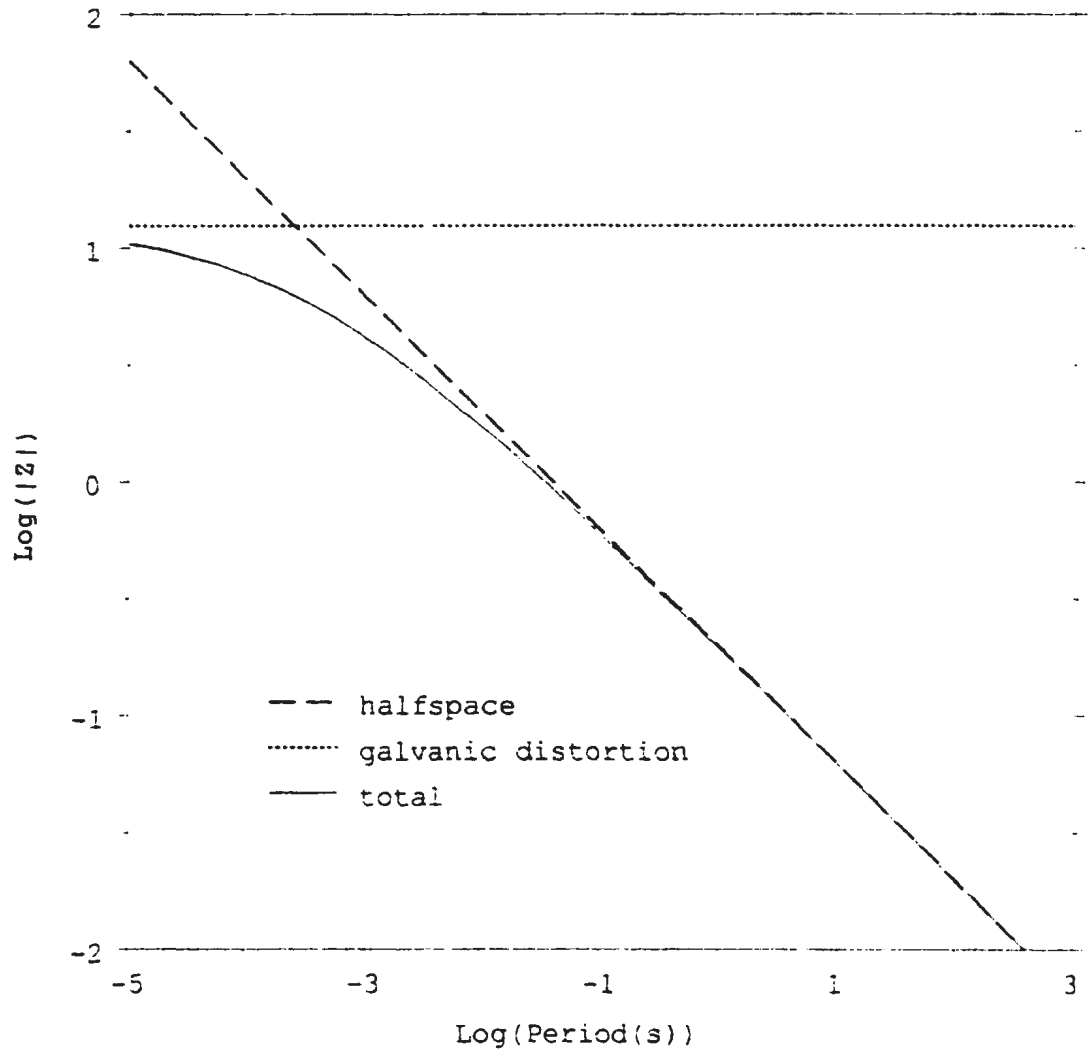

Figure 3.1 Galvanic magnetic distortion of a 5000 Ω·m halfspace impedance magnitude as a function of period. Distortion of the measured impedance magnitude becomes negligible at longer periods.

importance of magnetic distortion reduces as approximately $\sqrt{\omega}$, since as period increases the magnitude of $Z_{regional}$ decreases making the term $DZ_{regional}$ in the denominator of equation 3.50 insignificant ($I \gg DZ_{regional}$). As the magnitude of the regional impedance tensor never increases with increasing period it is reasonable to assume that the first order

effects of galvanic distortion are can explained solely by the distortion matrix C, especially at the longer periods of interest in regional studies.

Equation 3.52 shows that in the presence of a galvanic distorter the measured magnetic transfer function is the sum of the distorted regional transfer function (first term) and a local transfer function (second term) produced by the distorter (Zhang et al., 1993). As the magnitude of the regional impedance tensor decreases the measured transfer function will approach that of the regional structure ($T_{regional}$). The importance of distortion of the transfer functions is dependent on the magnitude of the regional transfer function, with the local transfer functions possibly making up a significant portion of the measured transfer function when the regional transfer function is small, especially at high frequencies where the magnitude of the regional impedance tensor is large.

The distortion of the observed magnetic fields is dependent on the regional conductivity structure, having its greatest importance in structures where the magnitude of the regional impedance tensor decays slowly as a function of period. Magnetic distortions will be most important therefore in regions having a conductive over resistive structure and of lesser importance when the conductivity structure is resistive over conductive. Regardless of the conductivity structure the effects of magnetic distortion become less important as period increases, with the electric field distortions describing the first order effects of the galvanic distorter.

When considering only the first-order effects of galvanic distortion the measured magnetic field is assumed to be that of the regional structure,

$$\vec{H}_{meas} = \vec{H}_{regional} \,. \tag{3.52}$$

Therefore, the distortion is represented by four real parameters and the measured impedance tensor in the regional coordinate system is given by

$$Z_{meas} = C\, Z_{regional} \,. \tag{3.53}$$

If the regional conductivity structure is one-dimensional the measured impedance tensor in the measurement axes system becomes

$$Z_{meas}(\omega) = R(\theta)\, C(\theta) \begin{bmatrix} 0 & Z(\omega) \\ -Z(\omega) & 0 \end{bmatrix} R'(\theta) \,, \tag{3.54}$$

having seven parameters per frequency. For a two-dimensional regional conductivity structure the measured impedance tensor is given by

$$Z_{meas}(\omega) = R(\theta)\, C(\theta) \begin{bmatrix} 0 & Z_{TE}(\omega) \\ -Z_{TM}(\omega) & 0 \end{bmatrix} R'(\theta) \,, \tag{3.55}$$

and the model contains 9 parameters per frequency.

Larsen (1977) provided a method of recovering the 1-D regional impedances in the presence of weak 3-D local effects. Zhang et al. (1987) provided a method of recovering 1-D and 2-D regional responses when the local galvanic effects are 2-D. A number of methodologies have been proposed to recover up to 2-D regional impedances in the

presence of 2-D or 3-D galvanic distortion (Bahr, 1988; Groom and Bailey, 1989; Chakridi et al., 1992; Chave and Smith, 1994; McNeice and Jones, 1996).

3.5 Summary

In this chapter, the magnetotelluric impedance tensor for an arbitrary Earth was derived. An impedance tensor measured at the surface of the Earth is dependent solely on the period of observation and conductivity structure of the Earth. Deriving information on the Earth's conductivity structure from magnetotelluric observations is achieved through the use of physical models which attempt to describe the impedance tensor's spatial and frequency dependence. In practice this is a difficult task, since for arbitrary Earth structures there is no obvious means of deriving the desired parameters.

Traditionally interpretation of the impedance tensor is approached by making simplifying assumptions about the dimensionality of the Earths conductivity structure. For a 1-D and 2-D conductivity structure the impedance tensor assumes a simplified form which is readily interpretable. However, in the interpretation of experimental data traditional 1-D and 2-D conductivity models are often unable to explain the observed impedance tensor and more complex conductivity models must be invoked.

In large scale regional investigations where the Earth's conductivity structure is relatively sparsely sampled interpretation essentially becomes an attempt to resolve larger scale regional features of the conductivity structure, treating smaller scale 3-D conductivity features as geological noise. Recognition of this problem has lead to the development of a

number of mathematical and physical impedance tensor decomposition procedures, which attempt to recover first-order features of the measured impedance tensor. Of these two classes of decompositions physical decompositions are by far the most successful as they are based on physical models of the conductivity structure and as a result the parameters derived are readily interpretable.

Physical decompositions for recovering regional impedances in the presence of 3-D galvanic distortion are based on the most complete physical model of the impedance tensor currently available. The model (eqn. 3.50) on which these methodologies are based includes simpler physical models as special cases, and as such the 3-D galvanic distortion model is the most widely applicable physical model of the impedance tensor. The regional impedances recovered with these methodologies can be interpreted using available one and two dimensional forward and inverse procedures.

CHAPTER 4

Extension of Groom-Bailey Decomposition

4.1 Introduction

In recent years, impedance tensor decomposition analysis (3D/2D model) has become an integral part of the interpretation of magnetotelluric data for 1D and 2D regional structures (Jones and Dumas, 1993; Jones et al., 1993a, 1993b; Kurtz et al., 1993; Ogawa et al., 1994; Boerner et al., 1995; Gupta and Jones, 1995). The goal of this analysis is to remove the first-order effects of galvanic distortion produced by near surface zones of anomalous conductivity, recovering the impedances and strike of the regional geoelectric structure. Of the parameters recovered during decomposition analysis the regional strike is often one of the poorest resolved parameters (Groom et al., 1993; Jones and Groom, 1993). This presents a problem, as the accuracy of the interpretation is dependent on the determination of a regional strike consistent with the data.

The instability of regional strike in the presence of noise and galvanic distortion leads to instability in decomposition procedures (Bahr, 1988; Chakridi et al., 1992) based on the rotation of the impedance tensor. Stable estimates of decomposition parameters can be obtained by fitting the decomposition model to an impedance tensor in a least squares sense (Groom and Bailey, 1989, 1991). In this analysis the galvanic decomposition parameters - shear, twist and regional strike - are then iteratively constrained to find frequency independent estimates required by the decomposition model. The regional

strike, determined for each of a set of sites, is then compared to obtain an estimate of regional strike for the entire data set (assuming the data is 2D and sensing the same regional 2D structure). To obtain an accurate estimate of regional strike, one really needs to perform a weighted average of the determined strike estimates, since the resolution of regional strike is a function of both frequency and site position.

In this chapter an extension to Groom-Bailey decomposition is proposed, in which all the constraints inherent to the decomposition model are imposed simultaneously on the data set. This procedure enables the determination of a strike estimate consistent with the data set in a statistical sense. The variation of strike resolution as a function of frequency and position is used in the determination of the strike estimate. This approach additionally provides the interpreter with information on the degree to which the data fits the model of regional two dimensionality with galvanic distortions.

Previously published synthetic data, as well as a synthetic 2D data set, are used to demonstrate the robustness of the proposed decomposition analysis. Additionally, the determination of confidence intervals for the derived parameters is discussed.

4.2 Groom-Bailey Decomposition

Groom and Bailey (1989) proposed a tensor decomposition method which fits the 3D/2D galvanic distortion model (Eqn. 3.54 and 3.55) to the observed data (GB analysis). The GB analysis is based on a factorization of the distortion tensor C as a product of modified Pauli spin matrices. This factorization allows the separation of determinant and

indeterminant elements of the distortion tensor C, as well as providing some physical insight into the distortion produced by elements of the distortion tensor.

Any rank 2 tensor such as the distortion tensor C can be represented as a sum of the Pauli spin matrices

$$I = \begin{bmatrix} 1 & 0 \\ 0 & 1 \end{bmatrix}$$

$$\Sigma_1 = \begin{bmatrix} 0 & 1 \\ 1 & 0 \end{bmatrix} \qquad (4.1)$$

$$\Sigma_2 = \begin{bmatrix} 0 & -1 \\ 1 & 0 \end{bmatrix}$$

$$\Sigma_3 = \begin{bmatrix} 1 & 0 \\ 0 & -1 \end{bmatrix}.$$

where

$$C = \alpha_0 I + \alpha_1 \Sigma_1 + \alpha_2 \Sigma_2 + \alpha_3 \Sigma_3 \qquad (4.2)$$

and α_0, α_1, α_2, and α_3 are scalar multipliers. In the GB method, modified forms of the Pauli spin matrices are used to represent C as a product factorization

$$C = g T S A , \qquad (4.3)$$

where g is a scalar termed "site gain" and T, S, and A are tensor factors termed "twist",

"shear" and "anisotropy" respectively. The tensor factors T, S, and A are given by

$$T = \frac{1}{\sqrt{1+t^2}}(I+t\Sigma_3) = \frac{1}{\sqrt{1+t^2}}\begin{bmatrix} 1 & -t \\ t & 1 \end{bmatrix},$$

$$S = \frac{1}{\sqrt{1+e^2}}(I+e\Sigma_1) = \frac{1}{\sqrt{1+e^2}}\begin{bmatrix} 1 & e \\ e & 1 \end{bmatrix}, \qquad (4.4)$$

$$A = \frac{1}{\sqrt{1+s^2}}(I+s\Sigma_2) = \frac{1}{\sqrt{1+s^2}}\begin{bmatrix} 1+s & 0 \\ 0 & 1-s \end{bmatrix},$$

and the distortion tensor C in the GB product factorization therefore becomes

$$C = g\begin{bmatrix} (1+s)(1-te) & (1-s)(e-t) \\ (1+s)(e+t) & (1-s)(1+te) \end{bmatrix}. \qquad (4.5)$$

The scalar multipliers of equation 4.4 are absorbed into the site gain g.

Some insight into the physical meaning of the factors T, S, and A can be gained by examining the effect of each of the tensors on the regional electric field. Figure 4.1 shows the distortion produced by each of the distortion tensors and their net effect on a regional electric field represented by a set of unit vectors.

The twist T and shear S tensors form the determinable portion of the distortion matrix. The twist tensor rotates the regional electric field clockwise by an angle $\tan^{-1} t$. While the shear tensor develops anisotropy on an axis which bisects the regional principal axis system, rotating a vector on the x-axis clockwise and a vector on the y-axis counter-

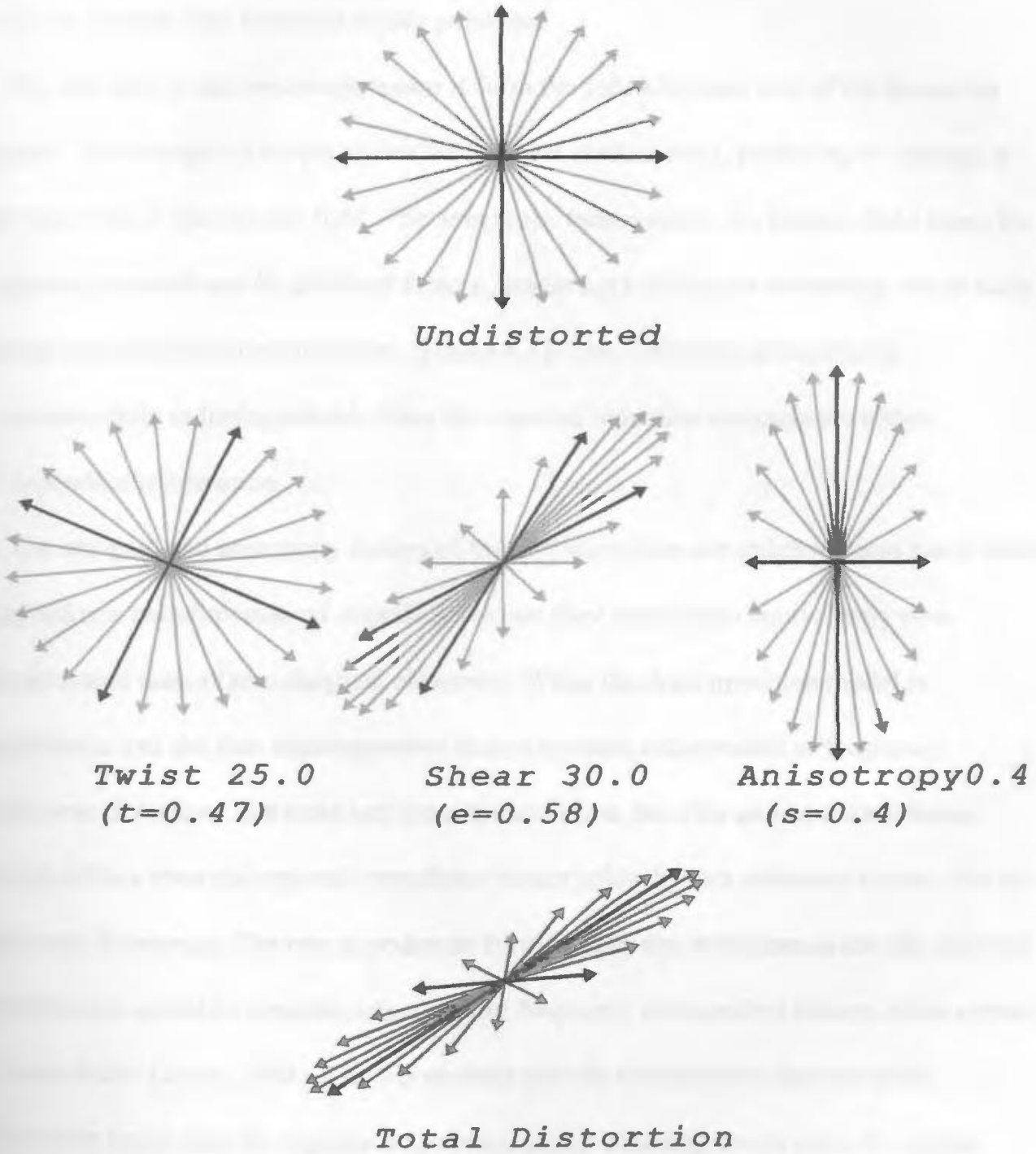

Figure 4.1 The effect of telluric distortion factors on a set of unit vectors representing the regional electric field (after Groom and Bailey, 1989).

clockwise by an angle of $\tan^{-1} e$ (Figure 4.1). For a shear e of 1 or -1 (shear angle of 45 or -45) the electric field becomes totally polarized.

The site gain g and anisotropy tensor A form the indeterminant part of the distortion matrix. The site gain g simply scales the regional electric field, producing no change in the direction of the electric field. The anisotropy tensor scales the electric field along the regional principal axis by different factors, producing a distortion anisotropy which adds to the regional inductive anisotropy (Figure 4.1). This distortion anisotropy is experimentally indistinguishable from the regional inductive anisotropy without independent information.

The site gain and anisotropy factors of the decomposition are indeterminant since when applied to a two-dimensional impedance tensor they result in an equivalently two-dimensional tensor (zero diagonal elements). When the decomposition model is applicable, and the four decomposition factors become independent of frequency (galvanic distortion), the twist and shear tensors alone describe an impedance tensor which differs from the regional impedance tensor solely by two unknown factors, the site gain and anisotropy. The two impedances recovered by the factorization are the regional impedances scaled by separate unknown but frequency independent factors, often termed "static shifts" (Jones, 1988). The GB method absorbs the unknown factors of the distortion tensor into the regional impedance tensor allowing one to solve for scaled regional impedances.

Absorbing the site gain g and anisotropy s into the regional impedances the measured

impedance tensor under the GB factorization becomes

$$Z_{meas} = RTSZ_{regional}R^T$$
$$= \begin{bmatrix}\cos\theta & -\sin\theta\\ \sin\theta & \cos\theta\end{bmatrix}\begin{bmatrix}1-te & e-t\\ e+t & 1+te\end{bmatrix}\begin{bmatrix}0 & A\\ -B & 0\end{bmatrix}\begin{bmatrix}\cos\theta & \sin\theta\\ -\sin\theta & \cos\theta\end{bmatrix}, \qquad (4.6)$$

where $Z_{regional}$ is the scaled regional impedance tensor ($gAZ_{regional}$). Groom and Bailey (1989) showed that when the measured impedance tensor obeys the decomposition model, the tensor is uniquely described by the seven parameters of the factorization (Eqn. 4.6), provided that the absolute value of shear e and anisotropy s are less than one (corresponding shear angles between 45 and -45 degrees and distortion anisotropy between 1 and -1). A shear e or anisotropy s (sum of distortion and regional) of absolute value one produces a singular impedance tensor for which the distortion model becomes underdetermined as the impedance tensor becomes singular.

The seven parameters of the GB factorization are the two descriptors of telluric distortion twist t and shear e, the regional strike θ, and the four parameters contained in the two complex regional impedances A and B (Z_{xy} and Z_{yx}). The parameters of the factorization are found by statistically fitting the seven parameters of the decomposition model to the 8 data of the measured impedance tensor. This is done by minimizing the Chi-squared misfit of the model and data summary decomposition coefficients given by equation 4.2. For the measured data the coefficients are

$$\begin{aligned}
\alpha_0 &= Z_{xx} + Z_{yy} \\
\alpha_1 &= Z_{xy} + Z_{yx} \\
\alpha_2 &= Z_{yx} - Z_{xy} \\
\alpha_3 &= Z_{xx} - Z_{yy} .
\end{aligned} \qquad (4.7)$$

For the model the summary decomposition coefficients are found by multiplying out equation 4.6,

$$\begin{aligned}
\alpha_0 &= t\sigma + e\delta \\
\alpha_1 &= (\delta - et\sigma)\cos 2\theta - (t\delta + e\sigma)\sin 2\theta \\
\alpha_2 &= -\sigma + et\delta \\
\alpha_3 &= -(t\delta + e\sigma)\cos 2\theta - (\delta - et\sigma)\sin 2\theta ,
\end{aligned} \qquad (4.8)$$

where

$$\sigma = A + B$$

and

$$\delta = A - B$$

are the sum and difference of the regional impedances. Equating 4.7 and 4.8 one obtains

four simultaneous complex nonlinear equations which are solved for the seven parameters of the factorization. The parameters of the factorization are overdetermined and therefore a solution to the system of equations always exists.

In GB analysis, the decomposition model is fit to the measured data frequency by frequency. Although, for the 3D/2D distortion model to hold, enabling the recovery of the regional impedances, frequency independent estimates of the twist, shear and regional strike must be found over a band of frequencies. In practice this is done by iteratively constraining the estimates of twist, shear and strike found at each frequency in an attempt to find a frequency band for which the constrained values result in an acceptable misfit error. If the regional conductivity structure is truly one- or two-dimensional, the model will hold in general at low frequencies reducing the task to finding an upper frequency limit below which the distortion becomes solely galvanic (distorter becomes inductively small) and the distortion parameters become frequency independent.

4.3 Extension of Groom-Bailey Decomposition

Of the parameters solved for in decomposition analysis of the impedance tensor, regional strike is by far the most important parameter. Accurate recovery of the regional impedances, and therefore accuracy of the interpretation, is dependent on recovery of the correct regional strike. Unfortunately, regional strike is often one of the poorest resolved parameters in decomposition analysis (Jones and Groom, 1993). The resolution of

regional strike is a function of both frequency and position and its recovery hampered by galvanic distortion and experimental error.

The importance of accurate recovery of the regional strike can be seen by examining properties of the measured impedance tensor under the Groom-Bailey factorization. In an arbitrary coordinate system, the measured impedance tensor is given by (Eqn. 4.6). The elements of the impedance tensor are distortion and rotation dependent mixtures of the two regional impedances. In the regional coordinate system however, equation 4.6 reduces to

$$Z_{meas}(\theta_{regional}) = \begin{bmatrix} -(e-t)B & (1-te)A \\ -(1+te)B & (e+t)A \end{bmatrix}, \qquad (4.9)$$

and the two columns of the impedance tensor contain scaled estimates of the regional impedances. The impedance elements contained in the two columns are linearly dependent, having the same impedance phase, differing solely in magnitude. The magnitude of the four elements is described by the twist (t) and shear (e) factors of the GB factorization.

Equation 4.9 shows that scaled estimates of the regional impedances can be found, even in the presence of galvanic distortion, by simply rotating the impedance tensor to the regional coordinate system. An error in the regional strike estimate will result in the recovery of impedances which are mixtures of the regional impedances, while errors in twist and shear result solely in errors in the magnitudes of the recovered regional

impedances. Recovery of the correct regional strike is therefore essential for accurate recovery of the regional impedances.

The linear dependence of the impedance elements in the regional coordinate system is both the basis of the decomposition procedures proposed by Zhang et al. (1987), Bahr (1988) and Chakridi et al. (1992) and the reason conventional 2D analysis fails. In conventional analysis, the strike angle is found by minimizing the diagonal elements of the impedance tensor,

$$minimize \ |Z_{xx} - Z_{yy}|^2 \qquad (4.10)$$

(Sims and Bostick, 1969). Using equation 4.6 the minimum becomes

$$\theta' = \theta_{regional} + \frac{1}{2}\tan^{-1}\left(\frac{t\delta + e\sigma}{\delta - et\sigma}\right). \qquad (4.11)$$

Equation 4.11 clearly shows that in the presence of distortion the strike angle θ' recovered in the conventional method will not equal the regional strike. In addition the 3D indicator (skew) used in the conventional analysis fails in the presence of galvanic distortion. Swift (1967) defined the skew as

$$\Gamma = \left|\frac{Zxx + Zyy}{Zxy - Zyx}\right|, \qquad (4.12)$$

which becomes

$$\Gamma = \left| \frac{t\sigma + e\delta}{\delta - et\sigma} \right|, \qquad (4.13)$$

where σ and δ are the sum and difference of the regional impedances. The skew can be significantly greater than zero when the regional structure is 2D. Low skew is therefore not a requirement of regional two dimensionality.

In the decomposition procedures proposed by Zhang et al. (1987), Bahr (1988) and Chakridi et al. (1992), the linear dependence of the columns of the impedance tensor is used to find the regional strike. Their procedures solve for a strike angle for which the elements of the two columns have equal impedance phases. This method however is unstable in the presence of noise since, depending on distortion (twist and shear), some of the elements of the tensor can be small in magnitude and dominated by error, producing significant errors in the recovered regional strike.

Groom-Bailey decomposition performs well in the presence of noise since it simultaneously solves for all the parameters of the decomposition model. The twist and shear are often better resolved than the regional strike as they are dependent on the relative magnitude of the impedance elements as opposed to phase properties of the elements. The inclusion of twist and shear into a model fitting all eight elements of the impedance tensor stabilizes the estimation of regional strike.

To improve the estimate of regional strike, one can extend the GB analysis to fit an entire data set statistically with the 3D/2D distortion model. Extension of the analysis can

improve the estimate of regional strike, since it accounts for the position and frequency dependence of strike resolution. The regional strike is usually only well defined over a small subset of the data. The dependence of model misfit on strike defines a regional strike statistically consistent with the entire data set.

In the extended GB analysis, S magnetotelluric sites having N frequencies ($SN8$ data) can be fit with $S(N4+2)+1$ unknowns. The unknowns are the SN regional complex impedances (A and B), the $S2$ descriptors of telluric distortion (twist t and shear e) and the regional strike angle (θ). In the extended model, the S sites are required to have the same regional strike. The distortion parameters shear and twist remain site dependent although independent of frequency. Assuming that all data are independent, the model has $S(N4-2)-1$ degrees of freedom. In the case of a single site, the extended model is equivalent to that of the GB method with the strike, twist and shear constrained to be independent of frequency, although the solutions are arrived at differently.

The model parameters are found in the extended analysis by minimizing the Chi-squared (χ^2) misfit of the observed and model summary decomposition coefficients given by equations 4.7 and 4.8 respectively. The elements of each of the modelled impedance tensors are described by four complex nonlinear equations. The minimization procedure seeks a simultaneous solution to the $SN8$ nonlinear equations (4 real and 4 imaginary equations for each of the SN impedance tensors) describing the measured data set. A χ^2 objective function was chosen in order to reduce any bias produced by frequency and position dependence of experimental error and the frequency dependence of impedance

magnitudes. Additionally, the χ^2 objective function allows one to derive significance levels for the parameter estimates obtained by the minimization procedure.

The χ^2 objective function is given by

$$\chi^2(a) = \sum_{k=1}^{SN} \left(\sum_{i=0}^{3} \left[\frac{\Re(\alpha_i^{obs}) - \Re(\alpha_i^{model}(a))}{\sigma_{\alpha_i}} \right]^2 + \sum_{i=0}^{3} \left[\frac{\Im(\alpha_i^{obs}) - \Im(\alpha_i^{model}(a))}{\sigma_{\alpha_i}} \right]^2 \right) \tag{4.14}$$

where σ is the standard deviation of the summary coefficients. Minimization of the objective function is performed with a sequential quadratic programming algorithm. The algorithm iteratively improves a user-supplied trial solution by minimizing a quadratic approximation of the objective function. Iterations proceed until the gradient of the objective function is zero with respect to all parameters, or when successive iterations produce changes in the estimated parameters less than a user specified tolerance.

For each iteration the objective function is approximated by a $S(N4+2)+1$ dimensional quadratic function derived from a Taylor series expansion of the objective function,

$$\begin{aligned} \chi^2(a) &= \chi^2(P) + \sum_i \frac{\partial \chi^2}{\partial a_i} a_i + \frac{1}{2} \sum_{i,j} \frac{\partial^2 \chi^2}{\partial a_i \partial a_j} a_i a_j + \ldots \\ &\approx c + J \cdot a + \frac{1}{2} a \cdot H \cdot a \end{aligned} \tag{4.15}$$

where a is the parameter set sought by the minimization routine, c is the value of the

objective function for the trial parameter set P, and J and H are the gradient (Jacobian) and Hessian of the objective function evaluated at the trial solution. If the approximation is good, the routine can jump from the trial solution P to the minimum a_{min} by minimizing the gradient of the approximation. The gradient of the equation 4.15 is easily calculated as

$$\nabla\chi^2 \approx H \cdot a + J . \qquad (4.16)$$

The approximate objective function will be at its minimum when the gradient vanishes, the minimum (a_{min}) therefore satisfies

$$H \cdot a_{min} + J = 0 . \qquad (4.17)$$

For the trial solution the gradient is

$$\nabla\chi^2(P) = H \cdot P + J . \qquad (4.18)$$

Subtracting equation 4.17 from 4.18 we obtain an equation for the minimum (a_{min}),

$$a_{min} = P - H^{-1} \cdot \nabla\chi^2(P) . \qquad (4.19)$$

If the approximation is good, and we can calculate the gradient and Hessian of the objective function, the routine can find the minimum of the objective function in one iteration.

Since equation 4.15 may be a poor local approximation to the true objective function,

the inverse Hessian in equation 4.19 is replaced by a constant determined from the magnitude of the Hessian. The constant is small enough to allow the algorithm to take a step down the gradient without exhausting the downhill direction. Successive approximations of the objective function iteratively approach the desired minimum (a_{min}) of the objective function.

The exact value of the Hessian has no effect at all on the final set of parameters a_{min} reached by the algorithm. The Hessian's value only affects the iterative route that is taken in getting to the minimum. This allows us to save computation time by using an approximation to the Hessian. Writing the summary coefficient equation differences as a $SN8$ vector

$$\chi_i(a) = \frac{\alpha_i^{obs} - \alpha_i^{model}(a)}{\sigma_{\alpha_i}} \quad i = 1,2,\ldots,SN8\,, \tag{4.20}$$

the objective function becomes

$$\chi^2(a) = \sum_{i=1}^{SN8} [\chi_i(a)]^2\,. \tag{4.21}$$

Taking the first derivative of equation 4.19, the Jacobian of the summary coefficient difference vector becomes a $SN8$ x $S(N4+2)+1$ matrix given by

$$\frac{\partial \chi_i(a)}{\partial a_j} = \frac{-1}{\sigma_{\alpha_i}} \frac{\partial \alpha_i^{model}(a)}{\partial a_j} \quad i = 1,2,\ldots,SN8 \qquad (4.22)$$

$$j = 1,2,\ldots,S(N4+2)+1 .$$

The Jacobian (gradient) of the objective function, a $S(N4+2)+1$ element vector containing sums of the partial derivatives of the $SN8$ subfunctions (4 real and 4 imaginary equations for each of the modelled tensors), can be found using equations 4.20 and 4.22

$$\frac{\partial \chi^2(a)}{\partial a_i} = 2\sum_{j=1}^{SN8} \chi_j(a) \frac{\partial \chi_j(a)}{\partial a_i} \quad i = 1,2,\ldots,S(N4+2)+1 \qquad (4.23)$$

Taking an additional partial derivative we obtain the Hessian of the objective function, a $S(N4+2)+1$ x $S(N4+2)+1$ matrix of second partial derivatives

$$\frac{\partial^2 \chi^2}{\partial a_i \partial a_j} = 2\sum_{k=1}^{SN8} \frac{1}{\sigma_{\alpha_k}^2} \left[\frac{\partial \alpha_k^{model}(a)}{\partial a_i} \frac{\partial \alpha_k^{model}(a)}{\partial a_j} + [\alpha_k^{obs} - \alpha_k^{model}(a)] \frac{\partial^2 \alpha_k^{model}(a)}{\partial a_i \partial a_j} \right] \qquad (4.24)$$

Note that the equation for the Hessian (Eqn. 4.24) contains terms in both first and second derivatives of the summary coefficients. For a successful model, the term containing the second derivative in equation 4.24 becomes negligibly small. The multiplier $[\alpha^{obs} - \alpha^{model}]$

approaches the random measurement error of the summary coefficient and the second derivative terms cancel each other on summation. The Hessian can therefore be approximated by the first derivative term in equation 4.24. Using equation 4.22 the approximate Hessian becomes

$$\frac{\partial^2 \chi^2(a)}{\partial a_i \partial a_j} \approx 2 \sum_{k=1}^{SN8} \frac{\partial \chi_k(a)}{\partial a_i} \frac{\partial \chi_k(a)}{\partial a_j} \qquad (4.25)$$

$$i,j = 1,2,\ldots,S(N4+2)+1 \; .$$

Therefore, to perform the minimization one needs only to calculate equations 4.20 and 4.22, from which the objective function, gradient and approximate Hessian can be obtained.

4.4 Recovery of Regional Impedances

4.4.1 NACP anomaly

To illustrate the performance of the proposed decomposition procedure in the presence of experimental noise, consider thirty-one realizations of a theoretical impedance tensor discussed by Jones and Groom (1993). Their theoretical response is taken from a 2D model of the North America Central Plans (NACP) conductivity anomaly (Jones and Craven, 1990).

In order to derive a distorted response Jones and Groom (1993) applied a distortion matrix C from Chakridi et al. (1992) to an impedance tensor exhibiting the maximum

induction for the NACP anomaly. This distorted tensor is given by

$$
\begin{aligned}
Z &= C Z_{2D} \\
&= \begin{bmatrix} 1.26 & 0.44 \\ 0.53 & 0.86 \end{bmatrix} \begin{bmatrix} 0 & (4.72,4.05) \\ (-8.25,-3.10) & 0 \end{bmatrix} \times 10 \\
&= \begin{bmatrix} (-3.63,-1.36) & (5.95,5.10) \\ (-7.10,-2.67) & (2.51,2.15) \end{bmatrix} \times 10^{-4} (\Omega).
\end{aligned}
\tag{4.26}
$$

Decomposition of the distortion tensor above in terms of the GB parameters yields a site gain (g) of 1.06, an anisotropy (s) of 0.172, a twist angle of -2.1° (t = -0.037), and a shear angle of 24.95° (e = 0.47). The inductive strike of the NACP anomaly, the regional structure, is 0°.

Gaussian noise, having a standard deviation of 4.5% of the magnitude of the largest impedance element, was added to the tensor (Eqn. 4.25) to produce thirty-one noise-contaminated realizations. These thirty-one realizations form an ideal data set to test the performance of the decomposition procedure in the presence of noise, as all the realizations are equally sensitive to the inductive strike and obey the telluric distortion model differing solely by experimental noise.

Figure 4.2 shows histograms of the strike, twist and shear found from an unconstrained GB analysis of the thirty-one realizations. The distribution of the GB parameters clearly shows that shear and twist are more stable under decomposition than strike angle determination. The strike directions determined poorly define the regional strike. This

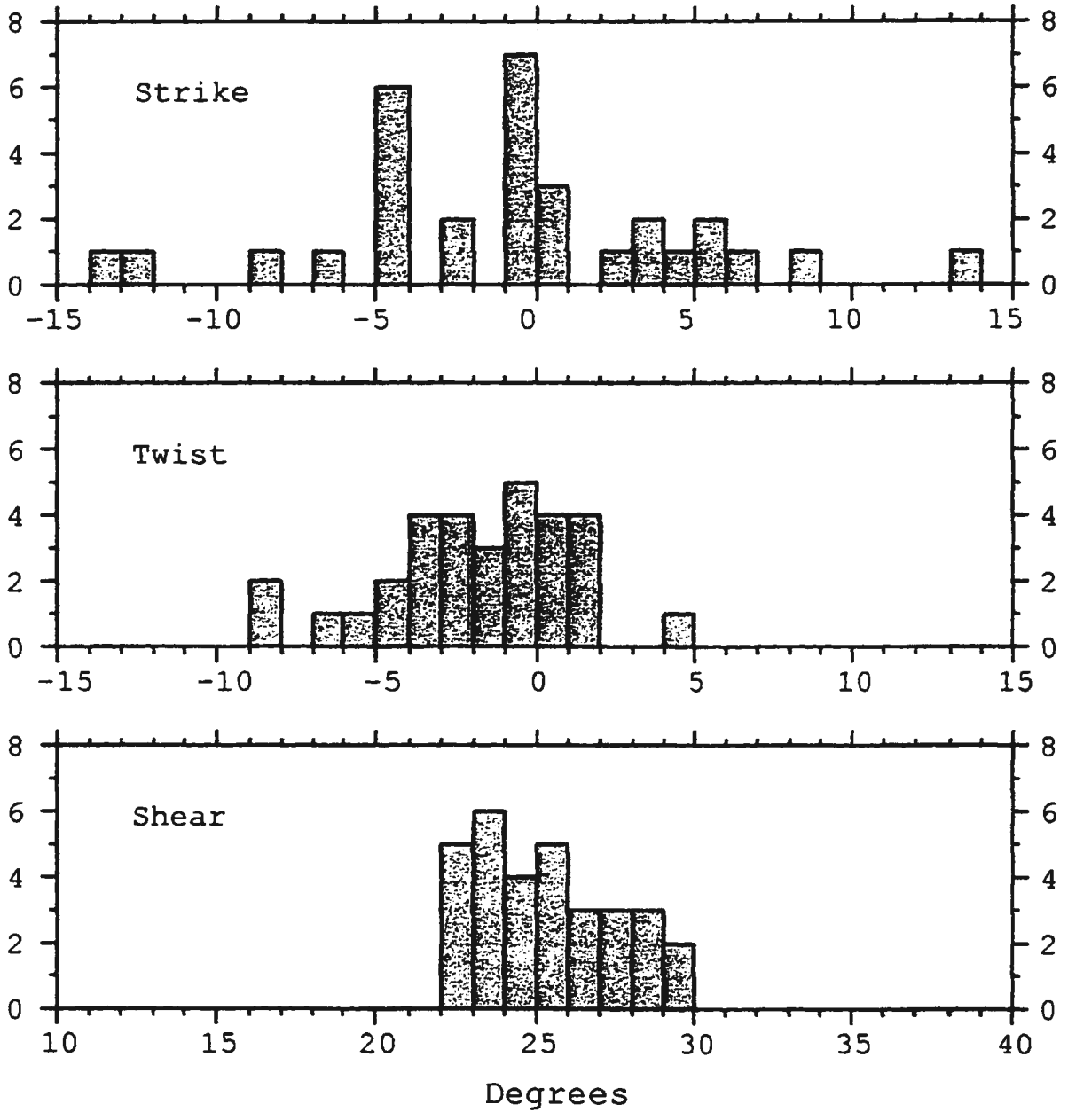

Figure 4.2 Histogram of strike, twist and shear determined through unconstrained GB analysis of the thirty-one relizations of the NACP impedance tensor. The results of extended decomposition analysis are indicted with dashed vertical lines.

example demonstrates the difficulty in obtaining an accurate estimate of the regional strike in the presence of distortion and experimental noise. The synthetic realizations exhibit the maximum induction for the NACP anomaly, and, as such, represent the best

case scenario for strike determination.

The results of the extended decomposition analysis are indicated in figure 4.2. This analysis yields a twist angle of -2.2°, a shear angle of 25.6° and strike direction of 0.1°, close to the correct values of -2.1°, 25° and 0° respectively. The results are accurate and free of noise bias. Although the data set is somewhat unrealistic, the performance of the extended decomposition analysis indicates that if the 3D/2D model is applicable to real data the extended GB analysis should yield a stable estimate of strike direction in the presence of experimental noise.

4.4.2 Groom-Bailey 3D/2D synthetic site

Now consider the question of decomposition analysis of a more realistic theoretical response, where sensitivity to the 2D inductive strike is a function of frequency. Groom and Bailey (1991) produced an accurate 3D/2D data set by superposing 2D numerical and 3D analytic responses (Figure 4.3). Decomposition of this theoretical response has been previously discussed by Groom and Bailey (1991) and Groom et al. (1993). The 3D analytical response is that of a small conducting hemisphere. For the frequencies considered the hemisphere has a negligible inductive response, however it has a significant effect on both the electric and magnetic fields of the regional 2D structure. For periods longer than 0.1 second, the distortion effects produced by the anomalous magnetic fields of the hemisphere become negligible and the hemisphere acts as a galvanic scatterer. Decomposition analysis should therefore be able to recover the regional 2D impedances for periods greater than 0.1s to within a static shift. The strike

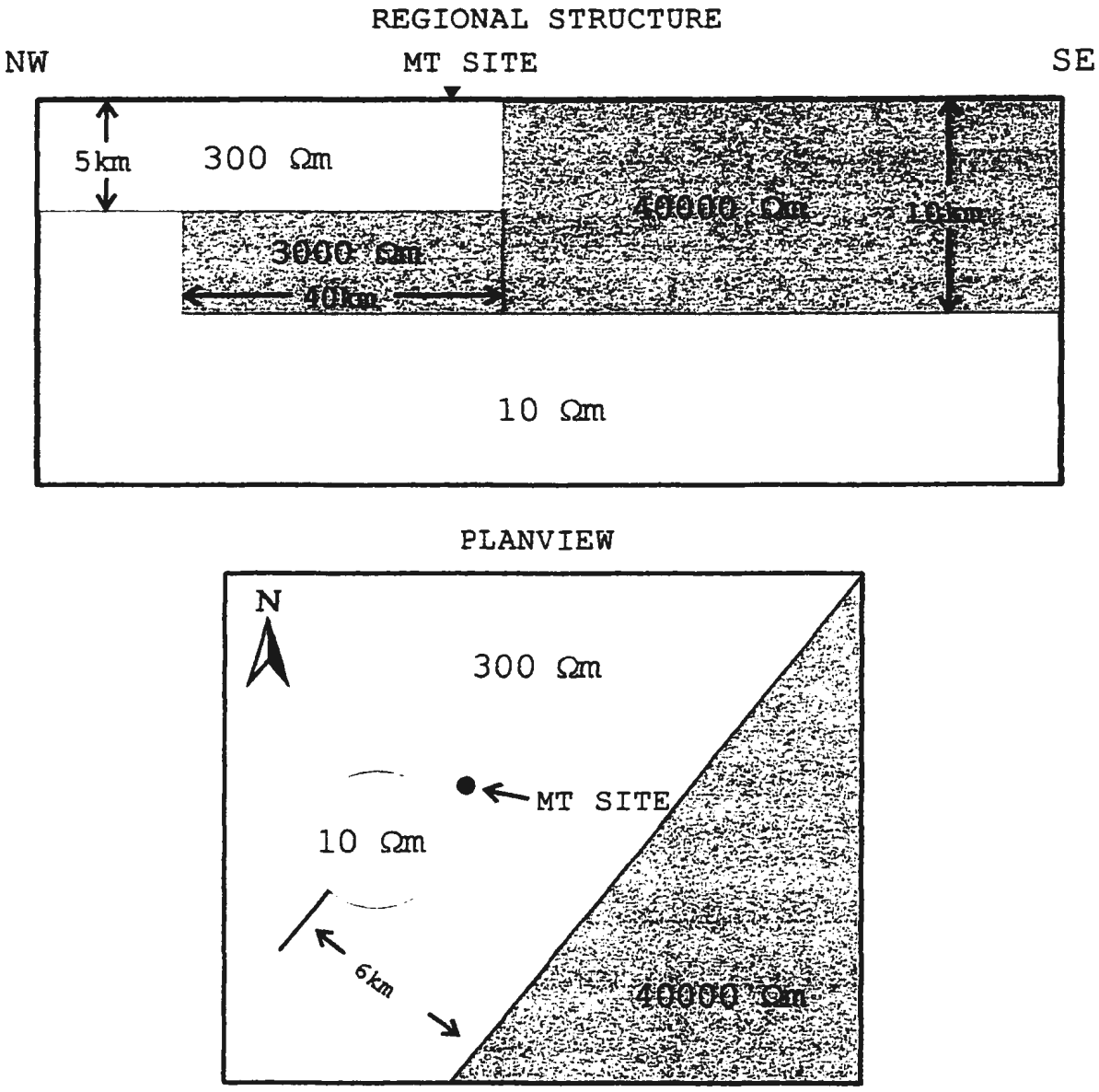

Figure 4.3 Conductivity model for a synthetic 3D/2D sounding (after Groom and Bailey, 1991).

of the regional 2D structure is 30° (Figure 4.3). Groom et al. (1993) have shown that the strike is poorly defined at both short and long periods. For short periods, the data are not sensitive to the 2D boundaries of the regional structure and are essentially 1D. At long periods, the 2D structure becomes inductively thin, having a galvanic response. The

phases of the two regional impedances become virtually identical and the regional response becomes an anisotropic 1D response (2D galvanic distortion of the response of

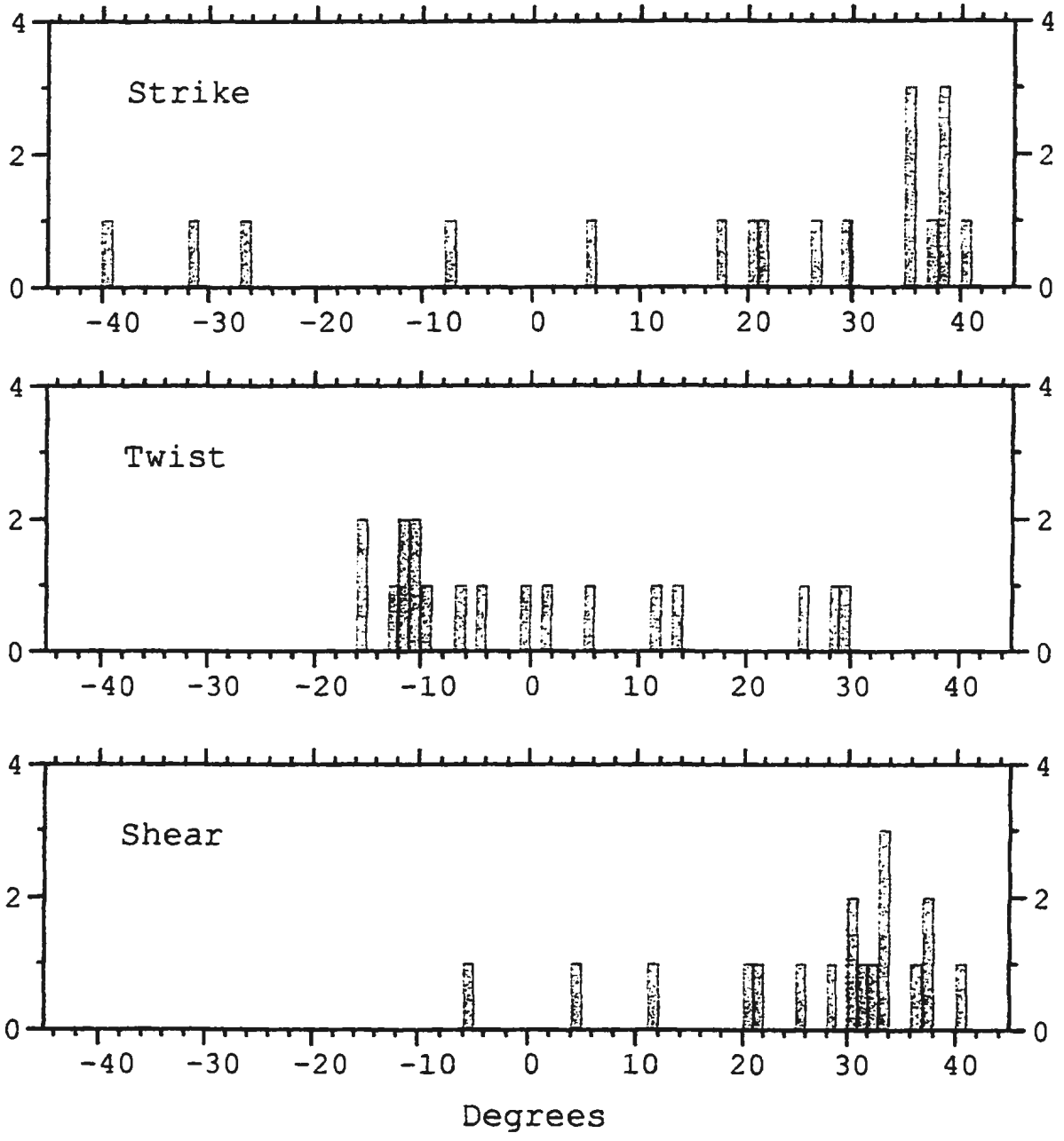

Figure 4.4 Histogram of strike, twist and shear determined through unconstrained GB analysis of the 3D/2D site. The results of the extended decomposition analysis are indicated with dashed vertical lines.

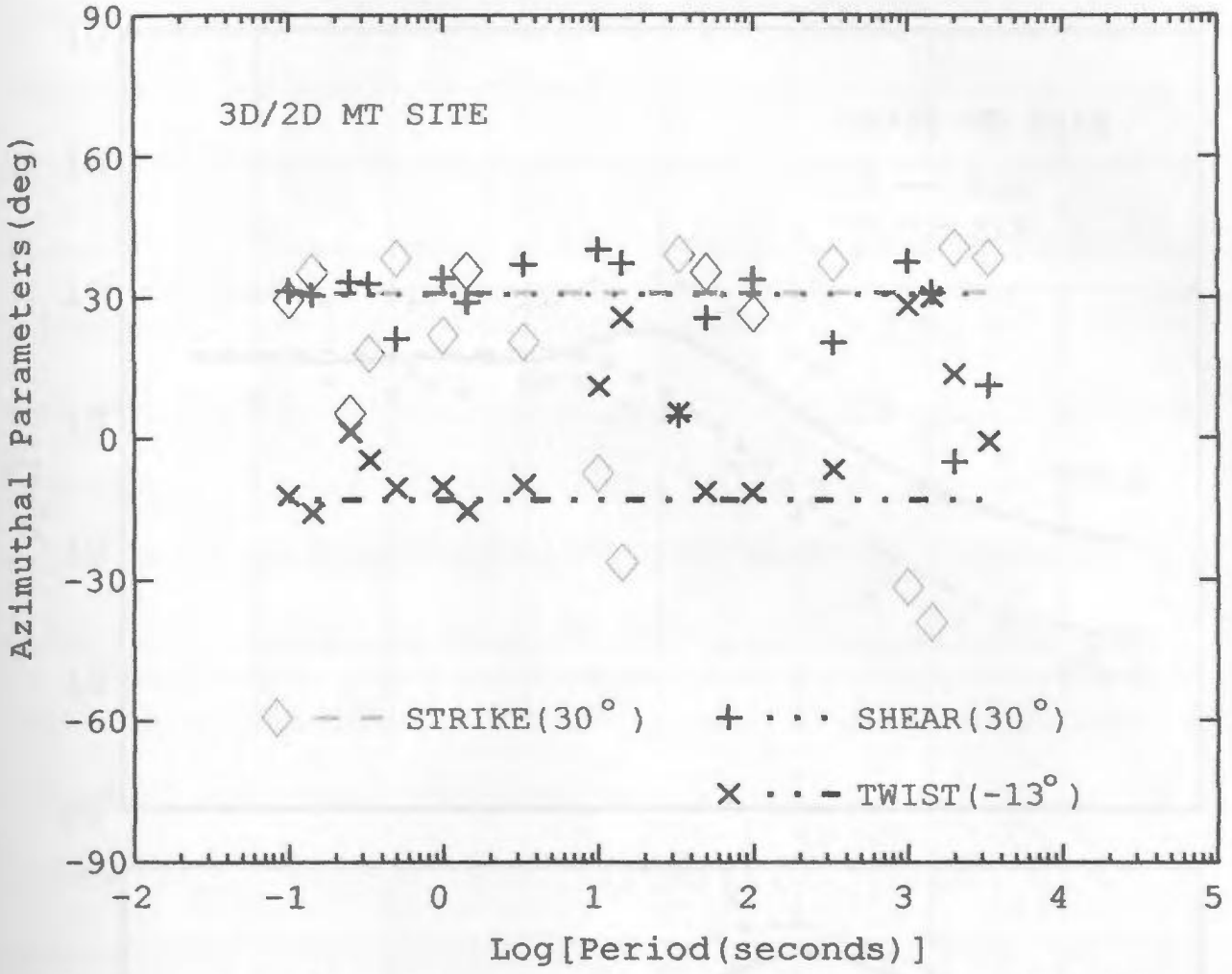

Figure 4.5 Comparison of the results of the unconstrained and extended GB analysis for the 3D/2D site, displayed as a function of period.

the deep regional 1D structure). To simulate experimental noise, 2% Gaussian noise was added to the theoretical responses. Decomposition analysis, prior to the addition of noise, yields a twist angle of -12° and shear angle of 30° (Groom et al., 1993). The 3D scattering effects of the hemisphere in this data set are first-order effects while the inductive response of the 2D structure has a much smaller effect, making this a good data set for testing the extended decomposition routine. Figure 4.4 shows histograms of the regional strike, twist and shear angles resulting from a GB analysis of the theoretical

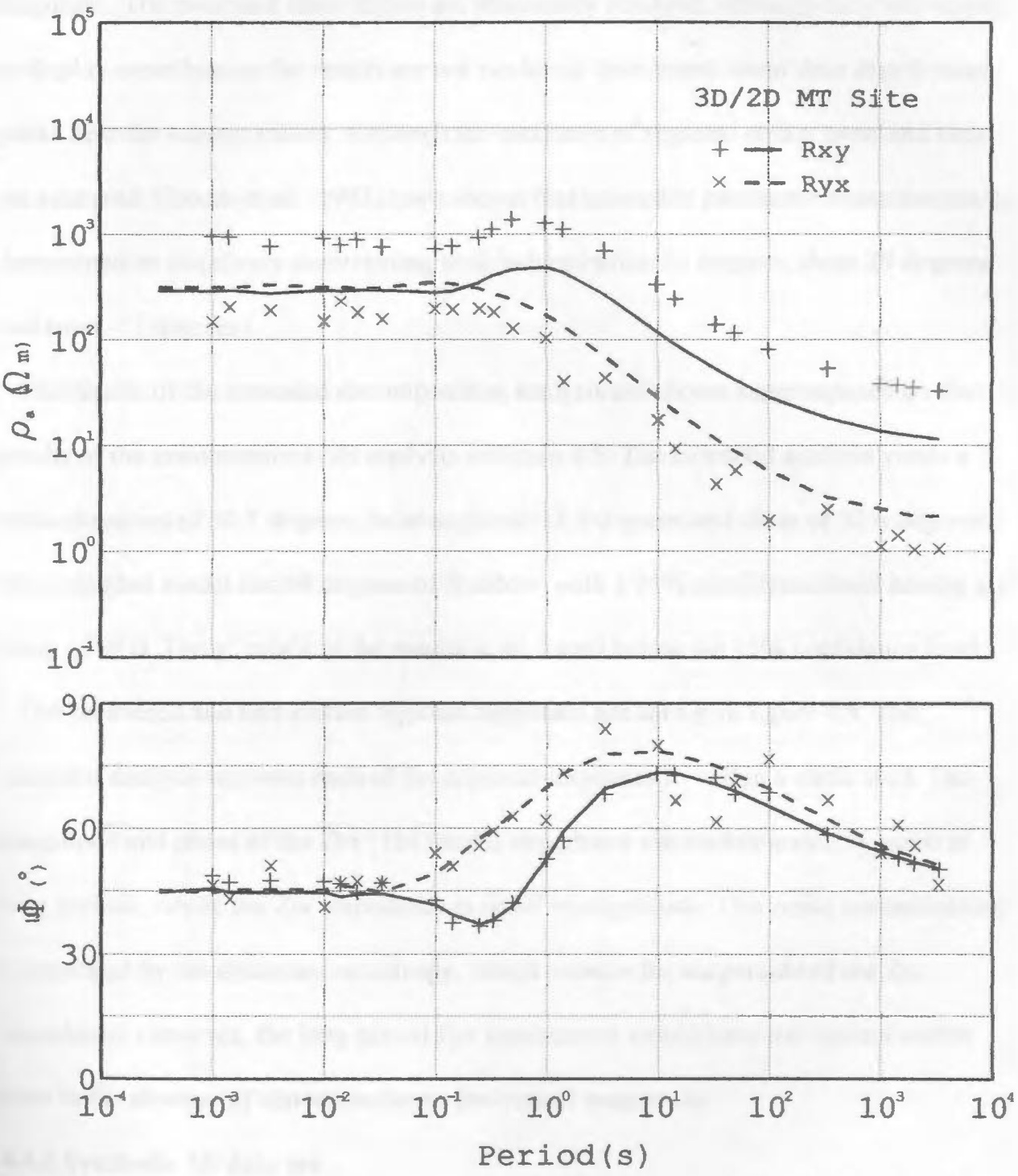

Figure 4.6 Plot of the undistorted and recovered regional impedances for the 3D/2D synthetic site. The undistorted response is indicated by the solid and dashed lines, the recovered response by the symbols + and x.

responses. The twist and shear angles are reasonably resolved, although they both appear to display some bias as the results are not randomly distributed about their distribution peaks near the correct values. Although the estimates of regional strike, twist and shear are scattered, Groom et al. (1993) have shown that easonable parameter estimates can be determined by iteratively constraining their values (strike 30 degrees, shear 29 degrees and twist -11 degrees).

The results of the extended decomposition analysis are shown superimposed on the results of the unconstrained GB analysis in figure 4.5. The extended analysis yields a strike direction of 30.7 degrees, twist angle of -13.0 degrees and shear of 30.6 degrees. The extended model has 69 degrees of freedom, with a 95% confidence level having a χ^2 value of 90.0. The χ^2 misfit of the model is 49.5 well below the 95% confidence level.

The recovered and undistorted regional responses are shown in figure 4.6. The extended analysis recovers each of the regional responses to within a static shift. The magnitude and phase of the *Zyx* (TM mode) impedance are contaminated by noise at long periods, where the *Zyx* impedance is small in magnitude. This noise contamination is enhanced by the distortion anisotropy, which reduces the magnitude of the *Zyx* impedance. However, the long period *Zyx* impedances would have the highest scatter even in the absence of distortion due to their small magnitude.

4.4.3 Synthetic 2D data set

As a final theoretical example, we will consider simultaneous decomposition analysis of an entire data set. Ten synthetic magnetotelluric sites were produced using

Wannamaker's finite element algorithm (Wannamaker et al., 1984). The conductivity structure used to compute the synthetic data set is shown in figure 4.7. The ten synthetic sites were distorted by multiplying their responses with synthetic distortion matrices (C). The twist and shear values of the synthetic distortion matrices applied to the data are given in table 4.1. The distortions are solely that of galvanic telluric distortion. The resultant sites therefore obey the decomposition model, having no 3D inductive effects or magnetic distortions. Gaussian noise, having a magnitude of 2% of the largest impedance element, was added to the distorted responses to simulate experimental noise.

Plots of the decomposition parameters found by unconstrained GB analysis of the synthetic data set are shown in figure 4.8. Examination of these plots indicates that for

Site	True Value		Decomposition Result	
	Shear	Twist	Shear	Twist
SYN001	20.0	-20.0	20.1	-20.1
SYN002	-10.0	40.0	-10.1	40.2
SYN003	25.0	-15.0	25.2	-15.1
SYN004	40.0	20.0	39.9	19.7
SYN005	-25.0	-40.0	-25.0	-40.0
SYN006	-20.0	30.0	-20.2	30.1
SYN007	-35.0	-50.0	-34.9	-50.1
SYN008	25.0	-10.0	25.1	-10.1
SYN009	35.0	-5.0	35.1	-5.3
SYN010	15.0	45.0	14.8	45.1

Table 4.1 Results of decomposition of synthetic 2-D data set. Joint decomposition found a regional strike of 30.3, close to the real value of 30.0 degrees.

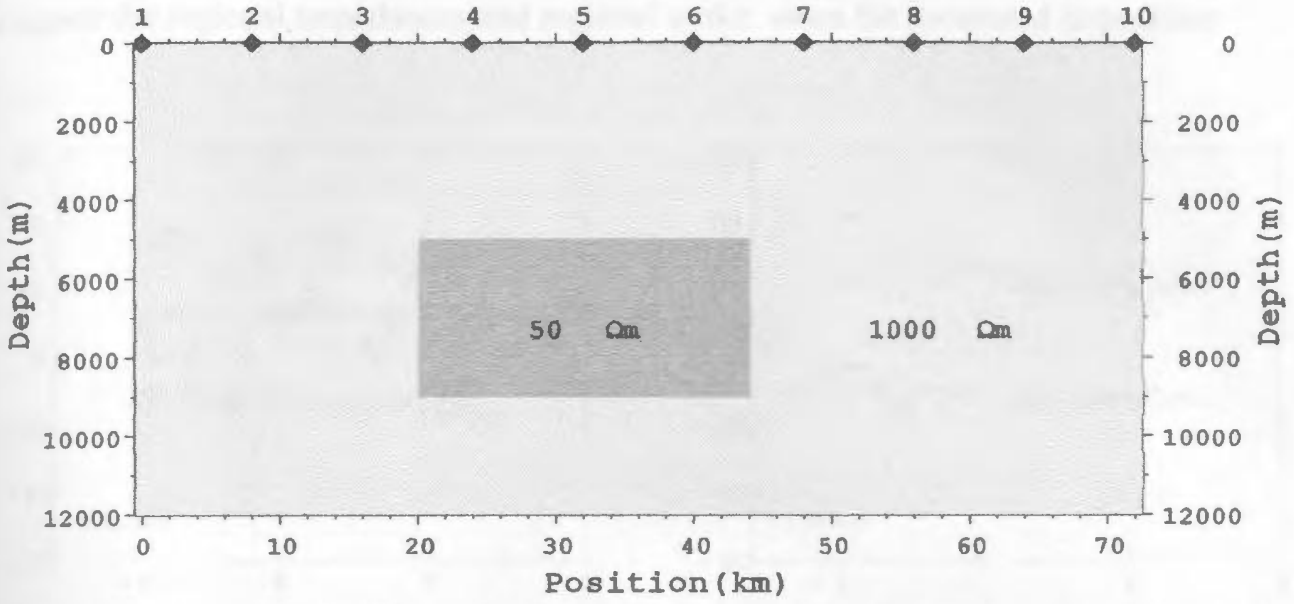

Figure 4.7 Conductivity structure used to produce a set of 10 synthetic MT soundings. The position of the 10 soundings are indicated along the top of the structure.

virtually all of the sites twist and/or shear are well-resolved parameters. However, the regional strike is poorly resolved for many of the sites. This example clearly demonstrates the effect galvanic distortion and noise can have on the resolution of strike.

The results of simultaneous decomposition of the ten sites are given in table 4.1. The extended decomposition routine found a regional strike of 30.3 degrees, very close to the correct value of 30.0 degrees. Additionally, the routine found accurate estimates of the twist and shear angles, enabling the accurate recovery of the regional responses (not shown). The extended decomposition model has 1219 degrees of freedom, with a 95% confidence level of 1303.4. The χ^2 misfit of the model was 512, well below the 95% confidence level.

4.4.4 Confidence limits

The theoretical examples demonstrate that the extended GB analysis can accurately

recover the regional impedances and regional strike, when the measured impedance

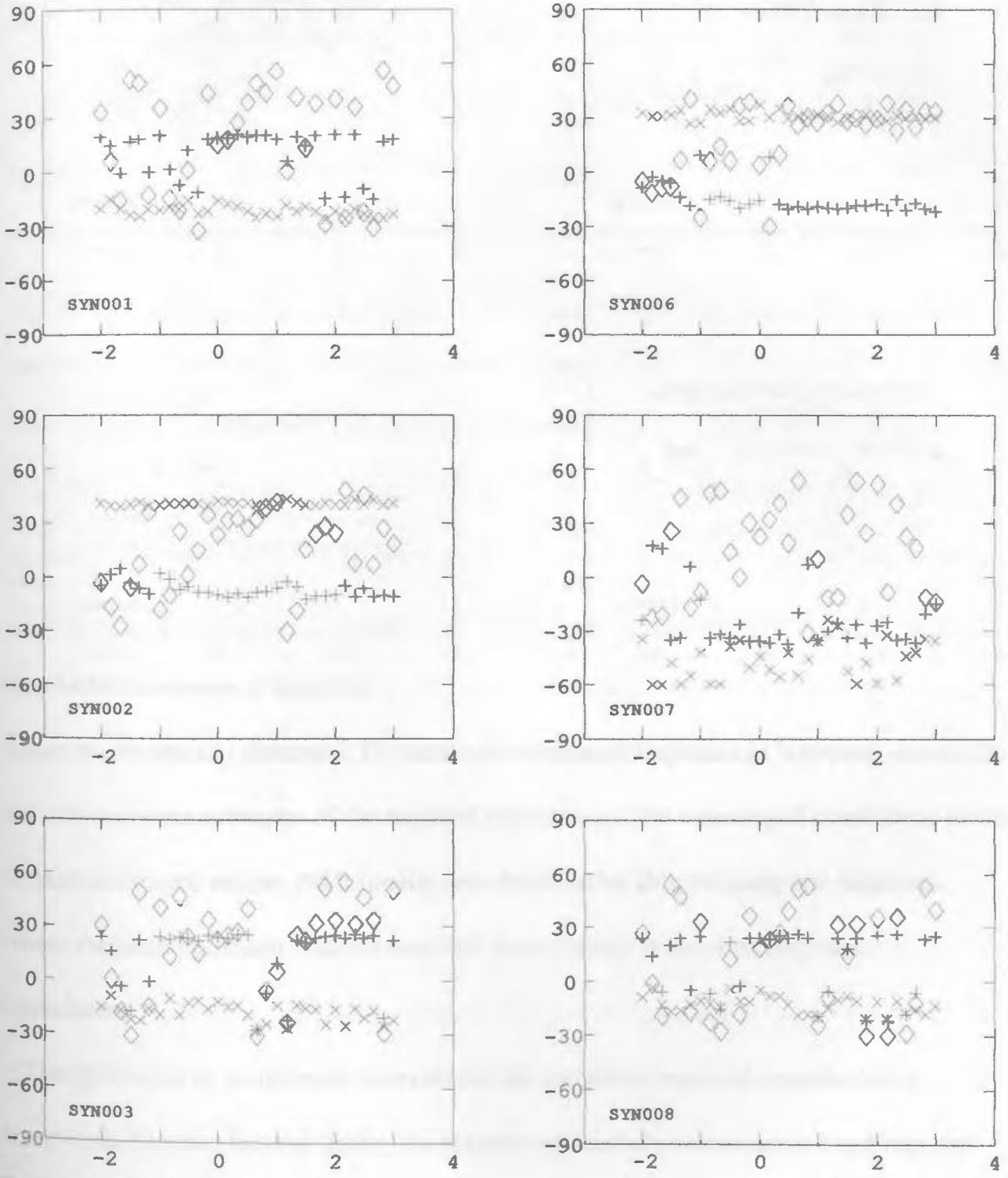

Figure 4.8a Plot of the decomposition parameters (strike ◊, twist X, shear +) for each of the 10 synthetic soundings, found using unconstrained GB analysis (continued in figure 4.8b).

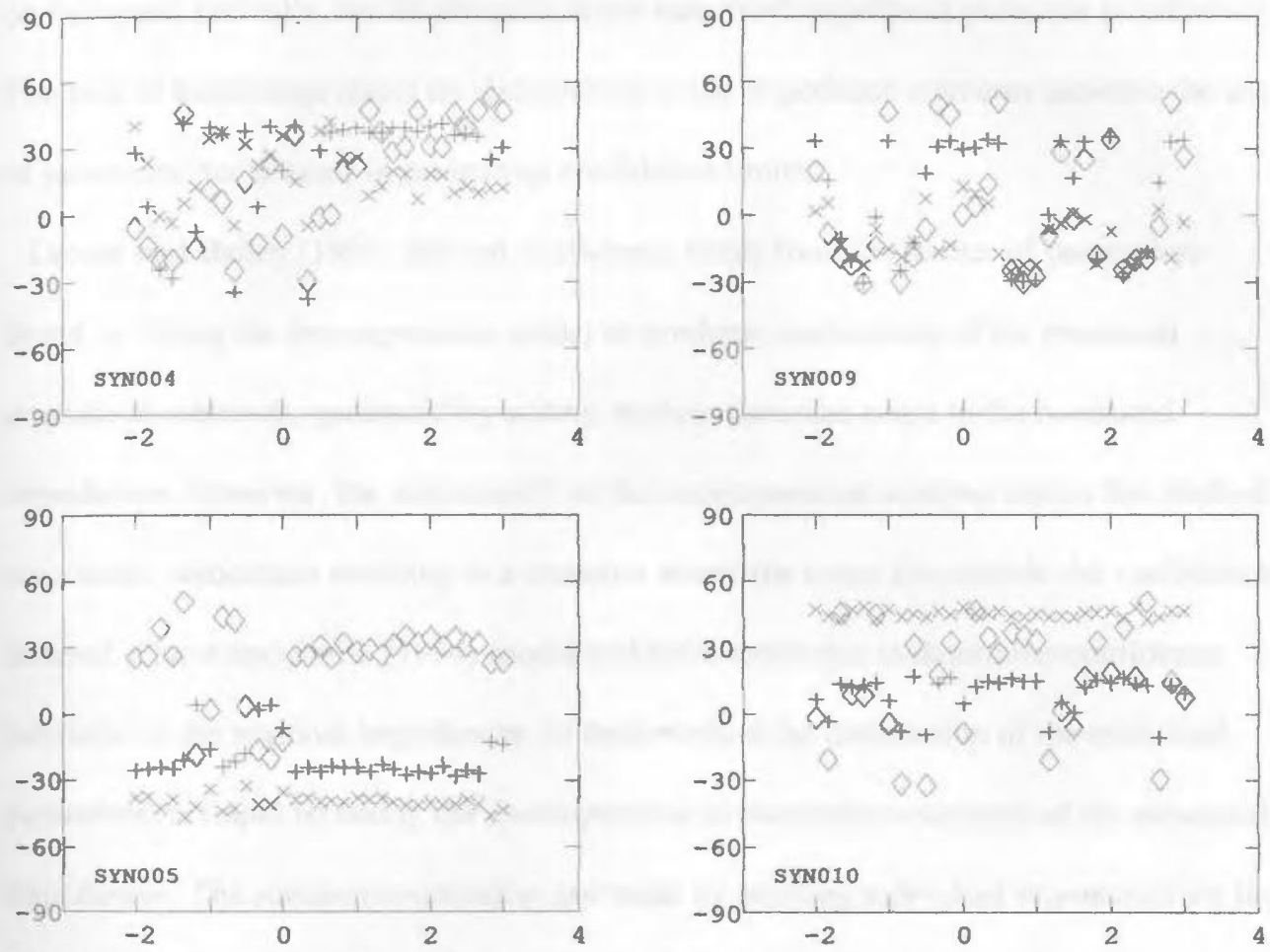

Figure 4.8b Continuation of figure 4.8a

tensor is galvanically distorted. To model the recovered impedances however, one needs not only accurate estimates of the regional impedances, but meaningful confidence limits on their estimated values. Additionally, one needs to be able to recognize situations where the decomposition analysis may fail to accurately recover the regional impedances.

The derivation of confidence intervals for the estimated regional impedances is complicated by two factors: firstly, the transformation between measured and regional impedances is nonlinear, and therefore the parameters do not have a linear dependence

on the noise; secondly, the distribution of the measured impedance elements is unknown. The lack of knowledge about the distribution of the impedance elements prevents the use of parametric techniques in estimating confidence limits.

Groom and Bailey (1991) derived confidence limits from the scatter of parameters found by fitting the decomposition model to synthetic realizations of the measured impedance elements, generated by adding random Gaussian noise to the measured impedances. However, the nonlinearity of the decomposition analysis makes this method inaccurate, sometimes resulting in a situation where the mean lies outside the confidence interval. Chave and Smith (1994) used a jackknife technique to determine confidence intervals on the regional impedances. In their method the distribution of the estimated parameters is found by fitting the decomposition to successive estimates of the measured impedances. The successive estimates are made by deleting individual estimates from the calculation of the mean impedances. This method is superior since it makes no assumptions about the distribution of the errors, although it requires all the estimates of the measured impedances tensor not just the mean value.

As the jackknife method cannot be performed without reprocessing from time series, a method similar to that of Groom and Bailey (1991) will be used to derive the desired confidence limits. The confidence limits on the distortion parameters are usually not of interest, only those on the regional impedances. The distortion parameters are therefore fixed at the values found from decomposing the mean measured impedance elements. When the distortion parameters are fixed, the measured impedances can be rotated to the

regional coordinate system linearizing the decomposition equations. In the regional coordinate system the summary decomposition equations given by equation 4.8 reduce to

$$\begin{aligned}
\alpha_0 &= Z_{xx} + Z_{yy} = e\delta + t\sigma \\
\alpha_1 &= Z_{xy} + Z_{yx} = \delta - te\sigma \\
\alpha_2 &= Z_{yx} - Z_{xy} = te\delta - \sigma \\
\alpha_3 &= Z_{xx} - Z_{yy} = -t\delta - e\sigma
\end{aligned} \qquad (4.26)$$

and the measured impedances are described by four complex linear equations. The measured impedances in the regional coordinate system can be found by rotating the Fourier spectra and calculating the impedance estimates from the re-calculated cross-spectral estimates. This provides accurate estimates of the errors on the measured impedances in the regional coordinate system. Synthetic realizations of the rotated measured impedances are then generated by adding Gaussian noise. These realizations are then decomposed (linear), and confidence limits are estimated from the spread of the resultant impedances. This method does not suffer from bias present in the Groom and Bailey (1991) method, as the decomposition is linear. The only limitation is the assumption that the error distribution is Gaussian; it is difficult to assess the error introduced by this assumption since the real distribution is unknown.

4.4.5 Decomposition versus Rotation

It is important to recognize that the regional impedances and confidence limits found

solely by rotating the measured impedances are not equivalent to those found through

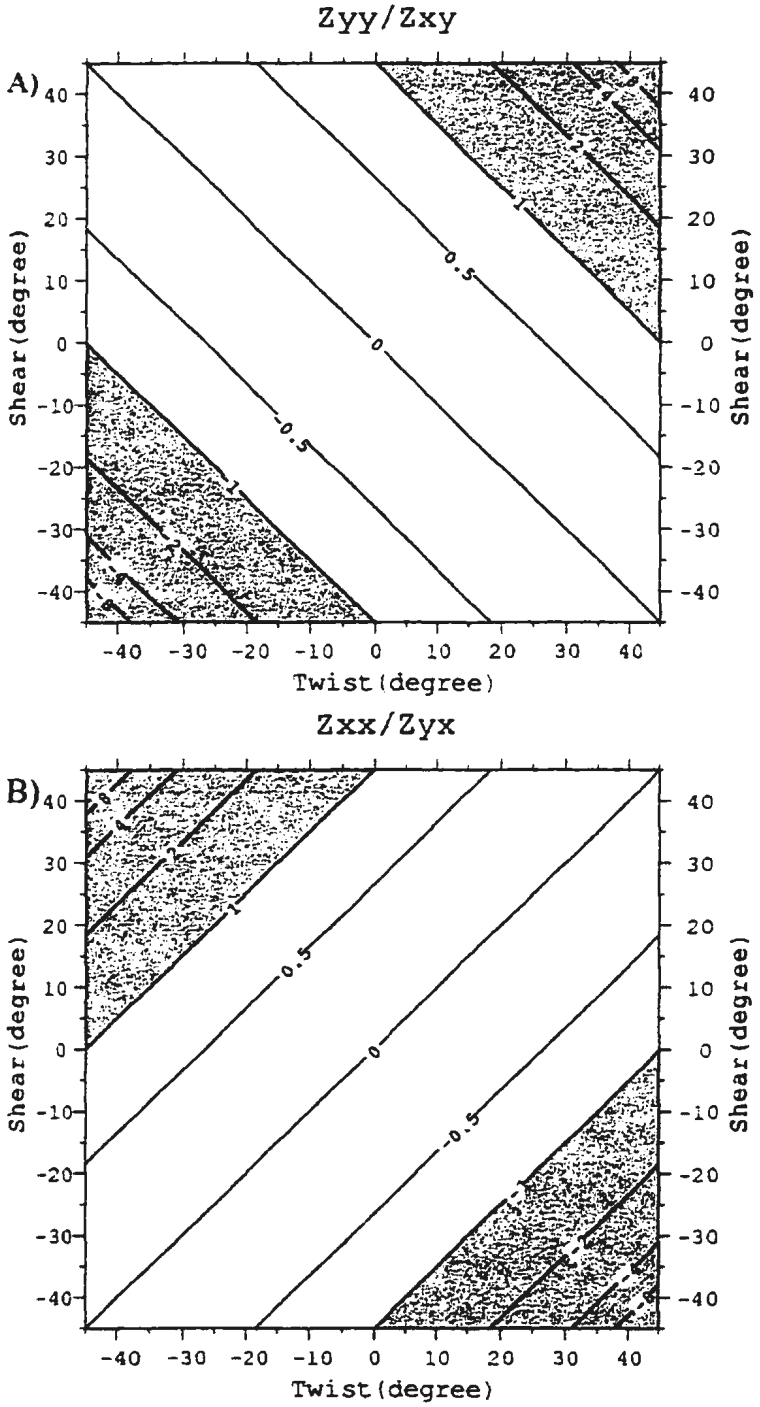

Figure 4.9 Plots of the ratios of the diagonal and anti-diagonal impedance magnitudes as a function of twist and shear. The ratio Zyy/Zxy is shown in A, the ratio Zxx/Zyx in B.

decomposition analysis, even if the regional strike is accurately known. When the measured impedance tensor is rotated to the regional coordinate system, each column of the tensor contains two estimates of one of the regional impedances (see equation 4.9). In rotation the anti-diagonal impedance elements are used as estimates of the regional impedances. While the anti-diagonal elements are scaled estimates of the true regional impedances in the presence of galvanic distortion, they may not represent the best estimates of the regional impedances. Depending on the values of the distortion parameters, twist and shear, one of the diagonal impedance elements (Z_{xx} or Z_{yy}) may contain a better estimate, i.e., better signal-to-noise characteristics, of a regional impedance. This can be seen by examining figure 4.9 which shows plots of the ratios of the diagonal and anti-diagonal impedances magnitudes (Z_{yy}/Z_{xy} and Z_{xx}/Z_{yx}) as a function of twist and shear. When the sum of the absolute shear and twist angles exceeds 45 degrees, indicated in figure 4.9 by the shaded regions, one of the diagonal impedances is greater in magnitude than the anti-diagonal impedance in its column. The larger magnitude estimate of the regional impedance will typically have a greater signal-to-noise ratio and is therefore a superior estimate of the regional impedance. Rotation does not account for the scaling produced by galvanic distortion, and in some situations will result in inferior estimates of the regional impedances. Decomposition analysis on the other hand performs essentially a weighted average of the two estimates of each regional impedances, providing a superior estimate in the presence of galvanic distortion and equivalent estimate in the absence of distortion.

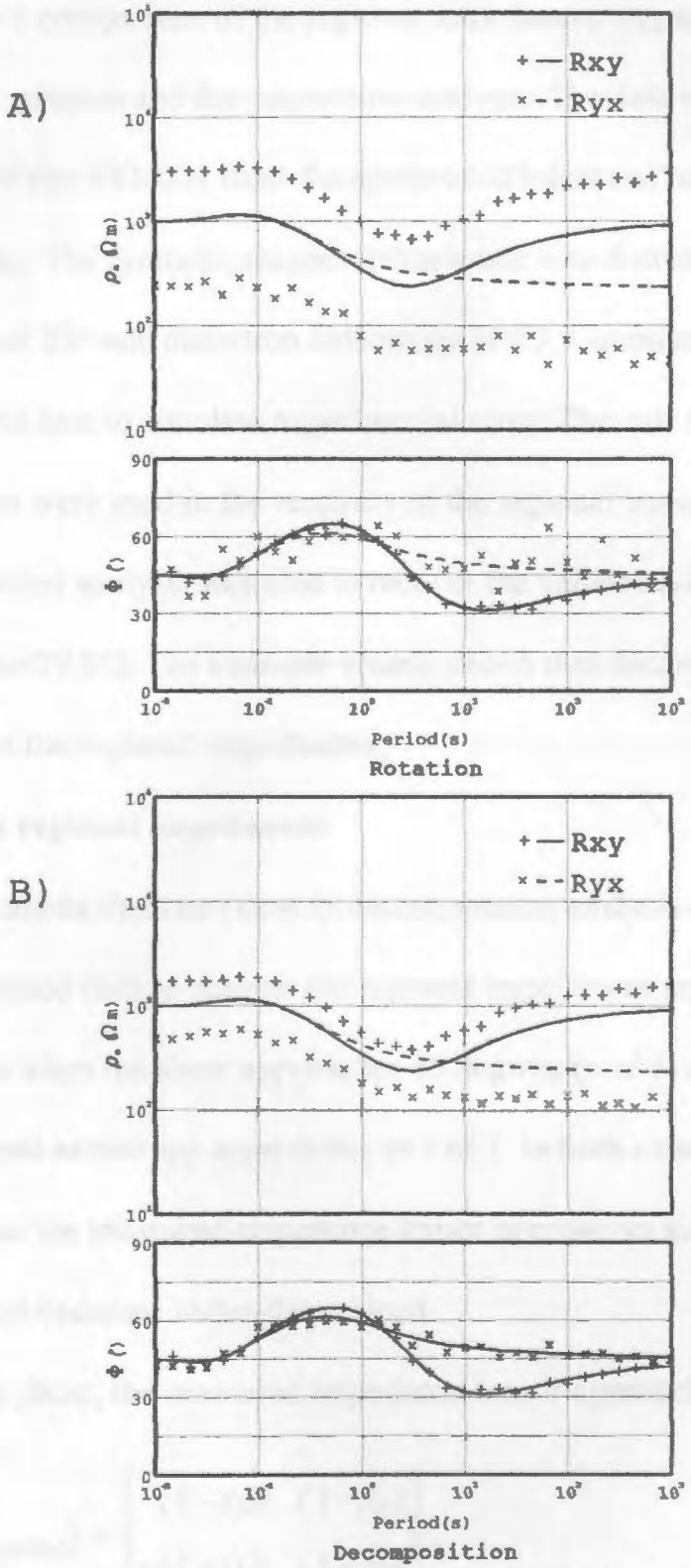

Figure 4.10 Comparison of regional responses recovered using rotation (A) and decomposition (B). The true response is indicated by the solid and dashed line, the recovered response is indicated by the + and X.

Figure 4.10 shows a comparison of the regional impedances (apparent resistivity and phase) recovered by rotation and decomposition analysis. The data used in this comparison is that of site SYN004 from the synthetic 2D data set, having a regional strike of 30.0 degrees. The synthetic magnetotelluric site was distorted by applying a twist of -35°, shear of 25° and distortion anisotropy of 0.3. Gaussian noise (3%) was added to the distorted data to simulate experimental error. The true regional strike and distortion parameters were used in the recovery of the regional impedances, however the extended decomposition analysis was able to recover the values accurately (shear -35.0°, twist 25.1° and strike 29.9°). The example clearly shows that decomposition recovers superior estimates of the regional impedances.

4.4.6 Irrecoverable regional impedances

There are two situations that can occur in decomposition analysis of the impedance tensor where the method fails to recover the regional impedances accurately. Decomposition fails when the shear approaches 45 degrees (e of 1) or when the sum of distortion and regional anisotropy approaches an s of 1. In both situations, decomposition analysis fails because the measured impedance tensor approaches singularity and the decomposition model becomes under-determined.

In the case of high shear, the measured impedance tensor approaches

$$Z_{meas}(\theta_{regional}) = \begin{bmatrix} -(1-t)B & (1-t)A \\ -(1+t)B & (1+t)A \end{bmatrix}, \qquad (4.27)$$

in the regional coordinate system. The two rows of the impedance tensor become linearly dependent. In fact the two rows of the impedance tensor are linearly dependent in any coordinate system. The strike therefore is unresolved, as the impedance tensor assumes the form of a distorted 2D tensor in any coordinate system. The shear angle will be well resolved by the linear dependence of the two rows, although only the sum of the regional strike and twist angles will be resolved. The twist t becomes

$$t(\theta) = t - \tan(\theta - \theta_{regional}) \qquad (4.28)$$

where $(\theta - \theta_{regional})$ is the regional strike error. In order to recover the regional impedances, the strike must be found from adjacent sites or other independent information.

In the high anisotropy case, the measured impedance tensor in the regional coordinate system will approach one of two forms

$$Z_{meas}(\theta_{regional}) = \begin{bmatrix} -(e-t)B & 0 \\ -(1+te)B & 0 \end{bmatrix}, \qquad (4.29)$$

or

$$Z_{meas}(\theta_{regional}) = \begin{bmatrix} 0 & (1-te)A \\ 0 & (e+t)A \end{bmatrix}. \qquad (4.30)$$

The distortion parameters will not be resolved and, while a strike angle is resolved, it

cannot be determined if it is that of the regional structure or local distorter. If the strike determined by decomposition is in agreement with the regional strike found at other sites it may be reasonable to assume that the recovered impedances are those of the regional structure.

4.5 Summary

In this chapter, an extension of Groom-Bailey decomposition analysis was developed. The extended analysis allows one to find the most consistent 2D parameters from a set of sites over a given frequency range. The estimate of regional strike found through this analysis is consistent with frequency, site location and data precision dependencies. The recovered impedances, where the 3D/2D decomposition model holds, are free of first-order effects of galvanic distortion, and the procedure provides a validation for further 2D interpretation. While the extended analysis provides a rapid method for data analysis, careful use of this global minimization is advocated, as the model parameters may vary with frequency.

CHAPTER 5

Regional Conductivity Structure

5.1 Introduction

A number of parameters calculated from magnetotelluric observations quantitatively delineate the regional conductivity structure of the Orogen. Magnetotelluric measurements are sensitive to changes in electrical conductivity both at depth and laterally. The depth and distance of investigation are governed by a skin-depth effect (equation 3.27), with high frequency observations (short periods) most sensitive to conductivity structure close to the site and low frequencies (long periods) to more distant conductivity structure. This frequency dependence allows one to the map geoelectrical structure of the Orogen as a function of pseudo depth.

Groom-Bailey strikes, induction vectors (transfer functions) and the determinant phases are useful parameters in mapping conductivity structure. However, since the depth of investigation is not solely dependent on frequency but additionally on the conductivity structure in the vicinity of the site, laterally distant sites may be sensitive to different depths and lateral distances of investigation. This possible variation in depth of investigation as a function of position complicates the interpretation of the parameter plots. However, regional trends in the parameters that correlate with changes in surface geology of the Orogen are most likely significant.

Before examining regional plots of the magnetotelluric parameters, estimating the response of the ocean surrounding the Island of Newfoundland is important. Conductive

sea water can have a significant response (Parkinson, 1959, 1962), obscuring the response of the regional conductivity structure. Recognition of portions of the data affected by coast effect allows one to separate trends associated with the ocean's response from those associated with changes in the regional conductivity structure.

5.2 Coast Effect

The term "coast effect" is used to describe the anomalous increase of the vertical/horizontal magnetic field ratio as a coastline is approached. The observed anomalous vertical magnetic field results from electric currents travelling along the coast in the ocean and ocean sediments. While distortion of the vertical magnetic field is the dominant effect observed, magnetotelluric impedances recorded near a coastline are also distorted. This distortion decays with increasing distance from the coast and increasing frequency of observation. In coastal regions, an estimate of the distortion produced by coast effect is essential to delineate portions of the recorded data free of distortion.

5.2.1 Coast effect at a two-dimensional coast

To illustrate coast effect, a set of eight magnetotelluric soundings, next to a simple two-dimensional ocean coast, was generated using Wannamaker's PW2D finite element algorithm (Wannamaker, 1984) (Figure 5.1a). The synthetic soundings were produced at 20 km intervals, placed from 10 km to 150 km from the coast.

The TE (Ex/Hy) and TM (Ey/Hy) mode apparent resistivities at periods of 10, 100 and 1000 seconds are plotted as a function of position in figures 5.1b and 5.1c respectively.

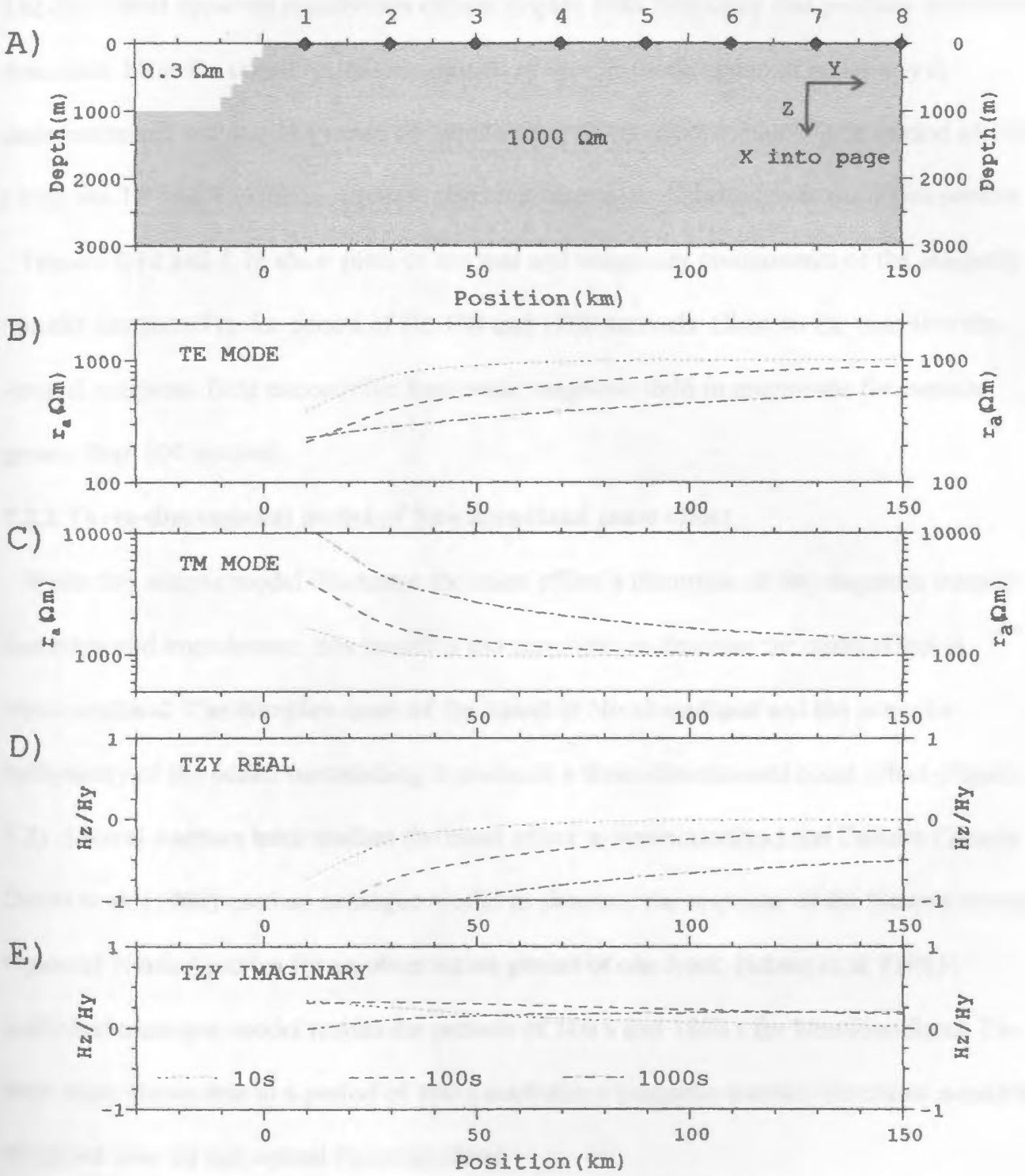

Figure 5.1 Diagram illustrating coast effect at a simple 2D coast. The 2D conductivity structure used to represent a simple coast is shown in A. TE and TM mode apparent resistivities as a function position are shown in B and C respectively. Parts D and E show the real and imaginary component of the magnetic transfer function Tzy.

The calculated apparent resistivities clearly display both frequency and position dependent distortion. Near the coastline, the magnitude of the TE mode apparent resistivity is underestimated and the TM mode apparent resistivity is overestimated. At a period of 1000 s both the TE and TM mode apparent resistivities remain distorted over the entire profile.

Figures 5.1d and 5.1e show plots of the real and imaginary components of the magnetic transfer function Tzy for period of 10, 100 and 1000 seconds. Close to the coastline the vertical magnetic field exceeds the horizontal magnetic field in magnitude for periods greater than 100 seconds.

5.2.2 Three-dimensional model of Newfoundland coast effect

While this simple model illustrates the coast effect's distortion of the magnetic transfer functions and impedances, this model is too simplistic to describe the coast effect in Newfoundland. The complex coast of the island of Newfoundland and the irregular bathymetry of the ocean surrounding it produces a three-dimensional coast effect (Figure 5.2). Several Authors have studied the coast effect in Newfoundland and Eastern Canada: Dosso et al. (1980) used an analogue model to simulate the response of the Eastern coastal region of North America for an observation period of one hour; Hebert et al. (1983) published analogue model results for periods of 100 s and 1800 s for Newfoundland. The later study shows that at a period of 100 s anomalous magnetic transfer functions would be observed over all but central Newfoundland.

To estimate the coast effect at periods above the published 100 s results, a three-dimensional model of Newfoundland and surrounding ocean was undertaken.

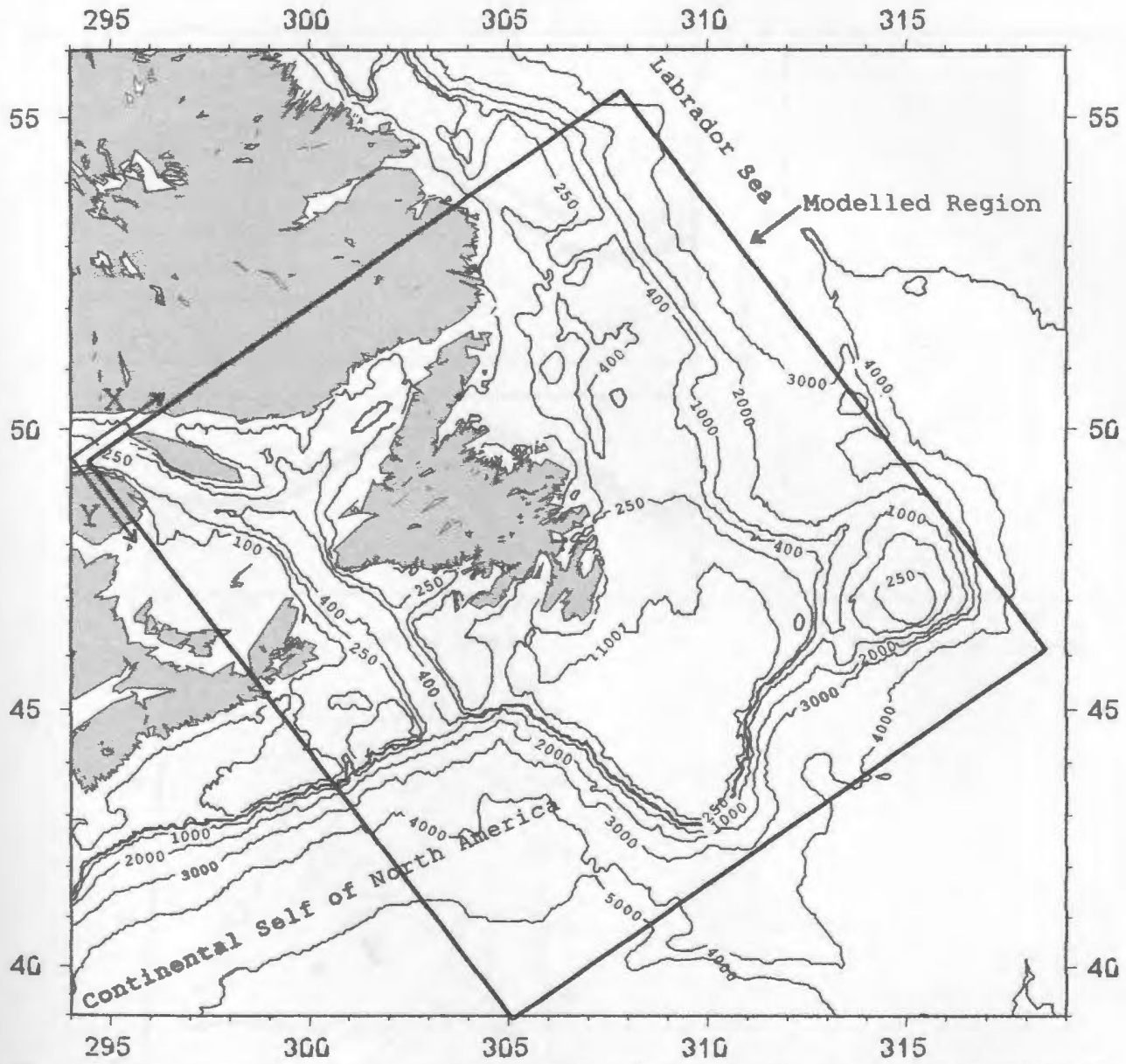

Figure 5.2 Bathymetry of the waters surrounding Newfoundland. The region modelled to estimate coast effect is indicated by the outlined region.

Using the difference equation 3D forward algorithm of Mackie et al. (1993), the island of Newfoundland and surrounding bathymetry were represented by a 28×31×16 (X×Y×Z) model.

The region modelled is shown in Figure 5.2, a bathymetry map of the waters surrounding

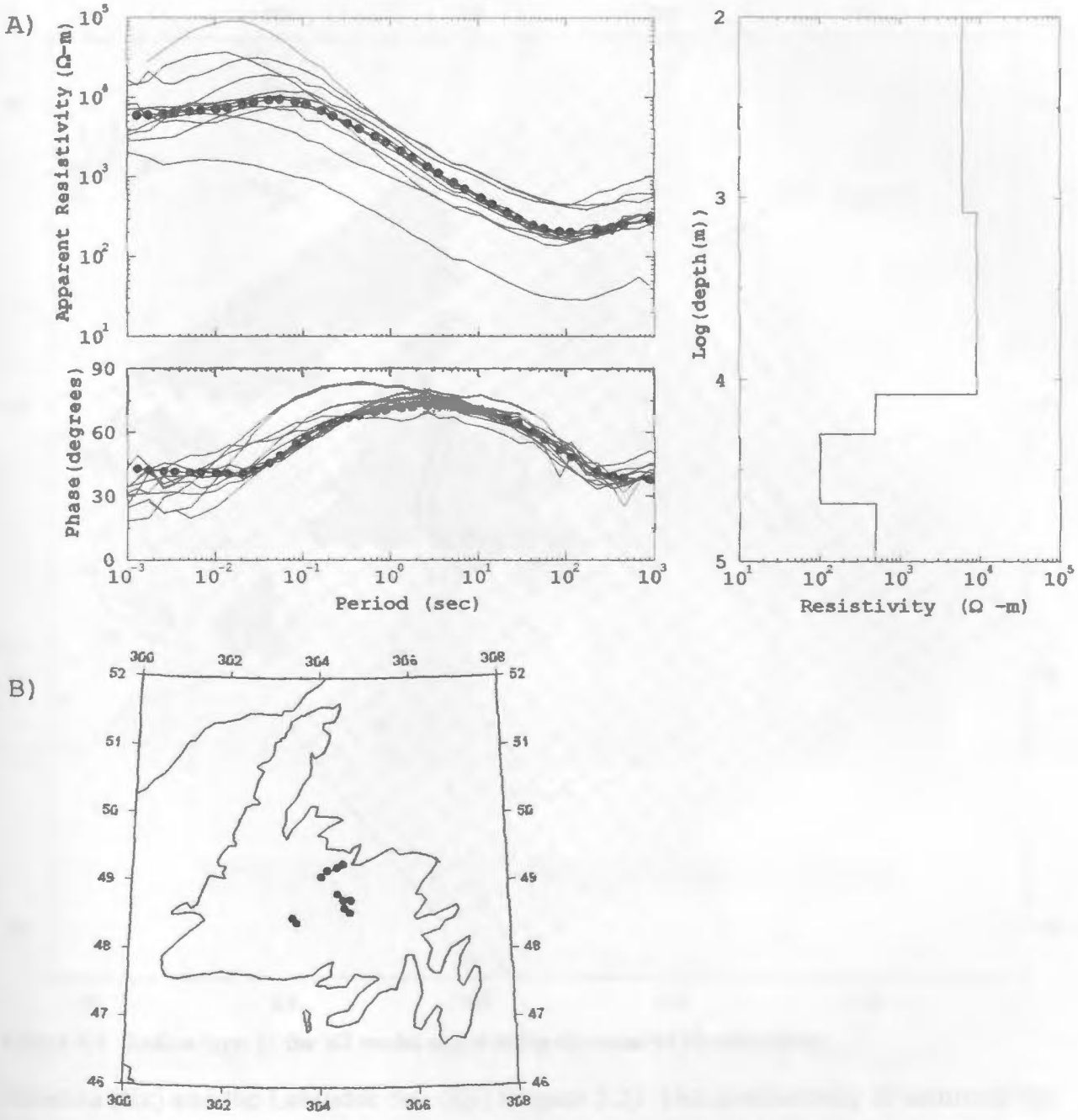

Figure 5.3 Calculation of a 1D resistivity-depth structure representative of the Newfoundland region. A shows the result of inverting the average of 11 apparent resistivity and phase curves (determinant average). The location of the 11 soundings is indicated in part B.

Newfoundland. A rotation of 57° east of north was used to produce the 3D model. This allows the models two electric field polarizations to parallel the continental self of North

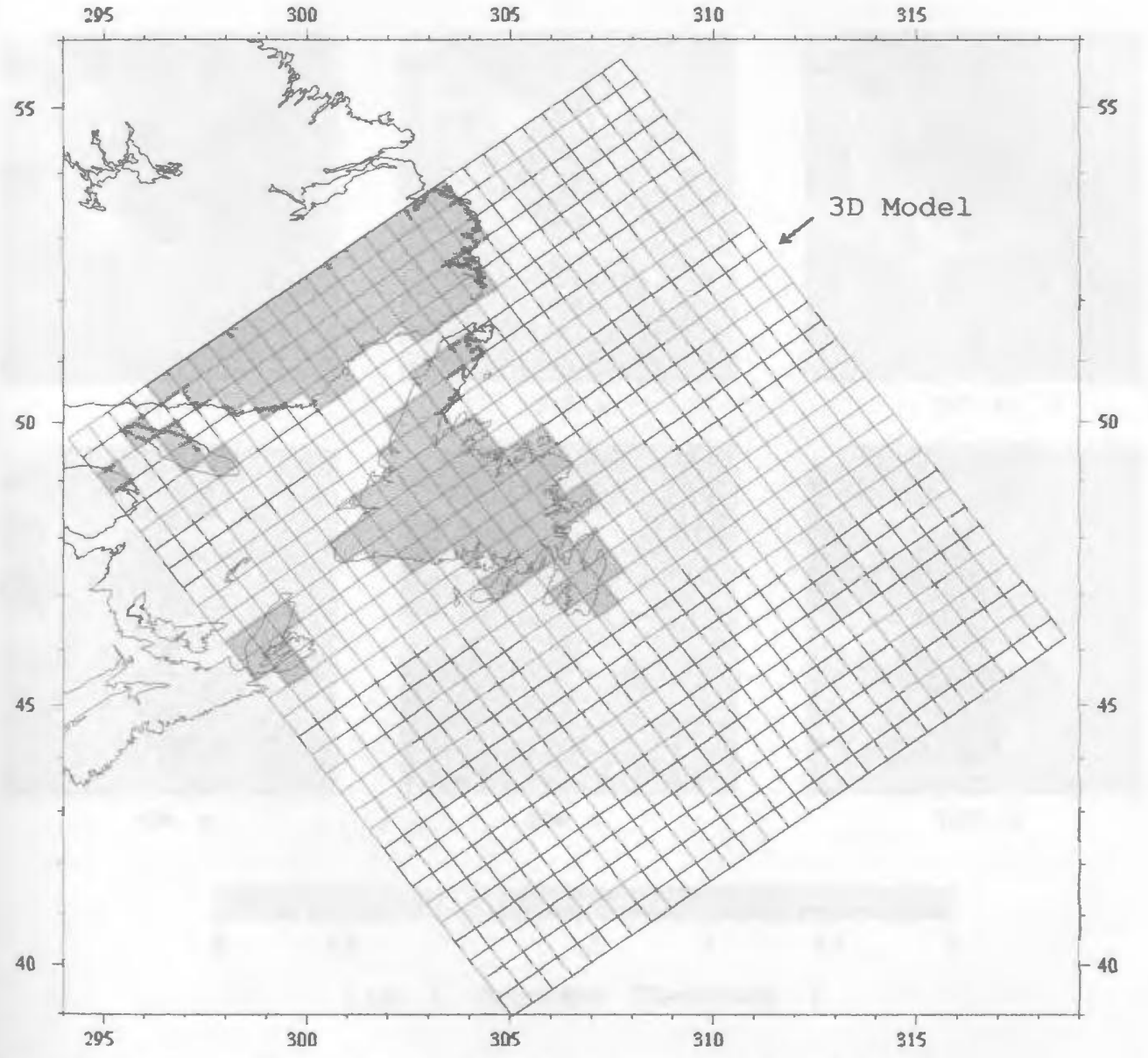

Figure 5.4 Surface layer of the 3D model representing the coast of Newfoundland.

America (Ex) and the Labrador Sea (Ey) (Figure 5.2). The conductivity structure of the region was simulated by superimposing the bathymetry of the region on a 16 layer one-dimensional Earth. A one-dimensional conductivity structure representative of the region was found through 1D inversion of the average of 11 magnetotelluric responses (Determinant average apparent resistivity and phase) (Figure 5.3a), recorded in north

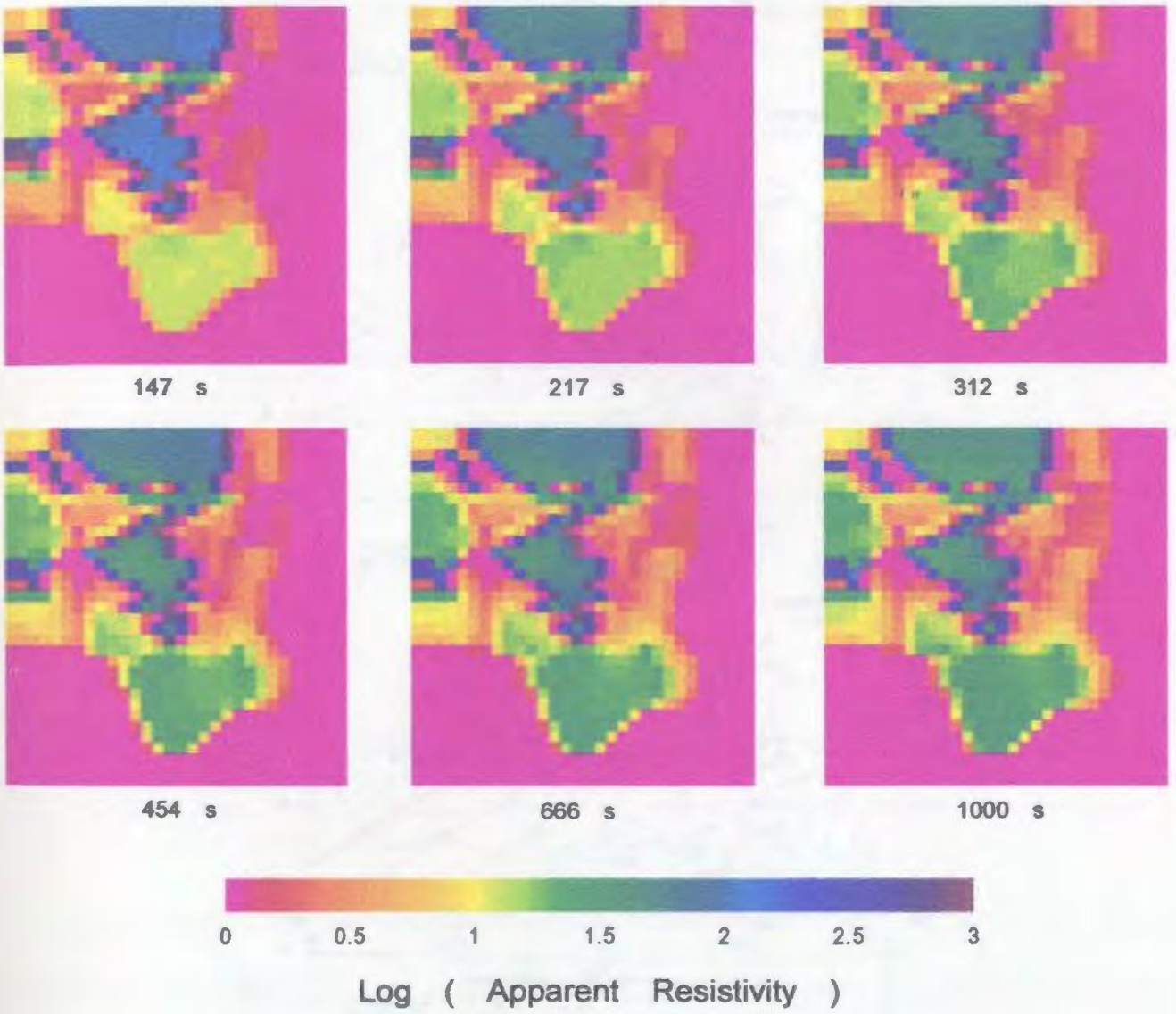

Figure 5.5 Modelled apparent resistivity (Rxy) for periods 147, 217, 312, 454, 666 and 1000 s.

central Newfoundland (Figure 5.3b). The model's accuracy in representing the coast of Newfoundland can be judged by examining Figure 5.4, a plot of the surface layer of the model. The coast of the island is reasonably approximated and should allow the model to predict a first-order estimate of Newfoundland coast effect.

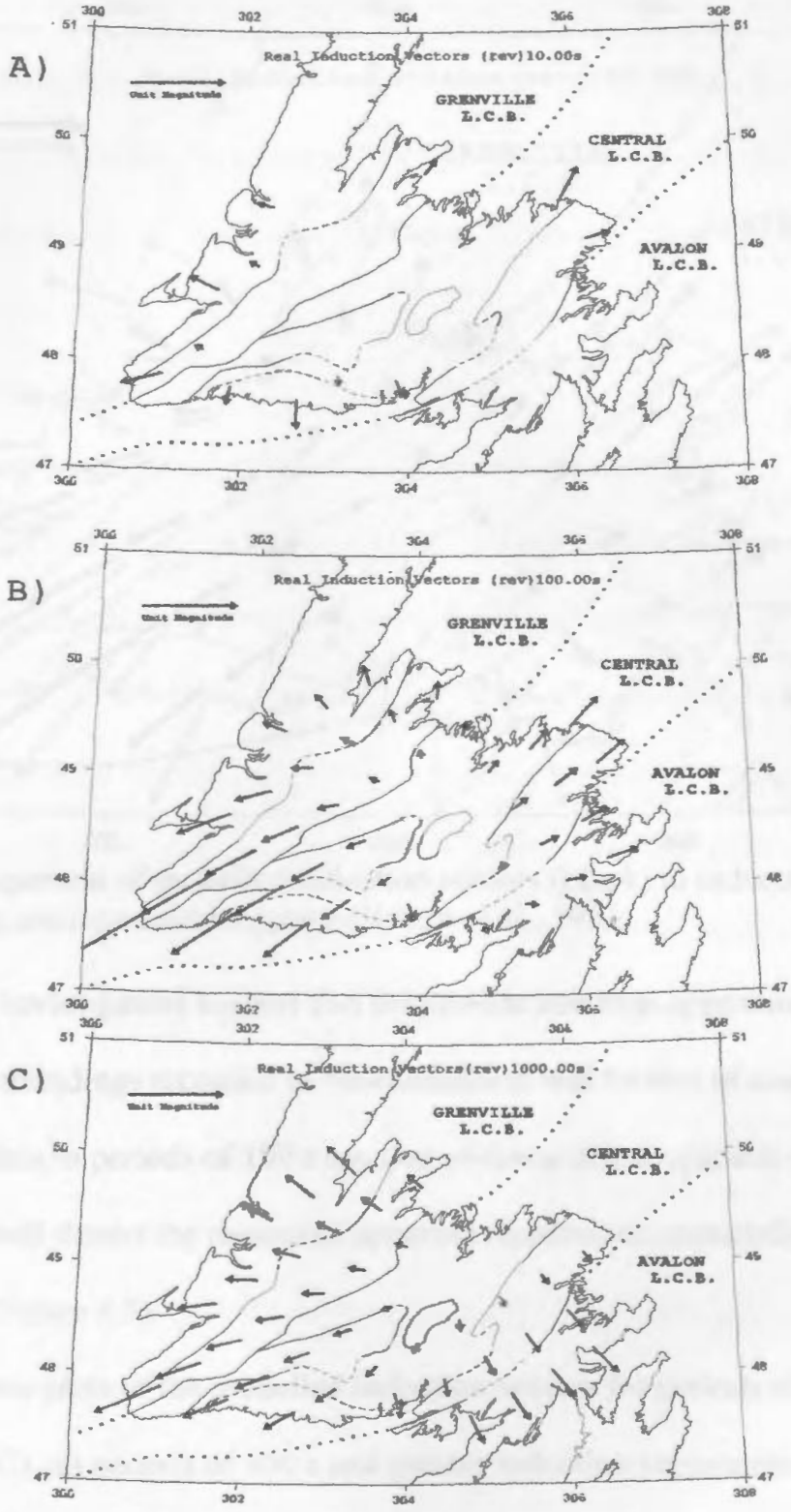

Figure 5.6 Modelled induction vectors for periods of 10, 100 and 1000 seconds.

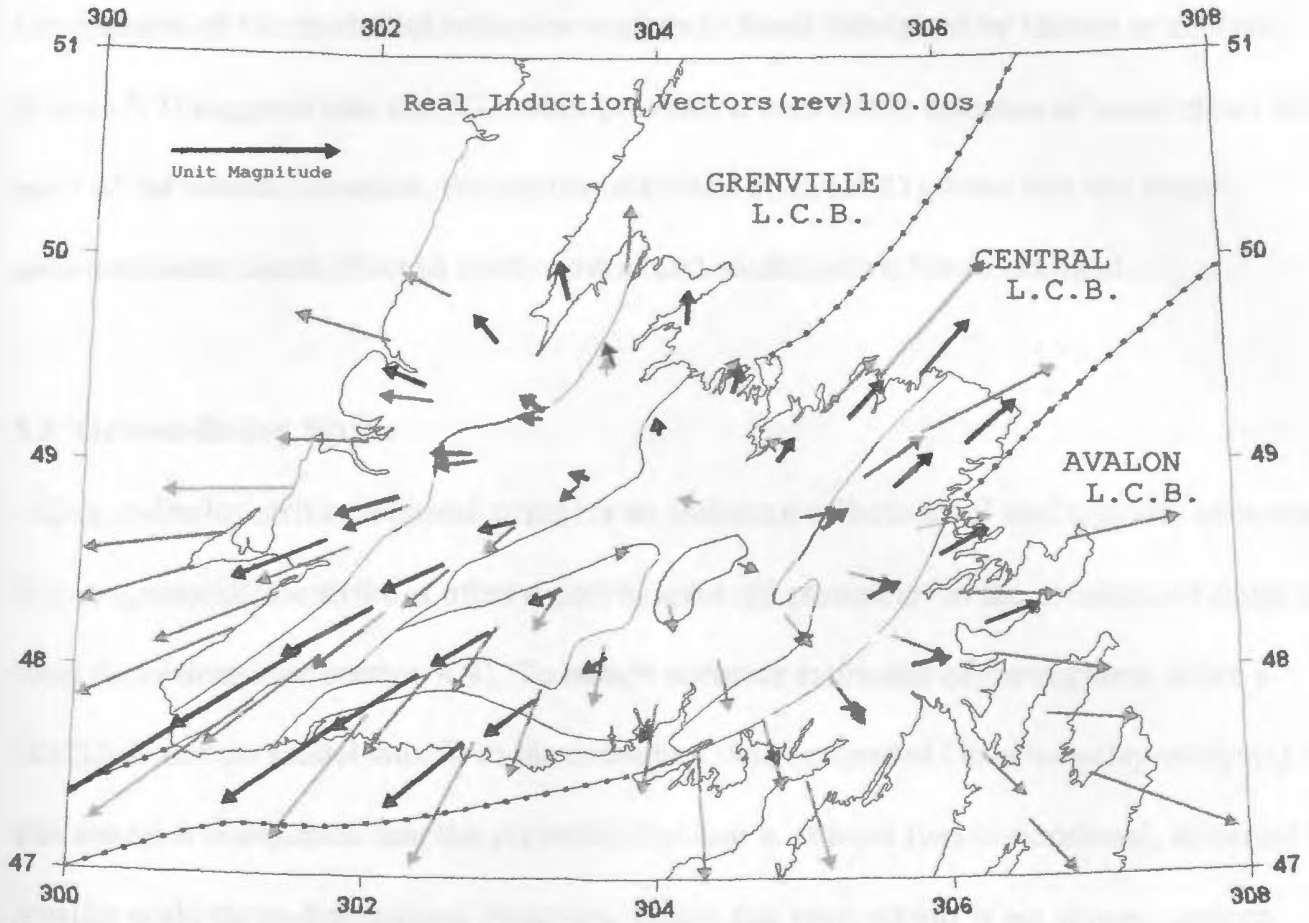

Figure 5.7 Comparison of modelled induction vectors (black) to induction vectors produced with an analogue model (grey) (Hebert et al., 1983).

Results of this investigation suggest that for periods less than approximately 10 s all the magnetotelluric soundings recorded in Newfoundland will be free of coast effect. In central Newfoundland data to periods of 100 s are free of distortion. At periods longer than 100 s the coast effect will distort the measured apparent resistivities, especially in southwestern Newfoundland (Figure 5.5).

Figure 5.6 shows plots of the modelled induction vectors for periods of 10 s (A), 100 s (B) and 1000 s (C). At periods of 100 s and greater induction vectors recorded in southwestern and northeastern Newfoundland will be significantly distorted by coast effect.

Comparison of the modelled induction vectors to those published by Hebert et al.(1983) (Figure 5.7) suggests that the 3D model provides a reasonable estimate of coast effect for most of the island. However, the results of Hebert et al. (1983) show that the model underestimates coast effect in south central and southeastern Newfoundland.

5.3 Groom-Bailey Strike

Groom-Bailey strike (regional strike) is an indicator of both local and regional structure. The magnetotelluric strike is often a poorly resolved parameter in the presence of noise and local distortions (see section 4.4). To obtain accurate estimates of the regional strike a 3D/2D distortion model was fit to the measured data (extended Groom-Bailey analysis). In this model it is assumed that the regional structure is at most two-dimensional, distorted by smaller scale three-dimensional structure. While this assumption is not always correct, application of the model provides constraints on the conductivity structure even when the model is not appropriate, as a large misfit error to the 3D/2D model is an indicator of three dimensionality.

Figure 5.8 shows plots of Groom-Bailey strikes found for the period (frequency) bands of 100Hz - 10Hz (A), 10Hz - 1Hz (B), 1s - 10s (C) and 10s - 100s (D). The strike arrows displayed in these figures are scaled by the normalized chi-squared misfit of the distortion model. The displayed error is the chi-squared error normalized by the 95% chi-squared value for the appropriate number of degrees of freedom for the period band. Large arrows on the plots therefore indicate regions of 2D regional structure, while small arrows are an

indication of 3D structue (induction), magnetic effects of galvanic charges, or of overly-optimistic error estimates.

Groom-Bailey strike directions are subject to a 90° ambiguity, as are all estimates of strike direction. Therefore whether the regional structure is parallel or perpendicular to the recovered strike direction must be inferred from other evidence. Strike ambiguity in figure 5.8 has been corrected by minimizing the angle between the regional electric strike and the regional geologic strike near the site (approximately 45°).

The regional strike is not displayed for sites having a shear with absolute value greater than 35°, as when the shear is large, the measured impedance tensor approaches singularity, and the strike is poorly defined (see section 4.4.6).

Observations (Figure 5.8)

100Hz to 10Hz (Upper Crust) (figure 5.8 (A))

- West of the GRUB line the regional strike estimates are fairly consistent at approximately 40° to 50° east of north.
- East of the GRUB line, strike angles in the Gander lake subzone and Avalon zone are approximately 10° to 20°, parallel to the Dover fault.

10Hz to 1Hz (Upper-Middle Crust) (figure 5.8 (B))

- The Humber zone and western Dunnage zone strike angles remain at a value of approximately 40° to 50°. The length of these strike arrows suggests that the northern Notre Dame subzone is reasonably 2D, with a consistent strike. In south central Newfoundland, near the Meelpaeg and Mount Cormack subzones and the

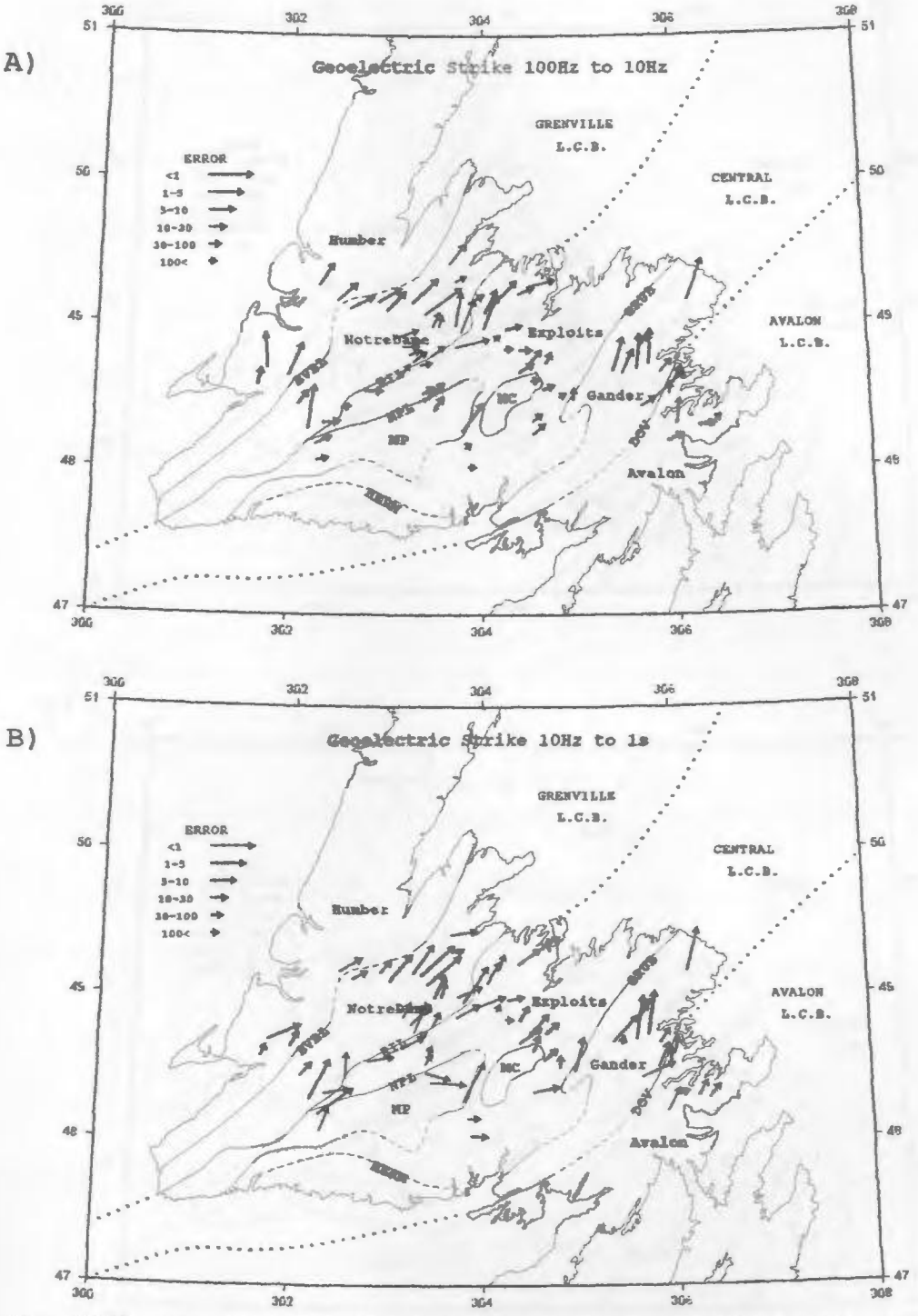

Figure 5.8a Groom-Bailey strike angles for the period (frequency) bands of 100Hz-10Hz (A), 10Hz-1Hz (B), 1s-10s (C) and 10s-100s (D) (observation point at base of arrow). Abbreviations: **Avalon**, Avalon zone; **BVBL**, Baie Verte Brompton Line; **DOV**, Dover fault; **Exploits**, Exploits subzone; **Gander**, Gander lake subzone; **GRUB**, Gander River Ultrabasic Belt; **HERM**, Hermitage Flexure; **Humber**, Humber zone; **MC**, Mount Cormack subzone; **MP**, Meelpaeg subzone; **Notre Dame**, Notre Dame subzone; **NPL**, Noel Paul's Line; **RIL**, Red Indian Line.

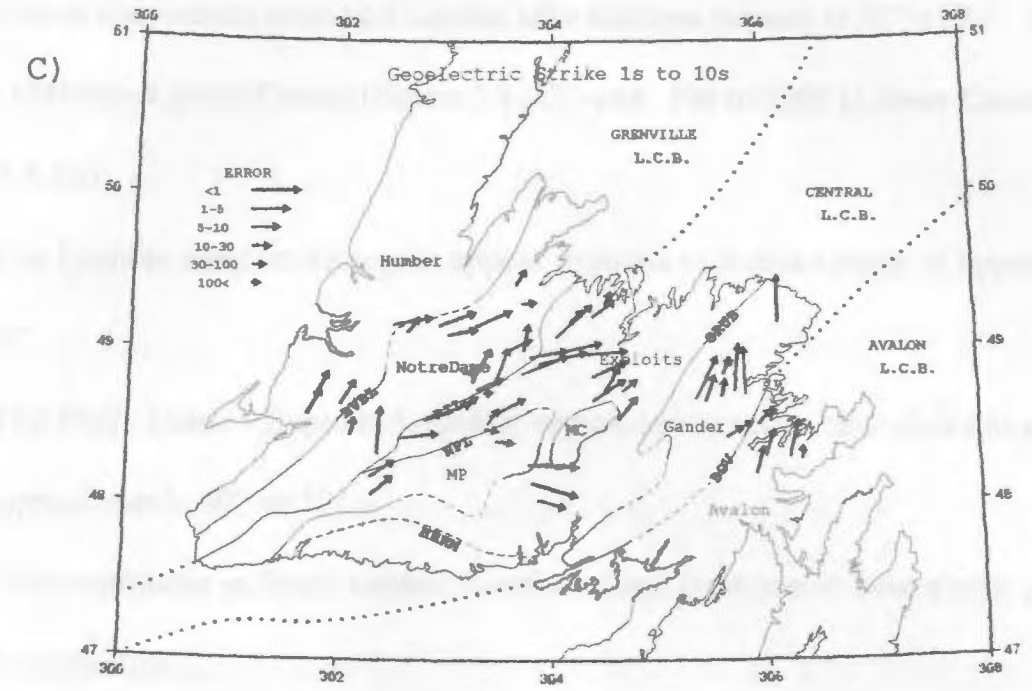

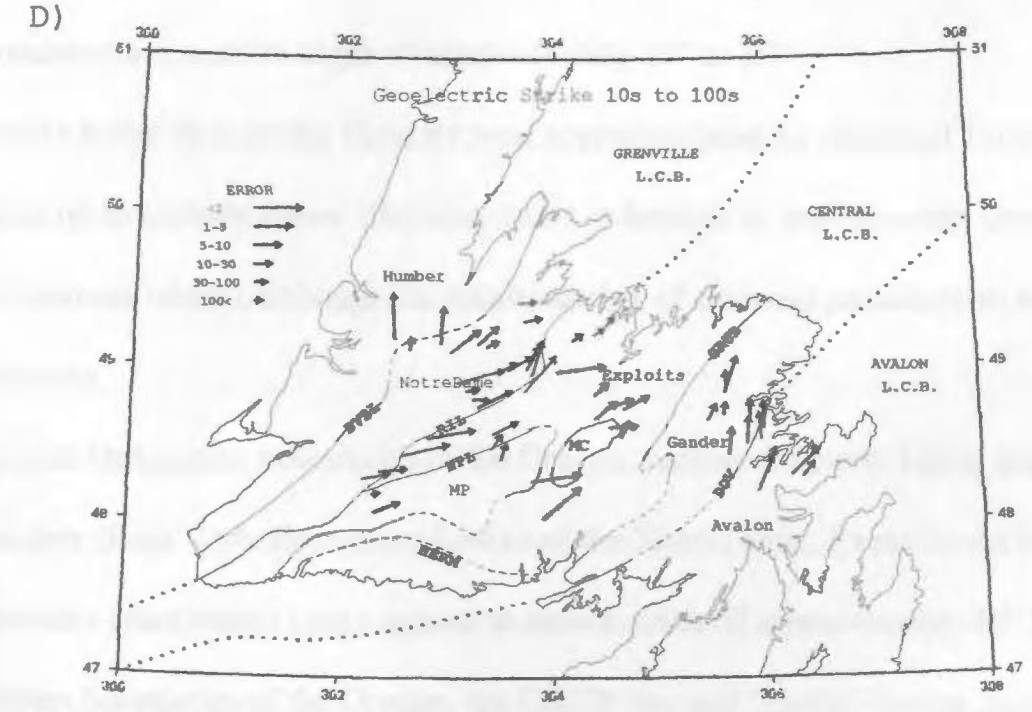

Figure 5.8b Continuation of figure 5.8a.

Hermitage flexure, the strike has changed to an angle of approximately 90° (east-west).

- Sites in the Avalon zone and Gander lake subzone remain at 10° to 20° degrees.

1s to 10s (Middle-Lower Crust) (figure 5.8 (C)) **and 10s to 100s (Lower Crust)** (figures 5.8 (D))

- The Humber zone strike angles appear to rotate to a strike angle of approximately 20°.
- The Notre Dame - Exploits boundary region continues to have strike angles of approximately 40° to 50°.
- Strike estimates in South central Newfoundland continue to have a near east-west in orientation.
- Soundings in the Avalon zone, Gander lake subzone and eastern most Exploits subzone have a strike angle of approximately 10° to 20°.

The middle-lower crust of the Humber zone appears to have an electrical strike that differs from more easterly zones. This may be an indication of pre-Taconian Grenvillian structure (tectonic fabric), although the small number of sites and proximity of the coast limit resolution.

Mid to Late Ordovician boundaries of the Orogen, such as the Notre Dame and Humber zone boundary (Baie Verte Bromptom Line) and the Notre Dame, Exploits and Gander zones boundary (Red Indian Line), appear to have a strike of approximately 40° to 50°. Later Silurian boundaries of the Orogen, the GRUB line and Gander-Avalon boundary (Dover fault and Hermitage flexure), have contrasting strike angles. The contrasting strikes of the later boundaries may have been imposed by the juxtaposition of the Avalon zone in

the mid-Silurian and similar age deformation that occurred along the Hermitage flexure and Dover fault. Deformation along the Hermitage Flexure and Dover fault was accompanied by the intrusion of large volumes of granite and sinistral shear, related to widespread Silurian Orogeny (Salinic Orogeny, Dunning et al. (1990). Earlier boundaries may have been reactivated at this time (Baie Verte, Red Indian and Noel Paul lines) (see Piasecki, 1995).

The regional strike of the Avalon and Gander Zones differs from that of the rest of the Island. This may be the result of changes in the tectonic processes responsible for the linkage of these tectono-stratigraphic zones or an indication of pre-existing tectonic fabric.

5.4 Induction Vectors

Induction vectors are another indicator of structure that can be used to map geologic and tectonic features of the Orogen. Induction vectors are a means of graphically displaying information contained in the magnetic transfer function, which relates the vertical magnetic field to the horizontal magnetic field. The magnetic transfer function is the complex ratio of the measured vertical and horizontal magnetic fields. Information contained in the transfer function can be displayed as two vectors, the real and imaginary induction vectors (Parkinson, 1959, 1962). A real induction vector, when reversed (Parkinson convention), usually points toward zones of enhanced conductivity (Jones, 1986). The magnitude or length of the induction vector is an indicator of proximity and magnitude of horizontal variations in electrical structure.

The real induction vector plots for Newfoundland are very complex. This complexity is introduced by the rapid variation of surface geology in Newfoundland. Near surface 3D structure distorts the vertical magnetic field similarly to the distortion of the horizontal electric fields discussed in Chapters three and four. This distortion however is dependent on frequency and decays with increasing period, making it difficult to distinguish. Another factor limiting the interpretation is the quality of the vertical magnetic field measurements; the air loop used for the vertical field measurements has a signal-to-noise ratio that decreases beyond approximately 20 s, making data collection beyond 100 s difficult.

Geological distortion of the vertical magnetic field and coast effect (see section 5.2.2) limit the interpretation of induction vectors to a band between 100Hz and 10s. Figure 5.9 shows plots of real (reversed) induction vectors for the periods (frequencies) of 18 Hz, 2.3Hz, 3.6s and 10.7s, sensitive to conductivity variations in the upper and middle crust.

Observations (Figure 5.9)

- For most of the sites in the Notre Dame subzone, induction vectors point toward nearest surrounding terrains. Induction vectors for sites in the western Notre Dame subzone point to the west and sites in the Eastern part of the subzone point east (Figure 5.9 (B) and (C)).
- In Northeastern Newfoundland induction vectors reverse direction near the GRUB line (Exploits subzone - Gander zone boundary). This reversal is partially obscured by the response of the coast however indicates an enhancement in crustal conductivity at this boundary (Figure 5.9 (C), (D) and 5.10).

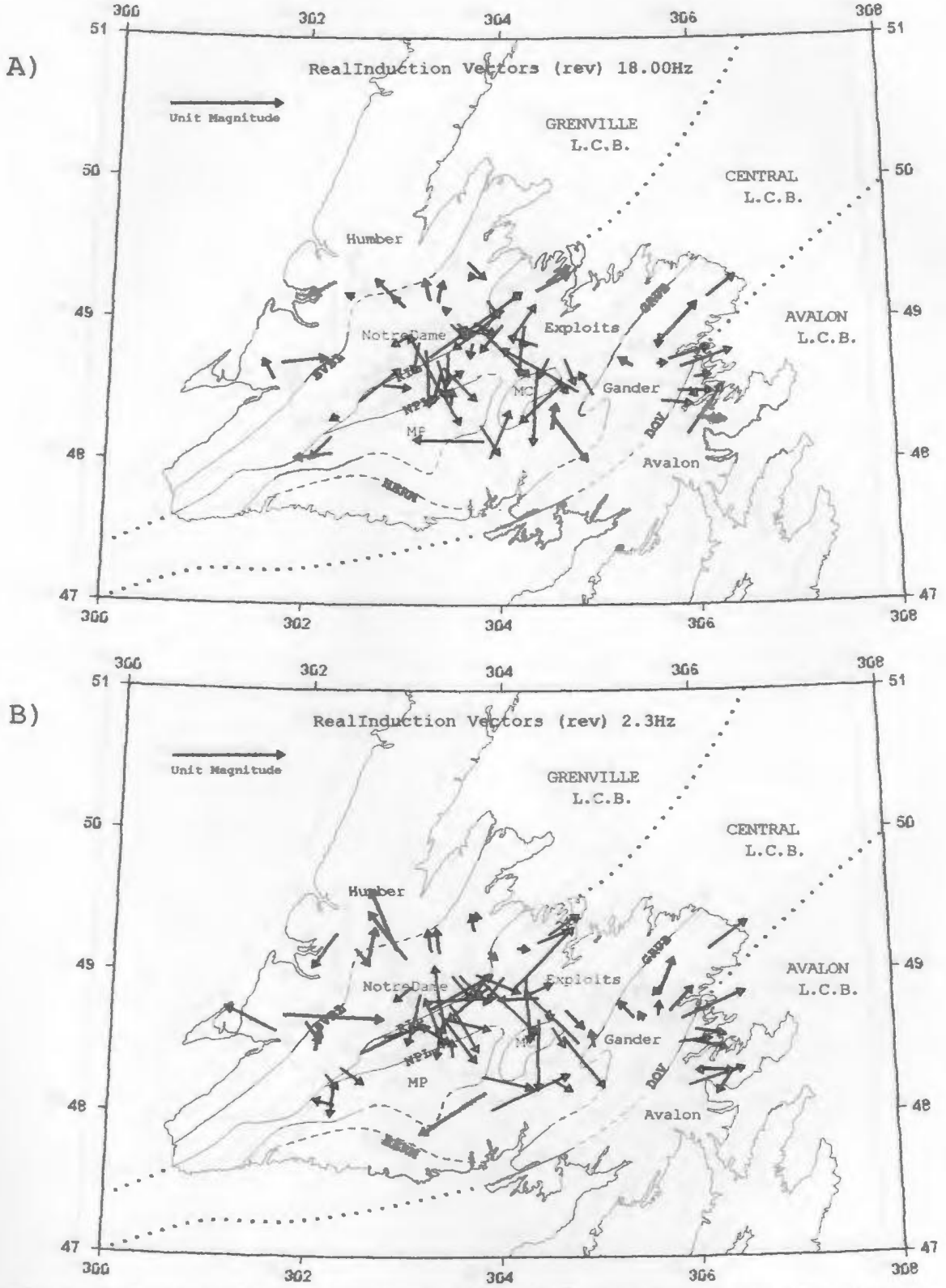

Figure 5.9a Real induction vector (reversed) plots for 18Hz (A), 2.3Hz (B), 3.6s (C) and 10.7s (D). Refer to figure 5.8 for explanation of abbreviations (observation point located at base of arrow).

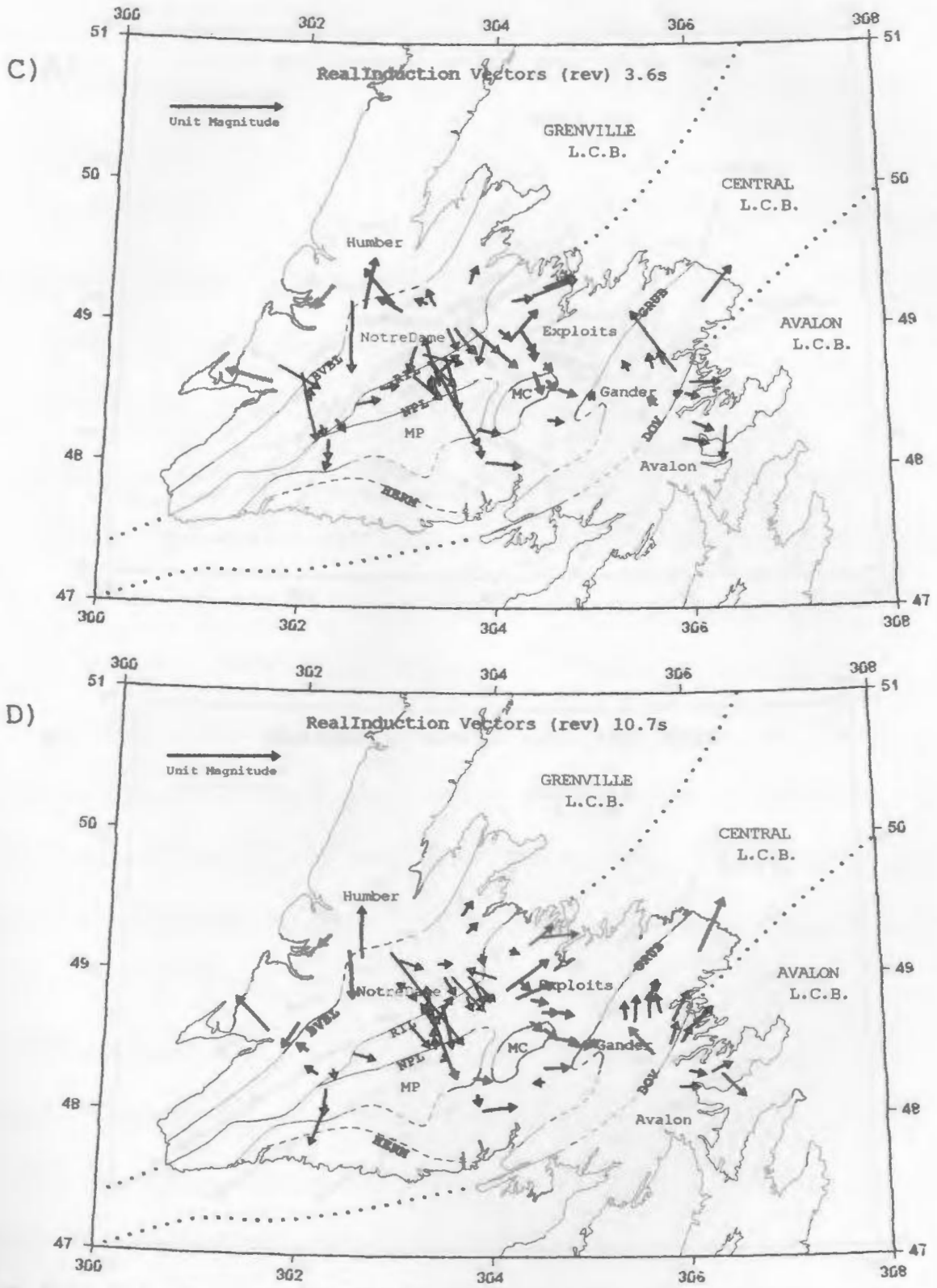

Figure 5.9b Continuation of Figure 5.9a .

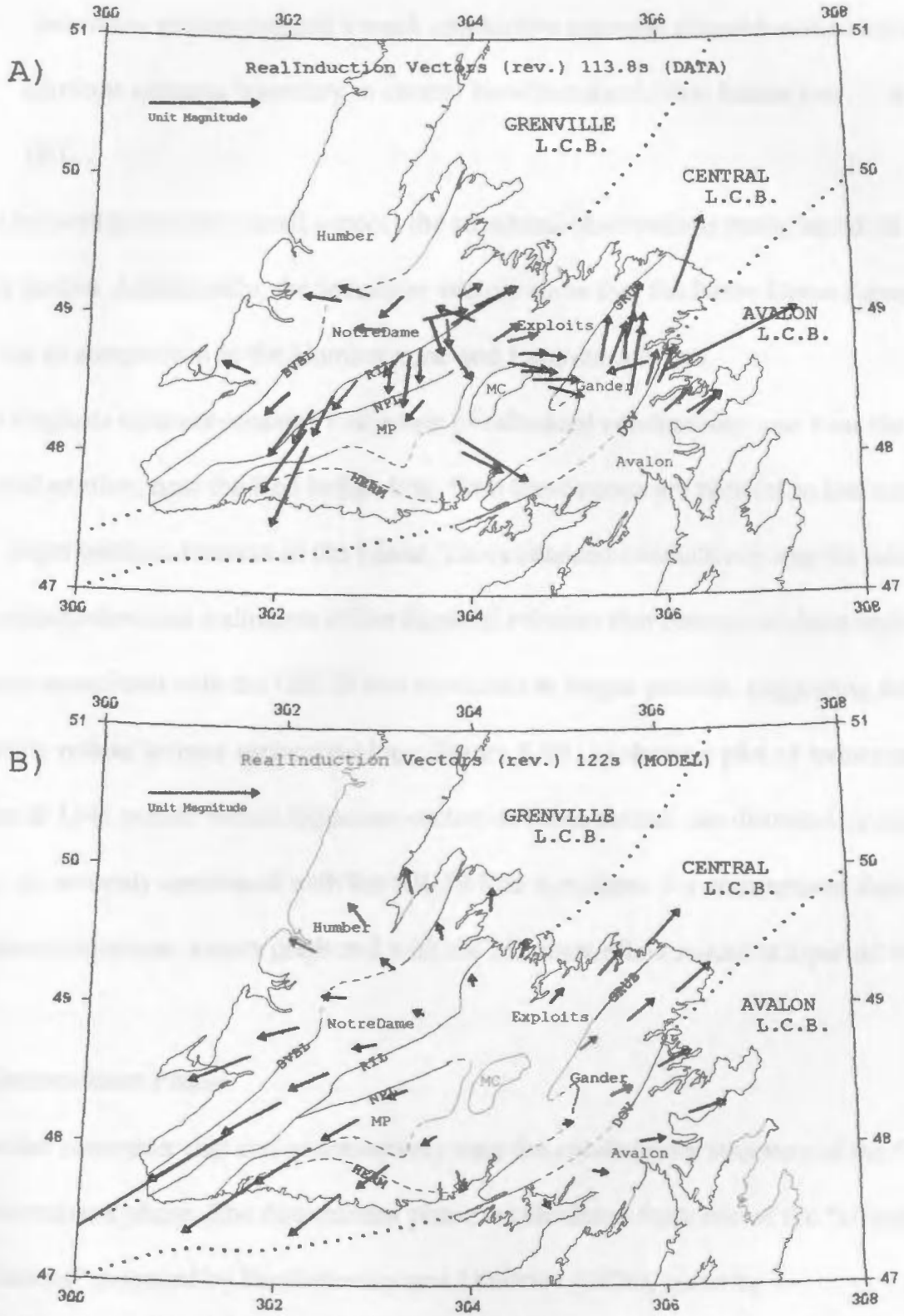

Figure 5.10 Comparison of measured (113s) (A) and modelled (3D coast effect) induction vectors (122s)(B). Refer to figure 5.8 for explanation of abbreviations.

- Induction vectors suggest a weak conductive anomaly situated at the Notre Dame Exploits subzone boundary in central Newfoundland (Red Indian line) (5.9 (A)and (B)).

The induction vectors overall support the structural observations made based on Groom-Bailey strikes. Additionally, the induction vectors show that the Notre Dame subzone is resistive in comparison to the Humber zone and Exploits subzone.

The Exploits subzone contains two zones of enhanced conductivity: one near the GRUB line; and another, near the Red Indian line. Both these zones are parallel to and coincident with, major tectonic features of the island. This enhanced conductivity may be related to Cambrian-Ordovician sediments of the Exploits subzone that outcrop in these regions. The anomaly associated with the GRUB line is evident at longer periods, suggesting that it is not solely related to near surface geology. Figure 5.10 (A) shows a plot of induction vectors at 114s period. While induction vectors at these periods are distorted by coast effect, an anomaly associated with the GRUB line is evident. For comparison, figure 5.10 (B) shows induction vectors predicted with the 3D coast effect model at a period of 122 s.

5.5 Determinant Phase

Another parameter that can quantitatively map the conductivity structure of the Orogen is the determinant phase. The determinant phase is calculated from one of the "effective impedances" proposed by Berdichevsky and Dmitriev (1976), given by

$$Z_{det} = \sqrt{Z_{xx}Z_{yy} - Z_{xy}Z_{yx}} \ .$$

The "effective impedances" are rotationally invariant averages of the impedance tensor (see section 3.3). They condense the information contained in the eight parameters of the impedance tensor into one complex impedance, which is thought to minimize multidimensional effects. The phase derived from this resultant "effective impedance" is useful in mapping structure as it is free of static shift that often complicates interpretation. However, modelling studies (eg. Agarwal et al., 1993) have shown that the success of the "effective impedances" in delineating structure is model dependent. Despite this model dependence, regional scale variations observed in the "effective impedances" are significant.

The magnetotelluric skin-depth relationship requires that longer periods of investigation are sensitive to greater depths and lateral distances. The determinant phase can therefore be used as a function of frequency to map regional structure as a function of depth. A determinant phase value rising greater than 45° is indicative of penetration into a zone of higher conductivity, while a phase decreasing less than 45° indicates penetration of a less conductive zone.

When interpreting determinant phase maps the spatial variation of values is more important than the absolute phase value observed. Because of the skin-depth relationship, the values at laterally distant sites may be sensitive to different depths, making comparison of the phase values of little use. On the other hand consistent values throughout a terrain,

differing in value from those of another terrain with consistent values implies a regionally significant change in electrical structure.

Figure 5.11 shows plots of the determinant phases for a frequency of 9 Hz and period of 5.3 seconds, sensitive to the upper and middle-lower crustal structure.

Observations

Upper Crust (Figure 5.11 (A))

- The Humber, western Dunnage (Notre Dame subzone) and Avalon zones have determinant phase values between 24° and 60°, which are lower than those observed over the Exploits subzones and the Gander zone.
- The highest determinant phase values (72° to 90°) occur in the Northwestern Exploits subzone, just to the southeast of the Red Indian line.

Middle-Lower Crust (Figure 5.11 (B))

- The Humber and Avalon zones have determinant phase values between 35° and 60°, which are lower than those observed over the Dunnage (Notre Dame and Exploits subzones) and the Gander zone.
- The highest determinant phase values (72° to 90°) occur in the Northwestern Exploits subzone, just to the southeast of the Red Indian line.
- The Notre Dame subzone and the eastern and southern edges of the Gander zone have consistent values along their length (50° to 65°).

The determinant phase maps agree with the information provided by the Groom-Bailey strikes and induction vectors. The Notre Dame subzone is very resistive, in contrast to its

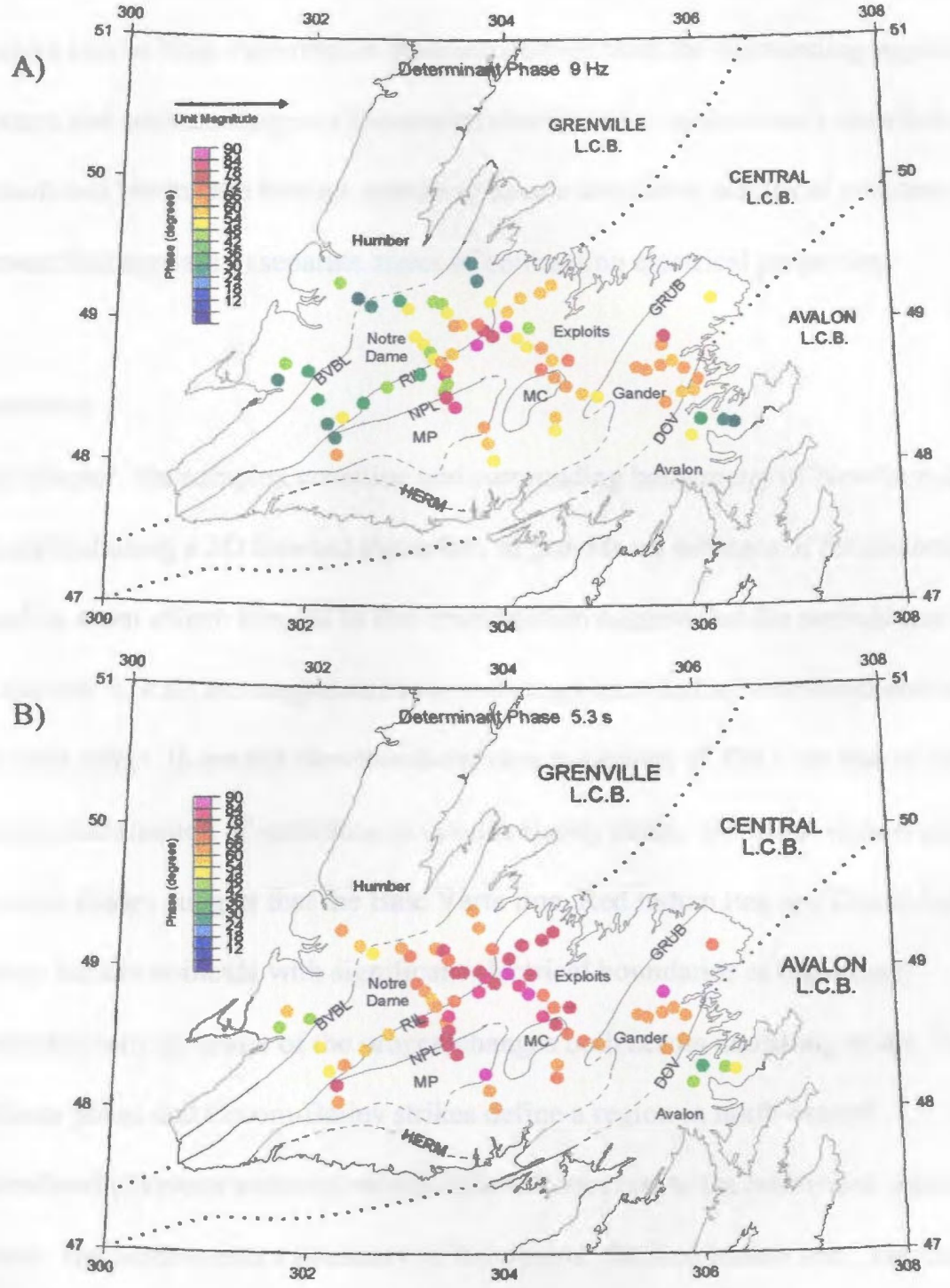

Figure 5.11 Determinant phases for a frequency of 9 Hz (A) and a period of 5.3 s (B). Refer to figure 5.8 for explanation of the abbreviations.

bordering zones. The determinant phases suggest that the Northwestern Exploits subzone (Red Indian line to Noel Paul line) is more conductive than the surrounding regions. The eastern and southern edges of the central mobile belt (Gander zone), parallelling the Dover fault and Hermitage flexure, appear to have a consistent electrical structure. The Dover fault appears to separate zones of contrasting electrical properties.

5.6 Summary

In this chapter, the complex coastline and surrounding bathymetry of Newfoundland were modelled using a 3D forward algorithm, to provide an estimate of the distortion produced by coast effect. Results of this investigation suggest that for periods less than approximately 10 s all the magnetotelluric soundings recorded in Newfoundland will be free of coast effect. In central Newfoundland data to periods of 100 s are free of distortion.

Regional examination of variations in Groom-Bailey strike, induction vectors and determinant phases suggest that the Baie Verte line, Red Indian line and Dover fault - Hermitage flexure coincide with significant electrical boundaries of the orogen.

The conductivity structure of the orogen changes both across and along strike. The determinate phase and Groom-Bailey strikes define a region in north-central Newfoundland (Exploits subzone) which differs from crust to the northwest, southeast and southwest. The north western boundary of this region, the Red Indian line, and the Baie Verte line further to the northwest are nearly two-dimensional, while the southwestern to southeastern boundary changes significantly along strike. This change in structure along

strike of the orogen is spatially coincident with deformation along the Hermitage flexure and Gander / Avalon boundary, possibly supporting the proposal of an Avalonian promontory in southern Newfoundland (Currie and Piasecki, 1989). If the seismic division of the lower crust of the orogen is valid, the three lower crustal blocks appear not to have a simple near two dimensional relationship in southern Newfoundland.

CHAPTER 6

Conductivity Structure of Major Boundaries of the Appalachian Orogen

6.1 Introduction

The regional conductivity structure of Newfoundland suggests that the Baie Verte line, Red Indian line and Dover fault - Hermitage flexure represent major conductivity boundaries within the orogen. In this chapter the conductivity structure of these three boundaries will be investigated through examination of apparent resistivity, phase and transfer function pseudosections and two-dimensional inversion along profiles crossing the three boundaries.

For each of the profiles examined the principal axis system for which Maxwell's equations decouple into the TE and TM modes was found by fitting a 3D/2D decomposition model to a subset of the transect data. For a period band sensitive to the conductivity structure of the transect (eg. 0.1 to 10 s), the data from all sites were inverted simultaneously for a single strike angle (See Chapter 4). In such a procedure, the twist and shear parameters required by the model are constrained to be frequency independent but site dependent. The undistorted 2D impedances (TE and TM impedances) are recovered by subsequently applying the decomposition model to the data at each site with the strike, twist and shear fixed to the values found. The result of this process should be a distortion free 2D data set for the transect, provided that the regional conductivity structure is reasonably 2D. This is shown to be a valid assumption by the low misfits of the decomposition model to the data.

Apparent resistivity, phase and transfer function pseudosections show quantitatively the location of major conductivity anomalies and variations in conductivity structure. Pseudosections are formed by contouring a magnetotelluric parameter (phase, apparent resistivity or transfer function) as a function of period (or psuedo-depth) along a profile.

Apparent resistivity pseudosections provide an approximate image of the conductivity structure along the transect. Examination of the structure on both the TE and TM mode sections can be useful in delineating conductivity structure, but these sections are complicated by static shifts (Jones, 1988). As the name implies, a static shift is a frequency independent shift of the apparent resistivity curve. Static shifts are the result of small scale near surface structure (same structure which produces 3D distortion of the data) and are indeterminant without additional independent information about the conductivity structure. There are two static shifts per site, one effecting the TE mode, and the other the TM mode. The two static shifts make up the indeterminant portion of the distortion matrix C, site gain and anisotropy (section 4.2). The static shifts can give the impression of lateral structure, therefore care must be taken in interpreting these sections.

Phase pseudosections do not suffer from the static shift problem that complicates the apparent resistivity sections. The phase sections are therefore very useful in delineating the conductivity structure, however the information contained within them is somewhat less intuitive. The phase value indicates whether the EM fields at a particular period are entering a more conductive or less conductive zone. A rising phase value > 45 indicates penetration of a zone more conductive than the zone above and a decreasing value < 45

indicates penetration of a less conductive zone.

Transfer function sections are primarily of use in locating lateral changes in conductivity structure (See section 5.4). For each transect there is a plot of the real component of the transfer functions projected along the transect. The major component of the transfer function should lie in the plane of the transect; in fact, for a structure to be truly 2D this is required. Anomalous transfer function values are usually caused by TE mode current concentrations, either as a result of a zone of enhanced conductivity parallel to strike or a boundary between a resistive and conductive region. They typically range in value from -1 to 1, with a value < 0 indicating a current concentration to the left (west for east-west profile) and value > 0 indicates a current concentration to the right (east).

All the parameters discussed so far have dealt with approximate or pseudo depth scales and parameters which are indicative of increasing or decreasing conductivity as opposed to the parameterization / interpretation one wishes to obtain, resistivity as a function of depth and position. In order to convert the magnetotelluric data into this parameterization, one must make use of 2D forward and / or 2D inverse codes. One difficulty with this process is that resistivity and depth are usually not an independent parameterization of the magnetotelluric data. For example, for a conductive layer the correct parameterization is in terms of resistance and conductance, the resistivity thickness product and conductivity thickness product respectively. Of these two orthogonal parameters only the conductance is usually well resolved.

Anomalous conductance and resistance are relative terms. To resolve a conductive zone

at depth, the zone's conductance must be greater than the total conductance from the surface down to the depth of the conductive zone. As well, a zone of enhanced conductivity is poorly resolved if it's lateral dimensions are much less than its depth (Jones, 1993).

The rapid relaxation inverse code (RRI) of Smith and Booker (1991) was used to convert the Newfoundland transect data to true depth sections. This inverse code is iterative and approximates horizontal derivatives of the electric and magnetic fields with values from previous iterations. This enables the code to treat the inverse problem at each site similar to a 1D inverse problem. The solutions to the uncoupled TE and TM inverses at each site are interpolated and a 2D forward calculation provides horizontal fields for the next iteration. The method is very fast, as the computations grow only linearly as the number of sites increase. The code has some limitations, primarily related to fitting the TM mode. One limitation occurs as a result of inaccuracies introduced by discontinuous electric fields produced when TM mode currents cross a surface boundary. Another limitation occurs as a result of small changes in structure producing significantly changes in laterally distant TM mode responses slowing convergence.

One problem that remains with the distortion corrected Newfoundland data are the static shifts which affect the TE and TM apparent resistivity curves. There have been a number of methods proposed in recent years to deal with this problem, although no correction is possible without external information. Vanyan et al. (1989) examined 399 magnetotelluric sites, and determined that the statistical standard deviation of static shift factors was half an

order of magnitude. Sternberg et al. (1988) found a standard deviation of one quarter to one third an order of magnitude for 70 magnetotelluric sites. It is reasonable to assume therefore that the static shift factors in Newfoundland should have a standard deviation on the order of one quarter to one half an order of magnitude in agreement with other observations. To represent accurately our confidence in the calculated apparent resistivity values, the error floor was set to twenty five percent in the inversion process. This confidence level should minimize the effects of static shifts, allowing the inversion algorithm to fit the phase data and shape of the apparent resistivity data without introducing structure based solely on apparent resistivity levels. (Note: If the magnetotelluric data is causal, the apparent resistivity curve can be calculated from the phase data to within a constant factor. Therefore for 1D, and possibly 2D, data the apparent resistivity and phase data is essentially redundant when the static shifts are considered. However, the apparent resistivity and phase refer to slightly different regions of model space.)

All of the true depth sections (inverse models) were found by jointly inverting the TM and TE modes, with error floors set to two percent for phase data and twenty five percent for the apparent resistivity data. The resultant models are have an RMS typically of 8 to 10 and are minimum structure models. The models are not unique, although they are the smoothest conductivity distribution that fits the data observations at the RMS calculated. Other models may be proposed but they will require more variation in conductivity structure.

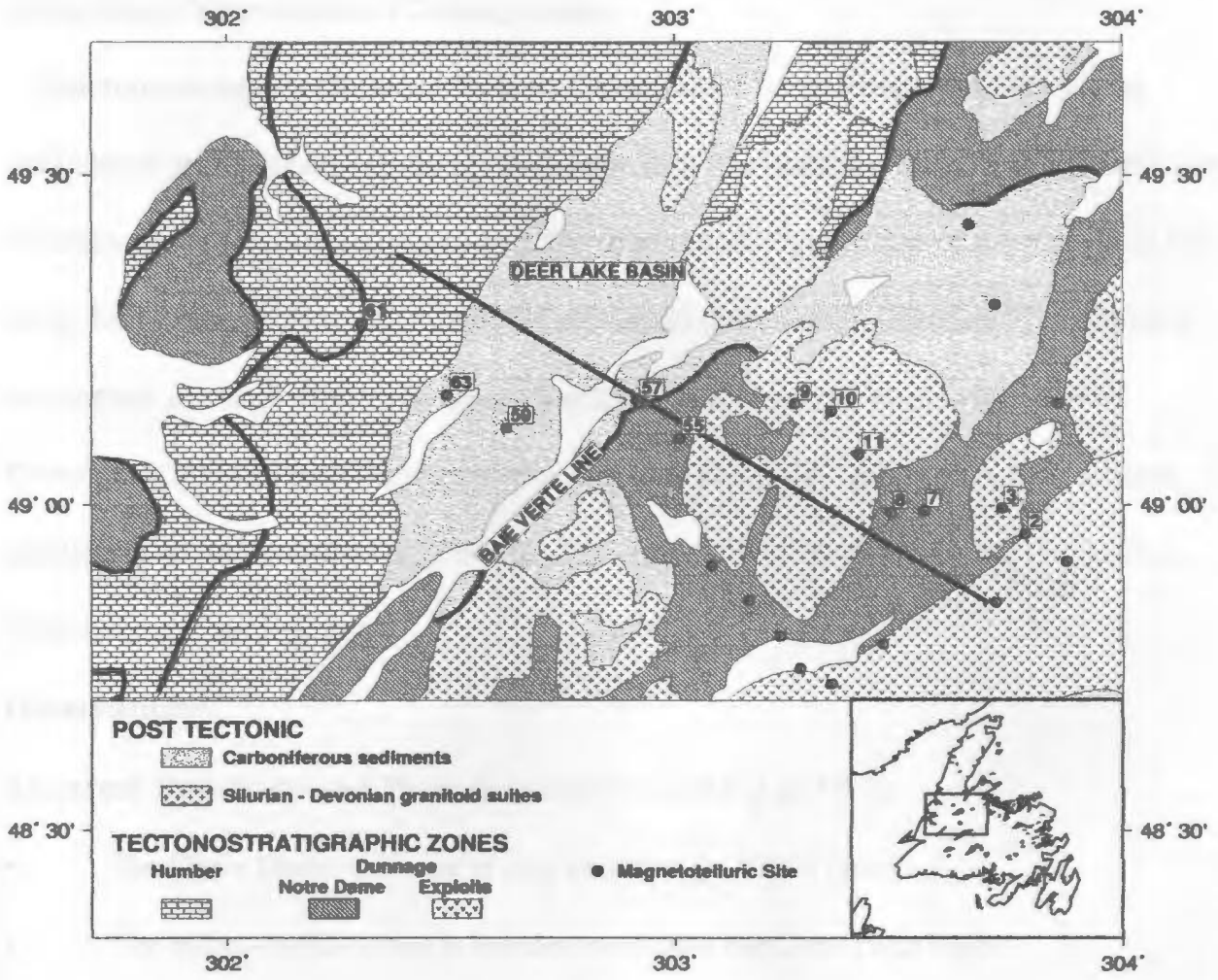

Figure 6.1 Geology map of the Humber - Dunnage zone boundary in western Newfoundland. The location of the magnetotelluric profile is indicated by the black line.

6.2 Humber-Dunnage Zone Boundary

This transect crosses the boundary of the Humber and Dunnage (Notre Dame) zones, marked by the Baie Verte line (Long Range fault) (Figure 6.1). From west to east the transect crosses passive margin rocks of the eastern margin of Iapetus (Humber Zone), Devonian-Carboniferous sediments of the Deer lake basin, and volcanic and intrusive rocks

of the Notre Dame subzone (Dunnage zone).

Structures along the transect are currently explained by an Early-Mid Ordovician collision of an island arc terrain (Notre Dame subzone) with the passive margin of North America as the result of eastward-directed subduction. Destruction of the margin in the Early-Mid Ordovician was followed by continued deformation (Silurian ?) resulting in duplication of the platform sequence (Stockmal and Waldron, 1990, 1991, 1993). Devonian-Carboniferous transcurrent movements along the Long Range fault system resulted in development of the Deer lake basin (positive flower structure) (Hyde et al., 1984).

Observations:

Apparent Resistivity and Phase Sections (Figures 6.2 and 6.3)

- The Notre Dame subzone is very resistive (> 10000 Ω·m).
- The upper-middle crust is conductive below the Deer Lake basin.
- The Baie Verte line (Long Range fault) marks the boundary between two electrically distinct zones.

Transfer Function Section (Figure 6.4)

- The Notre Dame subzone is bordered to the east and west by more conductive regions. This is indicated by transfer functions pointing east on eastern side of zone and west on western side.
- Transfer functions indicate the presence of a conductive zone beneath the Deer Lake basin, between site 63 and 57. This is indicated by the reversal of transfer

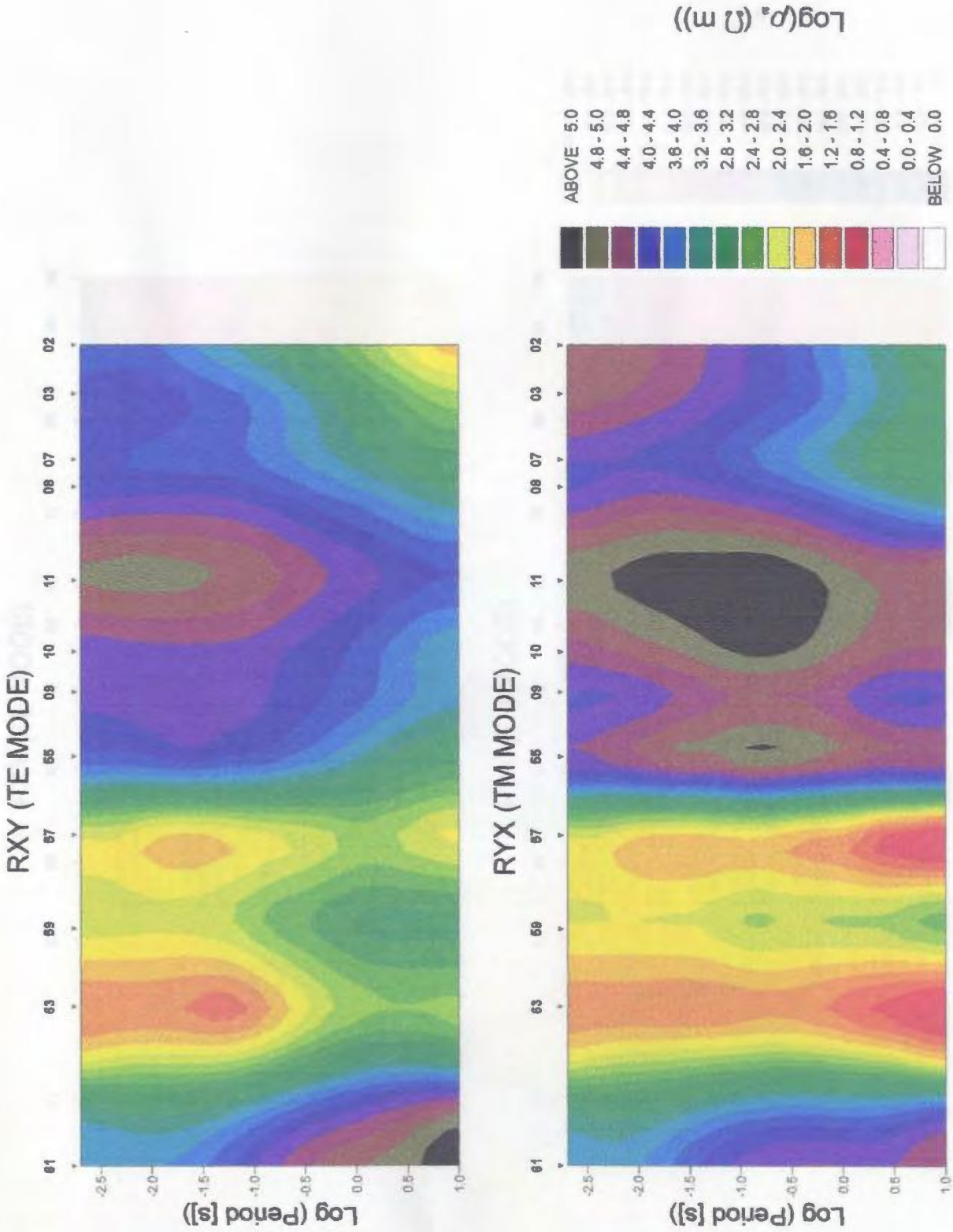

Figure 6.2 TE and TM apparent resistivity pseudosections for the Hummber - Dunnage boundary.

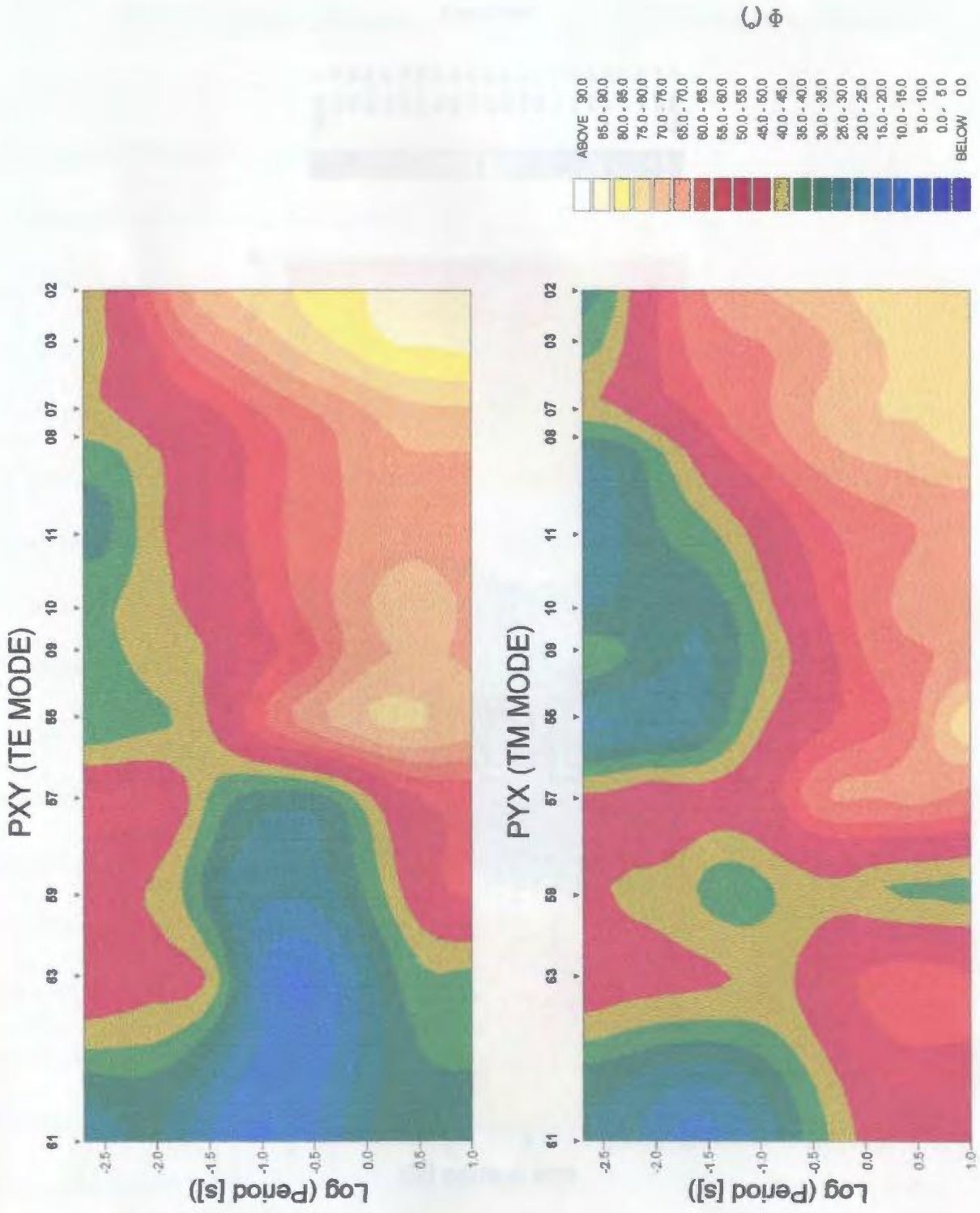

Figure 6.3 TE and TM phases pseudosections for the Humber - Dunnage boundary.

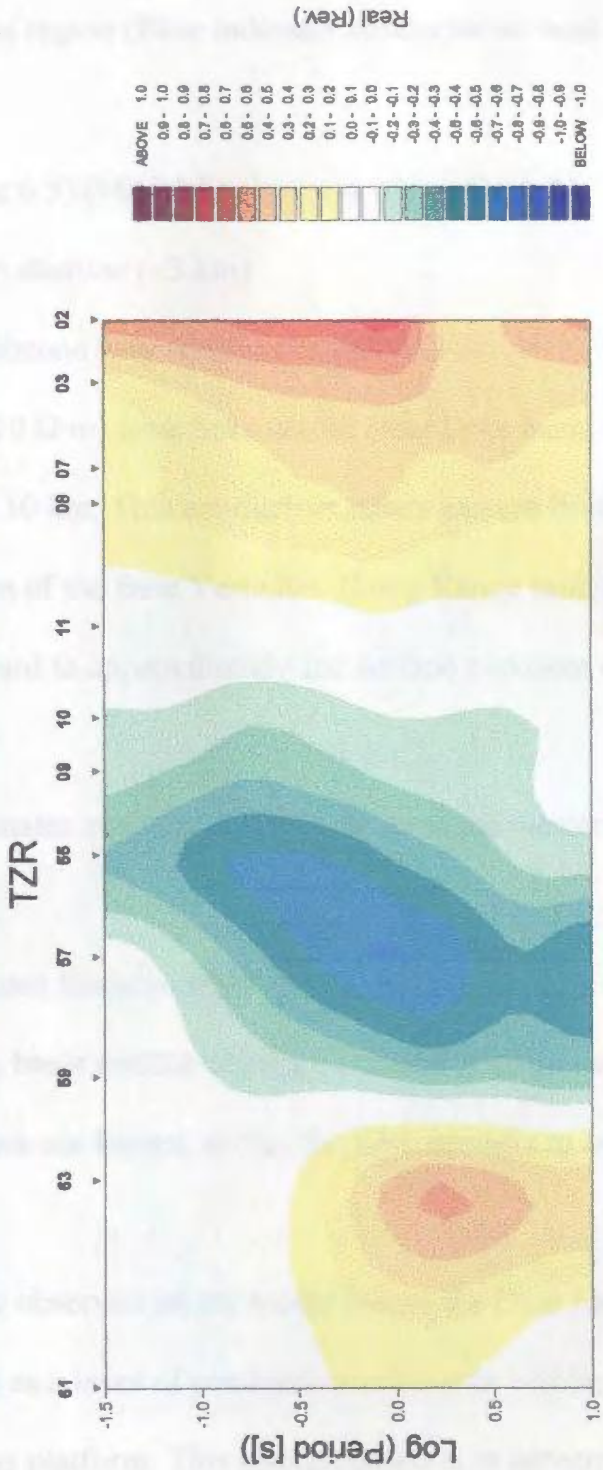

Figure 6.4 Transfer function pseudosection for the Humber - Dunnage boundary.

functions in this region (Blue indicates conductor to west and red conductor to the east).

Inverse Model (Figure 6.5) (Model fit shown in appendix A.1)

- Deer lake basin shallow (~3 km)
- Notre Dame subzone very resistive (~10000 Ω·m)
- Conductive (~10 Ω·m) zone beneath the Deer Lake basin at a depth of approximately 10 km. This conductive zone's eastern limit is coincident with the surface location of the Baie Verte line (Long Range fault). The conductive zone extends westward to approximately the surface exposure of platform rocks (Cormacks).
- Exposed carbonates and platform sediments at the western end of the line appear to be resistive

The two most dominant features of the inverse model are the conductive zone located beneath the Deer Lake basin and the change in crustal structure across the Baie Verte line (BVL). The two features are linked, in that the BVL appears to be the eastern limit of the conductive zone.

The conductive zone observed on the model below the Deer Lake basin is most reasonably interpreted as a layer of conductive sediments within, or deposited on top of, the para-autochthonous platform. This interpretation is in agreement with the tectonic model proposed by Stockmal and Waldron (1990, 1991 and 1993) on the basis of seismic reflection and structural observations. In their model, post collisional deformation of the

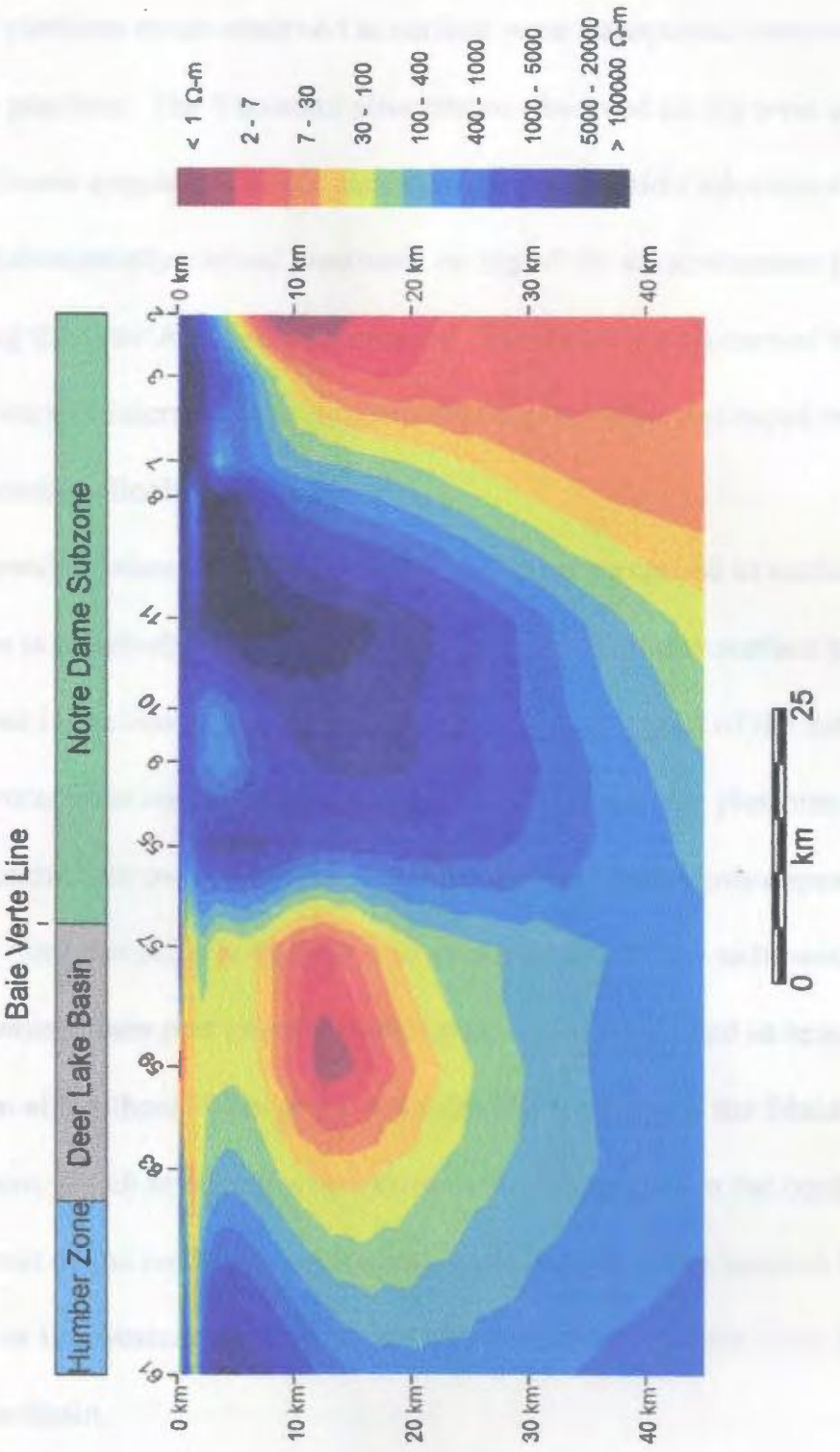

Figure 6.5 Two-dimensional inverse model (RRI) model of the Humber - Dunnage zone boundary.

eastern passive margin of Iapetus (Humber zone) resulted in duplication of the platform

sequence. The platform rocks observed at surface were transported westward over the autochthonous platform. The Taconian allochthons observed on the west coast of Newfoundland were emplaced on the platform during the mid-Ordovician Taconian Orogeny, and subsequently carried westward on top of the allochthonous platform sequence during the later Acadian deformation. The thrust which carried the platform sequence westward is interpreted as a reactivated normal fault produced in response to the load of the Taconian allochthons.

The inverse model indicates that the platform sequence exposed at surface west of the Deer lake basin is relatively resistive (western end of model near surface in Figure 6.5). This implies that if the conductive zone observed at depth is part of the autochthonous platform sequence these rocks apparently do not form part of the platform sequence at surface. The conductive zone therefore, may be related to sediments deposited on the autochthonous platform prior to the Acadian deformation. These sediments are the Goose Tickle Group which form part of a foreland basin sequence formed in response to the load of the Taconian allochthons. This group includes black shales of the Black Cove and Table Cove Formations, which may be the sediments imaged at depth in the conductive zone. The western limit of the conductive zone may therefore mark the western limit of the foreland basin or the western limit of deep water formations (Black Cove Formation) deposited in the basin.

The 8 to 12 km depth to the top of the conductive zone is in agreement with Stockmal and Waldron's (1991) interpretation of the horizontal reflectors seen on the western end of

line 2 between 3 and 5.5 seconds (TWT) as the autochthonous platform succession (Figure 6.6).

The eastern limit of the conductive zone in this model would mark the eastern limit of the autochthonous platform sequence. The coincidence of the eastern limit of the conductive zone and the BVL at surface suggests that the autochthonous platform may be truncated by the BVL. This relationship is unclear as the Acadian deformation model of Stockmal and Waldron (1993) would require an eastern limit to the autochthonous platform consistent with that observed in the inverse model (Figure 6.5). If the autochthonous platform is truncated by the BVL, movement on the BVL must post-date the Acadian deformation. This movement is most likely Carboniferous strike-slip movement of the Long Range Fault, which is coincident with the BVL in the study area. Stockmal et al. (1990) estimate a movement of approximately 140 km during Carboniferous times.

The crust on either side of the BVL has electrical conductivity structure which differs to at least 15 to 20 km. The relationship between the conductive zone and the BVL suggests that the contrasting electrical properties are most likely to be the result of strike-slip motion on the BVL as opposed to collisional tectonics. Surface structural investigations of the BVL (Goodwin and Williams, 1990) indicate that the BVL developed as a result of both dextral and sinistral strike-slip motion. The BVL experienced both ductile and brittle deformation throughout the entire development of the Orogen (Ordovician to Carboniferous) (Goodwin and Williams, 1990 and references therein). The Dunnage and Humber zones pre-strike histories therefore are likely to be different.

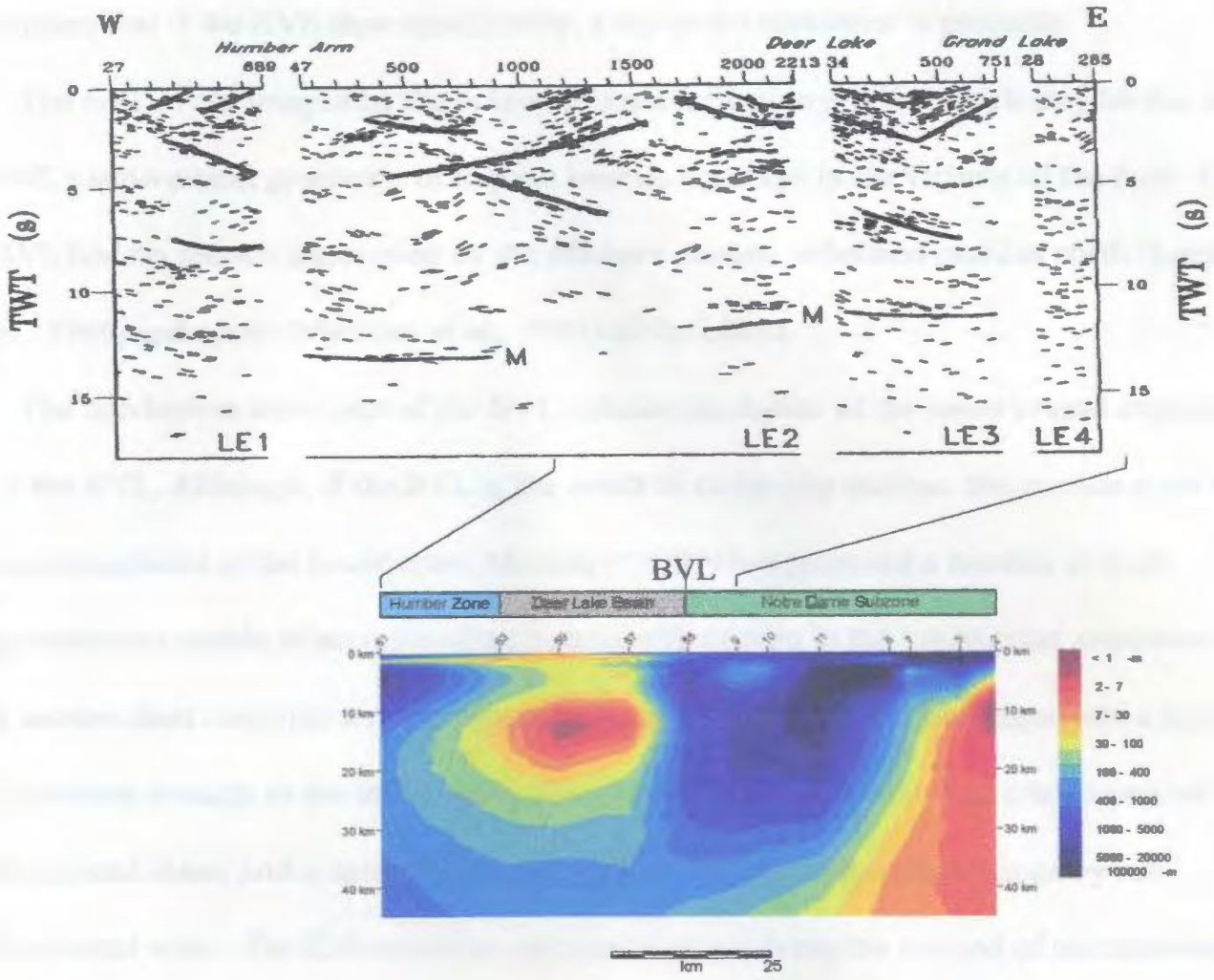

Figure 6.6 Comparison of Lithoprobe reflection seismic profiles 1-5 to the electromagnetic model.

The BVL appears to be nearly vertical on the inverse model, with it's surface expression coincident with the eastward limit of the conductive zone. This maybe partly a result of the inversion algorithm, although the eastern limit of the conductive zone should be resolved to within at least the site spacing (~10 km). The BVL therefore has a dip greater than 45 degrees, assuming a 10 km offset maximum between surface location and end of conductive zone and a depth of 10 km for the conductive zone. The data would favour moving the end of the conductive zone further to the west as opposed to the east. This

implies that if the BVL dips significantly, a dip to the northwest is probable.

The BVL is not imaged by the onland seismic reflection profile, which may be due to the BVL's sub-vertical geometry, or to poor seismic coverage in the vicinity of the fault. The BVL had no seismic expression on the offshore seismic reflection profiles north (Keen et al., 1986) and south (Marillier et al., 1989) of the island.

The conductive zone west of the BVL reduces resolution of the lower crustal expression of the BVL. Although, if the BVL is the result of strike-slip motion, this motion must be accommodated in the lower crust. McGeary (1989) has proposed a number of fault geometries capable of accommodating strike-slip motion in the lower crust: continuation of a narrow fault zone into a narrow shear zone, continuation of the fault zone into a zone of increasing breadth in the lower crust, decoupling of the fault zone into a wide zone of sub-horizontal shear, and a narrow fault zone offset from the upper crustal zone by sub-horizontal shear. The EM results are incapable of resolving the method of accommodation for the BVL, although they imply that strike-slip motion must be accommodated in the lower crust.

The middle and lower crustal reflectivity has been interpreted on both the onland (Quinlan et al., 1992) and offshore (Keen et al., 1986, and Marillier et al., 1989) seismic profiles as evidence that the lower crust is continuous across the BVL. Keen et al. (1986) and Marillier et al. (1989) proposed models based on reflectivity character in which the Grenville lower crust extends 70 km east of the BVL below an allochthonous western Dunnage zone (Notre Dame subzone). Quinlan et al. (1992) interpreted reflectivity

character observed on the onland profiles as evidence that the Gondwanan plate is continuous across Newfoundland, extending to the west coast of the island. In this model the Gondwanan plate (Central LCB) has under thrust the Laurentian plate (Grenville LCB) by up to 200 km. In the vicinity of the BVL, the Laurentian plate is sandwiched between a lower crust of the Gondwanan plate and upper crustal rocks of the Humber and Dunnage zone.

The strike-slip motion required by surface observations, and possibly imaged by the electromagnetic data, may be accommodated in the lower crust by reactivating earlier compressional structures (mid-lower crustal reflectors) as suggested by Quinlan et al. (1992). While it is entirely possible that the lower crust is continuous across the BVL, this is not required by continuity of reflective character across the fault. Continuity of reflective character may only imply a similar tectonic evolution.

6.3 Central Dunnage Zone (Notre Dame-Exploits Boundary)

Three magnetotelluric transects cross the major boundaries of the Central Mobile Belt (Figure 6.7). The most northerly transect crosses the boundaries near the Trans Canada Highway, the two more southerly transects cross the boundaries near Red Indian lake and the Burgeo road. The transects cross the Notre Dame - Exploits subzone boundary marked by the Red Indian Line and the Noel Paul Line, marking the boundary of the Exploits and Meelpaeg subzones. The geology of this region is some of the most complicated geology of the island, recording volcanism, sedimentation and deformation over much of the

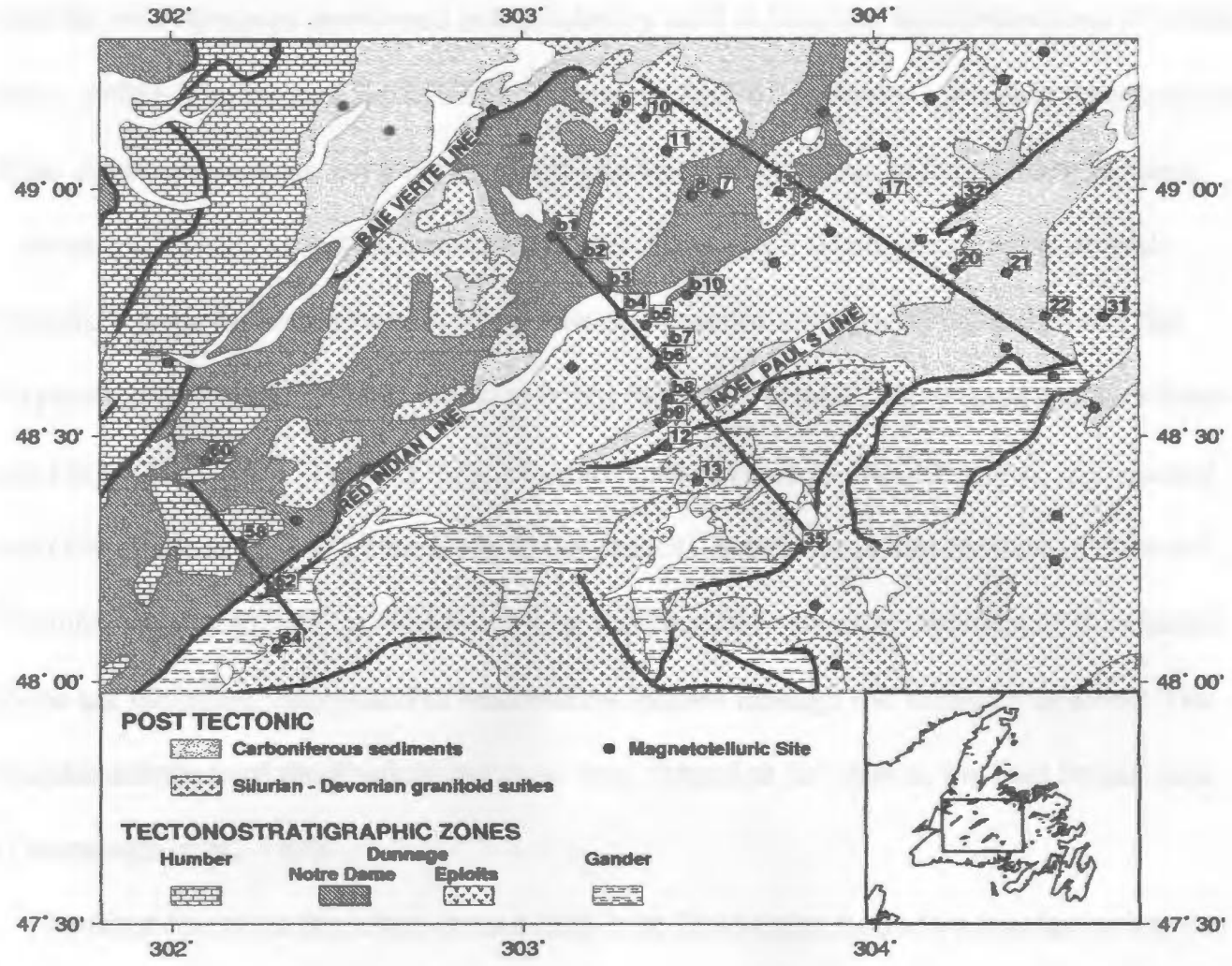

Figure 6.7 Geology map of the Notre Dame - Exploits subzone boundary. The location of three profiles crossing the boundary are indicated with a black line.

development of the orogen. An understanding of the relationships between the tectono-stratigraphic zones juxtaposed in this region is essential to the understanding of the tectonic history of the Appalachians in Newfoundland.

The Notre Dame and Exploit subzones together form the Dunnage zone, grouped on the basis of their similar arc and back-arc rocks. Although both subzones contain similar ophiolites and volcanic rocks, contrasts in stratigraphy, fauna and structural style suggests

that the two subzones developed independently until at least the late-Ordovician (Williams et al., 1988). The linkage of the Notre Dame and Exploits subzones possibly represents the final closure of Iapetus in Newfoundland (closure of a back-arc basin or marginal sea).

Relationships observed between the Gander Zone and Exploits subzone in central Newfoundland indicate that these two terranes were linked prior to the linkage of the Exploits and Notre Dame subzones, and that these two terranes developed together from the Early Ordovician. The Exploits subzone is interpreted as allochthonous, transported over Gander Zone rocks in the Early Ordovician (Colman-Sadd and Swinden, 1984 and Colman-Sadd et al., 1992). The Meelpaeg and Mount Cormacks subzones of the Gander Zone are therefore interpreted as basement windows through the Exploits subzone. The Gander substrate of the Exploits subzone may extend as far west as the Red Indian Line (Greenough et al., 1990).

The three transects therefore cross a Mid-Late Ordovician boundary amalgamating the eastern and western halves of the Dunnage Zone, deformed by orogenic events in the Early Ordovician. The Notre Dame subzone, which represents the western half of the three transects, is interpreted as an arc terrain accreted to the North American margin in the Taconian Orogen. The eastern half of the transects, the Exploits subzone, was thrust over the Gander Zone (eastern margin of Iapetus ?) in the Early Ordovician. The destruction of the eastern margin of Iapetus correlates with the Penobscot Orogeny of Maine, although the processes involved in this orogenic event remain unresolved.

Observations:

Apparent Resistivity and Phase Sections (Figures 6.8 and 6.9)

- The upper crust is resistive southeast of the projection of the Noel Pauls Line, approximately located between sites 32 and 20 (The Noel Pauls Line in this region may correlate with the Reach Fault).
- The upper-middle crust is resistive northwest of the Red Indian Line, located just west of site 2.
- There is a conductivity anomaly located in upper crust beneath sites 3, 2 and 17.
- A conductivity anomaly is observed near surface between sites 20 and 21.
- The TM mode phase indicates that there is a change in lower crustal conductivity structure near site 17.

Transfer Function Section (Figure 6.10)

- Sites 8 to 2 indicate the presence of enhanced conductivity southeast of site 2.
- The reversal of transfer functions between sites 32 and 21 indicates the presence of enhanced conductivity between these sites.
- The reversal of induction vectors for the enhanced conductivity southeast of site 2, observed at sites 8 to 2, may be masked by the enhanced conductivity between sites 32 and 21.

Inverse Model (Figure 6.11) (Model fit shown in appendix A.2.1)

- Entire crust west of the Red Indian Line (site 2) appears to be very resistive ($\geq$ 10000 Ω·m).

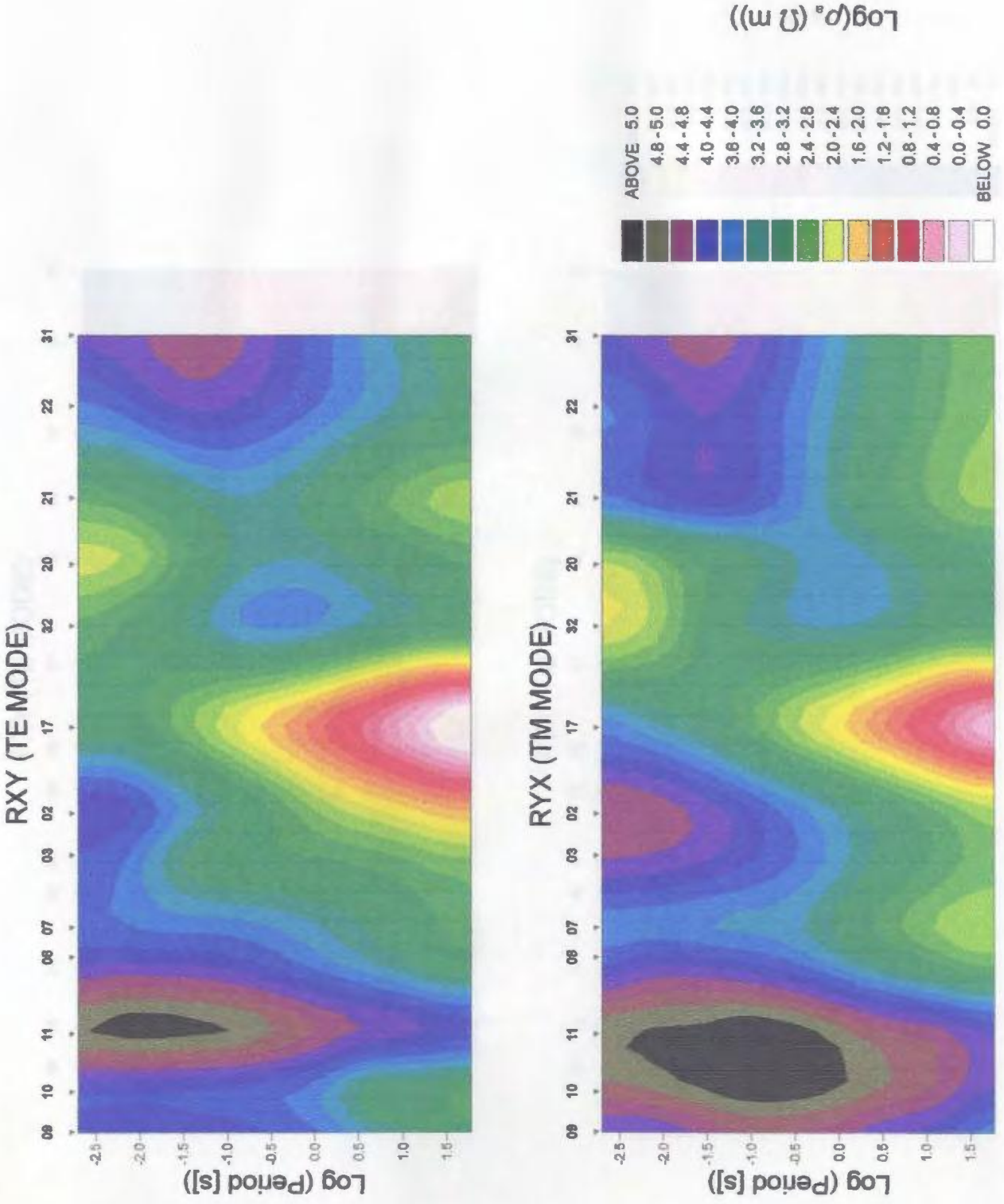

Figure 6.8 TE and TM apparent resistivity pseudosections for the Notre Dame -Exploits subzone boundary.

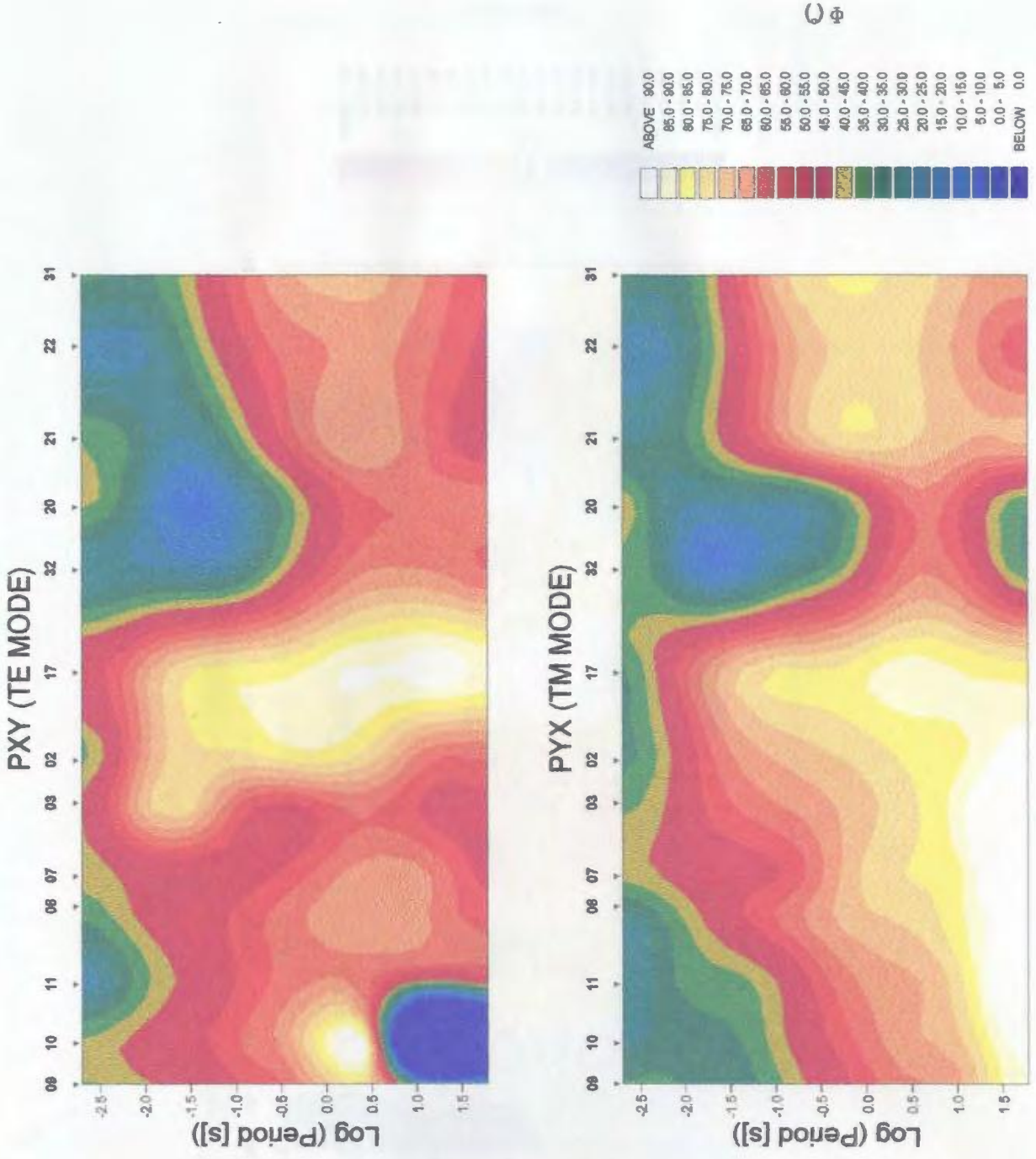

Figure 6.9 TE and TM phase pseudosections for the northern Notre Dame - Exploits boundary profile.

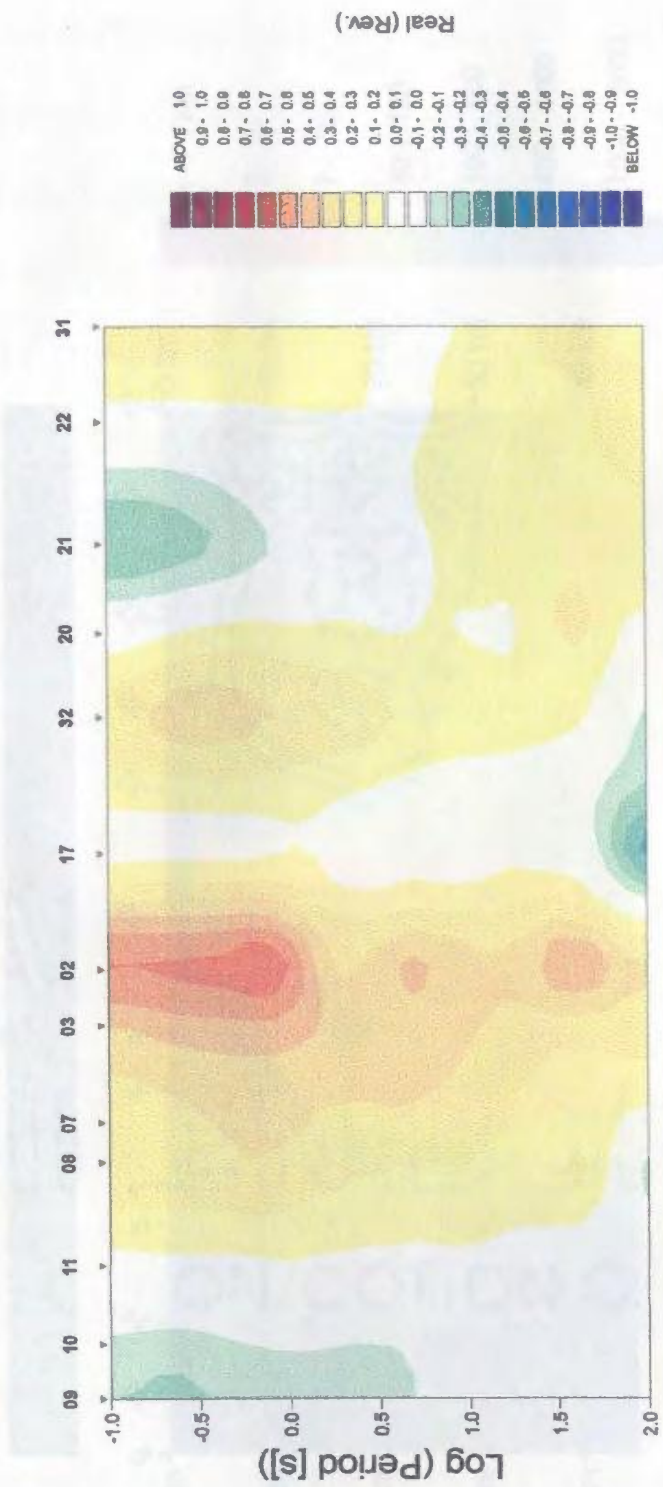

Figure 6.10 Transfer function pseudosection for the northern Notre Dame - Exploits boundary profile.

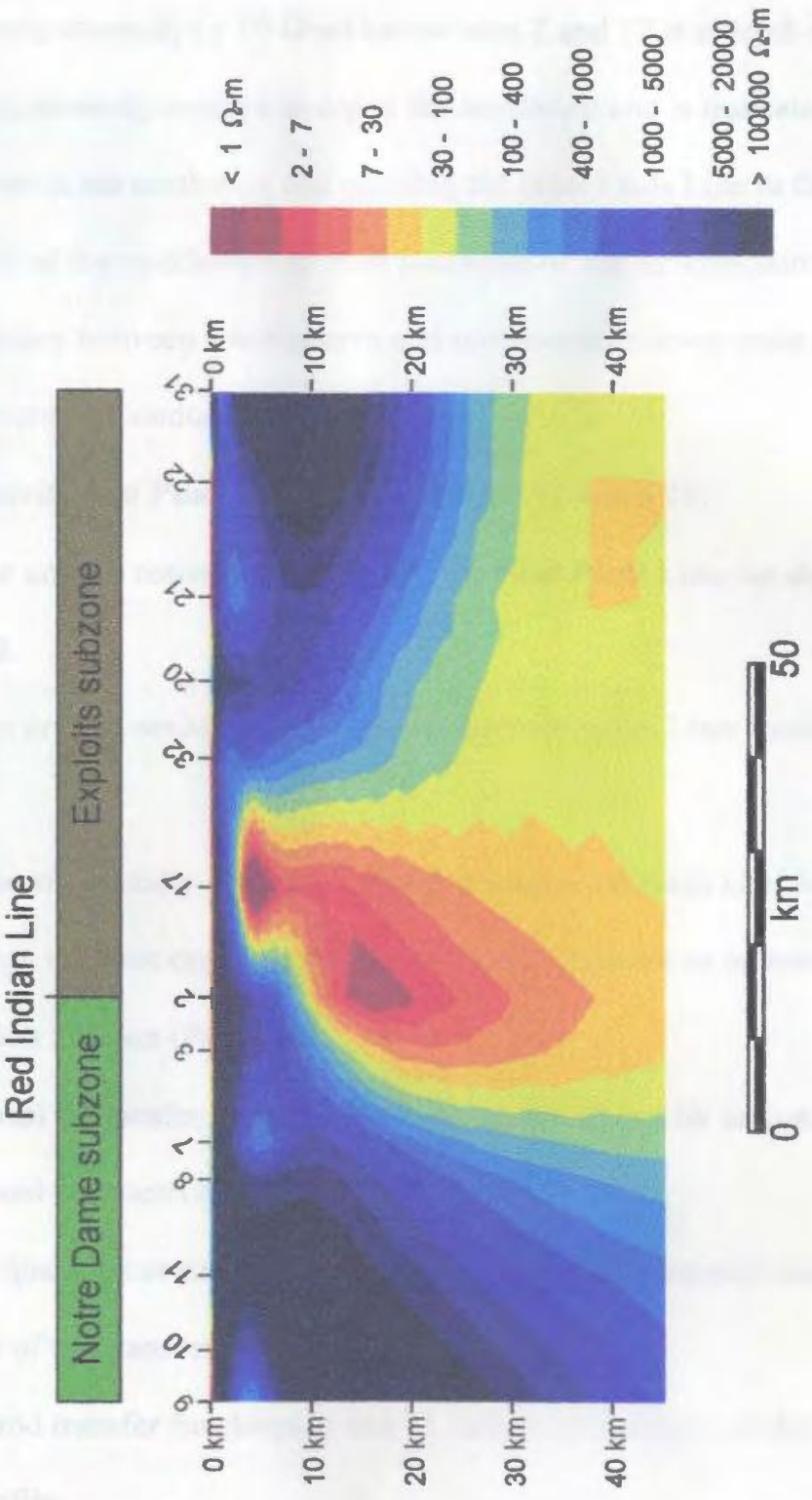

Figure 6.11 Two-dimensional inverse model (RRI) for the northern Notre Dame - Exploits boundary profile.

- Conductivity anomaly ($\leq$ 10 Ω·m) below sites 2 and 17 at a depth of approximately 5 km. This anomaly appears to dip to the northwest and is truncated by the Red Indian Line in the northwest and possibly the Noel Pauls Line in the southeast.
- Resistivity of the middle-lower crust southeast of site 32 approximately 500 Ω·m. The boundary between southeastern and northwestern lower crust is obscured by the upper crustal conductivity anomaly.

Apparent Resistivity and Phase Sections (Figures 6.12 and 6.13)

- The upper crust is resistive southeast of the Noel Pauls Line, located between sites b9 and 12.
- The upper crust is resistive northwest of the Red Indian Line, located just west of site b5.
- There is a conductivity anomaly located at surface between sites b6 and b7.
- The change in lower crustal conductivity not as apparent as on transect 2.

Transfer Function Section (Figure 6.14)

- The reversal of transfer functions between sites b10 and b8 indicates the presence of enhanced conductivity between these sites.
- Transfer functions at site 35 indicate the presence of enhanced conductivity southeast of the transect.
- Long period transfer functions at site b1 indicate enhanced conductivity northwest of the profile.

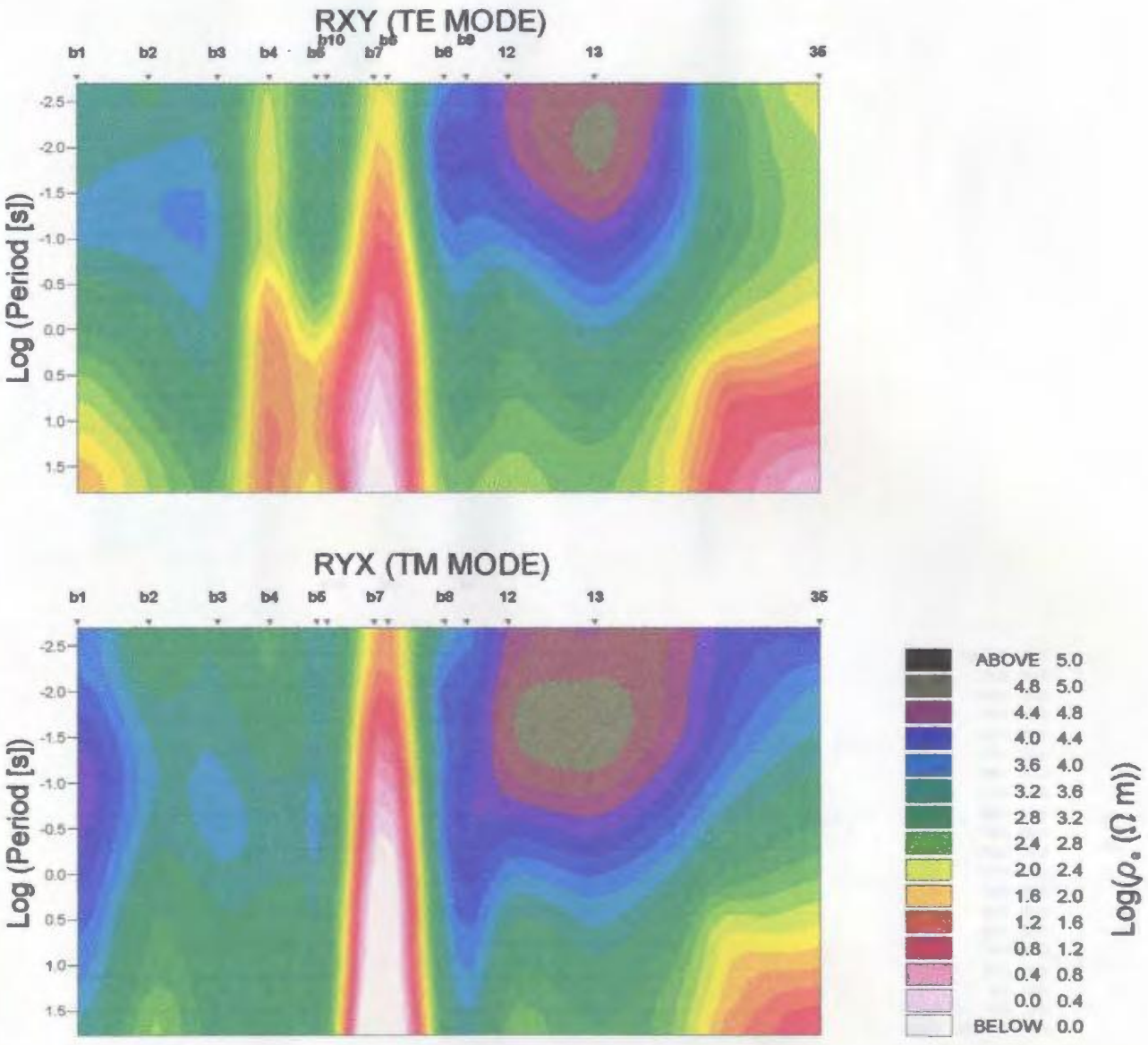

Figure 6.12 TE and TM apparent resistivity pseudosections for the central Notre Dame - Exploits subzone boundary.

Inverse Model (Figure 6.15) (Model fit shown in appendix A.2.2)

- The upper crust west of the Red Indian Line (site b5) appears to be very resistive ($\geq$ 10000 Ω·m). The conductive region in lower crust below site b1 may be an

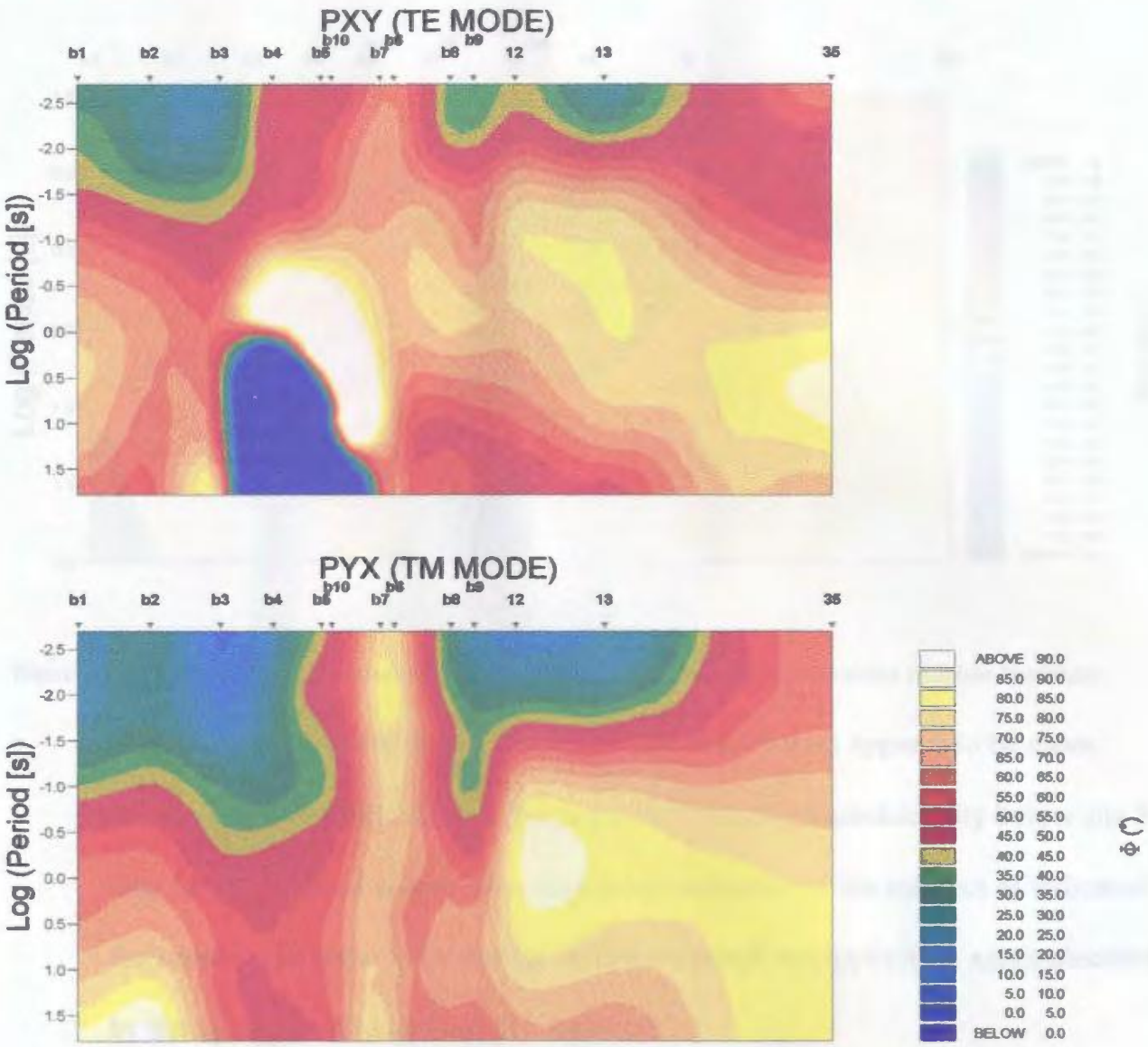

Figure 6.13 TE and TM phase pseudosections for the central Notre Dame - Exploits subzone boundary.

artifact produced by enhanced conductivity off the line.

- Conductivity anomaly (≤ 10 Ω·m) near surface below sites b6 and b7. This anomaly appears to be truncated by the Red Indian Line in the northwest and is similar to that observed on the northern transect.

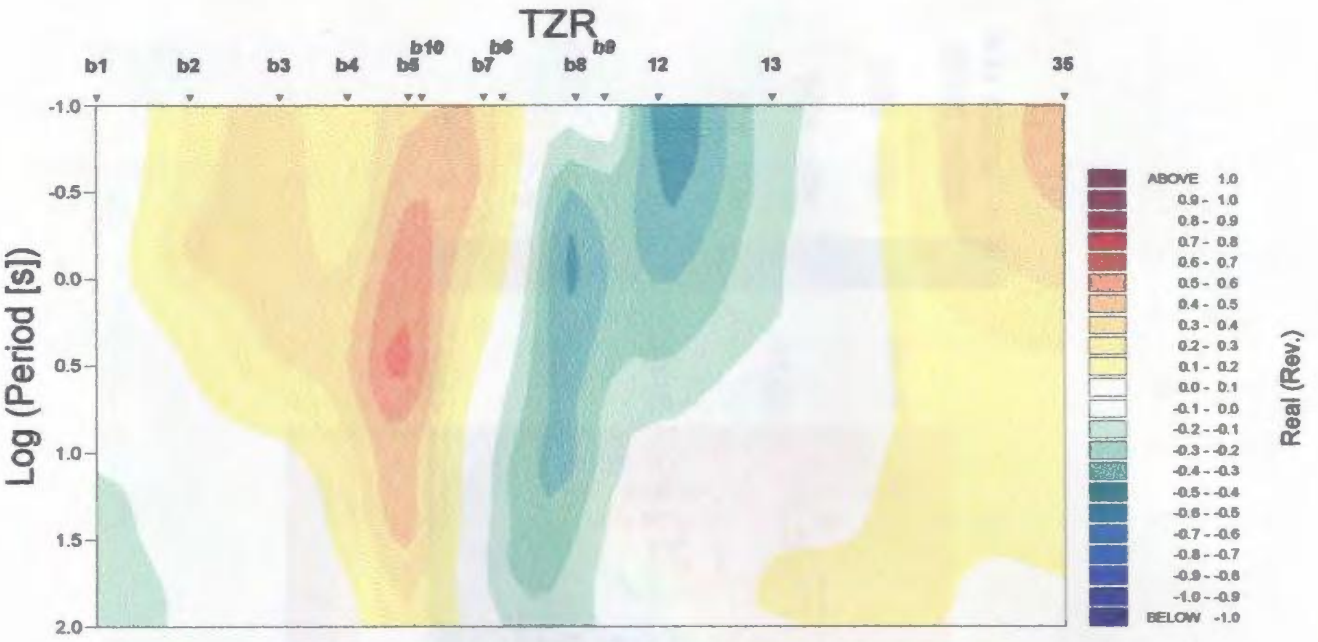

Figure 6.14 Transfer function pseudosection for the central Notre Dame - Exploits subzone boundary.

- Resistivity of the middle-lower crust southeast of site b8 appears to be more conductive than lower crust to the northwest. The high conductivity below site 35 may be the result of enhanced conductivity southeast of the transect as indicated by the transfer functions. The change in lower crustal conductivity is again obscured by the upper crustal conductivity anomaly.

Inverse Model (Figures 6.16) (Model fit shown in appendix A.2.3)

- Crust west of site 58 appears to be very resistive
- ($\geq$ 10000 Ω·m).
- The near surface conductivity anomaly observed on the two northern transects, between the Red Indian and Noel Pauls Lines, is absent.
- Resistivity of the middle-lower crust southeast of site 62 appears to be more

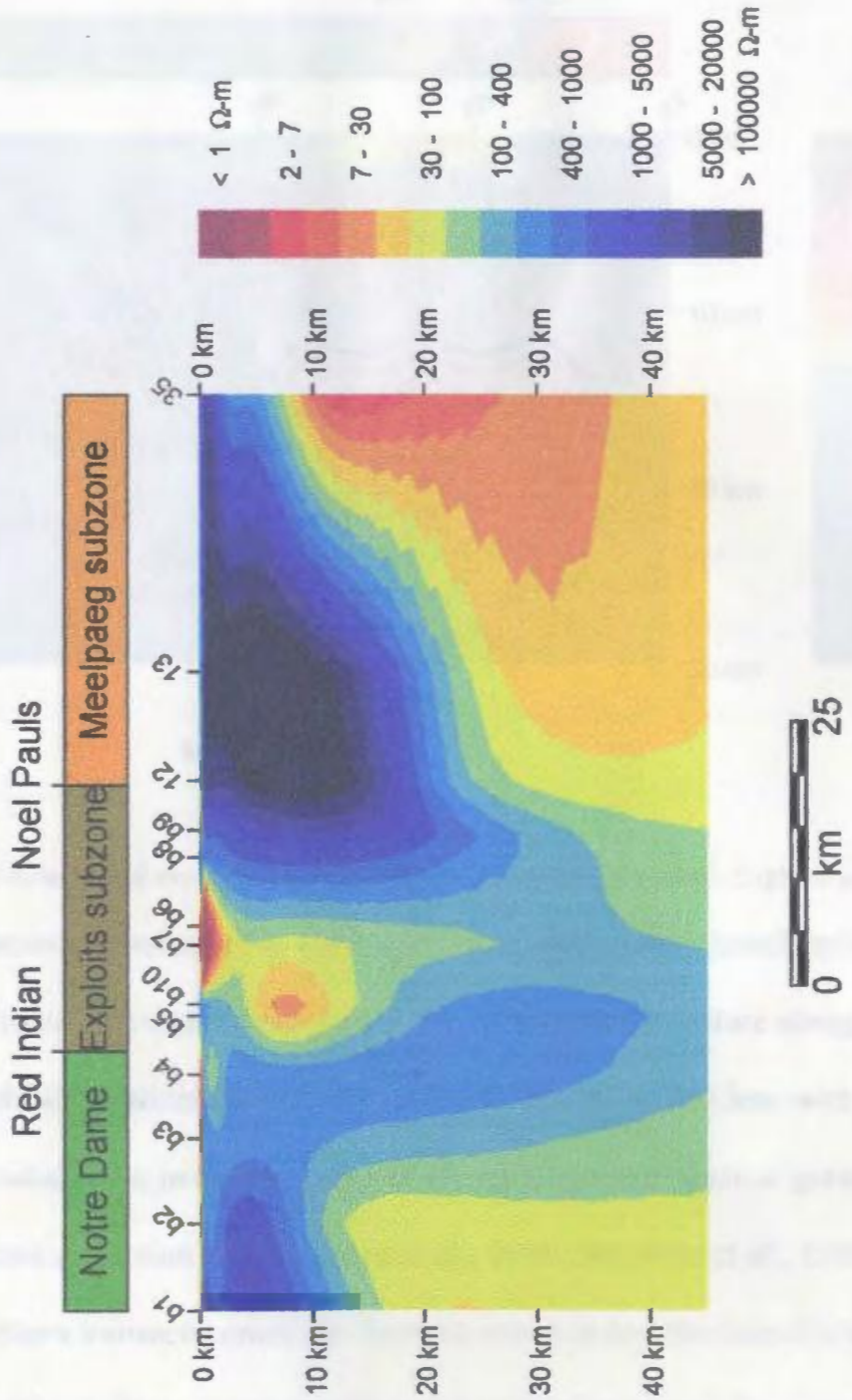

Figure 6.15 Two-dimensional inverse model (RRI) for the central Notre Dame - Exploits subzone boundary.

conductive than lower crust to the northwest.

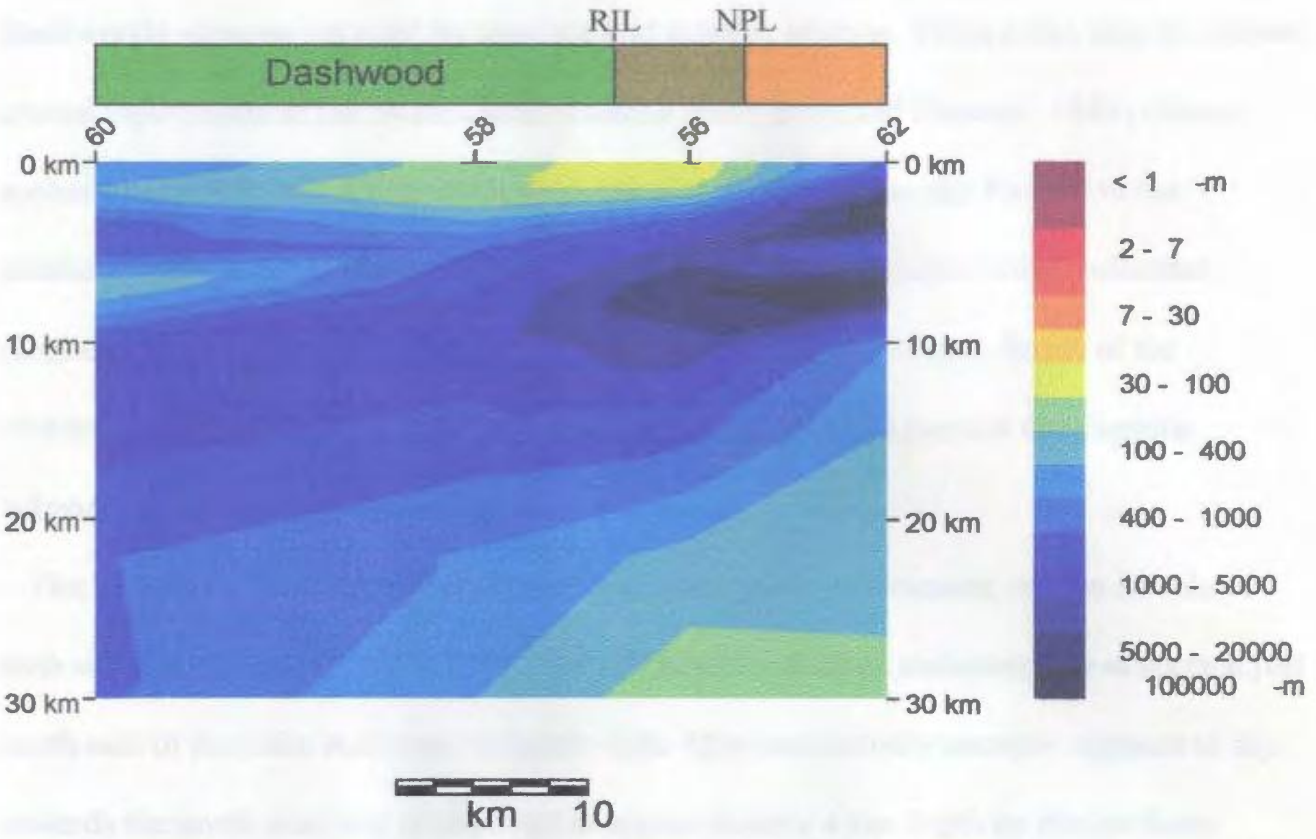

Figure 6.16 Two-dimensional inverse model (RRI) for the south Notre Dame - Exploits subzone boundary.

The three transects span approximately 150 km of the Notre Dame/Exploits subzone boundary and indicate a significant change in upper crustal structure along its length. The data and models also indicate that the boundary is roughly coincident with a change in lower crust conductivity, in agreement with changes in other physical parameters observed on earlier seismic reflection results (Keen et al., 1986; Marillier et al., 1989).

The two northern transects, cross the Topsail intrusive and Buchans-Roberts Arm volcanic of the Notre Dame subzone, volcanics and sediments of the Victoria Lake Group (Exploits subzone) bounded by the Red Indian and Noel Pauls Lines, and metasediments and intrusives of the Meelpaeg subzone. The southern transect crosses psamites of the

Dashwoods subzone intruded by tonalitic and granitic plutons. These rocks may be deeper crustal equivalents of the Notre Dame subzone (see Currie and Piasecki, 1989) (Some authors do not separate Dashwoods from the Notre Dame subzone). Further to the southeast the southern transect crosses a thin strip of Victoria Lake Group volcanics (Exploits) and granites and metasediments of the Meelpaeg subzone. South of the transects, the Red Indian Line converges with the Noel Pauls Line and the Exploits subzone is absent.

The surface conductivity anomaly, observed on the central transect, can be correlated with sediments of the Victoria Lake Group. These conductive sediments are at surface just north east of the Lake Ambrose Volcanic Belt. This conductivity anomaly appears to dip towards the north west and is observed at approximately 4 km depth on the northern transect, below post-Cardocian flysch and Cardocian black bhale. The black shale in overlying the Victoria Lake Group in this area may form part of the anomaly. To the south the conductive sediments of the Victoria Lake Group appear to be absent.

The apparent dip of the Victoria Lake Group, the convergence of the Red Indian and Noel Pauls line and changes in the geology of the Notre Dame subzone (Dashwoods versus Notre Dame), suggest that emergence of the Central Mobile Belt was greater to the southwest. Differential emergence may be the result of the collision of an Avalonian promontory in southwestern Newfoundland, as suggested by Currie and Piasecki (1989) and Lin et al. (1994).

The electromagnetic image of the Red Indian and Noel Pauls Lines indicates that they

are significant boundaries in the Appalachian Orogen. The Red Indian Line appears to be a near vertical boundary between the Exploits and Notre Dame subzones, extending to approximately 6 km depth and possibly more in north central Newfoundland (see northern transect). Relationships at the Noel Pauls Line are uncertain, although it appears to be an important upper crustal boundary in the conductivity structure of the region.

The Notre Dame/Exploits subzone boundary is roughly coincident with a change in the mid-lower crustal conductivity structure. The geometry of this lower crustal boundary is unresolved, as a result of lack of sensitivity below the conductive Victoria Lake Group. The change in conductivity is spatially coincident with a change from northwest to southeast dipping lower crustal reflectors seen on the southern Meelpaeg seismic reflection transect (Figure 6.17). This change in reflector dip may delineate the boundary.

This boundary may mark the northeastern limit of lower crust of Gondwanan affinity, although it remains uncertain as to whether this is a boundary between crust of Genvillian and Gondwanan affinity, as suggested by the offshore seismic reflection results (Keen et al., 1986; Marillier et al., 1989). The electromagnetic images of this boundary do not support the continuation of lower crust of Gondwanan affinity to the northwest below the Notre Dame subzone and Humber Zone suggested by Quinlan et al. (1992) on the basis of the onshore reflection data.

An understanding of the nature of this boundary and its relationship to the complex tectonics of the Orogen requires the full integration of seismic reflection and refraction, electromagnetic and geochemical constraints on the lower crust of the Orogen.

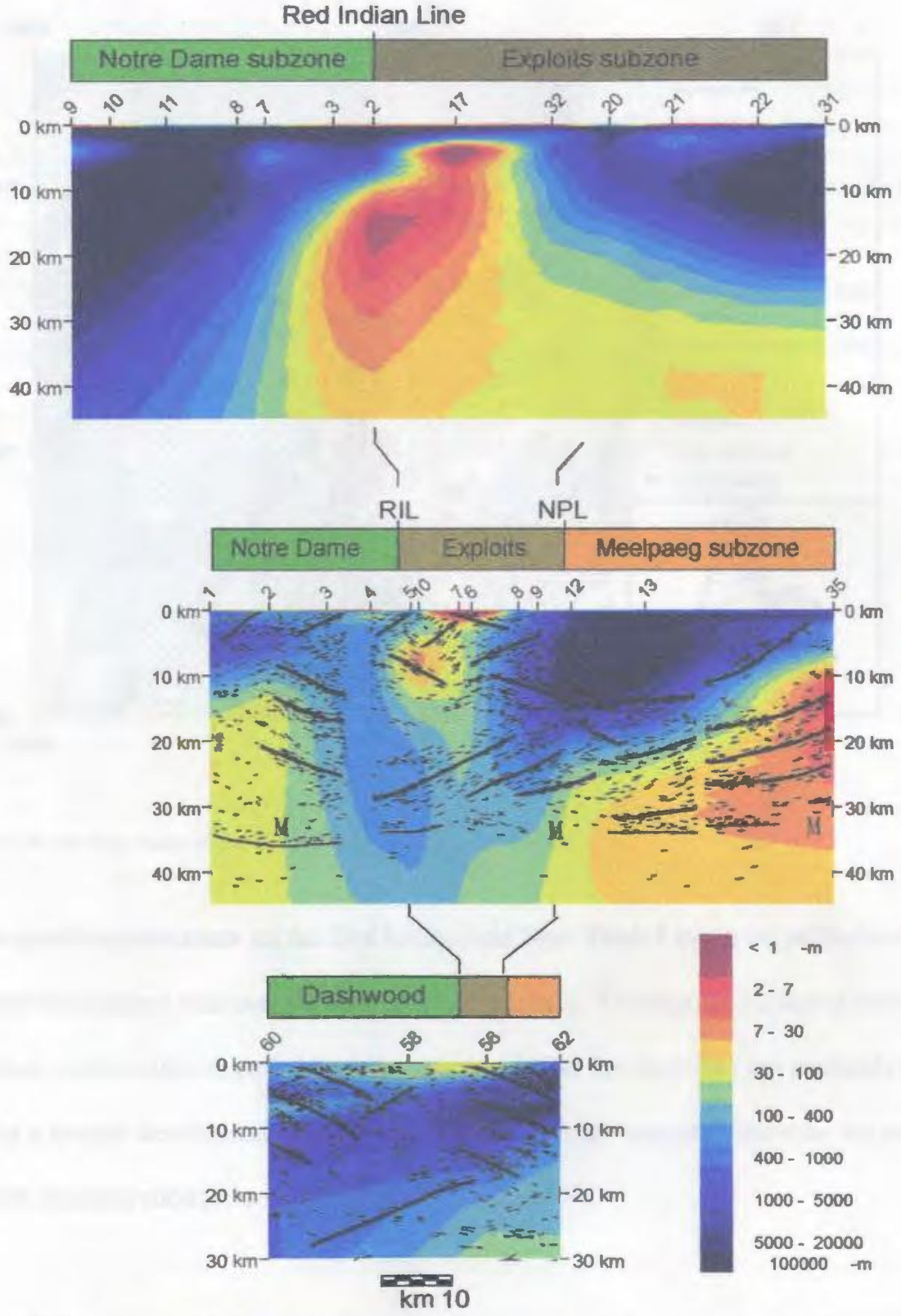

Figure 6.17 Comparison of the Notre Dame - Exploits inverse models to Lithoprobe reflection seismic profiles (Quinlan et al., 1992).

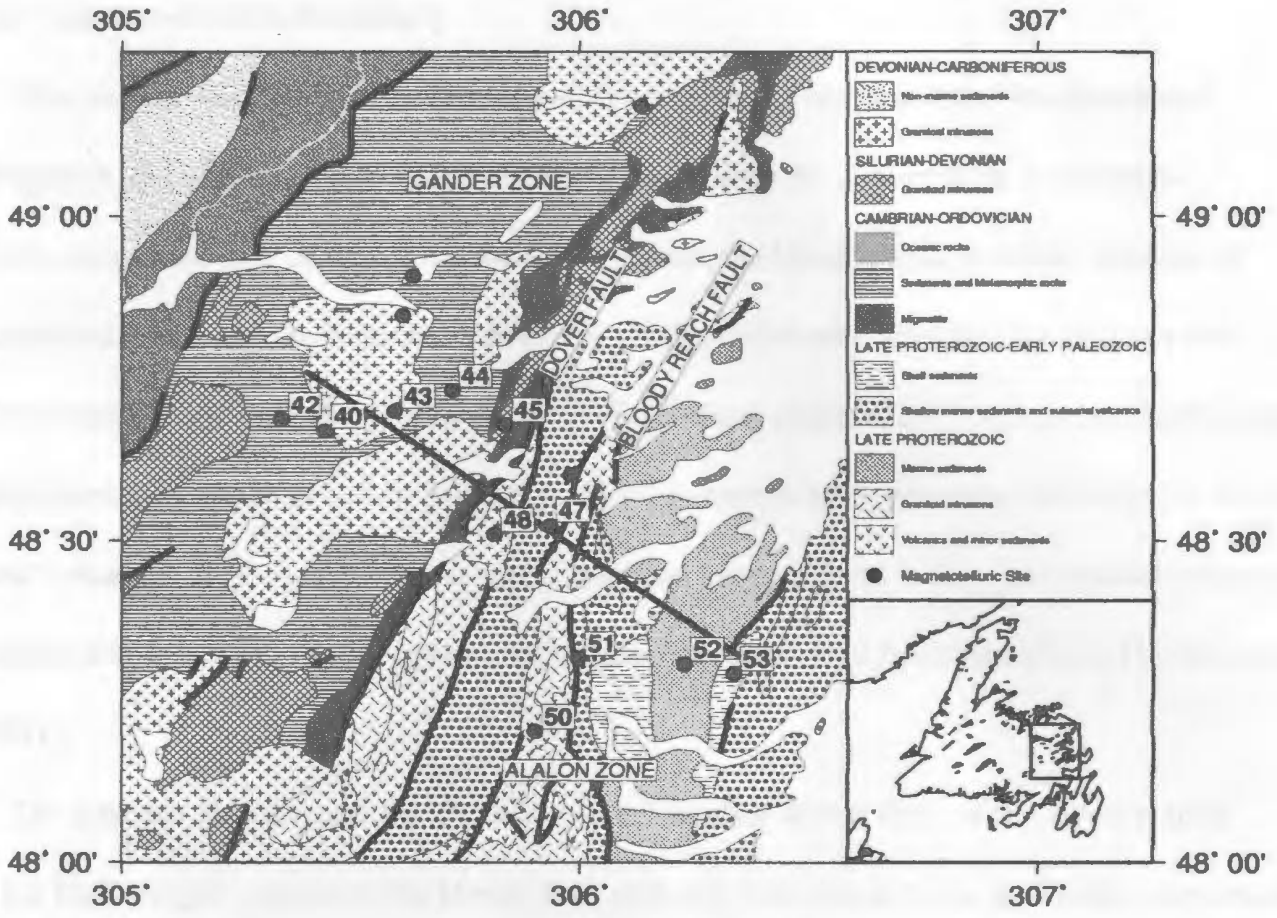

Figure 6.18 Geology map of the Gander - Avalon zone boundary.

Orogen parallel movement on the Red Indian and Noel Pauls Line have undoubtedly obscured the surface relationships across this boundary. The regions complex history of arc volcanism, sedimentation and deformation suggest that the tectonics are probably not the result of a simple development and destruction of a single marginal basin as the result of eastward directed subduction (See Dunning et al., 1991).

6.4 Gander-Avalon Boundary

This transect crosses the Gander - Avalon boundary in northeastern Newfoundland (Figure 6.18) The boundary in this region is marked by the Dover fault, a Silurian-Devonian strike-slip fault. To the west of the fault the Gander lake subzone consists of continental derived pre-Middle Ordovician clastic sediments, intruded by Silurian and Devonian granites. To the east of the fault the Avalon consists of Precambrian igneous and sedimentary rocks overlain by Paleozoic shallow marine and terrestrial sedimentary rocks and volcanics. The sharp contrast in deformation intensity and lack of correlatable features across the fault suggest that movement on the fault may have been significant (Holdsworth, 1991).

The transect also crosses the Bloody Reach/Paradise sound fault of the Avalon zone. This fault roughly parallels the Dover fault and may be related to the strike-slip movements on the Dover fault. Geologically it is recognized as the boundary between contrasting stratigraphic sequences (see Geology map of Newfoundland 1990).

Apparent Resistivity and Phase Sections (Figures 6.19 and 6.20)

- Dover fault (located between sites 46 and 48, with 48 located just east of the fault zone) is clearly a break in conductivity structure. To the west the Gander zone is resistive while to the east the Avalon zone is more conductive.
- The Bloody Reach fault (located between sites 50 and 51) also seems to be a break in the conductivity structure, with more conductive rocks at surface to the east of the fault.

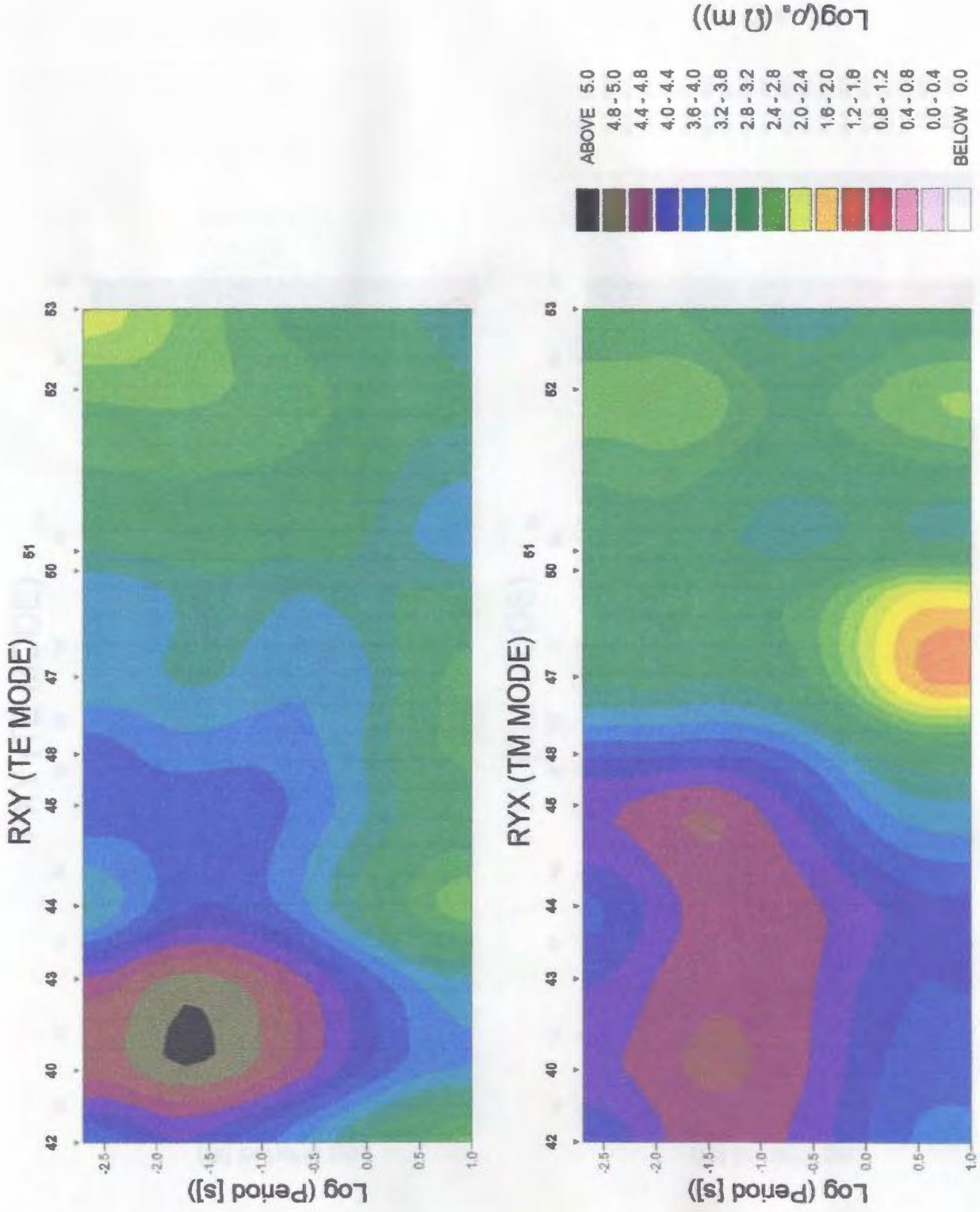

Figure 6.19 TE and TM apparent resistivity pseudosections for the Gander - Avalon boundary.

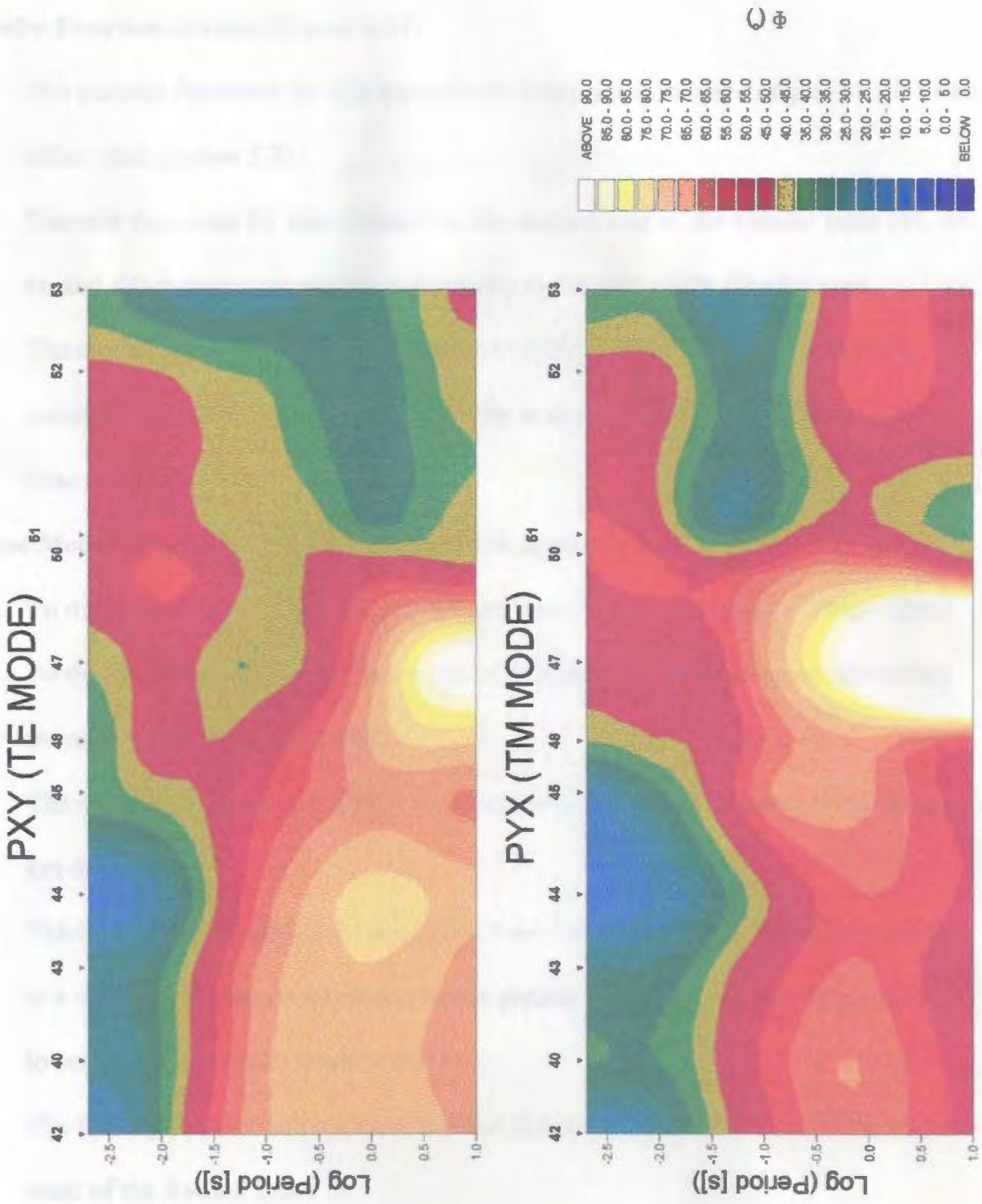

Figure 6.20 TE and TM phase pseudosections for the Gander - Avalon boundary.

Transfer Function Section (Figure 6.21)

- The transfer functions for this transect are overprinted to some degree by the coast effect (See section 5.2).
- Transfer functions for sites located on the eastern side of the Gander zone (43, 44, 46 and 48) indicate enhanced conductivity to the east of the Gander zone.
- The transfer functions for sites 52 and 53 (10Hz to 1Hz) seem to be reversed, possibly indicating enhanced conductivity at depth between the Dover and Bloody Reach faults.

Inverse Model (Figure 6.22) (Model fit shown in appendix A.3)

- To the west of the Dover fault the Gander Zone is very resistive ($\geq$ 10000 Ω·m).
- To the east the Avalon Zone has a complex upper crust consisting of alternating resistive and conductive layers.
- The middle crust of the Avalon is conductive (~ 200 Ω·m) below approximately 13 km depth.
- The contrasting conductivity structure of the Avalon and Gander Zones continues to a depth of at least 25 km and possibly greater (based on absence of conductive lower crust below the Gander Zone).
- The Bloody Reach Fault appears to offset the conductivity structure of the upper crust of the Avalon Zone.

The Dover fault is a the boundary between two terranes of contrasting electrical conductivity structures. The electromagnetic image of the Dover Fault is in agreement with

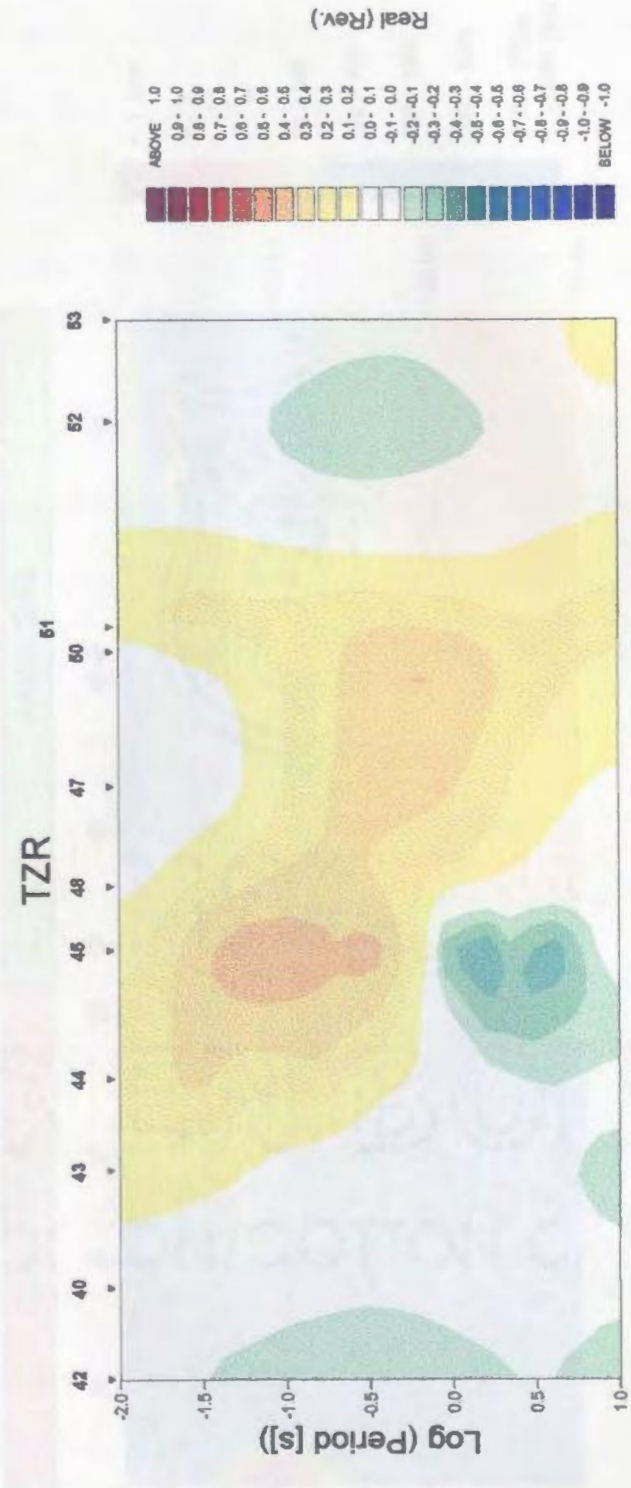

Figure 6.21 Transfer function pseudosection for the Gander - Avalon boundary.

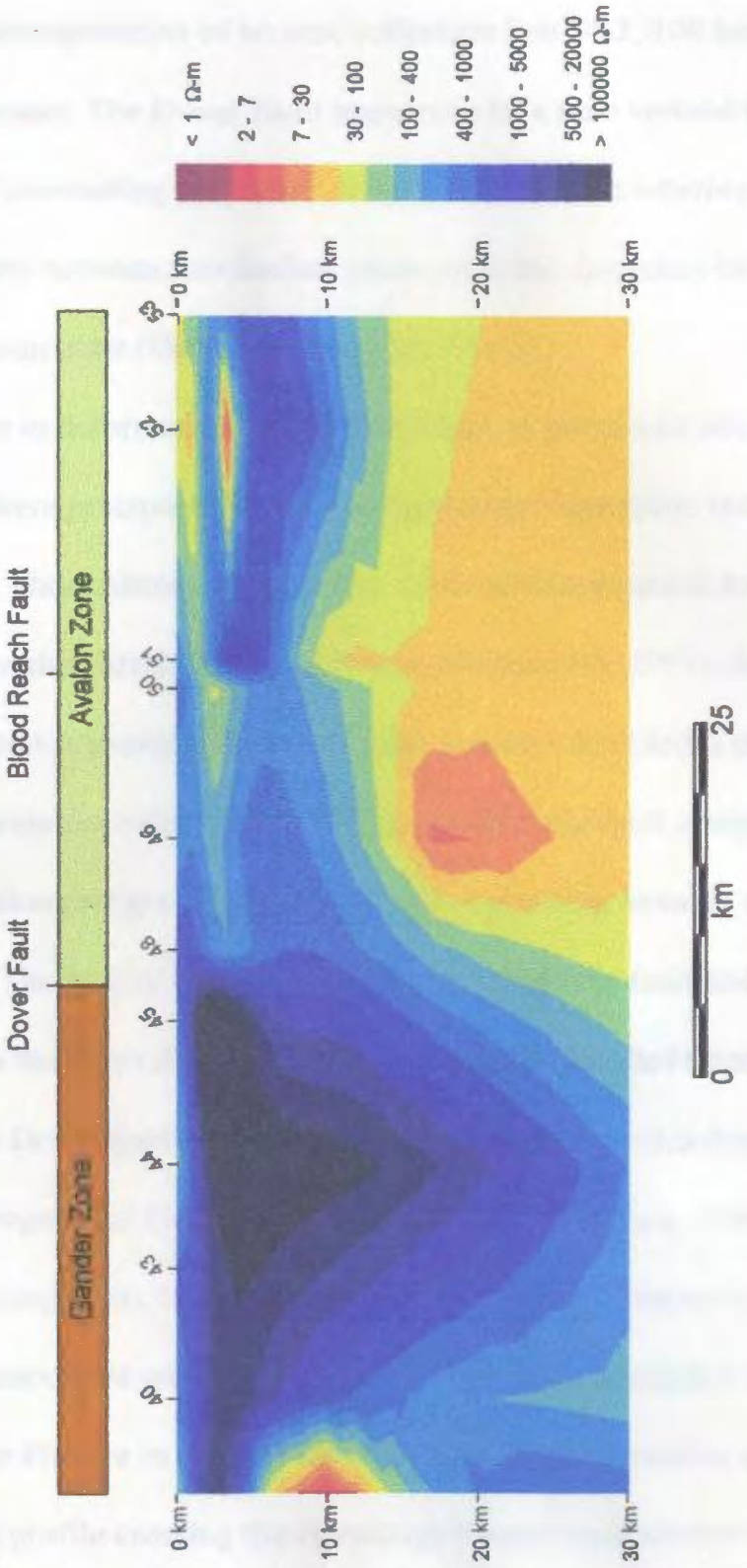

Figure 6.22 Two-dimensional inverse model (RRI) for the Gander - Avalon boundary.

Keen et al's (1986) interpretation of seismic reflection line 84-2, 100 km north of the electromagnetic transect. The Dover Fault appears to be a near vertical boundary between continental crust of contrasting properties. It remains uncertain whether the Dover Fault represents a boundary between two distinct plates or is the boundary between terranes of a composite Gondwanan plate (Gander and Avalon Zones).

The sharp contrast in deformation intensity and lack of overthrust allochthons suggest that the two zones were juxtaposed by strike-slip motion. Kinematic indicators indicate that the fault has a three phase history, with ductile sinistral transpression followed by ductile dextral transpression then brittle dextral motions (Holdsworth, 1991). An upper age limit for motion on the fault is provided by a Devonian granite which locks the fault (Ackley granite). The interpretation of the Dover fault as a strike-slip fault is supported by the change in regional Bouguer gravity anomalies and contrasting isotopic signatures of Devonian granites. The lack of correlatable features across the fault and sharp contrast in electrical properties indicates that movement on the fault must have been significant.

Movement on the Dover Fault may be related Silurian Orogenic activity observed elsewhere in the Orogen (see Hanmer, 1981; Dunning and O'Brien, 1989; Currie and Piaseki, 1989; Dunning et al., 1990 and Cawood et al., 1994). The early phase of sinistral transpression was associated with plutonism and is probably analogous to deformation along the Hermitage Flexure in south central Newfoundland (Dunning and O'Brien, 1989). The onland seismic profile crossing the Hermitage Flexure and southern extension of the Dover Fault, the Hermitage Bay Fault, is interpreted not to demonstrate the existence of a

crustal scale transcurrent fault in southern Newfoundland (Quinlan et al., 1992).

The swing in structural trends and conductivity structure (discussed in chapter 5) in south central Newfoundland and the similarity in deformation and plutonism along the Dover Fault - Hermitage Flexure, suggests that Silurian Orogenic deformation may have changed significantly along strike. Currie and Piasecki (1989) and Lin et al. (1994) have proposed models interpreting the swing in structural trends to an Avalonian promontory. In these models Silurian Orogen parallel motions observed in northern Newfoundland are accommodated by north over south thrusts and sinistral shear around the promontory in south central Newfoundland. If these models are substantiated they may be able to explain the differences between observations in southern and northern Newfoundland. The Hermitage Bay Fault in southern Newfoundland may therefore be a transcurrent fault separating Avalonian rocks displaying similar Precambrian histories, whereas the Hermitage Flexure (Bay D'Espoir Shear Zone) may be the equivalent boundary to the Dover Fault in northern Newfoundland. This boundary in south central Newfoundland however, would have a larger compressional component than the transcurrent Avalon/Gander boundary in northern Newfoundland.

The electromagnetic image of the crust of the Avalon Zone displays a number of interesting features. The upper crust appears to consist of alternating layers of resistive and conductive rocks. The resistive rocks at surface between the Dover and Bloody Reach Faults (sites 48 to 50) is consistent with the volcanics of the Love Cove Group observed at surface. East of the Bloody Reach Fault the conductive rocks at surface are sediments of

the Connecting Point Group. The Blood Reach Fault located between sites 50 and 51 seems to offset the conductivity structure of the Avalon Zone, although this may in part be due to the fault parallel offset of sites 50 and 51.

The upper crustal / middle crustal boundary observed in the inverse model at a depth of approximately 13 km may correlate with reflectors observed at around 5 second (TWT) on line 84-2 north of Newfoundland (See Keen et al., 1986) (Figure 2.7).

6.5 Summary

In this chapter the conductivity structure of three boundaries within the Appalachian orogen of Newfoundland was examined. Through two-dimensional inversion the conductivity structure of these boundaries was modelled and interpreted with respect to known geological and geophysical information.

Humber-Dunnage Boundary

The two most prominent features of the inverse model (Figure 6.5 and 6.6) are the conductive zone located beneath the Deer Lake basin and the change in conductivity structure coincident with the Baie Verte line (BVL).

The conductive zone is most reasonably interpreted as conductive sediments within or deposited on the autochthonous platform. This interpretation is in agreement with the tectonic evolution of the Humber zone proposed by Stockmal and Waldron (1991, 1993). The conductive sediments may form part of the Goose Tickle Group, deposited on the platform in a foreland basin created by emplacement of Taconian allochthons, prior to post

- Taconian westward transport and duplication of the platform sequence.

The eastern end of the conductive zone is coincident with the surface location of the BVL, the BVL may therefore mark the eastern end of the autochthonous platform. Structural investigations of the BVL suggest that the observed contrast in upper crustal electrical properties (< 20 km) coincident with the BVL are most likely the result of strike - slip motion as opposed to collisional tectonics (Goodwin and Williams, 1990). The conductivity of the lower crust west of the BVL is unresolved and it is therefore uncertain if the BVL is an electrical boundary in the lower crust. The BVL had no lower crustal seismic expression on any of the five Lithoprobe seismic reflection profiles which cross the BVL and it is uncertain how orogen parallel motion interpreted as important in the upper crust is accommodated in the lower crust (Quinlan et al., 1992; Marillier et al., 1989; Keen et al., 1986).

Notre Dame - Exploits Boundary

Three profiles crossing the Notre Dame - Exploits subzone boundary in central Newfoundland were inverted (Figures 6.11, 6.15, 6.16 and 6.17). The three inverse models indicate that the upper crust in the vicinity of the boundary changes significantly along strike and that the boundary is roughly coincident with a change in lower crustal conductivity.

On the two northern profiles conductive sediments of the Victoria Lake Group (VLG), bounded to the northwest by the Red Indian Line (RIL) and the Noel Paul's Line (NPL) to the southeast, are a dominant feature of the models. On the southern profile these

sediments appear to be absent. The models suggest that sediments of the VLG both dip and widen to the northwest. The eastern boundary of the VLG appears to be coincident with the NPL.

On all three profiles the lower crust to the southeast of the NPL appears to contrast with that to the northwest of the RIL. The boundary between the contrasting lower crusts is obscured by the conductive sediments of the VLG, although the coincidence of the boundary with northwest dipping reflectors observed on the Meelpaeg and Burgeo seismic reflection transects suggests the two may be related. This boundary may be the Grenville / Central lower crustal block boundary proposed by Keen et al. (1986).

Gander - Avalon Boundary

The electromagnetic image of the Gander-Avalon boundary in northeastern Newfoundland is consistent with the interpretation of the Dover fault as a near vertical strike-slip fault that penetrates the entire crust (Keen et al., 1986; Holdsworth, 1991). The Dover fault marks a near vertical boundary between upper-middle crusts of contrasting electrical properties and is a significant electrical boundary to a depth of at least 20 km (Figure 6.22). The sharp contrast in deformation intensity and lack of correlatable features across the fault suggests that movement on the fault must have been significant (Holdsworth, 1991).

The onshore seismic data do not demonstrate the existence of a crustal-scale fault coincident with the southern extension of the Dover fault, the Hermitage Bay fault (Quinlan et al., 1992). However, the offshore seismic reflection profiles, magnetotelluric

data and isotopic studies (Kerr et al., 1995) leave no doubt that the Dover-Hermitage fault is a major crustal-scale feature. Similarities in the Precambrian histories of the rocks juxtaposed by the Hermitage Bay fault (Dunning and O'Brien, 1989) and contrasting Precambrian isotopic signatures (Kerr et al., 1995) suggests that the fault may mark a late Precambrian boundary within a composite Gondwanan plate (Central and Avalon LCBs), reactivated during the Paleozoic tectonics.

CHAPTER 7

Conclusions

This thesis work was undertaken to improve our knowledge of the nature of the middle - lower crust of the Appalachian orogen of Newfoundland. The Appalachian orogen, records a late Precambrian - early Paleozoic cycle of ocean creation and destruction. Based on stratigraphic and structural contrasts the Newfoundland Appalachians have been divided into four tectono-stratigraphic zones (Williams, 1979). Variations in lower crustal reflectivity character, observed on early marine seismic reflection investigations, lead to a three-part division of the lower crust of the orogen (Keen et al., 1986; Marillier et al., 1989). The relationship between the tectono-stratigraphic zones observed at the surface and boundaries and affinity of the lower crust of the orogen are poorly understood, however essential for a full understanding of the tectonics of the orogen.

The Lithoprobe East magnetotelluric data, 77 soundings recorded to investigate the middle - lower crust of the orogen, proved to be one of the most complex data sets ever collected as part of Lithoprobe electromagnetic investigations. Outcropping graphitic units and rapid variations in surface geology distorted the natural electromagnetic fields, particularly the electric field, yielding responses that are very sensitive to analysis procedures. This distortion led to extending the standard distortion analysis approach of Groom and Bailey (1989) to solve simultaneously for multiple sites and multiple frequencies (McNeice and Jones, 1996). The extended analysis provides a method to recover two-dimensional regional impedances in the presence of complex near surface

geological variations and measurement noise.

The regional conductivity structure of the orogen suggests that the Baie Verte line, Red Indian line and Dover fault - Hermitage flexure represent significant electrical boundaries. The conductivity structure changes both across and along strike. The crust in north-central Newfoundland (Exploits subzone and Gander zone) differs from crust to the northwest, southeast and southwest. Tectonic boundaries to the northwest of this region, the Red Indian and the Baie Verte lines (RIL and BVL) are nearly two-dimensional, having an electrical strike of approximately 40° to 50°. To the southeast and southwest the strike of the Dover fault and Hermitage flexure changes significantly along strike. This change in structure across and along strike of the orogen is spatially coincident with deformation along the Hermitage flexure and Gander / Avalon boundary supports the proposal of an Avalonian promontory in southern Newfoundland (Currie and Piasecki, 1989). If the seismic division of the lower crust of the orogen is valid, the three lower crustal blocks appear not to have a simple near two dimensional relationship in southern Newfoundland.

The electromagnetic image of the Humber-Dunnage boundary (BVL) is in agreement with the tectonic evolution of the Humber zone proposed by Stockmal and Waldron (1991, 1993). A conductive zone observed to the west of the BVL is most reasonably interpreted as conductive sediments within or deposited on the autochthonous platform. The conductive sediments may form part of the Goose Tickle Group, deposited on the platform in a foreland basin created by emplacement of Taconian allochthons, prior to post - Taconian westward transport and duplication of the platform sequence.

The eastern end of the conductive zone is coincident with the surface location of the BVL, the BVL may therefore mark the eastern end of the autochthonous platform. Structural investigations of the BVL suggest that the observed contrast in upper crustal electrical properties (< 20 km) coincident with the BVL are most likely the result of strike - slip motion as opposed to collisional tectonics (Goodwin and Williams, 1990). The conductivity of the lower crust west of the BVL is unresolved and it is therefore uncertain if the BVL is an electrical boundary in the lower crust.

Electromagnetic images of the Notre Dame-Exploits subzone boundary in north, central and southern Newfoundland indicate that the upper crust in the vicinity of the boundary changes significantly along strike and that the boundary is roughly coincident with a change in lower crustal conductivity.

On the two northern profiles conductive sediments of the Victoria Lake Group (VLG), bounded to the northwest by the Red Indian Line (RIL) and the Noel Paul's Line (NPL) to the southeast, are a dominant feature of the models. On the southern profile these sediments appear to be absent. The models suggest that sediments of the VLG both dip and widen to the northwest.

On all three profiles the lower crust to the southeast of the NPL appears to contrast with that to the northwest of the RIL. The boundary between the contrasting lower crusts is obscured by the conductive sediments of the VLG, although the coincidence of the boundary with northwest dipping reflectors observed on the Meelpaeg and Burgeo seismic reflection transects suggests the two may be related. This boundary may be the Grenville /

Central lower crustal block boundary proposed by Keen et al. (1986).

The electromagnetic image of the Gander-Avalon boundary in northeastern Newfoundland is consistent with the interpretation of the Dover fault as a near vertical strike-slip fault that penetrates the entire crust (Keen et al., 1986; Holdsworth, 1991). The Dover fault marks a near vertical boundary between upper-middle crusts of contrasting electrical properties and is a significant electrical boundary to a depth of at least 20 km. The sharp contrast in deformation intensity and lack of correlatable features across the fault suggests that movement on the fault must have been significant (Holdsworth, 1991).

The onshore seismic data do not demonstrate the existence of a crustal-scale fault coincident with the southern extension of the Dover fault, the Hermitage Bay fault (Quinlan et al., 1992). However, the offshore seismic reflection profiles, magnetotelluric data and isotopic studies (Kerr et al., 1995) leave no doubt that the Dover-Hermitage fault is a major crustal-scale feature. Similarities in the Precambrian histories of the rocks juxtaposed by the Hermitage Bay fault (Dunning and O'Brien, 1989) and contrasting Precambrian isotopic signatures (Kerr et al., 1995) suggests that the fault may mark a late Precambrian boundary within a composite Gondwanan plate (Central and Avalon LCBs), reactivated during the Paleozoic tectonics.

The sharp change in upper-middle crustal conductivity observed in the magnetotelluric data suggest that orogen parallel motions were important in the development of many of the major boundaries of the orogen (BVL, RIL and Dover fault).

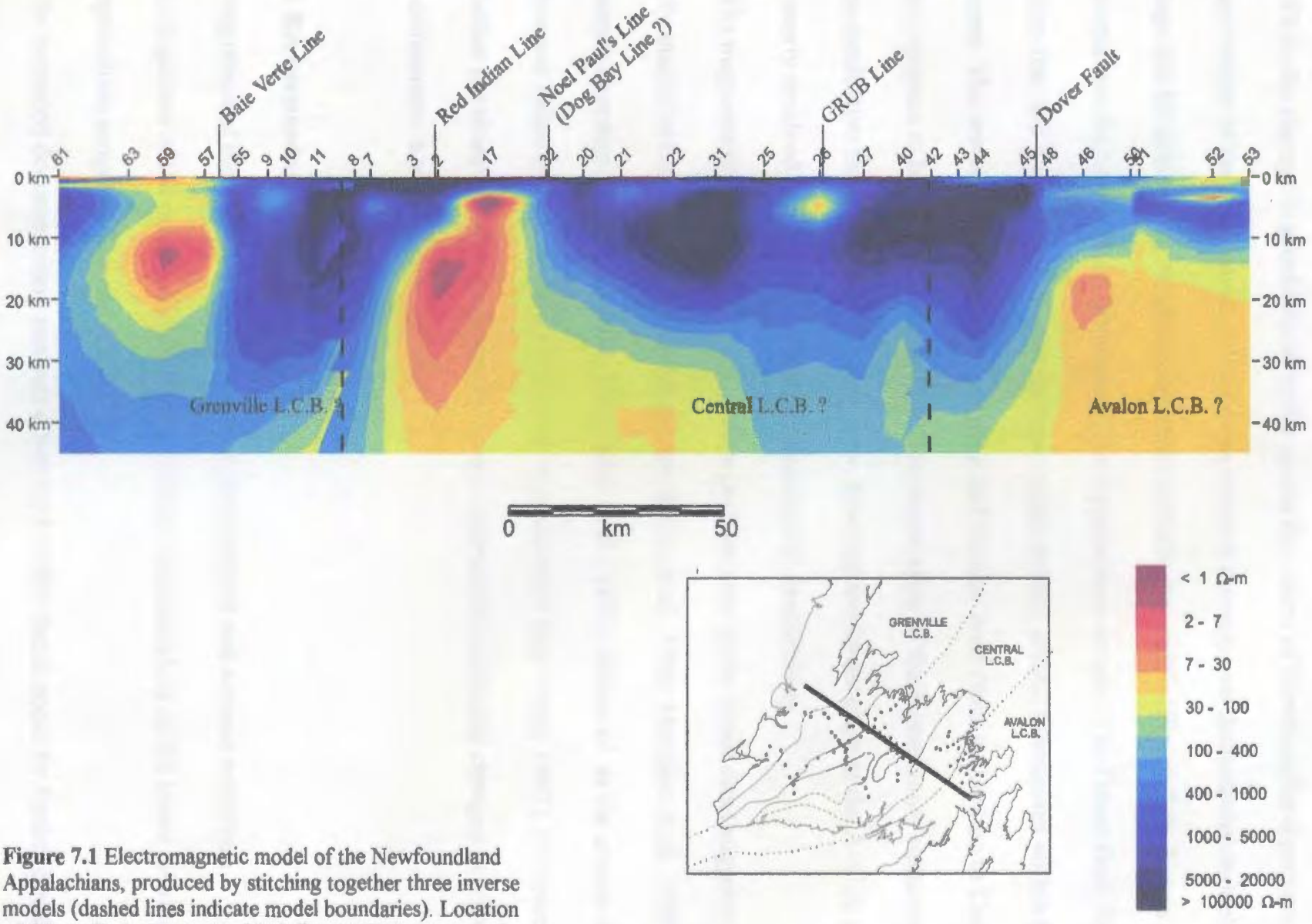

Figure 7.1 Electromagnetic model of the Newfoundland Appalachians, produced by stitching together three inverse models (dashed lines indicate model boundaries). Location of the profile is shown as a black line on the inset map of Newfoundland.

While the change in geoelectrical strike across the island of Newfoundland prevents examination of the conductivity structure as a whole through two-dimensional modelling an image can be obtained by stitching together conductivity models (Figure 7.1). Figure 7.1 summarizes the conductivity structure of the Appalachian orogen. The Dover fault, Red Indian line and Baie Verte line clearly mark upper-middle crustal boundaries within the orogen. The lower crust of Exploits subzone and Gander zone (Red Indian line to Dover fault) appears to be more conductive than the lower crust of the Notre Dame subzone and less conductive than that of the Avalon zone, however the lower crust of the Avalon zone is poorly resolved as a result of enhanced mid crustal conductivity.

The magnetotelluric data support the three part division of the lower crust suggested by early marine reflection seismic investigations (Keen et al., 1986; Marillier et al., 1989) and isotopic investigations (Fryer et al., 1992; Kerr et al., 1995). However, as the source of enhanced lower crustal conductivity is poorly understood (see Jones, 1992), it is uncertain whether the observed changes in lower crustal conductivity represent changes in petrology or differences in evolutionary history.

7.1 Recommendations for Future Work

Integration of the results of this thesis with geochemical and seismic refraction investigations of the orogen should lead to a better understanding of the lower crust of the Appalachian orogen in Newfoundland.

The extended decomposition analysis developed in this thesis could be further developed

to include magnetic distortion. Including magnetic distortion of both the magnetotelluric impedance tensor and magnetotelluric transfer functions would improve the recovered regional impedances and possibly extend the range of applicability of the distortion model.

REFERENCES

Agarwal, A.K., Poll, H.E., and Weaver, J.T. 1993. One and two dimensional inversion of MT data in continental regions. Physics of the Earth and Planetary Interiors, 81: 155-176.

Bahr, K. 1988. Interpretation of the magnetotelluric impedance tensor: regional induction and local telluric distortion. Journal of Geophysics, 62: 119-127.

Bahr, K. 1991. Geologic noise in magnetotelluric data: a classification of distortion type. Physics of the Earth and Planetary Interiors, 66: 24-38.

Bailey, R.C. 1970. Inversion of the geomagnetic induction problem. Proceedings of the Royal Society of London, Ser. A, 315: 185-194.

Beamish, D., and Smythe, D.K. 1986. Geophysical images of the deep crust: the Iapetus suture. Journal of the Geological Society, London, 143: 489-497.

Berdichevsky, M.N., and Dmitriev, V.I. 1976, Basic principles of interpretation of magnetotelluric curves. *In* Adam, A., Ed., Geolectric and Geothermal Studies. Akademini Kiado, 165-221.

Bird, J.M., and Dewey, J.F. 1970. Lithosphere plate-continental margin tectonics and the evolution of the Appalachian orogen. Geological Society of America Bulletin, 81: 1031-1060.

Boerner, D.E., Kurtz, R.D., Craven, J.A., Rodenay, S. and Qian, W. 1995. A burried Proterozoic foredeep under the Western Canada basin?. Geology, 23: 943-946.

Boerner, D.E., Kurtz, R.D. and Craven, J.A. 1996. Electrical conductivity and Paleo-Proterozoic foredeeps. Journal of Geophysical Research, 101: 13,775-13,791.

Cagniard, L. 1953. Basic theory of the magneto-telluric method of geophysical prospecting, Geophysics, 18: 605-635.

Cawood, P.A., Barnes, C.R., Botsford, J.W., James, N.P., Knight, I., O'Brien, S.J., O'Neill, P.P., Parsons, M.G., Stenzel, S.R., Stevens, R.K., Williams, H., and Williams, S.H. 1988. Field excursion guide book: a cross-section of the Iapetus ocean and its continental margins. 5th International Symposium on the Ordovician System, Aug. 1988, St. John's, Newfoundland, 144p.

Cawood, P.A., and Williams, H. 1988. Acadian basement thrusting, crustal delamination, and structural styles in and around the Humber Arm allochthon, western

Newfoundland. Geology, 16: 370-373.

Cawood, P.A., and Suhr, G. 1992. Generation and obduction of ophiolites: constraints from the Bay of Islands complex, western Newfoundland. Tectonics, 11: 884-897.

Cawood, P.A., Dunning, G.R., Lux, D., and van Gool, J.A.M. 1994. Timing of peak metamorphism and deformation along the Appalachian margin of Laurentia in Newfoundland: Silurian, not Ordovician. Geology, 22: 399-402.

Cawood, P.A., van Gool, J.A.M. and Dunning, G.R. 1995. Collisional tectonics along the Laurentian margin of the Newfoundland Appalachians. *In* Hibbard, J.P., van Staal, C.R. and Cawood, P.A., eds., Current Perspectives in the Appalachian-Caledonian Orogen. Geological Association of Canada, Special Paper 41, pp. 283-301.

Chakridi, R., Chouteau, M., and Mareschal, M. 1992. A simple technique for analysing and partly removing galvanic distortion from the magnetotelluric impedance tensor: application to Abitibi and Kapuskasing data (Canada). Geophysical Journal International, 108: 917-929.

Chave, A.D., and Smith, T.J. 1994,. On electric and magnetic galvanic distortion tensor decompositions. Journal of Geophysical Research, 99: 4669-4682.

Chave, A.D. and Jones, A.G., 1997. Electric and magnetic field distortion decomposition of BC87 data. Journal of Geomagnetism and Geoelectricity, in press.

Cochrane, N.A., and Hyndman, R.D. 1974. Magnetotelluric and magnetovariational studies in the Atlantic Canada. Geophysical Journal of the Royal Astronomical Society, 39: 385-406.

Cochrane, N.A., and Wright, J.A. 1977. Geomagnetic sounding near the northern termination of the Appalachian system. Canadian Journal of Earth Sciences, 14: 2858-2864.

Colman-Sadd, S.P. 1980. Geology of south-central Newfoundland and evolution of the eastern margin of Iapetus. American Journal of Science, 280: 991-1017.

Colman-Sadd, S.P. 1982. Two stage continental collision and plate driving forces. Tectonophysics, 90: 263-282.

Colman-Sadd, S.P., and Swinden, H.S. 1984. A tectonic window in central Newfoundland? Geological evidence that the Appalachian Dunnage Zone is

allochthonous. Canadian Journal of Earth Sciences, 21: 1349-1367.

Colman-Sadd, S.P., Dunning, G.R., and Dec, T. 1992. Dunnage-Gander relationships and Ordovician orogeny in central Newfoundland: A sediment provenamce and U/Pb age study. America Journal of Science, 292: 317-355.

Colman-Sadd, S.P., Stone, P., Swinden, H.S., and Barnes, R.P. 1992. Parallel geological developement in the Dunnage Zone of Newfoundland and the Lower Paleozoic terranes of southern Scotland: an assessment. Transactions of the Royal Society of Edinburgh: Earth Sciences, 83: 571-594.

Currie, K.L., and Piasecki, M.A.J., 1989. Kinematic model for southwestern Newfoundland based upon Silurian sinistral shearing. Geology, 17: 938-941.

Dainty, A.M., Keen, C.E., Keen, M.J., and Blanchard, J.F. 1966. Review of geophysical evidence on crust and upper mantle structure on the eastern seaboard of Canada. *In* Steinhart, J.S., and Smith, T.J., eds., The Earth Beneath the Continents. American Geophysical Union, Geophysical Monograph 10, pp. 349-369.

Dec, T., Swinden, H.S. and Dunning, G.R. 1997. Lithostratigraphy and geochemistry of the Cottrells Cove Group, Buchans - Roberts Arm volcanic belt: new constraints for the paleotectonic setting of the Notre Dame Subzone, Newfoundland Appalachians. Canadian Journal of Earth Sciences, 34: 86-103.

Dosso, H.W., Nienabar, W., Wright, J.A., Greenhouse, J.P., and Bailey, R.C. 1980. An analogue model study of electromagnetic induction in the eastern coastal region of North America. Physics of the Earth and Planetary Interiors, 23: 13-30.

Dubé, B., Dunning, G.R., Lauzière, K. and Roddick, J.C. 1996. New insights into the Appalachian Orogen from geology and geochronology along the Cape Ray fault zone, southwest Newfoundland. Geological Society of America Bulletin 108: 101-116.

Dunning, G.R., and Krogh, I.F. 1985. Geochronology of ophiolites of the Newfoundland Appalachians. Canadian Journal of Earth Sciences, 22: 1659-1670.

Dunning, G.R., Kean, B.F., Thurlow, J.G. and Swinden, H.S. 1987. Geochronology of the Buchans, Roberts Arm and Victoria Lake groups and Mansfield Cove complex, Newfoundland. Canadian Journal of Earth Science, 24: 1175-1184.

Dunning, G.R., and O'Brien, S.J., 1989. Late Proterozoic-early Paleozoic crust in the

Hermitage flexure, Newfoundland Appalachians: U/Pb ages and tectonic significance. Geology, 17: 548-551.

Dunning, G.R., O'Brien, S.J., Colman-Sadd, S.P., Blackwood, R.F., Dickson, W.L., O'Neill, P.P., and Krough, T.E. 1990. Silurian orogeny in the Newfoundland Appalachians. Journal of Geology, 98: 895-913.

Dunning, G.R., Swinden, H.S., Kean, B.F., Evans, D.T.W., and Jenner, G.A. 1991. A Cambrian island arc in Iapetus: geochronology and geochemistry of the Lake Ambrose volcanic belt, Newfoundland Appalachians. Geological Magazine, 128: 1-17.

Eggers, D.E. 1982. An eigenstate formulation of the magnetotelluric impedance tensor. Geophysics, 47: 1204-1214.

Fryer,B.J., Kerr, A., Jenner, G.A., and Longstaffe, F.J. 1992. Probing the crust with plutons: regional isotopic geochemistry of granitoid intrusions across insular Newfoundland. In Current Research (1992), Geological Survey Branch, Newfoundland Department of Mines and Energy Report 92-1. pp.119-140.

Goodwin, L.B., and Williams, P.F. 1990. Strike-slip movement along the Baie Verte Line. *In* Report of Lithoprobe East Meeting, Oct. 24-25, 1990, Memorial University, St. John's, Newfoundland, pp. 75-84.

Greenough, J.D., Fryer, B.J., and Owen, J.V. 1990. Evidence for sialic basement to the Dunnage Zone, Notre Dame Bay, Newfoundland. *In* Report of Lithoprobe East Transect Meeting, Oct. 24-25, 1990, Memorial University, St. John's, Newfoundland, pp. 85-87.

Groom, R.W. 1988. The effects of inhomogeneities on magnetotellurics. PhD Thesis, University of Toronto.

Groom, R.W., and Bailey, R.C. 1989. Decomposition of Magnetotelluric impedance tensors in the presence of local three-dimensional galvanic distortion. Journal of Geophysical Research, 94: 1913-1925.

Groom, R.W., and Bailey, R.C. 1991. Analytic investigations of the effects of near-surface three-dimensional galvanic scatters on MT tensor decompositions. Geophysics, 56: 496-518.

Groom, R.W., and Bahr, K. 1992. Corrections for near surface effects: decomposition of

the magnetotelluric impedance tensor and scaling corrections for regional resistivities a tutorial. Surveys in Geophysics, 13: 341-379.

Groom, R.W., Kurtz, R.D., Jones, A.G., and Boerner, D.E. 1993. A quantitative methodology for determining the dimensionality of conductivity structure and the extraction of regional impedance responses from magnetotelluric data. Geophysical Journal International, 115: 1095-1118.

Gupta, J. C. and Jones, A. G. 1995. Electrical conductivity structure of the Purcell Anticlinorium in southeast British Columbia and northwest Montana. Canadian Journal of Earth Sciences, 32: 1564-1583.

Haak V. and Hutton, V.R.S. 1986. Electrical resistivity in continental lower crust. *In* Dawson, J.B., Carswell, D.A., Hall, J. and Wedepohl, K.H., Eds., The Nature of the Lower Continental Crust. Geological Society of London, Special Publication, 24: 35-49.

Hall, J., Quinlan, G., Marillier, F., and Keen, C. 1990. Dipping shear zones and the base of the crust in the Appalachians, offshore Canada. Tectonophysics, 173: 581-593.

Hall, J., Barnes, P., Roberts, B., Spencer, C., and Wright, J. 1990. Lithoprobe East 1989 seismic reflection data. *In* Report of Lithoprobe East Transect Meeting, Oct. 24-25, 1990, Memorial University, St. John's, Newfoundland, pp.88-94.

Hall, J., Wright, J., Roberts, B., Cote, T., Luetgert, J., and Hughes, S. 1991. Delineating crustal blocks in the Appalachians: Results from the onland part of Lithoprobe East's 1991 seismic refraction / wide-angle reflection experiment in Newfoundland. American Geophysical Union, Program and Abstracts, EOS supplement 72: 297.

Hall, J., Marillier, F. and Dehler, S. 1998. Geophysical studies of the Appalachian Orogen in the Atlantic borderlands of Canada. Canadian Journal of Earth Sciences. (In press).

Hanmer, S. 1981. Tectonic significance of the northeastern Gander Zone, Newfoundland: an Acadian ductile shear zone. Canadian Journal of Earth Sciences, 18: 120-135.

Harland, W.B., and Gayer, R.A. 1972. The Arctic Caledonides and earlier oceans. Geological Magazine, 109: 289-314.

Hebert, D., Dosso, H.W., Nienaber, W., and Wright, J.A. 1983. Analogue model study of electromagnetic induction in the Newfoundland region. Physics of the Earth and

Planetary Interiors, 32: 65-84.

Holdsworth, R.E. 1991. The geology and structure of the Gander-Avalon boundary zone in northeastern Newfoundland. In Current Research (1991), Newfoundland Department of Mines and Energy Report 91-1. pp. 109-126.

Hughes, S., Hall, J., and Luetgert, J.H. 1994. The seismic velocity structure of the Newfoundland Appalachian Orogen. Journal of Geophysical Research, 99: 13,633-13,653.

Hutton, D.H.W. 1987. Strike-slip terranes and a model for the evolution of the British and Irish Caledonides. Geological Magazine, 124: 405-425.

Hutton, D.H.W. 1989. Pre-Alleghanian terrane tectonics in the British and Irish Caledonides. *In* Dallmeyer, R.D., ed., Terranes of the Circum-Atlantic Paleozoic Orogens. Geological Society of America, special paper 230, pp.47-57.

Hutton, V.R.S. and Jones, A.G. 1980. Magnetovariational and magnetotelluric investigations in S. Scotland. Journal of Geomagnetism and Geoelectricity, 32: SI 141 - SI 150.

Hyde, R.S. 1984.

Ingham, M.R. 1988. The use of invariant impedances in magnetotelluric interpretation. Geophysical Journal of the Royal Astronomical Society, 92: 165-169.

Jenner, J.A., Dunning, G.R., Malpas, J., Brown, M., and Brace, T. 1991. Bay of Islands and Little Port complexes, revisited: age, geochemical and isotopic evidence confirm supra subduction zone origin. Canadian Journal of Earth Sciences, 28: 1635-1632.

Jones, A.G. and Hutton, V.R.S. 1977. Magnetotelluric investigation of the Eskdalemuir anomaly S. Scotland - preliminary results. Acta Geodaet. Geophys. Mont, 12: 111-115.

Jones, A.G. and Hutton, V.R.S. 1979a. A multi-station magnetotelluric study in southern Scotland - I. Fieldwork, data analysis and results. Geophysical Journal of the Royal Astronomical Society, 56: 329-349.

Jones, A.G. and Hutton, V.R.S. 1979b. A multi-station magnetotelluric study in southern

Scotland - II. Monte-Carlo inversion of the data and its geophysical and tectonic implications. Geophysical Journal of the Royal Astronomical Society, 56: 351-368.

Jones, A.G. 1983. The problem of "current channelling": a critical review. Geophysical Surveys, 6: 79-122.

Jones, A.G. 1986. Parkinson's pointers' potential perfidy! Geophysical Journal of the Royal Astronomical Society, 87: 967-978.

Jones, A.G., and Garland, G.D. 1986. Preliminary interpretation of the upper crustal structure beneath Prince Edward Island. Annals of Geophysics, 4: 157-164.

Jones, A.G. 1987. MT and reflection: an essential combination. Geophysical Journal of the Royal Astronomical Society, 89: 7-18.

Jones, A.G. 1988. Static sift of magnetotelluric data and its removal in a sedimentary basin environment. Geophysics, 53: 967-978.

Jones, A.G., Chave, A.D., Egbert, G., Auld, D. and Bahr, K., 1989. A comparison of techniques for magnetotelluric response function estimation. Journal of Geophysical Research, 94: 14,201-14,213.

Jones, A.G. and Craven, J.A. 1990. The North American Central Plains conductivity anomaly and its correlation with gravity, magnetics, seismic, and heat flow data in the Province of Saskatchewan. Physics of the Earth and Planetary Interiors, 60: 169-194.

Jones, A.G. 1992. Electrical conductivity of the continental lower crust. *In* Fountain, D.M., Arculus, R.J, and Kay, R.W., eds., Continental Lower Crust. Elsevier, pp. 81-143.

Jones, A.G., and Groom, R. 1993. Strike angle determination from the magnetotelluric impedance tensor in the presence of noise and local distortion: rotate at your peril! Geophysical Journal International, 113: 524-534.

Jones, A.G. 1993. Electromagnetic images of modern and ancient subduction zones. Tectonophysics, 219: 29-45.

Jones, A.G., and Dumas, I. 1993. Electromagnetic images of a volcanic zone. Physics of the Earth and Planetary Interiors, 81: 289-314.

Jones, A.G., Groom, R.W., and Kurtz, R.D. 1993a. Decomposition and modelling of the BC87 dataset. Journal of Geomagnetism and Geoelectricity, 45: 1127-1150.

Jones, A.G., Craven, J.A., McNeice, G.W., Ferguson, I.J. Boyce, T., Farquarson, C. and Ellis, R.G. 1993b. The North American Central Plains conductivity anomaly within the Trans-Hudson orogen in northern Saskatchewan. Geology, 21: 1027-1030.

Kao, D., and Orr, D. 1982. Magnetotelluric studies in the Market Weighton area of eastern England. Geophysical Journal of the Royal Astronomical Society, 70, 323-337.

Karlstrom, K.E. 1983. Reinterpretation of Newfoundland gravity data and arguments for an allochthonous Dunnage Zone. Geology, 44: 263-266.

Keen, C.E., Keen, M.J., Nichols, B., Reid, I., Stockmal, G.S., Colman-Sadd, S.P., O'Brien, S.J., Miller, H., Quinlan, G., Williams, H., And Wright, J.A. 1986. Deep seismic reflection profile across the northern Appalachians. Geology, 14: 141-145.

Keen, C.E., Loncarevic, B.D., Reid, I., Woodside, J., Harworth, R.T., and Williams, H. 1990. Tectonic and Geophysical Overview; chapter 2. *In* Keen, C.E., and Williams, G.L., eds., Geology of the Continental Margin of Eastern Canada. Geological Survey of Canada, Geology of Canada, no. 2, pp.31-85.

Keppie, J.D. 1989. Northern Appalachian terranes and their accretionary history. *In* Dallmeyer, R.D., ed., Terranes in the circum-Atlantic Paleozoic orogens. Geological Society of America, special paper 230, pp.159-192.

Kerr, A., Jenner, G.A. and Fryer, B.J. 1995. Sm-Nd isotopic geochemistry of Precambrian to Paleozoic granitoid suites and the deep-crustal structure of the southeast margin of the Newfoundland Appalachians. Canadian Journal of Earth Science, 32: 224-245.

Kerr, A. 1996. Space-time-composition relationships amongst Appalachian-cycle plutonic suites in Newfoundland. *In* Sinha, J.B., Whalen, J.B. and Hogan, J.P., eds., The nature of magmatism in the Appalachian Orogen. Geological Society of America Memoir 191, pp. 193-219.

Kurtz, R.D., and Garland, G.D. 1976. Magnetotelluric measurements in eastern Canada. Geophysical Journal of the Royal Astronomical Society, 45: 321-347.

Kurtz, R.D., Craven, J.A., Niblett, E.R., and Stevens, R.A. 1993. The conductivity of the crust and mantle beneath the Kapuskasing Uplift: electrical anisotropy in the upper

mantle. Geophysical Journal International, 113: 483-498.

Larsen, J.C. 1977. Removal of local surface conductivity effects from low frequency mantle response curves. Acta Geodaet. Geophys. Mont, 12: 183-186.

LaTorraca, G.A., Madden, T.R., and Korringa, J. 1986. An analysis of the magnetotelluric impedance for three-dimensional conductivity structures. Geophysics, 51: 1819-1829.

Lin, S., van Staal, C.R. and Dubé, B. 1994. Promontory-promontory collision and tear faulting in the Canadian Appalachians. Geology: 897-900.

Mackie, R.L., Madden, T.R., and Wannamaker, P.E. 1993, Three-dimensional magnetotelluric modeling using difference equations - theory and comparison to integral equation solutions, Geophysics, 58: 215-226.

Madden, T., and Nelson, P. 1964. A defence of Cagniard's magnetotelluric method. Project NR-371-401, Geophysics Laboratory, M.I.T., Cambridge, Massachusetts.

Marillier, F., Keen, C.E., Stockmal, G.S., Quinlan, G., Williams, H., Colman-Sadd, S.P., and O'Brien, S.J. 1989. Crustal structure and surface zonation of the Canadian Appalachians: Implications of deep seismic reflection data. Canadian Journal of Earth Sciences, 26: 305-321.

Marillier, F., Roberts, B., Hall, J., Louden, K., Reid, I., Hughes, S., Lu, H., Cote, T., Clowes, R., Fowler, J., Guest, S., Luetgert, J., Quinlan, G., Spencer, C., Wright, J. 1994. Lithoprobe East onshore-offshore refraction survey - constraints on interpretation of reflection data in the Newfoundland Appalachians. Tectonophysics, 232: 1759-1772.

McGeary, S. 1989. Reflection seismic evidence for a Moho offset beneath the Walls Boundary strike-slip fault. Geological Society of London Journal, 146: 261-269.

McKerrow, W.S., and Cocks, L.R.M. 1977. The location of the Iapetus ocean suture in Newfoundland. Canadian Journal of Earth Science, 14: 488-499.

McKerrow, W.S., and Ziegler, A.M. 1971. The lower Silurian paleogeography of New Brunswick and adjacent areas. Journal of Geology, 79: 635-646.

M^{c}Neice, G.W. and Jones, A.G., 1996. Multi-site, multi-frequency tensor decomposition of magnetotelluric data. Contributed paper at *"66th Annual Society of Exploration*

Geophysics meeting", held in Denver, Colorado, on 10-15 November. Abstract publ. In Conference Proceedings.

Miller, H.G. 1990. A synthesis of the geophysical characteristics of terranes in eastern Canada. Tectonophysics, 177: 171-191.

Neuman, R.B., and Max, M.D. 1989. Penobscottian-Grampian-Finnmarkian orogenies as indicators of terrane linkages. *In* Dallmeyer, R.D., ed., Terranes in the Circum-Atlantic Paleozoic Orogens. Geological Society of America, special paper 230, pp.31-45.

O'Brien, B.H., O'Brien, S.J., and Dunning, G.R. 1991a. Silurian cover, Late Precambrian-Early Ordovician basement, and the chronology of Silurian orogenesis in the Hermitage Flexure, (Newfoundland Appalachians). American Journal of Science, 291: 760-799.

O'Brien, S.J., O'Brien, B.H., O'Driscoll, C.F., Dunning, G.R., Holdsworth, R.E., and Tucker, R. 1991b. Silurian orogenesis and the NW limit of Avalonian rocks in the Hermitage Flexure, Newfoundland Appalachians. Geological Society of America, Northeastern Section, Abstracts with Programs, 23: 86.

Ogawa, Y., Nishida, Y. and Makino, M. 1994. A collision boundary imaged by magnetotellurics, Hidaka Mountains, central Hokkaido, Japan. Journal of Geophysical Research, 99: 22,373-22,388.

Park, S.K. 1985. Distortion of magnetotelluric sounding curves by three-dimensional structures. Geophysics, 50: 785-797.

Park, S.K., and Livelybrooks, D.W. 1989. Quantitative interpretation of rotationally invariant parameters in magnetotellurics. Geophysics, 54: 1483-1490.

Parkinson, W.D., 1959. Direction of rapid geomagnetic fluctuations. Geophysical Journal of the Royal Astronomical Society, 2: 1-14.

Parkinson, W.D., 1962. The influence of continents and oceans on the geomagnetic variations. Geophysical Journal of the Royal Astronomical Society, 6: 441-449.

Piasecki, M.A.J. 1988. A major ductile shear zone in the Baie d'Espoir area, Gander Terrane, southeastern Newfoundland. In Current Research (1988), Newfoundland Department of Mines and Energy Report 88-1. pp. 135-145.

Piasecki, M.A.I., Williams, H., and Colman-Sadd, S.P. 1990. Tectonic relationships along the Meelpaeg, Burgeo and Burlington Lithoprobe transects in Newfoundland. *In* Current Research (1990), Newfoundland Department of Mines and Energy Report 90-1, pp. 327-339.

Piasecki, M.A.I. 1995. Terrane boundaries in Newfoundland. *In* Hibbard, J.P., van Staal, C.R. and Cawood, P.A., eds., Current Perspectives in the Appalachian-Caledonian Orogen. Geological Association of Canada, Special Paper 41, pp. 323-347.

Quinlan, G.M., Hall, J., Williams, H., Wright, J.A., Colman-Sadd, S.P., O'Brien, S.J., Stockmal, G.S., and Marillier, F. 1991. Onshore seismic reflection transects across the Newfoundland Appalachians. *In* Report of Lithoprobe East Transect Meeting, Nov. 29-30, 1991, Memorial University, St. John's, Newfoundland, pp.3-15.

Quinlan, G.M., Hall, J., Williams, H., Wright, J.A., Colman-Sadd, S.P., O'Brien, S.J., Stockmal, G.S., and Marillier, F. 1992. Lithoprobe onshore seismic reflection transects across the Newfoundland Appalachians. Canadian Journal of Earth Sciences, 29: 1865-1877.

Quinlan, G.M., Beaumont, C. and Hall, J., 1993. Tectonic model for crustal seismic reflectivity patterns in compressional orogens. Geology, 21, 663–666.

Quinn, L. 1995. Middle Ordovician foredeep fill in western Newfoundland. *In* Hibbard, J.P., van Staal, C.R. and Cawood, P.A., eds., Current Perspectives in the Appalachian-Caledonian Orogen. Geological Association of Canada, Special Paper 41, pp. 43-64.

Ranganayaki, R.P. 1984. An interpretive analysis of magnetotelluric data. Geophysics, 49: 1730-1748.

Sims, W.E., and Bostick,F.X. 1969. Methods of Magnetotelluric analysis. Research Laboratory, technical report 58, University of Texas, Austin.

Smith, J.T. and Booker, J.R. 1991. Rapid inversion of two- and three-dimensional magnetotelluric data. Journal of Geophysical Research, 96: 3905-3922.

Smith, J.T. 1995. Understanding telluric distortion matrices. Geophysical Journal International, 122: 219-226.

Soper, N.J., Strachan, R.A., Holdsworth, R.E., Gayer, R.A., and Greiling, R.O. 1992. Sinisral transpression and the Silurian closure of Iapetus. Journal of the Geological

Society, London, 149: 871-880.

Spitz, S. 1985. The magnetotelluric impedance tensor properties with respect to rotations. Geophysics, 50: 1610-1617.

Sternberg, B.K., Washburne, J.C. and Pellerin, L. 1988. Correction for the static shift in magnetotellurics using transient electromagnetic soundings. Geophysics, 53: 1459-1468.

Stockmal, G.S., Colman-Sadd, S.P., Keen, C.E., O'Brien, S.J., and Quinlan, G. 1987. Collision along an irregular margin: a regional plate tectonic interpretation of the Canadian Appalachians. Canadian Journal of Earth Sciences, 24: 1098-1107.

Stockmal, G.S., Colman-Sadd, S.P., Keen, C.E., Marillier, F., O'Brien, S.J., and Quinlan, G.M. 1990. Deep seismic structure and plate tectonic evolution of the Canadian Appalachians. Tectonics, 9: 45-62.

Stockmal, G.S., and Waldron, J.W.F. 1990. Structure of the Appalachian deformation front in western Newfoundland: Implications of multichannel seismic reflection data. Geology, 18: 765-768.

Stockmal, G.S. and Waldron, J.W.F 1991. Balanced cross sections through the Appalachian structural front, Port au Port Peninsula, Western Newfoundland. *In* Report of Lithoprobe East Transect Meeting, Nov. 29-30, 1991, Memorial University, St. John's, Newfoundland, pp.69-79.

Stockmal, G.S., and Waldron, J.W.F. 1993. Structural and Tectonic evolution of the Humber Zone, western Newfoundland, 1. Implications of balanced cross sections through the Appalachian structural front, Port au Port Peninsula. Tectonics, 12: 1056-1075.

Sule, P.O. and Hutton, V.R.S. 1986. A broad-band magnetotelluric study in southern Scotland. Data acquisition, analysis and one-dimensional modelling. Annales Geophysicae, 4B: 145-156.

Swift, C.M., Jr., 1967. A magnetotelluric investigation of an electrical conductivity anomaly in the southwestern United States. Ph.D. thesis, Mass. Inst. of Technol., Cambridge.

Thomas, W.A. 1977. Evolution of the Appalachian - Ouachita salients and recesses from reentrants and promontories in the continental margin. American Journal of

Science, 277A: 1233-1278.

van der Pluijm, B.A., and van Staal, C.R. 1988. Characteristics and evolution of the central mobile belt, Canadian Appalachians. Journal of Geology, 96: 535-547.

van Staal, C.R. 1994. Brunswick subduction complex in the Canadian Appalachians: Record of the Late Ordovician to Late Silurian collision between Laurentia and the Gander margin of Avalon. Tectonics, 13: 946-962.

van Staal, C.R. and de Roo, J.A. 1995. Mid-Paleozoic tectonic evolution of the Appalachian Central Mobile Belt in Northern New Brunswick, Canada: Collision, Extensional Collapse and Dextral Transpression. *In* Hibbard, J.P., van Staal, C.R. and Cawood, P.A., eds., Current Perspectives in the Appalachian-Caledonian Orogen. Geological Association of Canada, Special Paper 41, pp. 367-389.

Vanyan, L.L., Shilovsky, A.P., Okulessky, B.A., Semenov, V.Y. and Sidelnikova, P.P. 1989. Electrical conductivity of the crust of the Siberian Platform. Physics of the Earth and Planetary Interiors, 54: 163-166.

Vozoff, K. (editor), 1986. Magnetotelluric Methods. Society of Exploration Geophysicists Reprint Ser. No. 5, Society of Exploration Geophysicists, Tulsa, Oklahoma.

Wait, J.R. 1962. Theory of magneto-telluric fields. Journal of Research of the National Bureau of Standards-D, 66D: 509-541.

Wannamaker, P.E., Hohmann, G.W., and Ward, S.H. 1984.Magnetotelluric responses of three-dimensional bodies in layered earths. Geophysics, 49: 1517-1533.

West, G.F., and Edwards, R.N. 1985. A simple parametric model for the electromagnetic response of an anomalous body in a host medium. Geophysics, 50: 2542-2559.

Whelan, J.P., Brown, C., Hutton, V.R.S. and Dawes, G.J.K. 1990. A geoelectric section across Ireland from magnetotelluric soundings. Physics of the Earth and Planetary Interiors, 60: 138-146.

Wight, D.E. and Bostick, F.X. 1980. Cascade decimation - a technique for real time estimation of power spectra. Proceedings IEEE International Conference on Acoust., Speech, Signal Proc., Expanded Abstracts pp. 626-629, at Denver, Colorado, April 9-11, Reprinted in Vozoff (1987).

Williams, H. 1978. Tectonic lithofacies map of the Appalachians orogen: Memorial

University of Newfoundland, Map 1.

Williams, H. 1979. Appalachian orogen in Canada. Canadian Journal of Earth Sciences, 16: 792-806.

Williams, H., and Hatcher, R.D. 1982. Suspect terranes and accretionary history of the Appalachian orogen. Geology, 10: 530-536.

Williams, H., and Hatcher, R.D. 1983. Appalachian suspect terranes. *In* Hatcher, R.D., Williams, H., and Zietz, I., eds., Contributions to the tectonics and geophysics of mountain chains. Geological Society of America, Memoir 158, pp. 33-53.

Williams, H., Colman-Sadd, S.P., and Swinden, H.S. 1988. Tectonic-stratigraphic subdivisions of central Newfoundland. Current Research, Part B, Geological Survey of Canada, Paper 88-1B, pp. 91-98.

Williams, H., Piasecki, M.A.J. and Colman-Sadd, S.P. 1989. Tectonic relationships along the proposed central Newfoundland Lithoprobe transect and regional correlations. Current Research, Part B, Geological Survey of Canada, Paper 89-1B, pp. 55-66.

Williams, S.H., Harper, D.A.T., Neuman, R.B., Boyce, W.D. and Mac Niocaill, C. 1995. Lower Paleozoic fossils from Newfoundland and their importance understanding the history of the Iapetus Ocean. *In* Hibbard, J.P., van Staal, C.R. and Cawood, P.A., eds., Current Perspectives in the Appalachian-Caledonian Orogen. Geological Association of Canada, Special Paper 41, pp. 115-126.

Wilson, J.T. 1966. Did the Atlantic close and then re-open? Nature, 211: 676-681.

Wiseman, R. and Miller, H.G. 1994. Interpretation of gravity and magnetic data from southwestern Newfoundland and their correlation with Lithoprobe East seismic lines 89-11 and 89-12. Canadian Journal of Earth Sciences, 31: 881-890.

Wright, J.A. 1970. Anisotropic apparent resistivitiesarising from non-homogeneous, two-dimensional structures. Canadian Journal of Earth Sciences, 7: 527-531.

Wright, J.A., and Cochrane, N.A. 1980. Geomagnetic sounding of an ancient plate margin in the Canadian Appalachians Journal of Geomagnetism and Geoelectricity, 32: SI133-SI144.

Wu, N., Booker, J.R. and Smith, J.T. 1993. Rapid two-dimensional inversion of COPROD2 data. Journal of Geomagnetism and Geoelectricity, 45: 1073-1087.

Yee, E., and Paulson, K.V. 1986. The canonical decomposition and its relationship to other forms of magnetotelluric impedance tensor analysis for the magnetotelluric tensor. Journal of Geophysics, 61: 173-189.

Zhang, P., Roberts, R.G., and Pedersen, L.B. 1987. Magnetotelluric strike rules. Geophysics, 52: 267-278.

Zhang, P., Perersen, L.B., Mareschal, M., and Chouteau, M. 1993. Channelling contribution to tipper vectors: a magnetic equivalent to electrical distortion. Geophysical Journal International, 113: 693-700.

APPENDIX A

Two -Dimensional Model Fit Plots

A.1 Humber - Dunnage Zone Boundary

Figure A.1

A.2 Nortre Dame - Exploits Subzone Boundary

A.2.1 Northern transect

Figure A.2

A.2.2 Central transect

Figure A.3

A.2.3 Southern transect

Figure A.4

A.3 Gander - Avalon Zone Boundary

Figure A.5

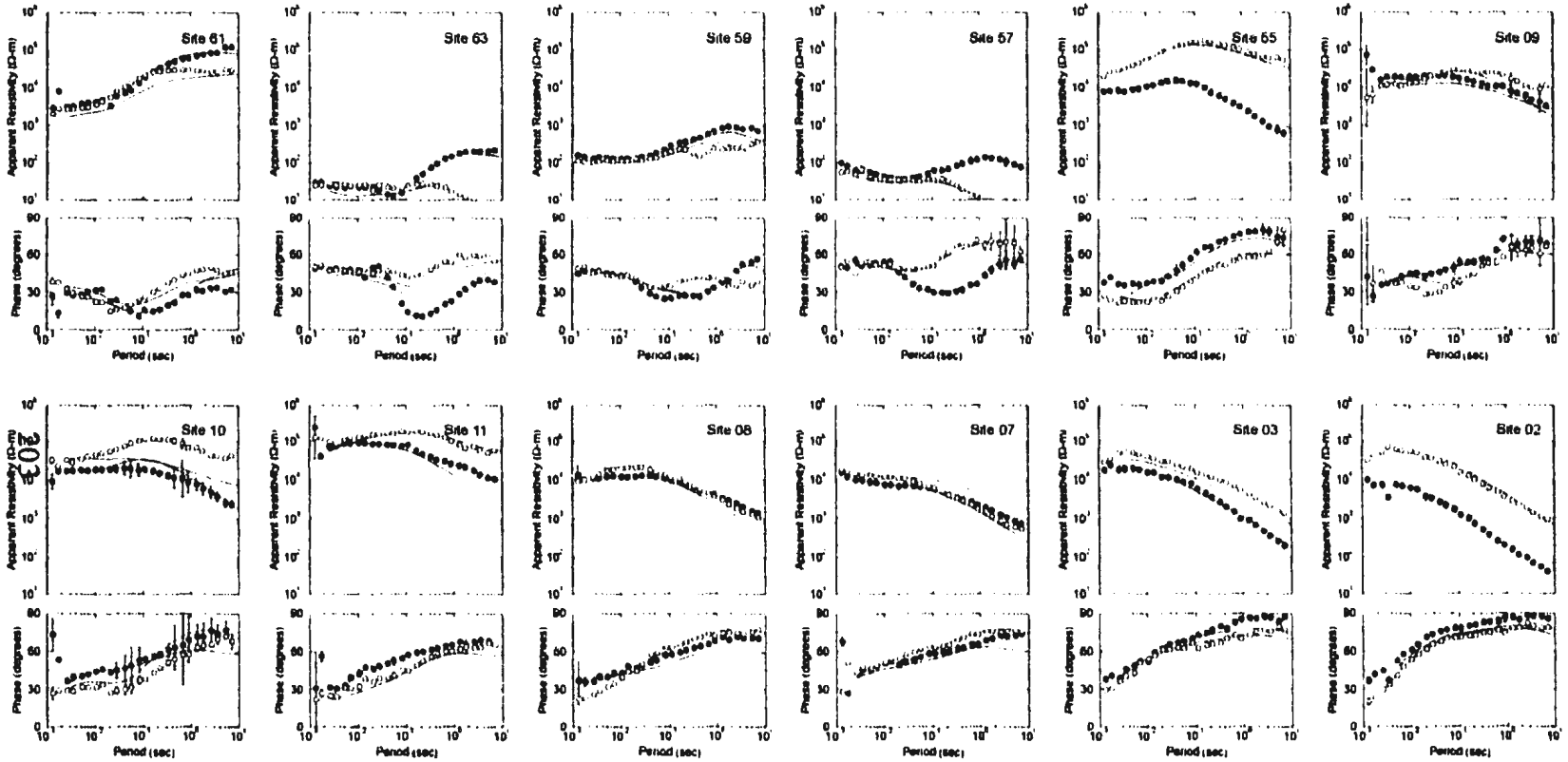

Figure A.1 Comparison of two-dimensional (RRI) model response to measured data for the Humber-Dunnage boundary.

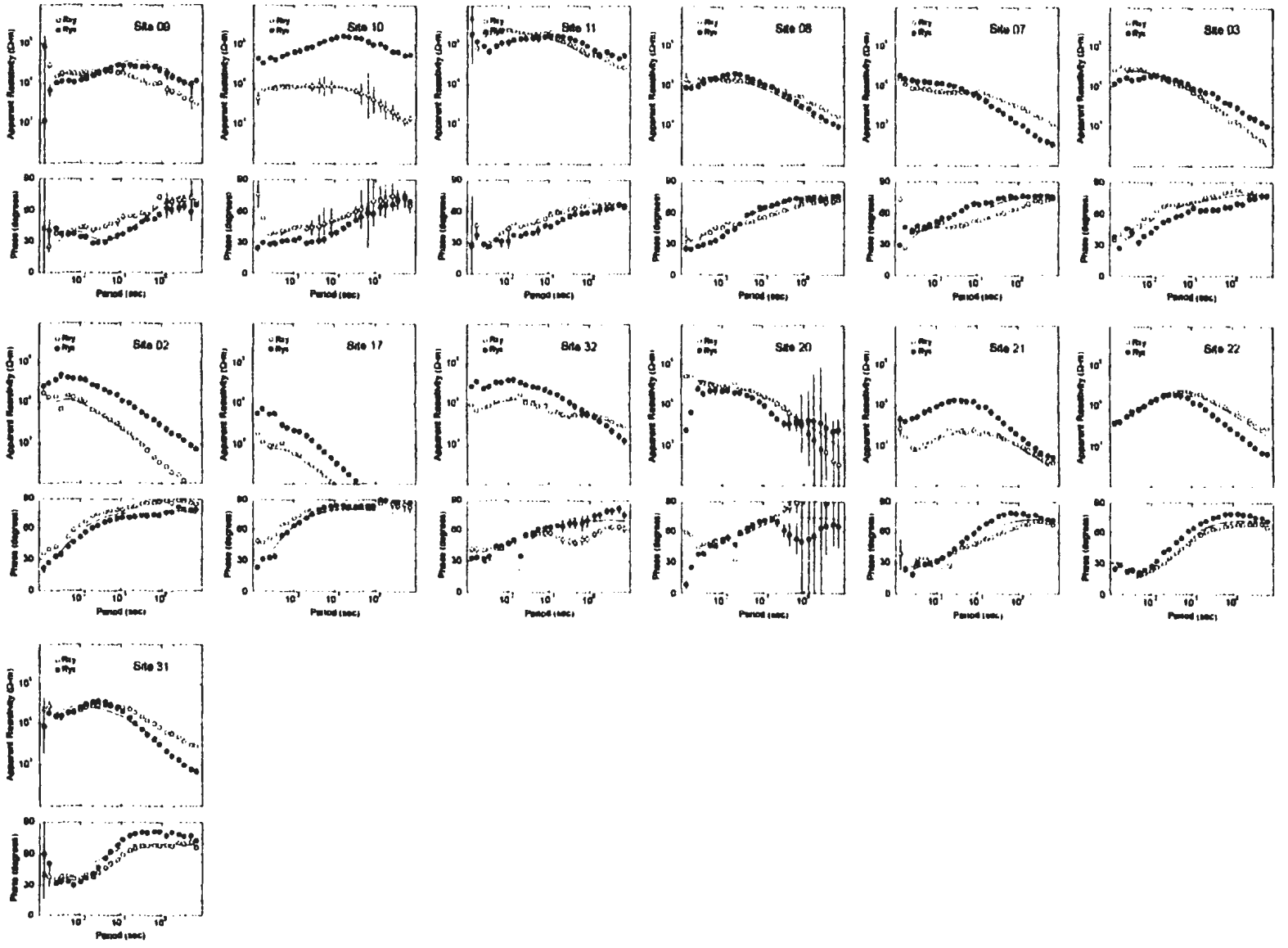

Figure A.2 Comparison of two-dimensional (RRI) model response to measured data for the northern Notre Dame-Exploits boundary.

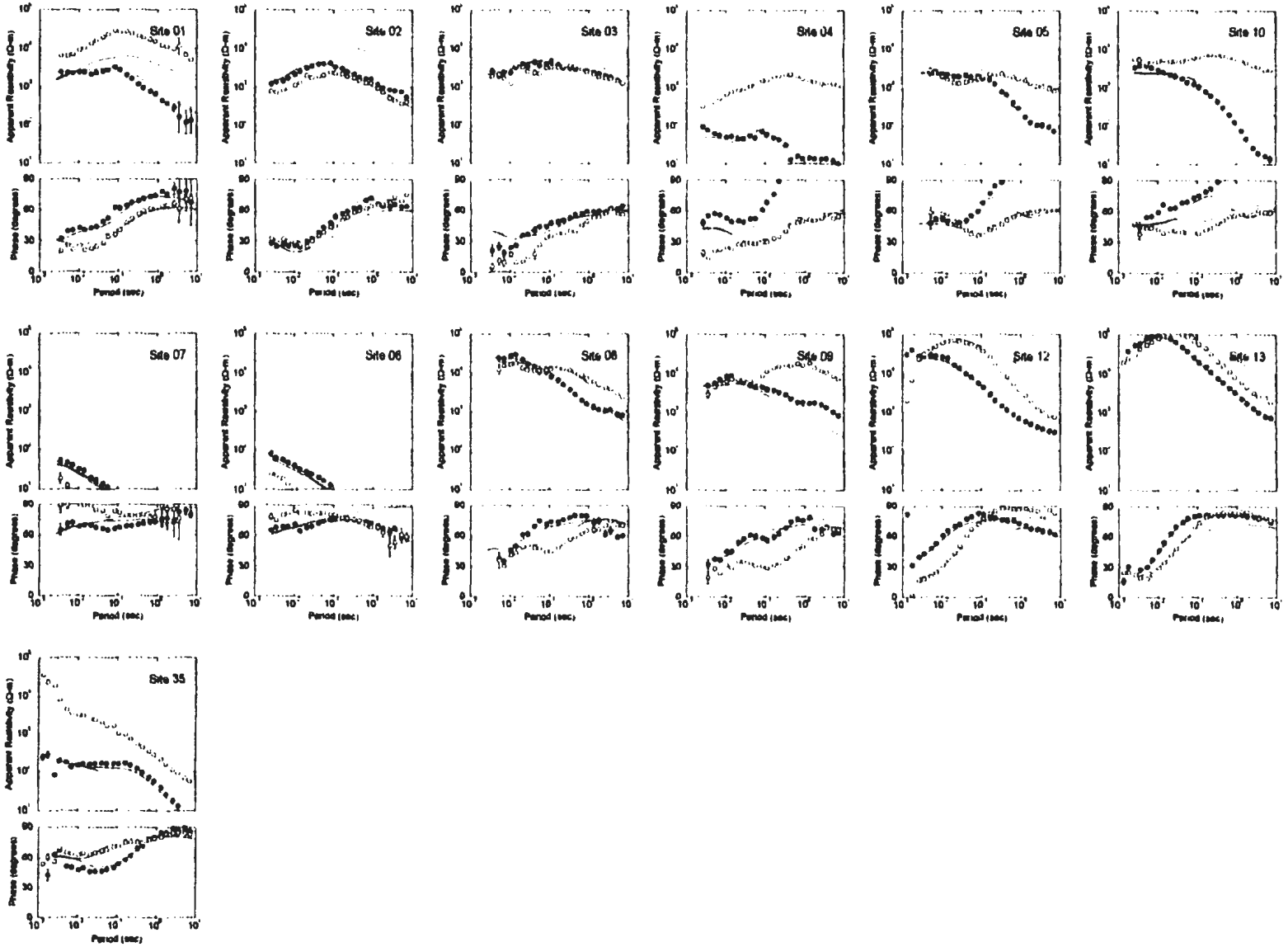

Figure A.3 Comparison of two-dimensional (RRI) model response to measured data for the central Notre Dame-Exploits boundary.

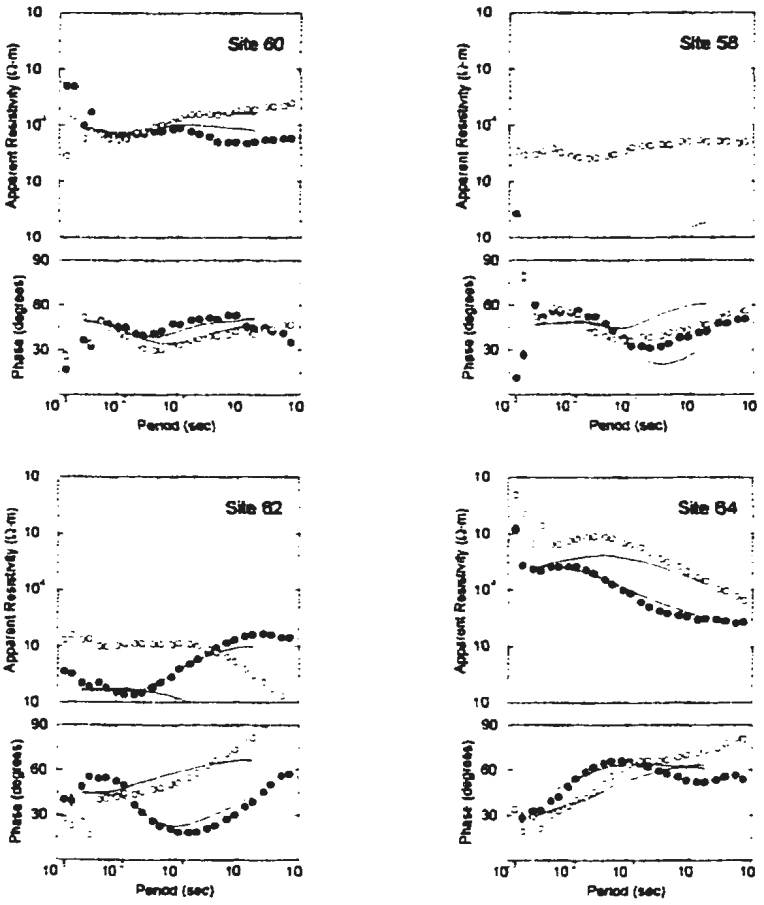

Figure A.4 Comparison of two-dimensional (RRI) model response to measured data for the southern Notre Dame-Exploits boundary.

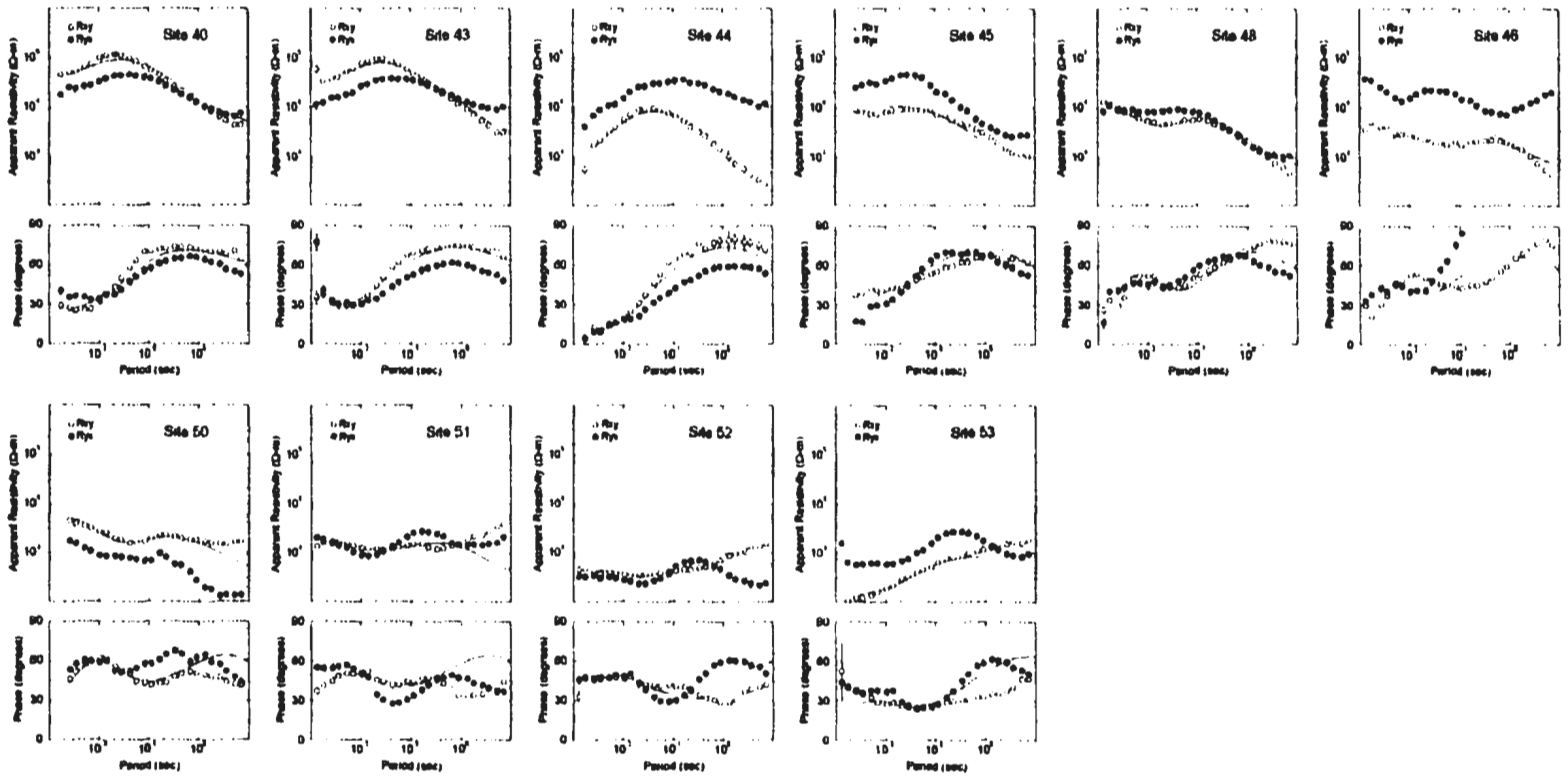

Figure A.5 Comparison of two-dimensional (RRI) model response to measured data for the Gander-Avalon boundary.